КРИСТАЛЛОГРАФИЯ

Kristallografiya

Soviet Physics

CRYSTALLOGRAPHY

Volume 1 1956

A Translation

of the journal

Crystallography

of the

Academy of Sciences of the USSR

Published by the

AMERICAN INSTITUTE OF PHYSICS

INCORPORATED

Soviet Physics
CRYSTALLOGRAPHY

A translation of the journal "Crystallography" of the Academy of Sciences of the USSR

Published by the

AMERICAN INSTITUTE OF PHYSICS

Soviet Physics – CRYSTALLOGRAPHY is a bimonthly journal published by the American Institute of Physics, with the cooperation of the American Crystallographic Association, for the purpose of making available in English reports of current Soviet research in crystallography as contained in the journal "Crystallography" of the Academy of Sciences of the USSR. The translations began with the 1957 issues.

The American Institute of Physics and its translators propose to translate faithfully all of the scientific material in the original articles. The views expressed in the translations are therefore those of the original authors and not those of the translators nor of the American Institute of Physics.

On the conviction that dissemination of the results of research is invaluable to the advancement of science, this translation and publication project was undertaken by the American Institute of Physics as a significant service to the physics community, not only in the United States but also in many other countries. The U. S. National Science Foundation encouraged the project initially and supplied partial financial support on a declining scale until the AIP translation program became self-supporting in July 1964. Translation and printing are handled by the Consultants Bureau Division of Plenum Publishing Corporation.

The transliteration of the names of Russian authors follows essentially the standard agreed upon by the British Standards Institution and Committee Z39/SC-5 of the American Standards Association.

One volume is published annually beginning with the July-August issue.

Subscriptions should be addressed to the American Institute of Physics, 335 East 45th Street, New York, N. Y. 10017.

Soviet Physics – CRYSTALLOGRAPHY is a bimonthly journal published at Prince and Lemon Streets, Lancaster, Pa. by the American Institute of Physics, Inc. Second Class postage paid at Lancaster, Pa.

Soviet Physics

CRYSTALLOGRAPHY

A Translation of "Kristallografiya"

Vol. 1, No. 1, pp. 1-111 January-February, 1956

CONTENTS

Vol. 1, No. 4, pp. 299-387 July-August, 1956

Vol. 1, No. 5, pp. 389-484 September-October, 1956

Vol. 1, No. 6, pp. 485-599 November-December, 1956

Soviet Physics
CRYSTALLOGRAPHY

Vol. 1, No. 1, pp. 1-111

January-February, 1956

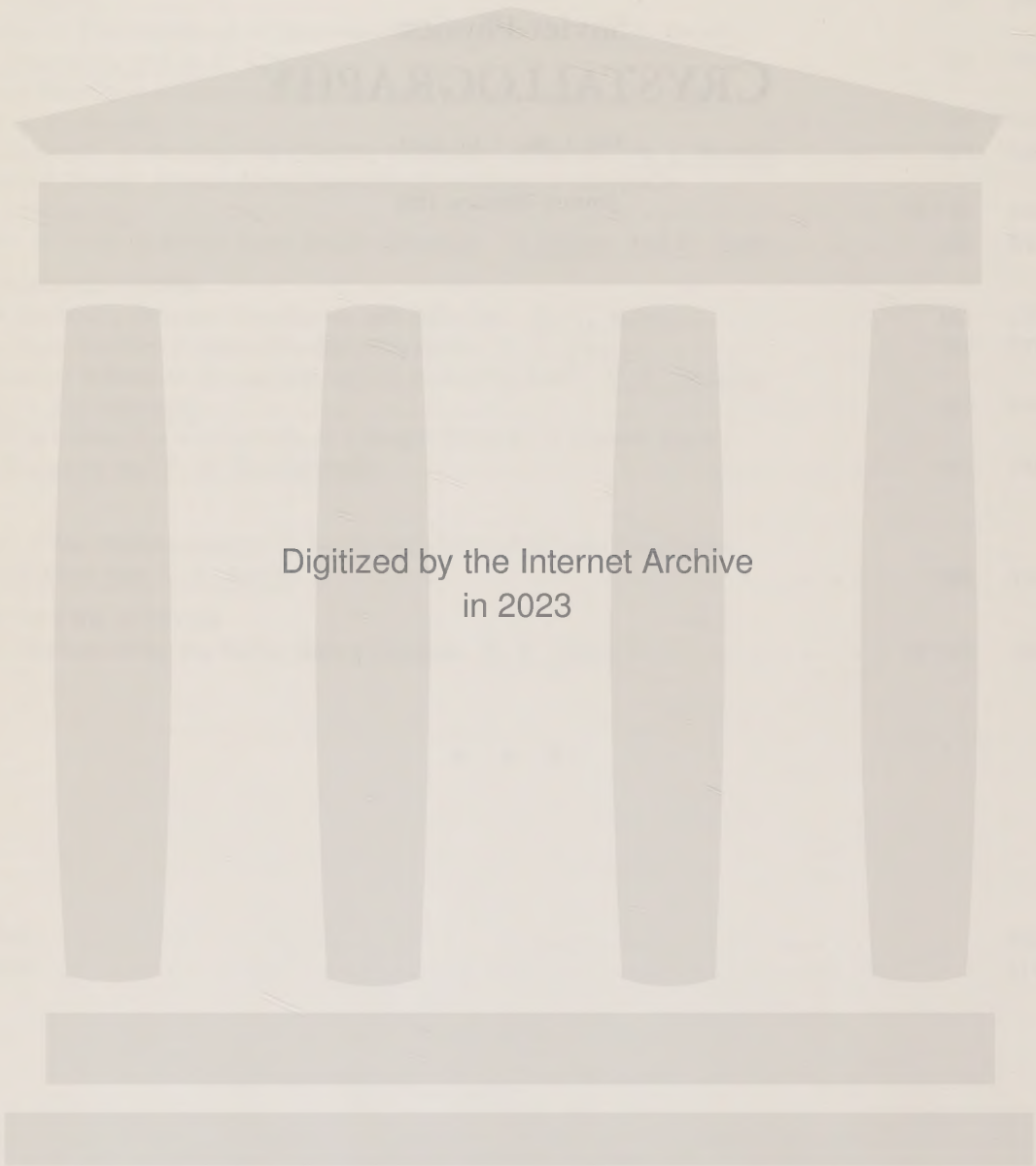

FROM THE EDITORS

Translated from Kristallografiya, Vol. 1, No. 1,
p. 3, January-February, 1956

This country was one of the leaders in crystallography even before the revolution. Gadolin made a considerable contribution to the subject with his derivation of the 32 symmetry classes, while Fedorov is world-famous for his work, including the deduction of the 230 symmetry groups for crystal structures, the invention of the theodolite goniometer and universal stage for optical examination of crystals, and the founding of chemical crystallography. Wulff made major contributions to physical and geometrical crystallography. Later development was even more extensive, however, because so many opportunities arose to apply the subject in industry and in neighboring disciplines. The publication of a journal devoted to crystallography is a natural consequence of this development.

The journal will cover the following areas.

1. Theoretical crystallography: symmetry, scattering theory, physical theories of solids, theory of crystal growth, computational techniques.

2. Analysis of crystal structures: x-ray, electron-diffraction, neutron-diffraction, and other such methods.

3. Chemical crystallography (crystal chemistry): of organic, inorganic, and mineral compounds; chemical bonding in crystals; methods of describing crystal structures; order–disorder effects.

4. Physical crystallography: optical, electrical, mechanical, magnetic, and other properties of crystals and textures.

5. Physicochemical crystallography: polymorphism, isomorphism, enantiomorphism, phase transitions, liquid crystals.

6. Crystal growth: nucleation, growth, equilibrium, morphology, structure, goniometry, and dissolution of real crystals.

7. Applied crystallography: methods and apparatus for crystal growing, crystal working, and technical uses of crystals.

8. History of crystallography and the training of crystallographers.

The journal will also carry brief communications, reviews, discussions, and conference reports.

COLOR SYMMETRY GROUPS

N. V. Belov and T. N. Tarkhova

Institute of Crystallography, Academy of Sciences of the USSR;
and Gor'kii State University

Translated from Kristallografiya, Vol. 1, No. 1,
pp. 4-13, January-February, 1956
Original article submitted November 1, 1955

A new method of selection from the 230 space groups is given for the 46 black-and-white (two-color) groups; this can be extended to 3, 4, and 6 colors; 15 of the color groups present in the 230 space groups are illustrated by specimens of infinite mosaics. Mosaics of low symmetry with 5, 7, or more colors that do not fit into the 230 space groups occur because there can be more than 14 Bravais lattices in a space in which one dimension is qualitatively different from the other two.

The infinite two-dimensional antisymmetry groups [1], or, in the usual representation, the black-and-white groups, were first derived by selecting from the 230 space groups those in which a figure remaining in a plane gives rise to derived figures, some of which may be reversed (turned over). This means that, if the figure (e.g., an irregular triangle) is viewed from the side facing us (colored white on that side) in the initial position, then in half of the derived positions it shows its other (black) side. There are 80 groups that leave a figure in the same plane [2-5]; deleting 17 one-sided planar symmetry groups (which do not reverse the figure), and the same number of groups in which each figure consists of two identical figures superimposed (principal plane a mirror plane; the gray groups in Shubnikov's terminology), we are left with 46 plane two-color groups in the strict sense of the word.

These groups can be deduced without resort to the 230 groups by the method used [6] in deducing the 1651 black-and-white (Shubnikov) antisymmetry space groups. To the well-known five planar Bravais lattices we add the two-color planar Bravais lattices, namely: a monoclinic one p'_b (p'_a, p'_c) in which any edge (or diagonal) of the elementary parallelogram is centered in the colored way (i.e., with the other color); three orthorhombic (rectangular) ones: p'_b (one edge centered in the colored way), p'_c (centered in the other color with respect to the area of the elementary rectangle), and c' (both edges of the ordinary centered rectangular cell centered in the colored way). The last planar color lattice p'_c is square and centered in the colored way. There are thus five color planar Bravais lattices in addition to the ordinary five, or ten in all (Fig. 1).[1]

We give below the international expressions for the 17 ordinary plane groups [7] containing not more

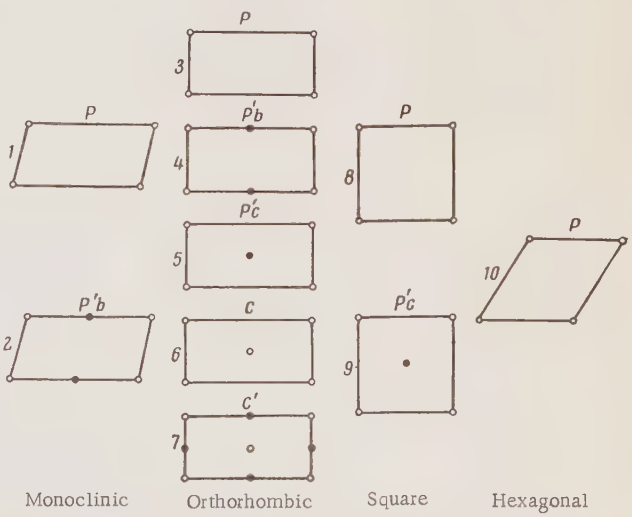

Fig. 1. The planar two-color Bravais nets (lattices).

[1]See the paper cited above for proof that these lattices exhaust the possible two-color ones in a plane (also for the 36 in space).

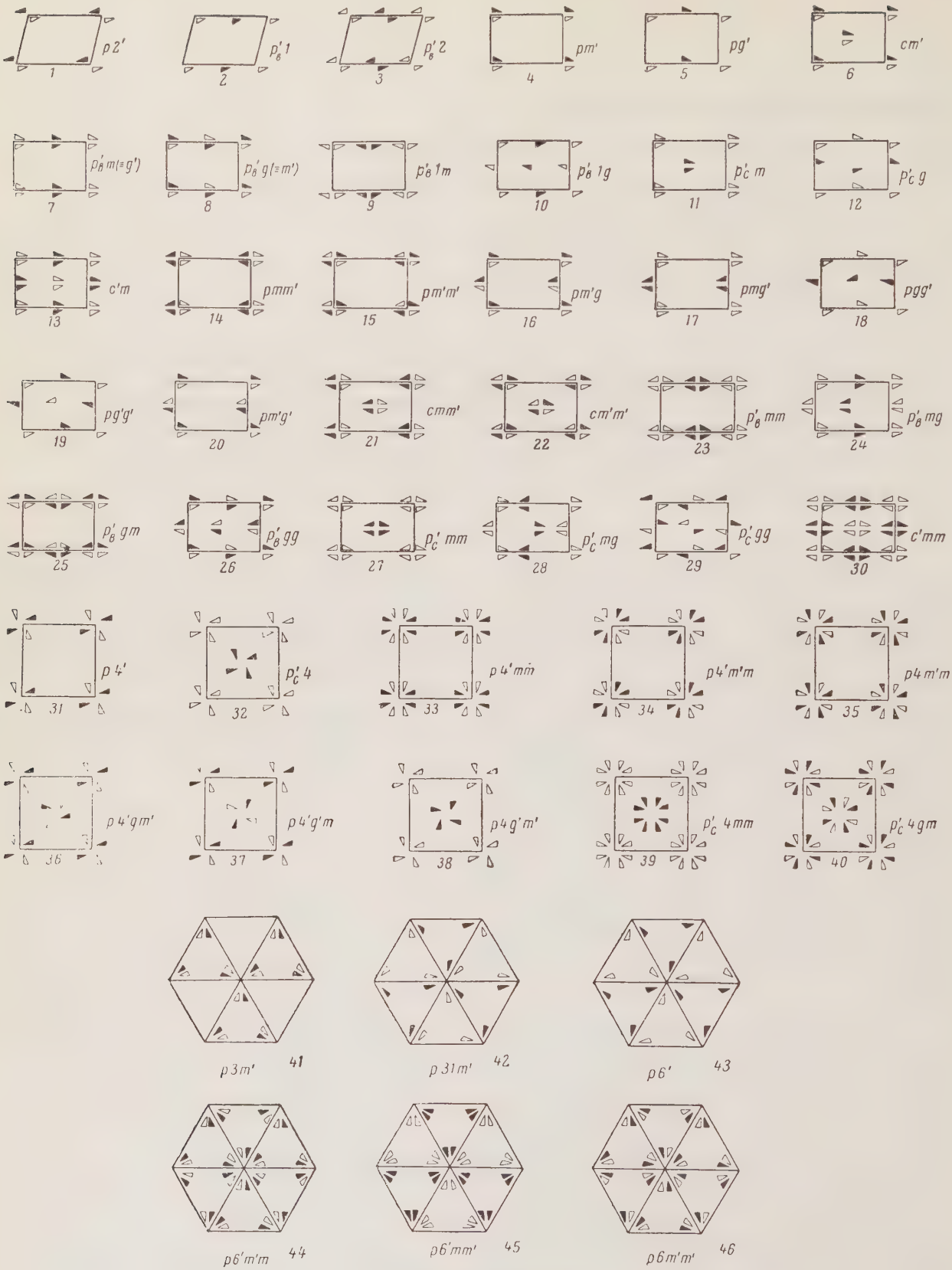

Fig. 2. The 46 two-color groups.

TABLE 1. List of the Planar Two-Color Groups

No.	Rational symbols	Cochran's symbols	Initial space group with reversing symmetry elements	Initial space group containing related objects at two levels
	1	2	3	4
1	$p2'$	$p2'$	$C_i = P\bar{1}$	$C_2^2 = P112_1$
2	$p_b'1$	pt'	$C_s = P11b$	$C_1^1 = A\,111$
3	$p_b'2$	$p2t'$	$C_{2h}^4 = P11\,\frac{2}{b}$	$C_2^1 = A\,112$
4	pm'	pm'	$C_2^1 = P121$	$C_s^2 = Pc11$
5	pg'	pg'	$C_2^2 = P\ 12_11$	$C_s^2 = Pn11$
6	cm'	cm'	$C_2^3 = C121$	$C_s^4 = Cc$
7	$p_b'm$	$pm + t'$	$C_{2v}^2 = Pm2_1b$	$C_s^3 = Am11$
8	$p_b'g$	$pg + t'$	$C_{2v}^3 = Pb2b$	$C_s^4 = Ab11$
9	$p_b'1m$	$pm + m'$	$C_{2v}^4 = P2mb$	$C_s^1 = A1m1$
10	$p_b'1g$	$pg + g'$	$C_{2v}^5 = P2_1ab$	$C_s^2 = A1a1$
11	$p_C'm$	$pm + g'$	$C_{2v}^7 = Pm2_1n$	$C_s^3 = Im11$
12	$p_C'g$	$pg + m'$	$C_{2v}^6 = Pb2n$	$C_s^4 = Ib11$
13	$c'm$	$cm + m'$	$C_{2v}^{15} = Cm2a$	$C_s^3 = Fm11$
14	pmm'	pmm'	$C_{2h}^1 = P\,\frac{2}{m}$	$C_{2v}^2 = Pmc$
15	$pm'm'$	$pm'm'$	$D_2^1 = P222$	$C_{2v}^3 = Pcc$
16	$pm'g$	$pm'g$	$C_{2h}^4 = P1\,\frac{2}{a}1$	$C_{2v}^5 = Pca$
17	pmg'	pmg'	$C_{2h}^2 = P\frac{2_1}{m}$	$C_{2v}^7 = Pmn$
18	pgg'	pgg'	$C_{2h}^5 = P\frac{2_1}{b}$	$C_{2v}^9 = Pbn$
19	$pg'g'$	$pg'g'$	$D_2^3 = P2_12_12$	$C_{2v}^{10} = Pnn$
20	$pm'g'$	$pm'g'$	$D_2^2 = P2_122$	$C_{2v}^6 = Pcn$
21	cmm'	cmm'	$C_{2h}^3 = C\,\frac{2}{m}$	$C_{2v}^{12} = Cmc$
22	$cm'm'$	$cm'm'$	$D_2^6 = C222$	$C_{2v}^{13} = Ccc$
23	$p_b'mm$	$pm, m + m'$	$D_{2h}^5 = Pmmb$	$C_{2v}^{14} = Amm2$
24	$p_b'mg$	$pm, g + g'$	$D_{2h}^{11} = Pmab$	$C_{2v}^{16} = Ama2$
25	$p_b'gm$	$pg, m + m'$	$D_{2h}^3 = Pbmb$	$C_{2v}^{15} = Abm2$
26	$p_b'gg$	$pg, g + g'$	$D_{2h}^8 = Pbab$	$C_{2v}^{17} = Aba$
27	$p_C'mm$	$pm + g',\ m + g'$	$D_{2h}^{13} = Pmmn$	$C_{2v}^{20} = Imm$
28	$p_C'mg$	$pm + g',\ g + m'$	$D_{2h}^7 = Pman$	$C_{2v}^{22} = Ima$
29	$p_C'gg$	$pg + m',\ g + m'$	$D_{2h}^4 = Pban$	$C_{2v}^{21} = Iba$
30	$c'mm$	$cm + m',\ m + m'$	$D_{2h}^{21} = Cmma$	$C_{2v}^{18} = Fmm$
31	$p4'$	$p4'$	$S_4^1 = P\bar{4}$	$C_4^3 = P4_2$
32	$p_C'4$	$p\ 4\ t'$	$C_{4h}^3 = P\,\frac{4}{n}$	$C_5^4 = I\,4$
33	$p\ 4'\ mm'$	$p\ 4'\ mm'$	$D_{2d}^5 = P\bar{4}\,m2$	$C_{4v}^7 = P\,4_2mc$
34	$p\ 4'\ m'm$	$p\ 4'\ m'm$	$D_{2d}^1 = P\bar{4}\,2m$	$C_{4v}^3 = P\,4_2cm$
35	$p\ 4\ m'm'$	$p\ 4\ m'm'$	$D_4^1 = P\,422$	$C_{4v}^5 = P\,4\,cc$
36	$p\ 4'\ gm'$	$p\ 4'\ gm'$	$D_{2d}^7 = P\bar{4}\,g2$	$C_{4v}^8 = P\,4_2gc$
37	$p\ 4'\ g'm$	$p\ 4'\ g'm$	$D_{2d}^3 = P\bar{4}\,2_1m$	$C_{4v}^4 = P\,4_2nm$
38	$p\ 4\ g'm'$	$p\ 4\ g'm'$	$D_4^2 = P42_12$	$C_{4v}^6 = P\,4\,nc$
39	$p_C'4\,mm$	$p\ 4m + g',\ m + m'$	$D_{4h}^7 = P\frac{4}{n}mm$	$C_{4v}^9 = I\,4\,mm$
40	$p_C'4\,gm$	$p\ 4g + m',\ m + m'$	$D_{4h}^3 = P\,\frac{4}{n}gm$	$C_{4v}^{10} = I\,4\,gm$
41	$p\ 3m'1$	$p\ 3m'1$	$D_3^1 = P312$	$C_{3v}^3 = P\,3\,c$
42	$p\ 31\,m'$	$p\ 31\,m'$	$D_3^2 = P321$	$C_{3v}^4 = P\,31\,c$
43	$p\ 6'$	$p\ 6'$	$C_{3i}^1 = P\bar{3}$	$C_6^6 = P\,6_3$
44	$p\ 6'\ m'm$	$p\ 6'\ m'm$	$D_{3d}^1 = P\,\bar{3}1\,\frac{2}{m}$	$C_{6v}^3 = P\,6_3\,cm$
45	$p\ 6'\ mm'$	$p\ 6'mm'$	$D_{3d}^2 = P\,\bar{3}\,\frac{2}{m}1$	$C_{6v}^4 = P6_3\,mc$
46	$p\ 6\ m'm'$	$p\ 6\ m'm'$	$D_6^1 = P\,622$	$C_{6v}^2 = P\,6\,cc$

than two principal generating symmetry elements; these we make colored (shown by primes) in turn, and then both together.

The theorem proved in the original derivation cited above indicates that any symmetry element in the direction of any color translation (in the two-color translational groups) either alternates with a (similar) uncolored element or coincides with the latter, so the complete list of the two-color groups is given by replacing in each of the 17 ordinary groups the uncolored symbol for the Bravais lattice in turn by all the colored ones of the same system. The two-color Bravais lattice may not relate in the same way to the generating elements in positions 1 and 2 in the symbol, in which case the number of corresponding groups is doubled. Table 1 gives all 46 two-color groups arranged in the order of deduction. The first column gives the representation in terms of colorless and two-color Bravais lattices, which we consider to be the most logical. The second column gives Cochran's rather illogical symbols from his paper in Acta Crystallographica [8], while the third column gives (in Schoenflies and international symbols) the space group (out of the 230) that corresponds to that color and which was the initial one in the original derivation of the 80 two-sided two-color groups. The last column gives a further space group from the 230 from which the two-color group may be deduced (see below for details of this).

Figure 2 gives schemes for all 46 two-color groups, which have been given before: in the first derivation by Alexander and Hermann [2], by Weber [3], and then by Shubnikov in his "Atlas" [4] and "Symmetry" [5]. Some of the schemes do not agree with those given in these sources, firstly because, in these sources, the orthorhombic lattice is centered (in the colored way) either on the $a-p'_a$ edge (mostly) or on the $b-p'_b$ edge, while we use always p'_b; secondly because preference was sometimes given in the earlier works to the color symmetry elements (i.e., the corresponding plane or axis was brought into coincidence with a coordinate one) when color symmetry elements alternate with uncolored ones (in groups with colored Bravais lattices). We have given preference to the uncolored elements, by virtue of the basic theorem; for instance, group p'_cg is given as p'_cg on account of the alternation of g with m' (Fig. 3a), whereas, in the earlier works, it is given as p'_cm' (Fig. 3b); group p'_cgg (Fig. 4a) is shown as $p'_cm'm'$ in Fig. 4b.

Antisymmetry was the basic concept in the early derivations of the two-color groups, especially by Shubnikov (front and rear in a plane figure, or plus and minus sides); this is not represented other than by implication if the two sides are given different colors. The groups may be deduced in another way, namely by selecting from the 230 space groups those that place all figures derived from a given one (an irregular triangle) at two levels only. Let the height of the three-dimensional cell be c, and the height of the initial figure be z; then half of the figures related by the symmetry of the group will remain at level z, while the other half will lie at $z+c/2$. However, z can always be taken as 0 in such groups. The symmetry elements that do this are screw axes (2_1, 4_2, 6_3) and c and n symmetry planes. In addition, the A, B, I, and F Bravais lattices can act in this way. The figures at z(0) are given one color, and those at $(z+c/2)$ or $c/2$ are given the other.

This method has the advantage of completely avoiding the one-color plane groups and the gray ones; it gives only the 46 two-color groups. Some of the aspects of the method are given below.

It is reasonable to extend this method to figures with more than two colors. The groups of multicolor symmetry are derived by isolating from the 230 those that place the figures at three levels only, at four levels only, and at six levels only, these levels being denoted by different colors.

The concepts of classical crystallography rule out five-color, seven-color, and other such symmetries (see below). The color symmetry elements (for numbers exceeding two) are 3_1, 3_2, 4_1, 4_3, 6_1, 6_5, 6_2, and 6_4 axes together with a d plane and Bravais lattice R.

The tetragonal color groups are $P4_1$ (I, II), $P4_3$, $I4_1$ (III), and multiples of these groups, namely $I4_1md$ (IV–V), $I4_1cd$ (VI). The trigonal subsystem contains $P3_1$ (X), $P3_2$, R3 (XI), R3m (XII), R3c (XIII) while the hexagonal one has $P6_1$ (XIV), $P6_5$, $P6_2$ (XV), $P6_4$. The sole group in the lower systems is the orthorhombic Fdd (VII, VIII, IX), which has figures at four levels.

We give color mosaics consisting of fairly large numbers of cells for 11 of these 15 groups (one of each enantiomorphic pair) as a separate table; the triangles used in the analogous schemes for the 46 two-color groups do not give a clear conception of these. The symmetry is given under each mosaic, while the above lists of groups contain (in parentheses) the Roman numerals representing the corresponding mosaics. Many of these mosaics are to be found in inlaid floors, etc., but some of them appear novel and have been constructed solely from the graphs of the corresponding space groups ($I4_1cd$

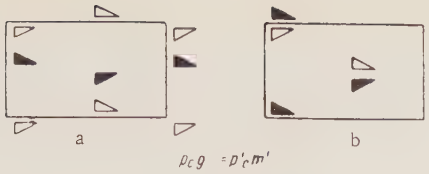

Fig. 3. Group $p'_c g$ in different aspects.

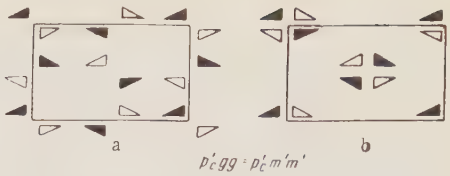

Fig. 4. Group $p'_c gg$ in different aspects.

–VI, R3c–XIII).

It is convenient to place a piece of tracing paper over the mosaic and mark in a unit cell, entering the symbols for the symmetry elements [7, 9]; the color action of these elements can then be followed.

A 4_1 axis places the figures at four levels, which in our figures are shown as yellow, blue, red, green, and then yellow again; operations 4_2 or 2_1 take us from yellow to red or from blue to green, as does the action of a c- or n-glide plane. The six colors for a 6_1 axis are white, red, green, black, yellow, blue, and white again. The 2_1 axis present in a 6_1 axis corresponds to the transitions white–black, red–yellow, and green–blue. These latter are also effected in hexagonal groups by c- and n-glide planes.

We at first thought that only the two enantiomorphic groups 6_1 and 6_5 were possible for six-color symmetry, but an examination of space group R3c gave us mosaic XIII not so far found in inlaid floors; this showed that the three levels generated by the triad screw axis are further divided in two by a c plane, and mosaic XIII may be split up either into hexagons of three kinds (each containing two colors with a difference of c/2) or into triangles of two kinds, one containing three colors with difference c/3 and the other also three colors with the same difference, but the complementary colors differing by c/2 from those in the first kind. The hexagons contain triad rotation axes at their centers; the triangles, triad screw ones.

The simpler pattern IV was obtained at first for group $I4_1md$, and it seemed that V represented a new symmetry group; but the two patterns have the same symmetry, the mirror planes in IV being parallel to the sides of the square plates, whereas, in V, they run along the diagonals of these plates.*

The orthorhombic mosaics corresponding to group Fdd are derived from the tetragonal ones with d planes by rhombic deformation, i.e., transformation of the square plates into rectangles or into rhombic ones, in accordance with whether the d planes lie along the sides of the plates (as in IV) or along the diagonals (in V). Elongation and compression always occur along the d planes, which persist in the orthorhombic symmetry and there define the coordinate directions, so the initial tetragonal cell must be taken in aspect F, not I. We arrive at the sole orthorhombic group Fdd not only from group $I4_1md = F4_1dm$ (mosaic VII from IV, mosaic VIII from V), but also from $I4_1cd = F4_1dc$ (mosaic IX from VI).

The lower systems contain (in classical crystallography) no symmetry elements (apart from d planes) that possess figures related by them at more than two levels, so it would appear that only group Fdd allows of multicolor groups with cells neither square nor hexagonal. But such groups (not space groups) do exist and are often found in mosaics; in addition, we find in them sets of 5, 7, and more colors forbidden by classical crystallography. Several such are shown, the first five (XVI to XX) being in colors, and the others being shown in the text as arrays of plates to be treated as colored in accordance with the numbers (the numbers of the levels in the other interpretation).

Mosaics XVI and XVII are similar in pattern, being centered with a symmetry plane (Cm) and having odd numbers (3 and 5) of colors; the second is forbidden by classical crystallography, but it is obvious that similar mosaics with 7, 9, and more colors are possible. Figure 5 shows schematically (in black) a seven-color one. Mosaic XVIII is analogous as regards symmetry and number of colors to XVI, but it consists of rectangular plates instead of rhombs. There are 6 colors in mosaics XIX and XX.

The symmetry of the first is Cm, while that of the second is Im; Fig. 6 shows a mosaic analogous to XIX but having eight colors, while Fig. 7 shows eight colors and no symmetry element apart from the triclinic F lattice. Figure 8 shows a cell of a mosaic consisting of six colors which has a primitive triclinic cell but an obvious law of succession in the colors.

These mosaics (not of space-group type) arise from special causes; lattices I and F can be referred in the monoclinic system to ones centered only on one rectangular face, on account of the absence of

*See correction at the end of the paper.

the requirement that the cell should have a right angle between the third axis and the centered face. Color symmetry replaces the continuous third dimension by a sequence of colors, which thereby eliminates the question of the various possible angles between the third axis and the rectangle ($b \times a$) formed by the first two. The impossibility of making these angles different causes the third dimension to be perpendicular (or in some other way specified) relative to the ba plane. This third axis does not have to be the direction of the shortest translation out of the plane of the other two if its direction has been specified; the ca (or cb) plane may be centered in two or more ways, not merely one.

Consider first an even number of centered points, especially 2. In this case the diagonal of the side rectangle is divided into 3 parts (3 levels), which enables us to construct mosaic XVI (three colors), which is the one most commonly encountered in inlaid floors. The side "rectangular" face may be centered by its four corners, in which case we have five levels and arrive at mosaic XVII containing five colors. In both cases the cell of the mosaic is centered, but the two side faces are uncentered.

In general, a mosaic with an even number of colors may have an odd number of centered points on face A; then, if face C is centered, the basic theorem of Bravais lattices shows that face B will be centered also (mosaic XVIII, Fig. 6). The last two examples have a symmetry plane each, whereas the sole symmetry element in Fig. 7 is lattice F.

The 14 Bravais lattices arise when we select six elementary parallelepipeds on the basis of the principal directions in crystals, these figures corresponding to the setting rules of classical crystallography (i.e., to the six systems); we then find that the vertices of such cells cannot take up all the lattice nodes. There is no reason why the third direction in a monoclinic cell (one special direction) should be perpendicular to the plane of the first two when the second direction has been taken perpendicular to the special one; on this basis we get only two monoclinic cells, to which all others can be reduced. Replacement of the third direction on color principles essentially makes that direction other than perpendicular, one result of which is the existence of cells centered in several ways. Colored mosaics thus illustrate Bravais lattices 15, 16, etc., which are not reducible to the basic 14.

This means that the lattice symbols cannot indicate only the faces centered in the sense of the 14 Bravais lattices (once and at the center of the face). The multiple centering must be allowed for and must appear in the formula. For instance, the formula for XVI will be $A^{II}PC$, for XVII and XVIII it will be $A^{IV}PC$, and for XIX it is $A^{V}BC$. The formula for Fig. 7 is (F) $A^{III}BC$. Indication of F is unnecessary in the last two cases, but the formula for XX, (I) $A^{II}PP$, requires the (I), for centering in the volume does not exclude centering of the faces (even number of nodes). The triclinic scheme of Fig. 8 has the formula $A^{V}B^{II}C^{II}$. The standard rule for the 14 Bravais lattices is replaced by a more general one for the color case: an odd number of centering nodes in two faces of the cell implies an odd number of nodes in the third face also.

Similar ideas appear in the early part of this paper in the third method of deducing the 46 color groups; Table 1 contains the side-centered triclinic cell A111, monoclinic cells centered on the face normal to the special direction (Am11 and Ab11), and even the monoclinic Fm11 face centered all around. All of these cells are impossible (are reduced to simpler ones) if the third edge is not per-

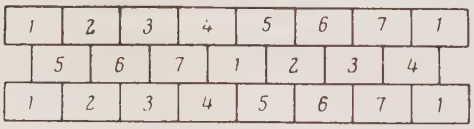

Fig. 5. The seven-color mosaic $A^{VI}PCm$.

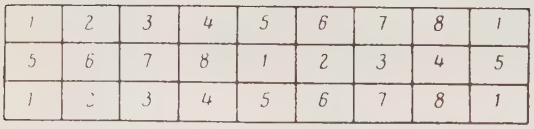

Fig. 6. The eight-color mosaic $A^{VIII}BCm$.

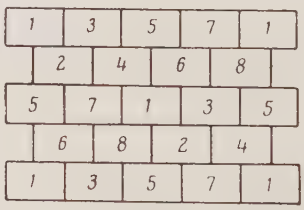

Fig. 7. The eight-color mosaic (F) $A^{III}BC$.

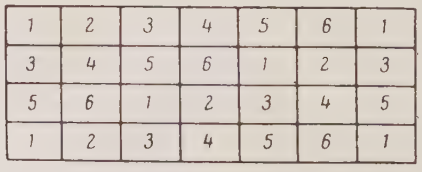

Fig. 8. The six-color mosaic $A^{V}B^{II}C^{II}$.

I

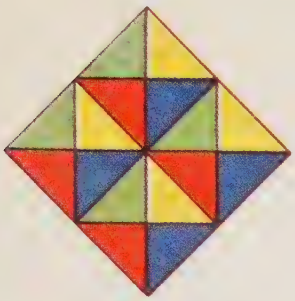

$P\,4_1$

IV

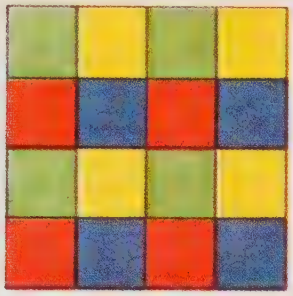

$I\,4\,md = F\,4\,dm$

VII

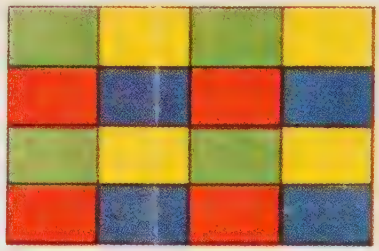

Fdd

X

P

II

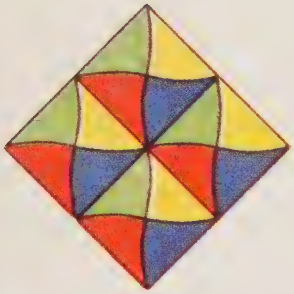

$P\,4_1$

V

$I\,4\,md = F\,4\,dm$

VIII

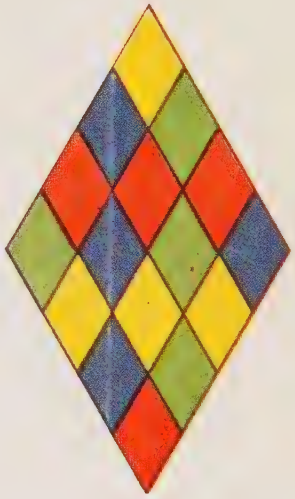

Fdd

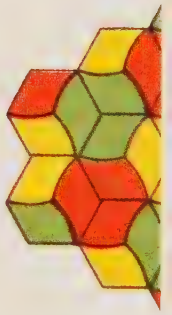

III

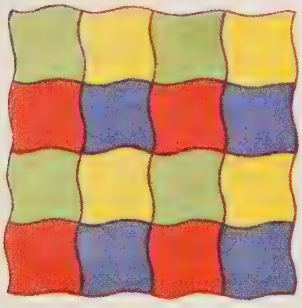

$I\,4_1$

VI

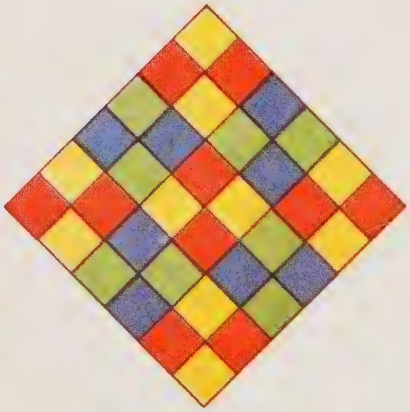

$I\,4\,cd = F\,4\,dc$

IX

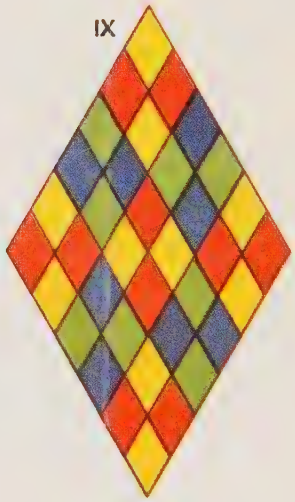

Fdd

R

$^{1}_{1}$

XIV

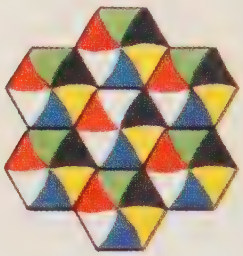

$P\,6_1$

XVI

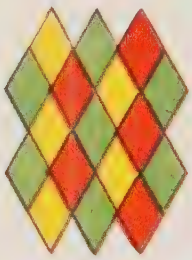

Cm

XVIII

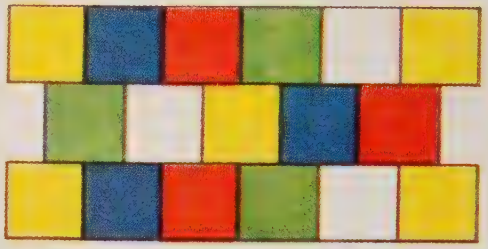

Cm

XI

R 3

XV

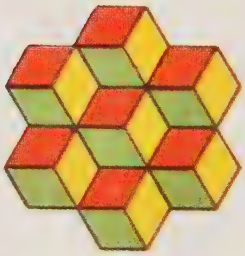

$P\,6_2$

XVII

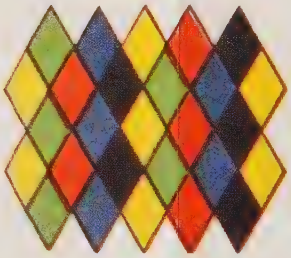

Cm

XIX

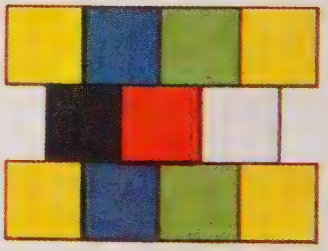

Pm

XII

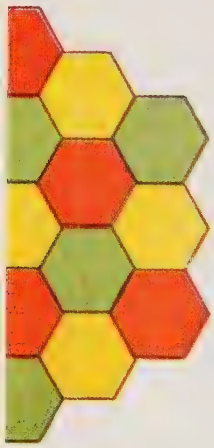

3 m

XIII

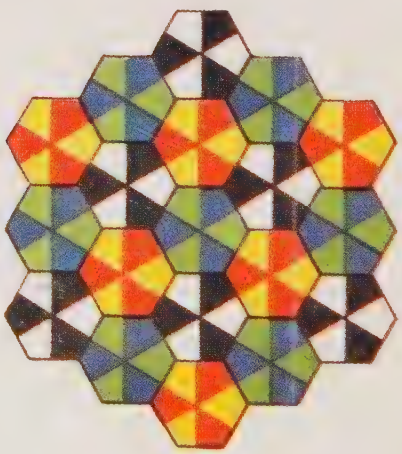

$R\,3_c$

XX

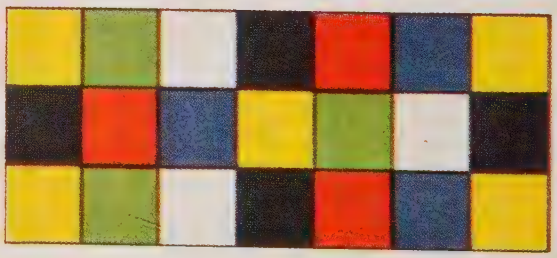

Cm

pendicular to the mutually perpendicular edges of the monoclinic cell, so even the two-color symmetry groups contain more than the 14 independent Bravais lattices (ones not mutually reducible).

LITERATURE CITED

1. A. V. Shubnikov, Symmetry and Antisymmetry of Finite Figures [in Russian] (Moscow, 1951).
2. E. Alexander and K. Hermann, Zur Theorie der flüssigen Kristalle, Z. Krist., 69, 285-299 (1928).
3. L. Weber, Die Symmetrie homogener ebener Punktsysteme, Z. Krist., 70, 309-327 (1929).
4. A. V. Shubnikov, Atlas of Crystallographic Symmetry Groups [in Russian] (Izd. AN SSSR, 1946).
5. A. V. Shubnikov, Symmetry [in Russian] (Moscow, 1960).
6. N. V. Belov, N. N. Neronova, and T. S. Smirnova, "The 1651 Shubnikov groups," Tr. Inst. kristallografii, 11, 33-67 (1955).
7. International Tables for X-ray Crystallography (Birmingham, 1952).
8. W. Cochran, "The symmetry of real periodic two-dimensional functions," Acta Cryst., 5, 630-633 (1952).
9. G. B. Bokii, Introduction to Chemical Crystallography [in Russian] (Moscow, 1954).
10. N. V. Belov, Structural Crystallography [in Russian] (AN SSSR, Moscow, 1951).

This paper contains an error in the uniform deformation of the tetragonal mosaics into orthorhombic ones. Mosaic IV should be compressed along the diagonal of the square, white mosaic V should be compressed along the sides, not the other way around. The same error occurs in the curvilinear outlines in mosaic XI, which thus illustrates group R3m instead of R3.

These faults have been corrected in the table in our second paper on the color groups, which appears on p. 487. In addition, new mosaics having only rectilinear boundaries in their components are shown there for all mosaics having curvilinear boundaries in the original paper.

DETERMINATION OF THE SIGN OF STRUCTURE AMPLITUDES

A. I. Kitaigorodskii

Institute of Heteroorganic Compounds, Academy of Sciences of the USSR
Translated from Kristallografiya, Vol. 1, No. 1,
pp. 14-16, January-February, 1956
Original article submitted October 20, 1955

A theory of the author is used to set up the simplest relations and tables for the certain and probable determination of the sign of structure products. The graphical and tabular material here presented may be successfully used to determine the signs of the structure amplitudes for crystals with cells containing up to 50 or 70 effective atoms.

1. The theory of structure-amplitude relations was developed by the author in papers published in Doklady Akademii Nauk SSSR in 1954-1955. In this article, we shall formulate very simple practical rules for determining the sign of structure amplitudes.

2. The theory developed enables us to consider relationships involving m amplitudes. In practice, however, calculations involving more than four amplitudes must be entrusted to a computer. The equations and rules governing relationships involving four amplitudes are set forth in the papers mentioned above.

Here we shall consider only the simplest case: relationships involving three amplitudes. Theory shows that such a relationship exists for the amplitudes of three reflections with indices $h_1h_2h_3$ (H), $k_1k_2k_3$ (K), and k_1-h_1, k_2-h_2, k_3-h_3 (K–H).

3. This relationship consists in the following. The value of the structure product $\hat{F}_H\hat{F}_K\hat{F}_{K-H}$, where $\hat{F}$ is a unitary structure amplitude, is positive definite for large amplitude values. The structure product is certainly positive if it is larger than $\frac{1}{8}$ in absolute magnitude. However, structure products smaller than $\frac{1}{8}$ may also be certainly positive. Exhaustive data for the certain determination of a positive sign for $\hat{F}_H\hat{F}_K\hat{F}_{K-H}$ are given by the graph presented in Fig. 1. Along the axes lie the values of $\hat{F}_H$ and $\hat{F}_K$, and each curve corresponds to a specific value of $\hat{F}_{K-H}$. The following rules govern the use of the graph:

(a) Choose the curve that corresponds to the given value of $|\hat{F}_{K-H}|$; plot the point with coordinates $|F_H|$, $|F_K|$ on the graph; if this point lies above the curve, the structure product will certainly be positive.

(b) Even if the structure product is not certainly positive, it still has a probability $W_+ > \frac{1}{2}$ of being positive.

Graphs of W_+ are given in Figs. 2 and 3 for several cases from the author's formula

$$W_+ = \frac{1}{1+\varepsilon},$$

where

$$\varepsilon = \sqrt{\frac{1-\hat{F}_H^2-\hat{F}_K^2-\hat{F}_{K-H}^2-2|\hat{F}_H\hat{F}_K\hat{F}_{K-H}|}{1-\hat{F}_H^2-\hat{F}_K^2-\hat{F}_{K-H}^2+2|\hat{F}_H\hat{F}_K\hat{F}_{K-H}|}} \times \exp -\frac{2|\hat{F}_H\hat{F}_K\hat{F}_{K-H}|}{\sigma^2}.$$

Here $\sigma^2 = \Sigma(Z_j^2/Z^2)$, where Z is the number of electrons in the cell and Z_j is the number of electrons in the atom. If all the atoms are identical, $\sigma = 1/\sqrt{N}$, where N is the number of atoms in the cell. It is convenient to call $1/\sigma^2$ the effective number of atoms in the cell.

The figures show curves of W_+ as a function of $|\hat{F}_{K-H}|$. In order to keep the graphs two-dimensional, we had to set $|\hat{F}_H| = |\hat{F}_K|$. It is noteworthy

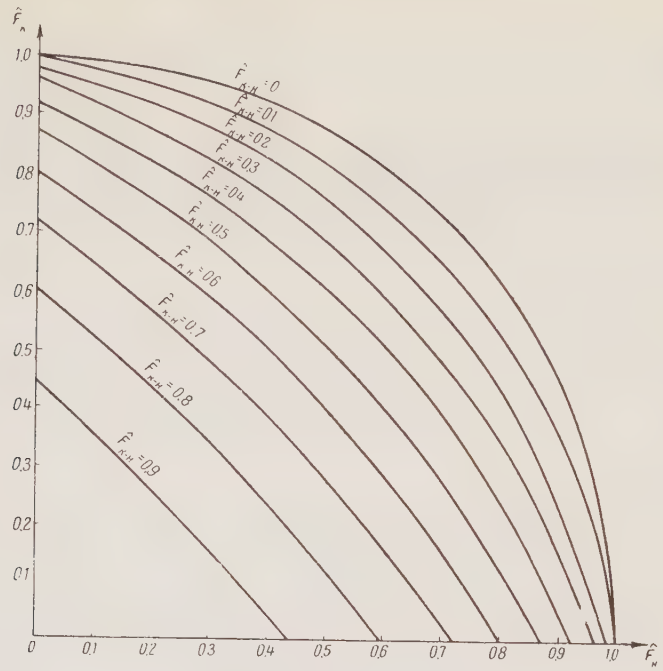

Fig. 1.

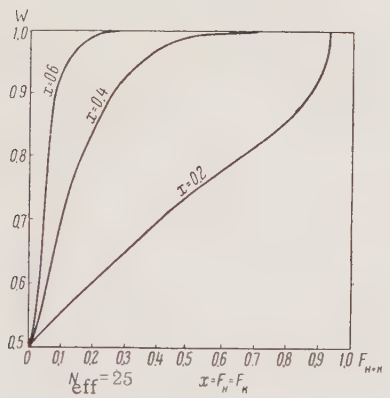

Fig. 2.

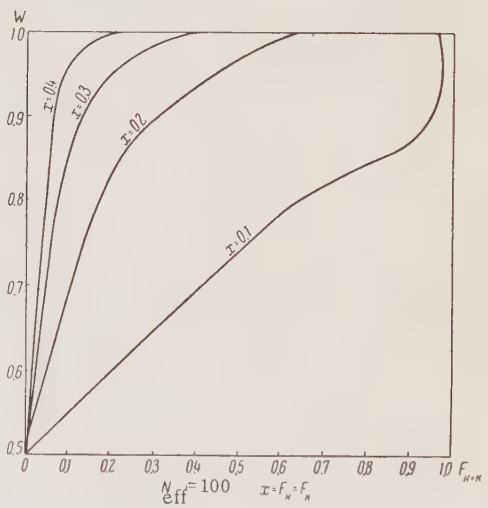

Fig. 3.

that a nearly asymptotic approach to $W_+ = 1$ takes place only for large values of $|\hat{F}|$.

4. The value of σ is a very important constant of the crystal. If it is known, the structure can be solved by direct methods.

Since the distribution of structure amplitudes, as Wilson demonstrated, is Gaussian, 31.74% of the experimentally determined amplitudes are greater than σ, 4.56% are greater than 2σ, 0.27% are greater than 3σ, and 0.01% are greater than 4σ. Analysis has shown that structures with values of σ smaller than 0.1 cannot be solved by direct methods while the solutions of those with $\sigma > 0.17$ are trivial.

5. To calculate $\hat{F}$ from experimental intensity data, we must know the curve of the mean atomic-temperature factor. If the number of reflections with which the investigator is operating is small, the curve of the atomic-temperature factor must be taken from published data. For a number of reflections of the order of several hundred, one should develop the reflection sphere in the region and find the $\overline{F^2}$ curve as a function of $(\sin\theta/\lambda)$. According to theory, this will also be the mean f-curve given on a relative scale.

With the help of this curve, the unitary structure amplitudes may be found apart from a constant factor. The constant factor is chosen in such a way

that the number of amplitudes larger than σ, 2σ, etc., coincides with the theoretical values indicated in paragraph 4.

6. What we have discussed exhausts the methods of determining structures with $\sigma > 0.17$-0.18 (up to 30 identical atoms in the cell). We make just two further comments. First, the direct method is fully applicable to crystals. Its effectiveness is determined by the number of atoms in the cell, and not by the number of crystallographically nonequivalent atoms. Second, for reliable results a three-dimensional experiment is necessary. However, in simple cases ($\sigma > 0.2$), investigations may be successfully carried out on the basis of projections.

THE KINEMATIC THEORY OF REFLECTION INTENSITIES ON ELECTRON-DIFFRACTION PATTERNS

Part 1. Spot Patterns

B. K. Vainshtein

Institute of Crystallography, Academy of Sciences of the USSR

Translated from Kristallografiya, Vol. 1, No. 1,
pp. 17-26, January-February, 1956
Original article submitted October 15, 1955

Kinematic electron scattering is discussed for single crystals, which give spot patterns; the integral intensity for the hk$l$ spot from an ideal crystal is given by formula (8b), which becomes (9a) and (9b) for the angle of regular reflection. Ideal crystals are very seldom encountered; the specimen is usually a mosaic, whose principal characteristic is the angular distribution function over a certain range. Formulas (18a) and (18b) give the integral intensity for the reflections from a mosaic film; the factor arising from the mosaic structure is of the form d_{hkl}/α, in which d_{hkl} is the interplanar distance for that reflection, and α is the effective angular spread of the crystals. The relationship is discussed between the kinematic-scattering formulas (which apply for thin blocks) and the dynamic-scattering ones (which lack the proportionality to thickness or volume characteristic of the kinematic ones). The mosaic factor is the same in both cases.

Introduction

A necessary step in a diffraction study of a crystal structure is conversion from the observed intensities to the structure amplitudes. The kinematic scattering theory is entirely satisfactory for x-ray work, but dynamic effects are very much more common in electron diffraction; nevertheless, the kinematic theory is very important in the latter area, because, very often, the specimen is such as to show that scattering.

Here we examine kinematic electron scattering by various types of specimen and deduce the intensity formulas for the various types of pattern.

The principal condition for kinematic scattering is that the scattered beams should be weak relative to the incident beam; secondary scattering can then be neglected, as can energy loss in the incident beam.

The solution to Schrödinger's equation in the kinematic approximation [1,2] gives the intensity scattered in a direction $\mathbf{s}$, relative to the incident intensity, as

$$J(\mathrm{s}) = J_0 |\Phi(\mathrm{s})|^2/r^2, \tag{1}$$

in which $\Phi(\mathbf{s})$ is the scattering amplitude, which is defined by the Fourier integral of the potential $\varphi(\mathbf{r})$ of the object [3]:

$$\Phi(\mathrm{s}) = K \int \varphi(\mathbf{r})\, e^{i(\mathbf{sr})}\, dv_{\mathrm{r}}, \quad K = \frac{2\pi me}{h^2}. \tag{2}$$

As applied to a single atom, the above condition, which gives rise to (2), is simply the Born approximation; the amplitude of (2) for a crystal is determined by that of a single elementary cell, Φ_{hkl} (the structure factor), and by the Laue interference function $|D|^2$:

$$J(\mathbf{h}) = J_0 |\Phi_{hkl}|^2 |D(\mathbf{h})|^2/r^2, \tag{3}$$

in which $\mathbf{h} = \mathbf{s}/2\pi$, and

$$\Phi_{hkl} = \sum_i f_{\mathrm{e}T_i} e^{2\pi i(\mathbf{rH})}. \tag{4}$$

Here the atomic temperature factor is $f_{\mathrm{e}T} = f_{\mathrm{e}} \exp\{-B(\sin\theta/\lambda)^2\}$, f_{e} being the atomic factor in absolute units [4]. The interference function is

$$|D(h_1h_2h_3)|^2 = \prod_{i=1,2,3} \frac{\sin^2 \pi A_i h_i}{\sin^2 \pi a_i h_i}, \quad (5)$$

in which h_i are the coordinates of reciprocal space, A_i are the linear dimensions of the crystal, and a_i are the cell repeat distances. The sine in the denominator may be replaced by its argument if we consider $|D|^2$ near a given node hk$l$ and reckon the h_i from its center; then each of the factors in (5) at the peak ($h_i = 0$) takes the value

$$\left[\frac{\sin^2 \pi A_i h_i}{(\pi a_i h_i)^2}\right]_{h_i \to 0} = \left(\frac{A_i}{a_i}\right)^2, \quad (6)$$

and the integral is

$$\int_{-\infty}^{+\infty} \frac{\sin^2 \pi A_i h_i}{(\pi a_i h_i)^2} dh_i = \frac{A_i}{a_i^2}. \quad (7)$$

Intensity Scattered by an Ideal Crystal [5]

Consider the integral intensity I_{hkl} of spot hk$l$; we have to integrate (3) over two directions in the plane of a screen on which reciprocal space is represented in a scale $L\lambda$, λ being wavelength and L(=r) being the specimen–screen distance. From (7),

$$I_{hkl} = \int J(h_1h_2h_3)\, L\lambda dh_1 L\lambda dh_2$$

$$= J_0\lambda^2 |\Phi_{hkl}|^2 \frac{A_1A_2}{a_1^2a_2^2} \frac{\sin^2 \pi A_3h_3}{(\pi a_3h_3)^2}. \quad (8a)$$

Let $S = A_1A_2$ be the area of the crystal (volume $V = SA_3$) and $\Omega = a_1a_2a_3$ be the volume of the cell. Then

$$\frac{I_{hkl}}{J_0S} = \lambda^2 \left|\frac{\Phi_{hkl}}{\Omega}\right|^2 \frac{\sin^2 \pi A_3h_3}{\pi^2 h_3^2}. \quad (8b)$$

Taking the I_{hkl} corresponding to the angle of true reflection, i.e., to intersection of the reflection sphere for node hk$l$ at the maximum ($h_3 = 0$), we have from (6) that (8a) and (8b) may be replaced by

$$I_{hkl} = J_0\lambda^2 \left|\frac{\Phi_{hkl}}{\Omega}\right|^2 VA_3, \quad (9a)$$

or

$$\frac{I_{hkl}}{J_0S} = \lambda^2 \left|\frac{\Phi_{hkl}}{\Omega}\right|^2 A_3^2. \quad (9b)$$

J_0S is the incident intensity received by area S, so the ratio of I_{hkl} to J_0S is proportional to the square of the structure amplitude, to the crystal thickness, and to the wavelength. Formula (9a) illustrates the proportionality between I_{hkl} and scattering volume characteristic of kinematic scattering.

The curvature of the reflection sphere generally allows not more than three reflections to appear in the scattering by an ideal single crystal. Real specimens give spot patterns containing all the reflections in a given zone, which can be explained only in terms of a mosaic of single crystals if the scattering is of three-dimensional type [6]. Therefore, (9a) and (9b) hardly ever correspond to actual experimental conditions, but they reflect the essential processes in an individual ideal block of the mosaic. The condition that (9b) equals one gives us [5] the critical thicknesses for ideal crystals as $A_3^* \approx (\lambda |\Phi_{hkl}/\Omega|)^{-1}$, which correspond to transition from kinematic scattering to dynamic. These thicknesses fall as the atomic number of the material increases, because f_e increases and hence, also, the Φ_{hkl} of (4); but they increase as the structure becomes more complex (with the number n of the atoms in the cell) because this reduces the mean value of the unit amplitudes $\hat{\Phi}_{hkl}$, and hence of Φ_{hkl} (see [5]). Simple structures (e.g., of cubic metals) give low critical thicknesses, e.g., about 50 Å for Au, and about 200 Å for Al. Moderately complex structures (n of 20-25) consisting of light atoms give $A_3^* \approx 1200$ Å, while for the same structures with medium-weight atoms A_3^* is 500-600 Å, and for heavy ones, 250-400 Å.

We assume that the beam is ideally monoenergetic and collimated in deriving (9a) and (9b); a real beam has an energy spread of about 0.1%, while the divergence at a single crystal does not exceed 0.0001 radian, so these have entirely negligible effects on (9a) and (9b).

Intensities of Reflections from a Mosaic Single-Crystal Film

A real specimen giving a spot pattern is a mosaic single crystal. The part of the crystal exposed to the beam contains many[1] ideal crystallites that are not strictly parallel (have a certain angular spread).

Oscillation or rotation at a certain angular velocity are used in x-ray work with microcrystals; the conception (which does not always correspond to the actual working conditions) is meaningless in electron diffraction, for the crystallites are at rest, but the assembly of them has a set of orientations in space, which replaces oscillations (i.e., a set of orientations in time).

[1] For instance, the beam might have an area of 1 mm^2 = 10^{14} A^2, the film being 500 A thick and the mean volume of a crystallite 200 × 200 × 200 A^3 ≈ 10^7 A^3; then there are about $5 \cdot 10^9$ crystallites.

This set of spatial orientations has the following consequences. First, not all the crystals are in the position corresponding to passage of the reflection sphere through the maximum of the interference function in the third direction, so it is necessary to integrate over that direction. Second, not all of the crystallites are in reflecting positions; some of them do not reflect at all, and the proportion participating may vary from one reflection to another.

Distribution Function. Let M (Fig. 1) be a reflecting plane; all of its orientations (and hence those of the crystallites in the mosaic) may be described in terms of the function for the distribution of the normal N to this plane over the angles α_2 and α_3. There is also a distribution in α_1 (Fig. 1), but this is of no significance in relation to the intensity, because these rotations leave the plane in the same position relative to the beam. Also, α_2 does not alter the angle ϑ between the plane and the incident beam, though the spot is thereby displaced through an angle α_2 on the screen. Only α_3 determines whether the given plane M lies in the reflecting position, so only the component distribution function $f(\alpha)$ (discarding the subscript in α_3) is significant in the intensity calculation. The film contains n identical crystallites, so the normalization condition for $f(\alpha)$ is

$$\int f(\alpha)\, d\alpha = n = V'/V, \tag{10}$$

in which V is the volume of a crystallite and V' is the volume of the film. There are $f(\alpha)$d crystallites in the range α to $\alpha + d\alpha$. We can usually assume that $f(\alpha)$ is the same for all reflecting planes, especially if the crystal is of isometric habit; in general, $f(\alpha)$ should be taken to be dependent on hkl, but it would be very difficult to consider this. A particular and rather different case of nonuniform distribution is a texture, when any orientation is possible around one of the crystallographic axes. This case is considered separately in the second part of this paper.

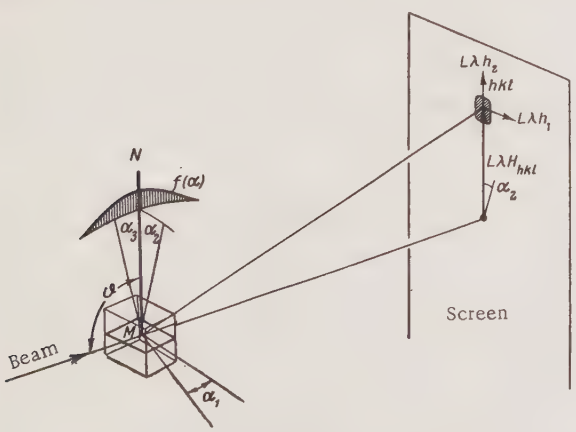

Fig. 1. Scheme for the angular distribution of the crystallites in a mosaic film.

General Formula. The mosaic film has $f(\alpha)$ as its distribution function; importance attaches only to the part of $f(\alpha)$ corresponding to displacement of the reciprocal-lattice nodes perpendicular to the reflection sphere (plane of the screen), so integration in the plane of the screen gives for the integral intensity, by analogy with (8a),

$$I_{hkl} = J_0 \lambda^2 |\Phi_{hkl}|^2 \frac{A_1 A_2}{a_1^2 a_2^2} G. \tag{11}$$

But here G is not $|D(h_3)|^2$, as it was in (8a), for it is also governed by $f(\alpha)$. We must find G by taking the integral of the interference function in the third direction over all possible positions given by $f(\alpha)$. Figure 2a indicates the mutual disposition of $f(\alpha)$, the reflection sphere in a position β, and the interference function $|D_3(\alpha - \beta)|^2$ for crystallites in position α, the last (as also f) being a function of angle. The intensity given by the crystallites in the range α to $\alpha + d\alpha$ is proportional to $f(\alpha)d\alpha$ (namely to the number in that position) and to the value for the interference function at its intersection with the reflection sphere at point $\alpha - \beta$. The integral over all positions of the crystallites gives G:

$$G(\beta) = \int |D(\alpha - \beta)|^2 f(\alpha)\, d\alpha. \tag{12}$$

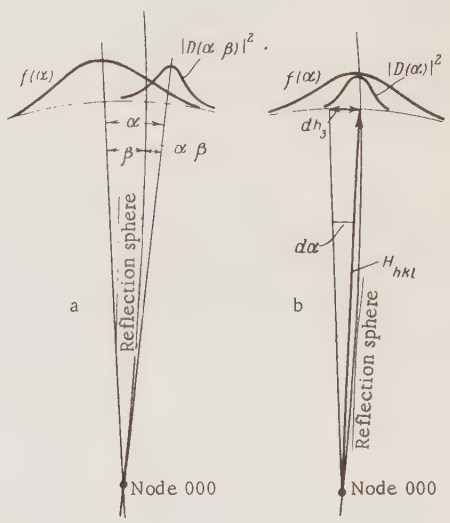

Fig. 2. (a) Mutual disposition of $f(\alpha)$, $|D_3|^2$, and reflection sphere; (b) the particular case when the origin is at the center of the reflection sphere.

The dependence on β shows that $G(\beta)$, and hence the intensity of (11), is dependent on the position of the mosaic crystal relative to the reflection sphere, i.e., on the angle of rotation of the specimen. It is convenient to take the origin at the center of the reflection sphere (i.e., to put $\beta = 0$; Fig. 2b) in order to evaluate G; then (12) becomes

$$G = \int |D(\alpha)|^2 f(\alpha)\, d\alpha. \qquad (13)$$

But here we should bear in mind that this fixes the reflection sphere at some definite point in the distribution function; the dependence on the angle of rotation is not seen. The element $d\alpha$ in (12) and (13) is related to the linear dimension dh_3 in reciprocal space by

$$d\alpha = \frac{dh_3}{H_{hkl}} = dh_3 \cdot d_{hkl}, \qquad (14)$$

as Fig. 2b shows; H_{hkl} in (14) is the distance to the given reciprocal-lattice node and d_{hkl} is the interplanar distance.

Uniform Distribution. Here we calculate G for the very simple case of a uniform distribution in angle (Fig. 3). The angular range is 3-4° ($\approx 1/15$ radian) for real mosaic films that give spot patterns. A uniform distribution makes $f(\alpha)$ constant within this range and equal to $n/(\alpha_1 - \alpha_2) = n/\alpha$, in which $\alpha = \alpha_1 - \alpha_2$ is the angular width of the range. Then the G of (13) becomes constant for all positions of the reflection sphere far from the edges of the region (α_1, α_2):

$$G = \frac{n}{\alpha} \int \frac{\sin^2 \pi A_3 h_3}{(\pi a_3 h_3)^2}\, d\alpha. \qquad (15)$$

Then (7) and (14) give

$$G = \frac{n \cdot A_3}{a_3^2} \cdot \frac{d_{hkl}}{\alpha}. \qquad (16)$$

This (reduced to one crystallite, $n = 1$) is less than the A_3^2/a_3^2 of (6), because d_{hkl}/α is less than A_3. The intensity of a reflection from a mosaic film is therefore less than that from an ideal single crystal of the same size. Then from (11) and (16)

$$I_{hkl} = J_0 \lambda^2 |\Phi_{hkl}|^2 \frac{A_1 \cdot A_2 A_3}{a_1^2 a_2^2 a_3^2} \cdot \frac{n \cdot d_{hkl}}{\alpha}. \qquad (17)$$

But $A_1 A_2 A_3 = V$ and $nV = V'$ from (10), in which V' is the volume of the film, so finally,

$$I_{hkl} = J_0 \lambda^2 \left| \frac{\Phi_{hkl}}{\Omega} \right|^2 V' \frac{d_{hkl}}{\alpha}, \qquad (18a)$$

or

$$\frac{I_{hkl}}{J_0 S} = \lambda^2 \left| \frac{\Phi_{hkl}}{\Omega} \right|^2 \frac{t \cdot d_{hkl}}{\alpha}, \qquad (18b)$$

which resemble (9a) and (9b); here, t is the mean thickness of the mosaic film,[2] which is not necessarily the thickness A_3 of the blocks (it can be greater or less), and S is the area of the film.

The d_{hkl} of (18a) and (18b) may be elucidated by estimating the fraction q of crystallites participating in reflection. The interference region has a half-width of $1/A_3$ (width $2/A_3$); the angular width for the hkl reflection is then $(2/A_3) q H_{hkl} = 2 d_{hkl}/A_3$, so,

$$q = \frac{2 d_{hkl}/A_3}{\alpha}. \qquad (19)$$

For instance, $A_3 = 200$ Å and $\alpha = 1/15$ give q close to 1 for $d \approx 5$ Å (near reflections) and $q \approx 0.1$ for $d \approx 0.7$ Å (far reflections). The proportional relation of q and of the I_{hkl} of (18) to d_{hkl} is explained by the fact that constant $1/\alpha$ produces a constant linear width in the interference region, not a constant angular width, the latter falling in proportion to d_{hkl} (Fig. 4).

Nonuniform Angular Distribution. A uniform distribution is an ideal case, but it can be extended to a nonuniform distribution of density $f(\alpha)$ subject to certain assumptions.

It is usual for $f(\alpha)$ to have a much greater angular width than $|D_3|^2$, so the G of (12) (for the real shape of the reciprocal-lattice nodes) has almost the form of $f(\alpha)$; hence the $f(\alpha)$ for a real mosaic film may be derived from the observed intensity variation at the screen of the diffraction apparatus as the specimen is rotated very slowly (the same result is attained from a series of photographs at small angular intervals, e.g., 1/4°). The most characteristic case is the following: the spot gradually appears, the intensity rises to a maximum, and then there is a fall to zero. The distribution function has the bell-shaped form shown in Figs. 1, 2, and 5.

We consider two extreme cases of this type of $f(\alpha)$; the first (Fig. 5a) is that where the range between α_1 and α_2 [limits of range where $f(\alpha) > 0$] is much greater than the width of the interference region for all reflections. The region where the interference function is finite is much narrower than the angular range of finite $f(\alpha)$, so we can take

[2] By S in (18b) we should understand the area of the beam, if this is less than that of the film; the V of (18a) is then the volume of the film exposed to the beam, not the total volume.

$f(\alpha)$ as constant within that region and extract it from the integral in (13):

$$G \approx f(\alpha) \int \frac{\sin^2 \pi A_3 h_3}{(\pi a_3 h_3)^2}\, d\alpha. \qquad (20)$$

Strictly speaking, the $f(\alpha)$ extracted in this way will vary from one order of reflection to another (Fig. 6), because the reflection sphere has a certain curvature and the α_{hkl} are different. This can be neglected if $f(\alpha)$ varies sufficiently slowly.

The natural approach is to operate at maximum intensity. The bell-shaped function of Fig. 5a may be taken as having a peak height equal to twice the mean; then, from (10),

$$f(\alpha)_{max} \approx 2\,\frac{1}{\alpha'} \int f(\alpha)\, d\alpha = \frac{2n}{\alpha'}, \qquad (21)$$

where $\alpha' = \alpha_1 - \alpha_2$ is the region in which $f(\alpha)$ is defined, i.e., the angular range between emergence and extinction of the interference spot for the rotating sample. From (20), (21), and (16) it follows that, in this case,

$$G \approx \frac{2A_3 n}{a_3^2}\,\frac{d_{hkl}}{\alpha'}, \qquad (22)$$

and the effective α in (18a) and (18b) is $\alpha'/2$.

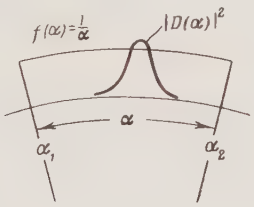

Fig. 3. Uniform angular distribution of crystallites.

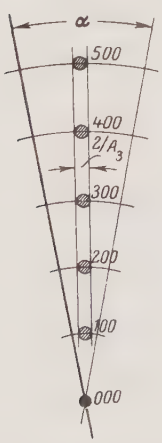

Fig. 4. Reduction in proportion of crystals participating in reflection with increase in order of reflection.

More rapid variation in $f(\alpha)$ (narrower angular range) may cause (Fig. 6) the $f(\alpha_{hkl})$ to differ substantially. Samples of this type do occur, and then it is found that the near and far reflections attain their maximum intensities at slightly different angles of rotation. The best approach then is to take several photographs at similar angles and take the maximum intensity for each reflection; this corresponds to the maximum (constant) value $f(\alpha)_{max}$, so the G of (11) will also be constant and may be evaluated from (22).

The other limiting case is that where the limits of finite $f(\alpha)$ are much narrower than the interference region for all reflections (Fig. 5b), i.e., there is very little angular spread in the crystallites. Then (6) shows that the interference function is close to A_3^2/a_3^2 throughout the range (α_1, α_2), so we extract it from the integral and get from (10) that

$$G = \frac{A_3^2}{a_3^2} \int_{\alpha_1}^{\alpha_2} f(\alpha)\, d\alpha = nA_3^2/a_3^2. \qquad (23)$$

Substituting (23) into (11), we get

$$\frac{I_{hkl}}{J_0 S} = \lambda^2 \left| \frac{\Phi_{hkl}}{\Omega} \right|^2 tA_3, \qquad (24)$$

in which t is the thickness of the film. The blocks may form a single layer ($t = A_3$), in which case we return to the ideal crystal of (9a) and (9b). This is entirely to be expected, because the mosaic approximates to an ideal crystal as α decreases.

The intermediate case (interference region of about the same width as the distribution function) is the most complicated; the intensities are then very inconvenient to use. It is clear that here G will approximate to (23) when d is large, and to (22) when d is small.

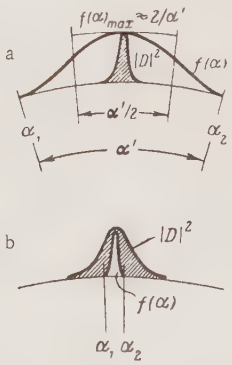

Fig. 5. Nonuniform angular distribution: (a) $f(\alpha)$ much larger than $|D_3|^2$; (b) the converse case.

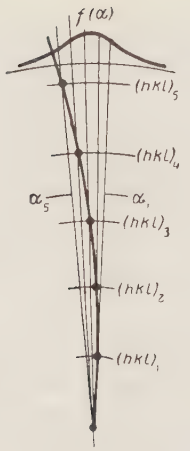

Fig. 6. Effects of curvature of reflection sphere.

Change in Type of Scattering with Specimen Thickness

The kinematic formulas are applicable only when the blocks are thin; the dynamic ones apply to thick blocks. Here, we consider the relation between the two sets of formulas as the thickness increases.

Ideal Single Crystal. The dynamic theory [7, 8] (see also [2, 6, 9]) gives the integrated intensity at the reflection angle as

$$I_{hkl} = I_0 \sin^2 \frac{v_{hkl} \cdot H}{2k}. \qquad (25)$$

Here, I_0 denotes the incident intensity, namely J_0S, where S is the area of the crystal. The v_{hkl}, H, and k of [2,6-8] correspond to our $v_{hkl} = 4\pi|\Phi_{hkl}/\Omega|$, $H = A_3$ (thickness of crystal), and $k = 2\pi/\lambda$. Then (25) becomes

$$I_{hkl} = J_0 S \sin^2 \left\{ \lambda \left| \frac{\Phi_{hkl}}{\Omega} \right| A_3 \right\}. \qquad (26)$$

The argument of the sine is simply the quantity whose square determines the reflection intensity in the kinematic theory. Blackman [8] has shown that we may replace the square of the sine in (26) by the square of the argument for A_3 small, which gives (9b), which is a particular case of the general expression (8b) for the kinematic scattering for $h_3 = 0$.

Formulas (8a), (8b), (9a), and (9b) are applicable if A_3 is less than the critical thickness A_3^* (see above).

Mosaic of Large Blocks. This case has not been considered in the dynamic theory, but the integral intensity has been calculated for a crystal rotating with an angular velocity ω [6, 7]. Then (after averaging with respect to thickness),

$$I_{hkl} = I_0 \frac{\pi v_{hkl}}{2k^2 \vartheta_0 \omega}. \qquad (27)$$

Rotation is not used in electron diffraction, but the mosaic structure produces an angular distribution, so ω may be replaced by the effective angular range α (see above). Now, $\vartheta_0 \approx \lambda/2d_{hkl}$ [note also the change in notation from (25) to (26)], so (27) becomes

$$\frac{I_{hkl}}{J_0 S} = \lambda \left| \frac{\Phi_{hkl}}{\Omega} \right| \frac{d_{hkl}}{\alpha}. \qquad (28)$$

The linear relation to volume (thickness) characteristic of the kinematic theory does not appear in (26) and (28). The mosaic structure (which is independent of the type of scattering in each block) in both cases gives the same factor d_{hkl}/α [cf. (18a) and (18b)], so the other factor dependent on the structure of the specimen (the analog of the Lorentz factor for x rays) remains unchanged when we pass from the kinematic theory to the dynamic one; the square of $\lambda|\Phi/\Omega|$ is merely replaced by the first power together with loss of the volume (thickness) dependence. The general formula will be intermediate between (18b) and (28) if the film consists of blocks of various sizes, some of which scatter kinematically and others dynamically. The spot reflections are replaced by Kikuchi lines if the blocks are very large.

Thick Films of Small Blocks. Let the size of the blocks be subcritical; the scattering in each is then kinematic, so (18a) and (18b) imply that I_{hkl} is proportional to t. The analogous formula for an isolated block is the rise in I_{hkl} with A_3 given by (9) up to $I_{hkl} \approx J_0S$, which means that we have the transition to dynamic scattering; (9a) and (9b) are inapplicable for $A_3 \geq A_3^*$. Also, (18a) and (18b) involve the assumption that $A_3 < A_3^*$, but here sufficiently large t can give the physically meaningless result $I_{hkl} > J_0S$. The point here is that (18a) and (18b) require correction for secondary extinction for t large, i.e., for screening by the layers of blocks preceding the one in question. At this point the treatment is no longer purely kinematic, because allowance must be made for the loss in intensity in the primary beam as it penetrates into the material; but no account is taken of the phase relations considered in the dynamic theory (primary extinction). In addition, absorption cannot be neglected for thick layers.

Secondary scattering can also occur [9-11] at the high scattered intensities encountered for thick films, no matter what the type of scattering within the blocks.

Conclusions

Kinematic scattering has the scattered intensity proportional to the volume (thickness) of the specimen and to the squares of the wavelength and the structure amplitude. A major characteristic of the specimen is the angular distribution of the crystallites (mosaic structure).

An ideal single crystal and a mosaic film with only small angular spread will have scattering described as appropriate by (8a), (8b), (9a), (9b), and (24); here the relative moduli of the structure amplitudes are related to the relative integral intensity by $|\Phi_{hkl}^{rel}| = \sqrt{I_{hkl}^{rel}}$ But these cases (which correspond to occurrence of only a few reflections from a zone) are hardly ever encountered in practice. It is most usual to find all the reflections in a given zone appearing simultaneously, on account of a range in α commonly about 3-4° (mosaic). The factor for the mosaic structure is d_{hkl}/α, so from (18a),

$$|\Phi_{hkl}^{rel}| = \sqrt{I_{hkl}^{rel}/d_{hkl}}. \qquad (29)$$

A film of large blocks each having dynamic scattering will have a factor for the structure of the same form as for a film of small blocks that scatter kinematically; in particular, for a mosaic film of large blocks,

$$|\Phi_{hkl}^{rel}| = I_{hkl}^{rel}/d_{hkl}. \qquad (30)$$

It is very desirable to employ the intensities of spot patterns in structure studies, but these are sensitive to the distribution function and to the thickness, and there is always the possibility of secondary scattering, so it is always necessary to make a careful study of the type of scattering to establish whether a given formula is applicable, the most common case being that described by (18a) and (18b), i.e., (29).

LITERATURE CITED

1. M. Born, Quantenmechanik der Stossvorgänge, Z. Phys. 38, 803-827 (1926).
2. M. von Laue, Materiewellen und ihre Interferenzen (Leipzig, 1948).
3. B. K. Vainshtein, Structural Electron Diffraction [in Russian] (Author's abstract, 1955).
4. B. K. Vainshtein, "Atomic scattering factors for electrons," ZhÉTF, 25, 157-168 (1953).
5. B. K. Vainshtein, "Kinematic scattering of electrons by an ideal crystal," DAN SSSR, 104, 537-539 (1955).
6. Z. G. Pinsker, Electron Diffraction [in Russian] (Izd. AN SSSR, 1949).
7. H. Bethe, Theorie der Beugung von Elektronen an Kristallen. Ann. Physik, 87, 55-129 (1928).
8. M. Blackman, "On the intensities of electron-diffraction rings," Proc. Roy. Soc., A173, 68-82 (1939).
9. Z. G. Pinsker and B. K. Vainshtein, "Dynamic scattering of electrons," Izv. AN SSSR, ser. fiz., 14, 212-222 (1950).
10. J. M. Cowley, A. L. G. Rees, and J. A. Spink, "Secondary elastic scattering in electron diffraction," Proc. Phys. Soc., A64, 609-619 (1951).
11. B. K. Vainshtein, "Some features of spot electron-diffraction patterns associated with secondary scattering," Trudy Inst. Kristallografii, 12 (1956).

DERIVATION OF WORKING FORMULAS FOR THE ELECTRON DENSITY AND STRUCTURE AMPLITUDES FROM THE SYMMETRY AND ANTISYMMETRY OF TRIGONOMETRIC FUNCTIONS

M. A. Porai-Koshits

Kurnakov Institute of General and Inorganic Chemistry
Translated from Kristallografiya, Vol. 1, No. 1,
pp. 27-48, January-February, 1956
Original article submitted October 1, 1955

The derivations are considered for the various space groups in all settings on the basis of the symmetry and antisymmetry of trigonometric functions. Combinations of these functions are derived having even and odd h, k, and *l*; these correspond to particular symmetry elements. The formulas for a set of symmetry elements are derived from the general formula simply by eliminating terms contrary to the required symmetry. The relations between the Fourier coefficients are used only in the final stage [conversion of the limits of summation from $(-\infty, +\infty)$ to $0 \rightarrow \infty$]. Of the 230 space groups, only C_{2v}^{19}, D_{2h}^{24}, T_h^4, O_h^7, and O_h^8 are excluded in this method of finding the formulas. The method can also be applied to the formulas for the structure amplitude for crystals in the lower systems.

Introduction

The International Tables [1] give formulas for the structure amplitudes of all 230 space groups, but these are not the working formulas, for they require rather laborious manipulation to give the practical forms. Lonsdale's [2] simplified formulas are much more convenient, for these take account of the changes and simplifications arising from multiple values and combinations of the hk*l*. Lonsdale's book also gives formulas for the electron density, but these are only in a general form not convenient for practical use.

Lonsdale's formulas are reproduced in the new English edition of the International Tables [3]; two settings of the unit cell differing in choice of origin are given for 23 of the 230 space groups, whereas it is very common to encounter different choices of coordinate system in practical analysis, not merely for these groups, either. The most pronounced changes in the formulas occur when the origin is transferred to a point characterized by another set of symmetry elements. Belov [4] has shown (for groups D_{4h}^4, D_{4h}^{15}, D_{2h}^2, D_{2h}^4, etc.), that transfer of the origin from an inversion center to certain other positions leads to a marked simplification in the formulas.

There are very few copies of Lonsdale's tables and of the new edition of the International Tables in the USSR, and there is no corresponding work in Russian, if we ignore the obviously out-of-date Handbook on X-Ray Analysis [5], which was published in 1940.

The formulas are also much altered if the directions of the coordinate axes are changed. The choice of coordinate system is often related to aspects of the habit for various reasons of chemical crystallography, etc., so the setting of the crystal very often differs from the generally accepted one. This is especially so for monoclinic crystals; the space groups have at times to be considered in their body-centered, face-centered, and even stranger aspects.

This means that the practical worker has usually to deduce the electron-density formulas separately for each particular case on the basis of the particular setting of the crystal.

The strips method is presently the most common in the summation of Fourier series; most of the mechanized techniques of electron-density computation employ this method, as does one of the techniques for the structure amplitude [6,7]. However, it implies that the two- or three-dimensional distribution is considered as a set of parallel one-dimensional ones, so it is inevitable that the computation takes account only of those symmetry elements that correspond to such a distribution, namely symmetry planes perpendicular to the coordinate axes, diad symmetry axes parallel to the coordinate axes, and inversion centers.

The working formulas for the electron density thus involve referring the actual space group of the crystal to a subgroup belonging to one of the lower systems; only the latter require detailed consideration.

The usual derivation of the electron-density formulas is based on the relations between the F_{hkl} (Fourier coefficients) for the various signs of the indices with subsequent transformation of the trigonometric functions of the formula. A much shorter derivation may be based on the symmetry and antisymmetry of the trigonometric functions; this readily gives the formulas corresponding to particular symmetry elements in different combinations simply by elimination of trigonometric terms contrary to the required symmetry. The relations between the Fourier coefficients are used in explicit form only in the final stage, during conversion from summation between limits $-\infty \rightarrow +\infty$ to the same between limits $0 \rightarrow \infty$.

The same method can be used to derive formulas for the structure amplitude for all space groups in the lower systems, on account of the analogy between the electron density and the structure amplitude.

Symmetry and Antisymmetry of Trigonometric Functions

We may consider the terms in the Fourier expansion for the electron density as density waves in three-dimensional space, so we may consider the symmetry of the terms separately. The density wave represented by $\cos 2\pi hx$ has m symmetry planes perpendicular to the X axis and passing through the origin and the middle of the cell edge *a* (Fig. 1a, b). Conversely, $\sin 2\pi hx$ has a plane of antisymmetry ш, i.e., it transforms the density at point xyz into one equal in magnitude but opposite in sign at point xyz (Fig. 1c, d). Further, $\cos 2\pi hx$ has an m plane at $x = 1/4$ when h is even and an ш plane when h is odd. Conversely, $\sin 2\pi hx$ has an ш plane at $x = 1/4$ when h is even and an m plane when h is odd. These properties have been used [8, 9] to shorten the strips.

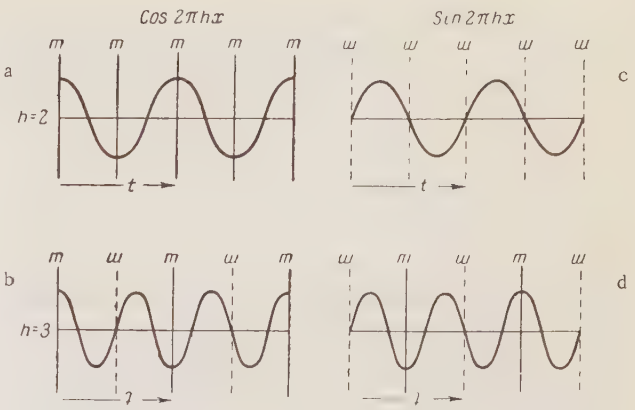

Fig. 1. Symmetry and antisymmetry elements of $\cos 2\pi hx$ and $\sin 2\pi hx$ for $h = 2n$ and $h = 2n - 1$.

A further aspect of the symmetry is that the second half of the cycle repeats the first when h is even; the repeat distance is half the cell period. We denote a translation of this magnitude by t and call it a half translation. The second half of the cell reproduces the first with the sign changed if h is odd for $\cos 2\pi hx$ as well as $\sin 2\pi hx$; this may be called an anti-half translation and be denoted by $\frac{1}{2}$. Table 1 summarizes these features of $\cos 2\pi hx$ and $\sin 2\pi hx$.

These properties are sufficient for the discussion of all space groups in the triclinic, monoclinic, and orthorhombic systems apart from C_{2v}^{19} = Fdd and D_{2h}^{24} = Fddd, which contain d glide planes; in addition, the setting of the coordinate system causes various symmetry elements to pass through points displaced from the origin by $1/8$ of a period. These two features force us to take account of additional symmetry features of the trigonometric functions when h is even; but it is then laborious to derive the formulas via the properties of the functions, and the device appears extremely artificial. These space groups are therefore excluded from the general discussion.

Other excluded space groups are T_h^4 = Fd3, O_h^7 = Fd3m, and O_h^8 = Fd3c, which reduce to Fddd' after removal of the higher-order symmetry elements and their equivalents. The other space groups of the tetragonal and cubic systems have d glide planes, as orthorhombic subgroups contain combinations of symmetry elements that do not include such planes. For instance, groups D_{2d}^{12} = $I\bar{4}2d$, T_d^6 = $I\bar{4}3d$, and O_h^{10} = Ia3d reduce to $I2_12_12_1$; group C_{4v}^{11} = I4md reduces to Imm; group D_{4h}^{19}

TABLE 1. Symmetry Properties of $\cos 2\pi hx$ and $\sin 2\pi hx$

Function	h even			h odd		
	$x=0$	$x=1/4$	$\Delta x=1/2$	$x=0$	$x=1/4$	$\Delta x=1/2$
$\cos 2\pi hx$	$m_0(x)$	$m_{1/4}(x)$	$t(x)$	$m_0(x)$	$u_{1/4}(x)$	$\tau(x)$
$\sin 2\pi hx$	$u_0(x)$	$u_{1/4}(x)$	$t(x)$	$u_0(x)$	$m_{1/4}(x)$	$\tau(x)$

= I4/amd reduces to Imma; group C_{4v}^{12} = I4cd reduces to Iba, and group D_{4h}^{20} = I4/acd reduces to Ibca. These groups, and all the others, may thus be discussed solely on the basis of the symmetry and antisymmetry features dealt with above.

However, it may be that for those of these groups that have inversion centers it will prove convenient or necessary to preserve the inversion center at any point having one or more components equal to $1/8$ (or $3/8$, $5/8$, or $7/8$). The corresponding formulas then clearly cannot be deduced on the basis of the above properties; this applies to groups D_{2d}^{12}, D_{4h}^{19}, D_{4h}^{20}, T_d^6, and O_h^{10}. The present method of deriving the electron-density formulas thus applies fully to 220 of the 230 groups and, with certain restrictions, to 5 more groups. Only five groups are ruled out altogether: C_{2v}^{19}, D_{2h}^{24}, T_h^4, O_h^7, and O_h^8.

Superposition of the Operations m, u, t, and τ

These elements of generalized symmetry are sufficient to represent all the other symmetry operations encountered in the space groups of the lower systems. We may combine the functions $\begin{matrix}\cos\\ \sin\end{matrix} 2\pi hx$, $\begin{matrix}\cos\\ \sin\end{matrix} 2\pi ky$, $\begin{matrix}\cos\\ \sin\end{matrix} 2\pi lz$, (and hence these elements) to obtain a function having any of the possible sets of symmetry elements.

It is obviously simplest to construct a function having two or three mutually perpendicular symmetry planes [functions of symmetry m(x)m(y) or m(x)m(y)m(z)]. The other elements (rotation and screw axes, glide-reflection planes, inversion centers) may be formed by superposing these simple combinations. For example, a diad rotation axis parallel to the Z axis may be formed by superposing a function m(x)m(y) (which thus has a symmetry axis along the line of intersection of the two planes) and a function u(x)u(y) (and thus a diad axis along the line of intersection):

$$m(x)\cdot m(y)+u(x)\cdot u(y). \tag{1}$$

This leaves only the common element, namely, the diad axis parallel to Z. An inversion center may be formed similarly by superposing four functions having inversion:

$$m(x)\,m(y)\,m(z)+m(x)\,u(y)\,u(z)+u(x)\,m(y)\,u(z)+u(x)\,u(y)\,m(z). \tag{2}$$

All other symmetry and antisymmetry elements present in each function individually are eliminated by the superposition.

The situation is rather more complicated with glide-reflection planes and screw axes.

We assume that the glide-reflection plane is perpendicular to the X axis and has its glide along the Z axis, which means that the function should not change in sign or magnitude after two successive operations (reflection at a plane perpendicular to the X axis and displacement through half a translation along the Z axis).

This is satisfied by combinations of trigonometric functions of symmetries m(x)t(z) and u(x)τ(z); but each alone has excess symmetry elements: the first has a symmetry plane and a half translation t, while the second has an antisymmetry plane and an anti-half translation τ. Superposition

$$m(x)\,t(z)+u(x)\,\tau(z) \tag{3}$$

removes these unwanted elements and leaves only the glide-reflection. Transfer by half a translation along the YZ diagonal may be considered as the result of two successive operations t(y) and t(z) or τ(y) and τ(z); similarly, an anti-half translation along the YZ diagonal may be considered as the combinations t(y) · τ(z) or τ(y) · t(z), so a diagonal glide-reflection plane with a half glide is represented by

$$m(x)\,[t(y)\,t(z)+\tau(y)\cdot\tau(z)]+u(x)\,[t(y)\,\tau(z)+\tau(y)\,t(z)]. \tag{4}$$

A 2_1 screw axis parallel to the Z axis may be represented as a superposition of a function of symmetry 2(z)t(z) and one of symmetry ζ(z)τ(z), where ζ is a diad antiaxis:

$$[m(x)\cdot m(y)+u(x)\,u(y)]\,t(z)+[m(x)\,u(y)+u(x)\,m(y)]\,\tau(z). \tag{5}$$

All of these relations are used below to derive the working formulas for the electron density in terms of Fourier series.

General Working Formula for the Three-Dimensional Electron-Density Distribution and General Formula for the Structure Amplitude

In the general case,

$$\rho(xyz)=\frac{1}{V}\sum_{\substack{hkl\\-\infty}}^{\infty}F_A(hkl)\cos 2\pi(hx+ky+lz)+$$

$$+\frac{1}{V}\sum_{\substack{hkl\\-\infty}}^{\infty} F_B(hkl)\sin 2\pi(hx+ky+lz), \qquad (6)$$

where $F_A(hkl)$ and $F_B(hkl)$ are, respectively, the real and imaginary parts of the structure amplitude.[1] We transform the cos and sin sums via the usual trigonometric formulas to get:

$$\rho(xyz)=\frac{1}{V}\sum_{\substack{hkl\\-\infty}}^{\infty} F_A(hkl)$$

$$\times[\cos 2\pi hx\cos 2\pi ky\cos 2\pi lz-\cos 2\pi hx\sin 2ky\sin 2\pi lz$$

$$-\sin 2\pi hx\cos 2\pi ky\sin 2\pi lz-\sin 2\pi hx\sin 2\pi ky\cos 2\pi lz]$$

$$+\frac{1}{V}\sum_{\substack{hkl\\-\infty}}^{\infty} F_B(hkl)[-\sin 2\pi hx\sin 2\pi ky\sin 2\pi lz$$

$$+\sin 2\pi hx\cos 2\pi ky\cos 2\pi lz$$

$$+\cos 2\pi hx\sin 2\pi ky\cos 2\pi lz+\cos 2\pi hx\cos 2\pi ky\sin 2\pi lz].$$

For brevity we denote cos by C and sin by S, with the triple products representing in the first position h with x, the second k with y, and the third l with z. Then

$$\rho(xyz)=\frac{1}{V}\sum_{\substack{hkl\\-\infty}}^{\infty} F_A(hkl)[CCC-CSS-SCS-SSC]$$

$$+\frac{1}{V}\sum_{\substack{hkl\\-\infty}}^{\infty} F_B(hkl)[-SSS+SCC+CSC+CCS]. \qquad (6a)$$

It remains to complete the conversion to summation from 0 to ∞ for each of the indices; $F_A(hkl) = F_A(\overline{hkl})$ and $F_B(hkl) = -F_B(\overline{hkl})$, from which we get the relations of Table 2 [formula (6b)]. These relations are basic to the derivation of detailed working formulas for the electron density that apply in the presence of the various symmetry elements.

The structure amplitude in the general case is given by

$$F(hkl)=\sum_{j=1}^{N} f_j\cos 2\pi(hx+ky+lz)$$

$$+i\sum_{j=1}^{N} f_j\sin 2\pi(hx+ky+lz), \qquad (7)$$

and so may be put in a form analogous to (6a):

$$F(hkl)=\sum_{j=1}^{N} f_j[CCC-CSS-SCS-SSC]$$

$$+i\sum_{j=1}^{N} f_j[-SSS+SCC+CSC+CCS]. \qquad (7a)$$

Electron-Density Formulas for Single Symmetry Elements

The presence of a symmetry element gives rise to relations between the structure amplitudes for different reflections, which enables us to simplify and manipulate the Fourier expansions for the electron density. Each of the eight terms in (6b) bears a certain combination of m, ш, t, and ↿; summation is equivalent to superposition of these combinations, so only the symmetry operations that are in common are retained. To each real symmetry element in the structure there corresponds a certain set of terms in the sum of (6b); in deriving the working formulas, it is sufficient to note that of the eight terms listed in Table 2, we must retain only those that are in accordance with the symmetry of the structure.

Consider the effects of single symmetry elements on (6b).

1. Mirror plane perpendicular to the X axis.

a) The m plane passes through the origin; symmetry condition $m_0(x)$. The formula for ρ (xyz) must retain only the terms that contain cos 2πhx as a factor, so

$$\rho(xyz)=\frac{8}{V}\sum_{\substack{hkl\\0}}^{\infty}\{[A_{CCC}CCC-A_{CSS}CSS]$$

$$+[B_{CSC}CSC+B_{CCS}CCS]\}. \qquad (8a)$$

b) The m plane intersects the X axis at x = ¼; symmetry condition $m_{1/4}(x)$. This means that the trigonometric part of the formula must retain only those functions that contain cos 2πhx with h even and sin 2πhx with h odd:

$$\rho(xyz)=\frac{8}{V}\sum_{\substack{hkl\\0}}^{\infty}\{[A_{CCC}CCC-A_{CSS}CSS]$$

for $h=2n$

$$+[B_{CSC}CSC+B_{CCS}CCS]\}+$$

[1] Allowance has been made in (6) for the requirement $F^*(\overline{hkl}) = F(hkl)$, i.e., that a function expanded as a Fourier series must be real.

TABLE 2

$$\rho(xyz) = \frac{8}{V}\sum_{\substack{h,k,l\\0}}^{\infty}[A_{CCC}\,CCC - A_{CSS}\,CSS - A_{SCS}\,SCS - A_{SSC}\,SSC] + \frac{8}{V}\sum_{\substack{h,k,l\\0}}^{\infty}[-B_{SSS}\,SSS + B_{SCC}\,SCC + B_{CSC}\,CSC + B_{CCS}\,CCS]$$

I_A

$$A_{CCC}(hkl) = \frac{1}{4}[F_A(hkl) + F_A(h\bar{k}\bar{l}) + F_A(\bar{h}k\bar{l}) + F_A(\bar{h}\bar{k}l)]$$

$$A_{CCC}(hk0) = \frac{1}{4}[F_A(hk0) - F_A(\bar{h}\bar{k}0)]$$

$$A_{CCC}(h0l) = \frac{1}{4}[F_A(h0l) + F_A(h0\bar{l})]$$

$$A_{CCC}(0kl) = \frac{1}{4}[F_A(0kl) + F_A(0\bar{k}\bar{l})]$$

$$A_{CCC}(h00) = \frac{1}{4}F_A(h00)$$

$$A_{CCC}(0k0) = \frac{1}{4}F_A(0k0)$$

$$A_{CCC}(00l) = \frac{1}{4}F_A(00l)$$

$$A_{CCC}(000) = \frac{1}{8}F_A(000)$$

II_A

$$A_{CSS}(hkl) = \frac{1}{4}[F_A(hkl) + F_A(h\bar{k}\bar{l}) - F_A(\bar{h}k\bar{l}) - F_A(\bar{h}\bar{k}l)]$$

$$A_{CSS}(0kl) = \frac{1}{4}[F_A(0kl) - F_A(0\bar{k}\bar{l})]$$

$$A_{CSS}(hk0) = A_{CSS}(h0l) = 0$$

$$A_{CSS}(h00) = A_{CSS}(0k0) = A_{CSS}(00l) = A_{CSS}(000) = 0$$

III_A

$$A_{SCS}(hkl) = \frac{1}{4}[F_A(hkl) - F_A(h\bar{k}\bar{l}) + F_A(\bar{h}k\bar{l}) - F_A(\bar{h}\bar{k}l)]$$

$$A_{SCS}(h0l) = \frac{1}{4}[F_A(h0l) - F_A(h0\bar{l})]$$

$$A_{SCS}(hk0) = A_{SCS}(0kl) = 0$$

$$A_{SCS}(h00) = A_{SCS}(0k0) = A_{SCS}(00l) = A_{SCS}(000) = 0$$

IV_A

$$A_{SSC}(hkl) = \frac{1}{4}[F_A(hkl) - F_A(h\bar{k}\bar{l}) - F_A(\bar{h}k\bar{l}) + F_A(\bar{h}\bar{k}l)]$$

$$A_{SSC}(hk0) = \frac{1}{4}[F_A(hk0) - F_A(\bar{h}\bar{k}0)]$$

$$A_{SSC}(h0l) = A_{SSC}(0kl) = 0$$

$$A_{SSC}(h00) = A_{SSC}(0k0) = A_{SSC}(00l) = A_{SSC}(000) = 0$$

I_B

$$B_{SSS}(hkl) = \frac{1}{4}[F_B(hkl) + F_B(h\bar{k}\bar{l}) + F_B(\bar{h}k\bar{l}) + F_B(\bar{h}\bar{k}l)]$$

$$B_{SSS}(hk0) = B_{SSS}(h0l) = B_{SSS}(0kl) = 0$$

$$B_{SSS}(h00) = B_{SSS}(0k0) = B_{SSS}(00l) = B_{SSS}(000) = 0$$

II_B

$$B_{SCC}(hkl) = \frac{i}{4}[F_B(hkl) + F_B(h\bar{k}\bar{l}) - F_B(\bar{h}k\bar{l}) - F_B(\bar{h}\bar{k}l)]$$

$$B_{SCC}(hk0) = \frac{i}{4}[F_B(hk0) - F_B(\bar{h}\bar{k}0)]$$

$$B_{SCC}(h0l) = \frac{i}{4}[F_B(h0l) + F_B(h0\bar{l})]$$

$$B_{SCC}(0kl) = 0$$

$$B_{SCC}(h00) = \frac{i}{4}F_B(h00)$$

$$B_{SCC}(0k0) = B_{SCC}(00l) = B_{SCC}(000) = 0$$

III_B

$$B_{CSC}(hkl) = \frac{i}{4}[F_B(hkl) - F_B(h\bar{k}\bar{l}) + F_B(\bar{h}k\bar{l}) - F_B(\bar{h}\bar{k}l)]$$

$$B_{CSC}(hk0) = \frac{i}{4}[F_B(hk0) + F_B(\bar{h}\bar{k}0)]$$

$$B_{CSC}(0kl) = \frac{i}{4}[F_B(0kl) - F_B(0\bar{k}\bar{l})]$$

$$B_{CSC}(h0l) = 0$$

$$B_{CSC}(0k0) = \frac{i}{4}F_B(0k0)$$

$$B_{CSC}(h00) = B_{CSC}(00l) = B_{CSC}(000) = 0$$

IV_B

$$B_{CCS}(hkl) = \frac{1}{4}[F_B(hkl) - F_B(h\bar{k}\bar{l}) - F_B(\bar{h}k\bar{l}) + F_B(\bar{h}\bar{k}l)]$$

$$B_{CCS}(h0l) = \frac{1}{4}[F_B(h0l) - F_B(h0\bar{l})]$$

$$B_{CCS}(0kl) = \frac{1}{4}[F_B(0kl) + F_B(0\bar{k}\bar{l})]$$

$$B_{CCS}(hk0) = 0$$

$$B_{CCS}(00l) = \frac{1}{4}F_B(00l)$$

$$B_{CCS}(h00) = B_{CCS}(0k0) = B_{CCS}(000) = 0$$

$$+\frac{8}{V}\sum_{\substack{hkl\\ \text{for } h=2n-1}}^{\infty}\{[-A_{SCS}SCS-A_{SSC}SSC]$$

$$+[-B_{SSS}SSS+B_{SCC}SCC]\}. \qquad (8b)$$

2. Glide-reflection plane perpendicular to the X axis with the glide along the Z axis.

a) The plane passes through the origin; symmetry condition $m_0(x)t(z)+w_0(x)\eta(z)$. Either of the functions $\cos 2\pi lz$ and $\sin 2\pi lz$ has symmetry t(z) for $l = 2n$ and $\eta(z)$ for $l = 2n-1$, so the formula must contain only terms in $\cos 2\pi hx$ for $l = 2n$ and in $\sin 2\pi hx$ for $l = 2n-1$; for $l = 2n$ we retain terms CCC, CSS, CSC, and CCS, while for $l = 2n-1$ we retain SCS, SSC, SSS, and SCC.

b) The plane intersects the X axis at $x = 1/4$; symmetry condition $m_{1/4}(x)t(z)+w_{1/4}(x)\eta(z)$. For $h+l = 2n$ we retain CCC, CSS, CSC, and CCS, while for $h+l = 2n-1$ we retain SCS, SSC, SSS, and SCC.

3. Glide-reflection plane perpendicular to the X axis with the glide along the YZ diagonal.

a) The n plane passes through the origin; symmetry condition

$$m_0(x)[t(y)t(z)+\eta(y)\eta(z)]+w_0(x)[t(y)\eta(z)+\eta(y)t(z)].$$

The formula must contain $\cos 2\pi hx$ for $k+l = 2n$ and $\sin 2\pi hx$ for $k+l = 2n-1$, so the terms in CCC, CSS, CSC, and CCS are retained only for $k+l = 2n$, and those in SCS, SSC, SSS, and SCC for $k+l = 2n-1$.

b) The plane intersects the X axis at $x = 1/4$; symmetry condition

$$m_{1/4}(x)[t(y)t(z)+\eta(y)\eta(z)]+w_{1/4}(x)[t(y)\eta(z)+\eta(y)t(z)].$$

The formula contains CCC, CSS, CSC, and CCS for $h+k+l = 2n$ and SCS, SSC, SSS, and SCC for $h+k+l = 2n-1$.

The various cases of a symmetry plane of a given orientation show that the electron-density formulas are extremely similar; the only differences lie in the conditions on the indices of the reflections (Table 3).

The trigonometric terms in the formulas split up into two groups. A plane perpendicular to the X axis causes the functions containing $\cos 2\pi hx$ to be active for one combination of the indices and those containing $\sin 2\pi hx$ for another.

4. Diad rotation axis parallel to Z axis.

a) The 2 axis passes through the origin; symmetry condition $m_0(x)m_0(y)+w_0(x)w_0(y)$, which is satisfied by functions containing as factors $\cos 2\pi hx \cdot \cos 2\pi ky$ and $\sin 2\pi hx \cdot \sin 2\pi ky$. Consequently,

$$\rho(xyz)=\frac{8}{V}\sum_{hkl}^{\infty}\{[A_{CCC}CCC-A_{SSC}SSC]$$

$$+[-B_{SSS}SSS+B_{CCS}CCS]\}. \qquad (9a)$$

b) The 2 axis passes through the point $x = 1/4$, $y = 0$; symmetry condition $m_{1/4}(x)m_0(y)+w_{1/4}(x)\cdot w_0(y)$, which is satisfied by functions containing as factors $\cos 2\pi hx \cdot \cos 2\pi ky$ and $\sin 2\pi hx \cdot \sin 2\pi ky$ for h even, and by ones in $\cos 2\pi hx \cdot \sin 2\pi ky$ and $\sin 2\pi hx \cdot \cos 2\pi ky$. Then,

$$\rho(xyz)=\frac{8}{V}\sum_{\substack{hkl\\ \text{for } h=2n}}^{\infty}\{[A_{CCC}CCC-A_{SSC}SSC]$$

$$+[-B_{SSS}SSS+B_{CCS}CCS]\}$$

$$+\frac{8}{V}\sum_{\substack{hkl\\ \text{for } h=2n-1}}^{\infty}\{[-A_{CSS}CSS-A_{SCS}SCS]$$

$$+[B_{SCC}SCC+B_{CSC}CSC]\}. \qquad (9b)$$

c) The 2 axis passes through the point $x = 1/4$, $y = 1/4$; symmetry condition $m_{1/4}(x)m_{1/4}(y)+w_{1/4}(x)w_{1/4}(y)$, which gives the same functions but with different relations between the indices:

for $h+k = 2n$, functions CCC, SSC, SSS, and CCS;

for $h+k = 2n-1$, functions CSS, SCS, SCC, and CSC.

5. Screw axis parallel to the Z axis.

a) The 2_1 axis passes through the origin; symmetry condition

$$[m_0(x)m_0(y)+w_0(x)w_0(y)]t(z)$$

$$+[m_0(x)w_0(y)+w_0(x)m_0(y)]\eta(z).$$

This means that for $l = 2n$, i.e., t(z) symmetry, we have CCC, SSC, SSS, and CCS, while for $l = 2n-1$, i.e., for $\eta(z)$ symmetry, we have CSS, SCS, SCC, and CSC.

b) The 2_1 axis passes through the point $x = 1/4$, $y = 0$; the symmetry condition has $m_0(x)$ and $w_0(x)$ replaced by $m_{1/4}(x)$ and $w_{1/4}(x)$, so the formula contains the same combinations of the trigonometric functions, but for $h+l = 2n$ and $h+l = 2n-1$ instead of $h = 2n$ and $h = 2n-1$.

TABLE 3. Formulas for the Three-Dimensional Electron-Density Distribution for Various Dispositions of Single Symmetry Elements

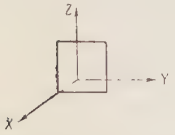

I. Symmetry Plane Perpendicular to X Axis

Functions present in formula		Relation between F(hkl)	A(hkl) and B(hkl) in Fourier series	Conditions on the indices					
				m plane		c plane		n plane	
				$x=0$	$x=1/4$	$x=0$	$x=1/4$	$x=0$	$x=1/4$
I	$\lvert CCC,$ $-CSS\rvert_A$ $\lvert CSC,$ $CCS\rvert_B$	$F(hkl) = -F(\bar{h}kl)$	$A_{CCC}=1/2\lvert F_A(hkl)+F_A(\bar{h}k\bar{l})\rvert$ $A_{CSS}=1/2\lvert F_A(hkl)-F_A(\bar{h}k\bar{l})\rvert$ $B_{CSC}=1/2\lvert F_B(hkl)+F_B(\bar{h}k\bar{l})\rvert$ $B_{CCS}=1/2\lvert F_B(hkl)-F_B(\bar{h}k\bar{l})\rvert$	hkl — all	$h=2n$	$l=2n$	$h+l=2n$	$k+l=2n$	$h+k+l=2n$
II	$\lvert -SCS,$ $-SSC\rvert_A$ $\lvert -SSS,$ $SCC\rvert_B$	$F(hkl) = -F(\bar{h}kl)$	$A_{SCS}=1/2\lvert F_A(hkl)+F_A(\bar{h}k\bar{l})\rvert$ $A_{SSC}=1/2\lvert F_A(hkl)-F_A(\bar{h}k\bar{l})\rvert$ $B_{SSS}=1/2\lvert F_B(hkl)+F_B(\bar{h}k\bar{l})\rvert$ $B_{SCC}=1/2\lvert F_B(hkl)-F_B(\bar{h}k\bar{l})\rvert$	None	$h=2n-1$	$l=2n-1$	$h+l=2n-1$	$k+l=2n-1$	$h+k+l=2n-1$

II. Symmetry Plane Parallel to Z Axis

Functions present in formula		Relation between F(hkl)	A(hkl) and B(hkl) in Fourier series	Conditions on the indices					
				2 rotation axis			2_1 screw axis		
				$x=0$ $y=0$	$x=1/4$ $y=0$	$x=1/4$ $y=1/2$	$x=0$ $y=0$	$x=1/4$ $y=0$	$x=1/4$ $y=1/2$
I	$\lvert CCC,$ $-SSC\rvert_A$ $\lvert -SSS,$ $CCS\rvert_B$	$F(hkl) = F(\bar{h}\bar{k}l)$	$A_{CCC}=1/2\lvert F_A(hkl)+F_A(h\bar{k}\bar{l})\rvert$ $A_{SSC}=1/2\lvert F_A(hkl)-F_A(h\bar{k}\bar{l})\rvert$ $B_{SSS}=1/2\lvert F_B(hkl)+F_B(h\bar{k}\bar{l})\rvert$ $B_{CCS}=1/2\lvert F_B(hkl)-F_B(h\bar{k}\bar{l})\rvert$	hkl — all	$h=2n$	$h+k=2n$	$l=2n$	$h+l=2n$	$h+k+l=2n$
II	$\lvert -CSS,$ $-SCS\rvert_A$ $\lvert SCC,$ $CSC\rvert_B$	$F(hkl) = -F(\bar{h}\bar{k}l)$	$A_{CSS}=1/2\lvert F_A(hkl)+F_A(h\bar{k}\bar{l})\rvert$ $A_{SCS}=1/2\lvert F_A(hkl)-F_A(h\bar{k}\bar{l})\rvert$ $B_{SCC}=1/2\lvert F_B(hkl)+F_B(h\bar{k}\bar{l})\rvert$ $B_{CSC}=1/2\lvert F_B(hkl)-F_B(h\bar{k}\bar{l})\rvert$	None	$h=2n-1$	$h+k=2n-1$	$l=2n-1$	$h+l=2n-1$	$h+k+l=2n-1$

*In addition, $F(hkl) = F^*(\overline{hkl})$, i.e., $F_A(hkl) = F_A(\overline{hkl})$ and $F_B(hkl) = -F_B(\overline{hkl})$.

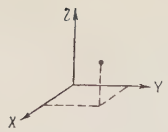

III. Inversion Center

	Functions present in formula	Relation between F(hkl)	A(hkl) and B(hkl) in Fourier series	Conditions on the indices: x=0, y=0, z=0	x=1/4, y=0, z=0	x=1/4, y=1/4, z=0	x=1/4, y=1/4, z=1/4
I	$[CCC, -CSS, SCS, -SSC]_A$	$F(hkl) = F(\bar{h}\bar{k}\bar{l})$	$A_{CCC} = 1/4\,[F_A(hkl) + F_A(h\bar{k}\bar{l}) + F_A(\bar{h}k\bar{l}) + F_A(\bar{h}\bar{k}l)]$ $A_{CSS} = 1/4\,[F_A(hkl) + F_A(h\bar{k}\bar{l}) - F_A(\bar{h}k\bar{l}) - F_A(\bar{h}\bar{k}l)]$ $A_{SCS} = 1/4\,[F_A(hkl) - F_A(h\bar{k}\bar{l}) + F_A(\bar{h}k\bar{l}) - F_A(\bar{h}\bar{k}l)]$ $A_{SSC} = 1/4\,[F_A(hkl) - F_A(h\bar{k}\bar{l}) - F_A(\bar{h}k\bar{l}) + F_A(\bar{h}\bar{k}l)]$	hkl — all	h = 2n	h + k = 2n	h + k + l = 2n
II	$[-SSS, SCC, CSC, CCS]_B$	$F(hkl) = -F(\bar{h}\bar{k}\bar{l})$	$B_{SSS} = 1/4\,[F_B(hkl) + F_B(h\bar{k}\bar{l}) + F_B(\bar{h}k\bar{l}) + F_B(\bar{h}\bar{k}l)]$ $B_{SCC} = 1/4\,[F_B(hkl) + F_B(h\bar{k}\bar{l}) - F_B(\bar{h}k\bar{l}) - F_B(\bar{h}\bar{k}l)]$ $B_{CSC} = 1/4\,[F_B(hkl) - F_B(h\bar{k}\bar{l}) + F_B(\bar{h}k\bar{l}) - F_B(\bar{h}\bar{k}l)]$ $B_{CCS} = 1/4\,[F_B(hkl) - F_B(h\bar{k}\bar{l}) - F_B(\bar{h}k\bar{l}) + F_B(\bar{h}\bar{k}l)]$	None	h = 2n − 1	h + k = 2n − 1	h + k + l = 2n − 1

c) The 2_1 axis passes through the point x = 1/4, y = 1/4; the symmetry condition causes further change in the condition on the indices in (9b), h = 2n being replaced by h + k + l = 2n and h = 2n − 1 by h + k + l = 2n − 1.

A symmetry axis parallel to the Z axis thus causes functions containing cos 2πhx · cos 2πkx or sin 2πhx · sin 2πky to be active for one combination of the indices, and those containing cos 2πhx · sin 2πky or sin 2πhx · cos 2πky for another.

6. Inversion center.

a) Inversion center at the origin; symmetry condition:

$$m_0(x)\,m_0(y)\,m_0(z) + m_0(x)\,u_0(y)\,u_0(z) + u_0(x)\,m_0(y)\,u_0(z) + u_0(x)\,u_0(y)\,m_0(z).$$

Working formula:

$$\rho(xyz) = \frac{8}{V}\sum_{\substack{hkl\\0}}^{\infty}[A_{CCC}\,CCC - A_{CSS}\,CSS - A_{SCS}\,SCS - A_{SSC}\,SSC]. \qquad (10a)$$

b) Inversion center at x = 1/4, y = 0, z = 0; the symmetry condition has $m_0(x)$ and $u_0(x)$ replaced by $m_{1/4}(x)$ and $u_{1/4}(x)$, and, therefore, cos 2πhx becomes sin 2πhx when h = 2n − 1 and, conversely, so

$$\rho(xyz) = \frac{8}{V}\sum_{\substack{hkl\\0}}^{\infty}[A_{CCC}\,CCC - A_{CSS}\,CSS - A_{SCS}\,SCS - A_{SSC}\,SSC] \quad \text{for } h=2n$$

$$+\frac{8}{V}\sum_{\substack{hkl\\0}}^{\infty}[-B_{SSS}\,SSS + B_{SCC}\,SCC + B_{CSC}\,CSC + B_{CCS}\,CCS] \quad \text{for } h=2n-1 \qquad (10b)$$

c) Inversion center at x = 1/4, y = 1/4, z = 0; the conditions on the indices become h + k = 2n for the first sum, and h + k = 2n − 1 for the second.

d) Inversion center at x = 1/4, y = 1/4, z = 1/4; the conditions on the indices become h + k + l = 2n for the first sum, and h + k + l = 2n − 1 for the second.

An inversion center thus causes one group of functions to consist of combinations containing an even number of sines (or CCC alone) and the other group to contain an odd number of sines.

Table 3 collects these results, which are presented in separate parts for symmetry planes, symmetry axes, and inversion centers.

Each part has two horizontal sections: I, for the terms of the Fourier series that appear for the first (even) combination of the indices, and II, for those for the second (odd) combination.

Each section gives the functions that are retained and the conditions (combinations) for the indices for all types of symmetry element in all positions. It also gives the relations between the structure amplitudes arising from the symmetry elements and the values of A(hk$l$) and B(hk$l$) for h $\neq 0$, k $\neq 0$, and $l \neq 0$ implied by these.

The general formula of Table 2 may be used with the data of Table 3 to write in expanded form the electron-density formula for any symmetry element and any setting of the crystal. No particular difficulty arises in permutation of the letter symbols in the functions and indices that is necessitated by a setting differing from that of Table 3.

Working Fourier Series for the Electron Density for the Various Space Groups

Tables 2 and 3 form the basis of the derivation for the space groups considered here; we retain in (6a) only terms that do not conflict with any of the symmetry elements in the group, so we have to take from Table 3 the functions characterizing the individual symmetry elements (permuting C and S in accordance with the orientation of the element). These are compared to leave only the ones present in all. The A(hk$l$) and B(hk$l$) are simultaneously derived from the relations between the structure amplitudes.

The following are some examples.

1. Space group D_{2h}^2 = Pnnn (Fig. 2).

a) Origin at the inversion center, i.e., at the intersection of the three planes.

The inversion center requires us to retain only [CCC, –CSS, –SCS, –SSC]$_A$ for all hk$l$; the n plane perpendicular to the X axis, only [CCC, –CSS]$_A$, [CSC, CCS]$_B$ for k + l = 2n, and [–SCS, –SSC]$_A$, [–SSS, SCC]$_B$ for k + l = 2n – 1; and the diad axis parallel to the Z axis and passing through x = 1/4, y = 1/4 requires us to retain [CCC, –SSC]$_A$, [–SSS, CCS]$_B$ for h + k = 2n and [–CSS, –SCS]$_A$, [SCC, CSC]$_B$ for h + k = 2n – 1. All three conditions are satisfied by

$$\begin{aligned} CCC &\quad \text{for} \quad h+k=2n \quad \text{and} \; k+l=2n \quad (a),\\ -CSS &\quad \text{for} \quad h+k=2n-1 \; \text{and} \; k+l=2n \quad (b),\\ -SCS &\quad \text{for} \quad h+k=2n-1 \; \text{and} \; k+l=2n-1 \quad (c),\\ -SSC &\quad \text{for} \quad h+k=2n \quad \text{and} \; k+l=2n-1 \quad (d), \end{aligned}$$

so

$$\rho(xyz) = \frac{8}{V}\sum_{\substack{hkl\\ 0(a)}}^{\infty} A_{CCC}\cos 2\pi hx \cos 2\pi ky \cos 2\pi lz -$$

$$-\frac{8}{V}\sum_{\substack{hkl\\ 0(b)}}^{\infty} A_{CSS}\cos 2\pi hx \sin 2\pi ky \sin 2\pi lz$$

$$-\frac{8}{V}\sum_{\substack{hkl\\ 0(c)}}^{\infty} A_{SCS}\sin 2\pi hx \cos 2\pi ky \sin 2\pi lz$$

$$-\frac{8}{V}\sum_{\substack{hkl\\ 0(d)}}^{\infty} A_{SSC}\sin 2\pi hx \sin 2\pi ky \cos 2\pi lz,$$

in which (a), (b), (c), and (d) denote the above conditions imposed on the indices.

b) Origin at the intersection of the diad axes.

The inversion center at 1/4, 1/4, 1/4 leaves [CCC, –CSS, –SCS, –SSC]$_A$ for h + k + l = 2n and [–SSS, SCC, CSC, CCS]$_B$ for h + k + l = 2n – 1; the plane perpendicular to the X axis and passing through x = 1/4 removes half of each set of functions, leaving [CCC, –CSS]$_A$ for h + k + l = 2n and [–SSS, SCC]$_B$ for h + k + l = 2n – 1, while the diad axis coincident with the Z axis necessitates [CCC, –SSC]$_A$ and [–SSS, CCS]$_B$ for all hk$l$. Then all elements are satisfied by

$$\rho(xyz) = \frac{8}{V}\sum_{\substack{h,k,l=0\\ (h-k+l=2n)}}^{\infty} A_{CCC}\cos 2\pi hx \cos 2\pi ky \cos 2\pi lz$$

$$-\frac{8}{V}\sum_{\substack{h,k,l=0\\ h-k+l=2n-1}}^{\infty} B_{SSS}\sin 2\pi hx \sin 2\pi ky \sin 2\pi lz.$$

2. Space group C_{2h}^6 = C2/c (Fig. 3).

a) Origin at the inversion center. The glide-reflection plane perpendicular to the Y axis passes through the origin and has its glide in the direction of the Z axis, so a permutation is necessary in the formulas of Table 3 (Y is replaced by X). The c plane leaves [CCC, –SCS]$_A$, [SCC, CCS]$_B$ for l = = 2n and [–CSS, –SSC]$_A$, [–SSS, CSC]$_B$ for l = 2n – 1.

The inversion center lies at the origin, so the formula can retain only functions in the brackets

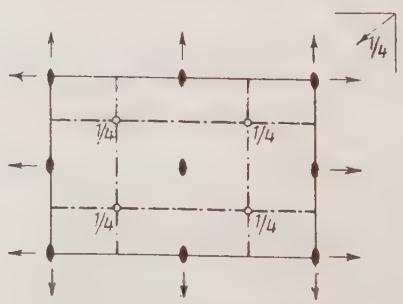

Fig. 2. Space group D_{2h}^2 = Pnnn.

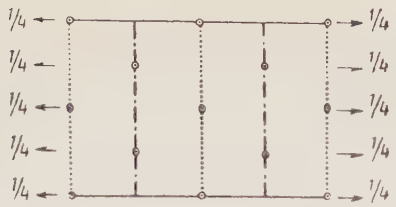

Fig. 3. Space group C_{2h}^6 = C2/c.

with subscript A. The centering of the cell imposes a condition on all reflections present: h + k must be even. These three elements are sufficient to generate the others, and hence the conditions are sufficient. The working formula is

$$\rho(xyz) = \frac{8}{V} \sum_{\substack{hkl \\ 0 \\ h=2n,\ l=2n}}^{\infty} [A_{CCC} \cos 2\pi hx \cos 2\pi ky \cos 2\pi lz - A_{SCS} \sin 2\pi hx \cos 2\pi ky \sin 2\pi lz]$$
$$+ \frac{8}{V} \sum_{\substack{hkl \\ 0 \\ h=2n-1,\ l=2n-1}}^{\infty} [- A_{CSS} \cos 2\pi hx \sin 2\pi ky \sin 2\pi lz - A_{SSC} \sin 2\pi hx \sin 2\pi ky \cos 2\pi lz].$$

b) Origin at the intersection of the rotation axis with the c glide plane. The latter necessitates the same functions subject to the same conditions. The inversion center is at x = 0, y = 0, z = 1/4, so it leaves group A functions for l = 2n and group B for l = 2n − 1. Then,

$$\rho(xyz) = \frac{8}{V} \sum_{\substack{hkl \\ 0 \\ h=2n,\ l=2n}}^{\infty} [A_{CCC} \cos 2\pi hx \cos 2\pi ky \cos 2\pi lz - A_{SCS} \sin 2\pi hx \cos 2\pi ky \sin 2\pi lz]$$
$$+ \frac{8}{V} \sum_{\substack{hkl \\ 0 \\ h=2n-1,\ l=2n-1}}^{\infty} [- B_{SSS} \sin 2\pi hx \sin 2\pi ky \sin 2\pi lz + B_{CSC} \cos 2\pi hx \sin 2\pi ky \cos 2\pi lz].$$

It is equally simple to find the expansion when the origin is placed at the intersection of the screw axis with the c plane or the n plane, or at another inversion center.

3. Space group T_h^7 = Ia3. The orthorhombic subgroup of group Ia3 is D_{2h}^{27} = Icab (Fig. 4). It is most convenient to take as basis the c plane perpendicular to the X axis, the 2_1 axis parallel to the Z axis, and the inversion center.

We assume that the origin is placed at the inversion center, the c plane passing through the origin and the 2_1 axis being displaced by 1/4 repeat distance along the X axis. Table 3 gives directly that

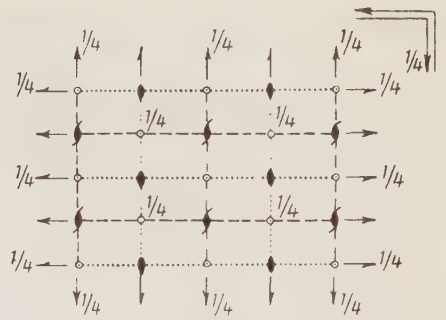

Fig. 4. Space group $D_2^{27}{}_h$ = Icab

$$\rho(xyz) = \frac{8}{V} \sum_{\substack{hkl \\ 0 \\ h=2n,\ l=2n}}^{\infty} A_{CCC} \cos 2\pi hx \cos 2\pi ky \cos 2\pi lz$$
$$- \frac{8}{V} \sum_{\substack{hkl \\ 0 \\ h=2n-1,\ l=2n}}^{\infty} A_{CSS} \cos 2\pi hx \sin 2\pi ky \sin 2\pi lz$$
$$- \frac{8}{V} \sum_{\substack{hkl \\ 0 \\ h=2n,\ l=2n-1}}^{\infty} A_{SCS} \sin 2\pi hx \cos 2\pi ky \sin 2\pi lz$$
$$- \frac{8}{V} \sum_{\substack{hkl \\ 0 \\ h=2n-1,\ l=2n-1}}^{\infty} A_{SSC} \sin 2\pi hx \sin 2\pi ky \cos 2\pi lz.$$

There is no need to examine the transformation of A(hk$l$) and B(hk$l$) for each group separately.

No relation between the F(hk$l$), F($\bar{h}$kl), and F(h$\bar{k}\bar{l}$), etc., can reduce any of the A(hk$l$) or B(hk$l$) to zero, because this would imply loss of the corresponding trigonometric function and hence change in the symmetry of the distribution. Then equality in the absolute values of two amplitudes, e.g., |F(hk$l$)| and |F($\bar{h}$k$\bar{l}$)|, can lead only to simplification (not loss) of the corresponding coefficients: A_{CCC}(hk$l$) = 1/2[F(hk$l$) + F($\bar{h}$k$\bar{l}$)] will be replaced by A_{CCC}(hk$l$) = F(hk$l$) or A_{CSS}(hk$l$) = 1/2[F(hk$l$) − F($\bar{h}$k$\bar{l}$)] by A_{CSS} = F(hk$l$) [the F($\bar{h}$k$\bar{l}$) reflection is obliged to have the sign corresponding to this change in the formula].

On the other hand, we know that the amplitudes for the eight reflections that differ in the signs of the indices always split up into two independent sets of four that differ in absolute value:

$$|F(hkl)| = |F(h\bar{k}l)| = |F(\bar{h}\bar{k}\bar{l})| = |F(\bar{h}k\bar{l})|$$

and

$$|F(\bar{h}kl)| = |F(\bar{h}\bar{k}l)| = |F(h\bar{k}\bar{l})| = |F(hk\bar{l})|$$

(we assume that the special axis is the Y axis of the monoclinic crystal). Similarly, the absolute values

TABLE 4. Coefficients for Fourier Expansion of the Electron Density

I. Monoclinic System, Y Axis the Special Direction

Indices	A_{CCC}	A_{CSS}	A_{SCS}	A_{SSC}	B_{SSS}	B_{SCC}	B_{CSC}	B_{CCS}
hkl	$\frac{1}{2}[F_A(hkl) + F_A(\bar{h}kl)]$	$\frac{1}{2}[F_A(hkl) + F_A(\bar{h}kl)]$	$\frac{1}{2}[F_A(hkl) - F_A(\bar{h}kl)]$	$\frac{1}{2}[F_A(hkl) - F_A(\bar{h}kl)]$	$\frac{1}{2}[F_B(hkl) - F_B(\bar{h}kl)]$	$\frac{1}{2}[F_B(hkl) - F_B(\bar{h}kl)]$	$\frac{1}{2}[F_B(hkl) + F_B(\bar{h}kl)]$	$\frac{1}{2}[F_B(hkl) + F_B(\bar{h}kl)]$
$hk0$	$\frac{1}{2}F_A(hk0)$	0	0	$\frac{1}{2}F_A(hk0)$	0	$\frac{1}{2}F_B(hk0)$	$\frac{1}{2}F_B(hk0)$	0
$h0l$	$\frac{1}{4}[F_A(h0l) + F_A(\bar{h}0l)]$	0	$\frac{1}{4}[F_A(h0l) - F_A(\bar{h}0l)]$	0	0	$\frac{1}{4}[F_B(h0l) - F_B(\bar{h}0l)]$	0	$\frac{1}{4}[F_B(h0l) + F_B(\bar{h}0l)]$
$0kl$	$\frac{1}{2}F_A(0kl)$	$\frac{1}{2}F_A(0kl)$	0	0	0	0	$\frac{1}{2}F_B(0kl)$	$\frac{1}{2}F_B(0kl)$
$h00$	$\frac{1}{4}F_A(h00)$	0	0	0	0	$\frac{1}{4}F_B(h00)$	0	0
$0k0$	$\frac{1}{4}F_A(0k0)$	0	0	0	0	0	$\frac{1}{4}F_B(0k0)$	0
$00l$	$\frac{1}{4}F_A(00l)$	0	0	0	0	0	0	$\frac{1}{4}F_B(00l)$
000	$\frac{1}{8}F_A(000)$	0	0	0	0	0	0	0

II. Monoclinic System, Z Axis the Special Direction

Indices	A_{CCC}	A_{CSS}	A_{SCS}	A_{SSC}	B_{SSS}	B_{SCC}	B_{CSC}	B_{CCS}
hkl	$\frac{1}{2}[F_A(hkl) + F_A(\bar{h}kl)]$	$\frac{1}{2}[F_A(hkl) + F_A(\bar{h}kl)]$	$\frac{1}{2}[F_A(hkl) - F_A(\bar{h}kl)]$	$\frac{1}{2}[F_A(hkl) - F_A(\bar{h}kl)]$	$\frac{1}{2}[F_B(hkl) - F_B(\bar{h}kl)]$	$\frac{1}{2}[F_B(hkl) - F_B(\bar{h}kl)]$	$\frac{1}{2}[F_B(hkl) + F_B(\bar{h}kl)]$	$\frac{1}{2}[F_B(hkl) + F_B(\bar{h}kl)]$
$hk0$	$\frac{1}{4}[F_A(hk0) + F_A(\bar{h}k0)]$	0	0	$\frac{1}{4}[F_A(hk0) - F_A(\bar{h}k0)]$	0	$\frac{1}{4}[F_B(hk0) - F_B(\bar{h}k0)]$	$\frac{1}{4}[F_B(hk0) + F_B(\bar{h}k0)]$	0
$h0l$	$\frac{1}{2}F_A(h0l)$	0	$\frac{1}{2}F_A(h0l)$	0	0	$\frac{1}{2}F_B(h0l)$	0	$\frac{1}{2}F_B(h0l)$
$0kl$	$\frac{1}{2}F_A(0kl)$	$\frac{1}{2}F_A(0kl)$	0	0	0	0	$\frac{1}{2}F_B(0kl)$	$\frac{1}{2}F_B(0kl)$
$h00$	$\frac{1}{4}F_A(h00)$	0	0	0	0	$\frac{1}{4}F_B(h00)$	0	0
$0k0$	$\frac{1}{4}F_A(0k0)$	0	0	0	0	0	$\frac{1}{4}F_B(0k0)$	0
$00l$	$\frac{1}{4}F_A(00l)$	0	0	0	0	0	0	$\frac{1}{4}F_B(00l)$
000	$\frac{1}{8}F_A(000)$	0	0	0	0	0	0	0

III. Orthorhombic System

Indices	A_{CCC}	A_{CSS}	A_{SCS}	A_{SSC}	B_{SSS}	B_{SCC}	B_{CSC}	B_{CCS}
hkl	$F_A(hkl)$	$F_A(hkl)$	$F_A(hkl)$	$F_A(hkl)$	$F_B(hkl)$	$F_B(hkl)$	$F_B(hkl)$	$F_B(hkl)$
$hk0$	$\frac{1}{2}F_A(hk0)$	0	0	$\frac{1}{2}F_A(hk0)$	0	$\frac{1}{2}F_B(hk0)$	$\frac{1}{2}F_B(hk0)$	0
$h0l$	$\frac{1}{2}F_A(h0l)$	0	$\frac{1}{2}F_A(h0l)$	0	0	$\frac{1}{2}F_B(h0l)$	0	$\frac{1}{2}F_B(h0l)$
$0kl$	$\frac{1}{2}F_A(0kl)$	$\frac{1}{2}F_A(0kl)$	0	0	0	0	$\frac{1}{2}F_B(0kl)$	$\frac{1}{2}F_B(0kl)$
$h00$	$\frac{1}{4}F_A(h00)$	0	0	0	0	$\frac{1}{4}F_B(h00)$	0	0
$0k0$	$\frac{1}{4}F_A(0k0)$	0	0	0	0	0	$\frac{1}{4}F_B(0k0)$	0
$00l$	$\frac{1}{4}F_A(00l)$	0	0	0	0	0	0	$\frac{1}{4}F_B(00l)$
000	$\frac{1}{8}F_A(000)$	0	0	0	0	0	0	0

of all eight amplitudes are identical for any group in the orthorhombic system.

The transformed expressions for A_{CCC}, A_{CSS}, etc., will thus be the same for all monoclinic groups; the same is true for the orthorhombic groups, and so these can be written down in the necessary form in advance (Table 4).

The space group of a crystal of higher symmetry is referred for the purpose of electron-density calculation to the highest subgroup in one of the lower systems, so the relations of Table 4 apply for any symmetry group. The higher groups that are referred to monoclinic ones are usually oriented with the special axis along the Z axis (not Y), so both possible settings are considered.

Working Formulas for the Structure Amplitude for the Lower Systems

The general series formulas of (6a) and (7a) are very similar, for they contain the same combinations of functions with the same signs. The functions present in the real part of F(hk$l$) coincide with those multiplied by the A coefficients in ρ (xyz), while those in the imaginary part of F(hk$l$) coincide with those multiplied by the B in ρ (xyz). The same combinations are lost in the two cases when a symmetry element is introduced.

The loss of a function from ρ(xyz) occurs because the symmetry of the function must satisfy the requirements on the symmetry of the crystal. The F(hk$l$) lose functions on account of summation over atoms related by symmetry elements; but here the only functions that can persist are those whose symmetry coincides with that of the array of atoms, otherwise the repeated functions would have (for the given f_j), opposite signs and so would cancel out.

Thus, the formula for ρ(xyz) as a Fourier series, must resemble that for the structure amplitude for all space groups; Table 3 may be used for both.

This gives a somewhat curious air to Nowacki's book [10] on the derivation of electron-density formulas on the basis of those for the structure amplitude. For instance, for group $D_2^4 = P2_12_12_1$, that derivation takes about four pages, whereas the final result can be written down directly from the analogy with the initial formula.

Plane Symmetry Groups

The present approach can also be applied to two-dimensional cases (projections and sections); difficulty in discarding the unwanted dimension can be avoided by drawing up separate tables for the general formula (12) (Table 5) and for the combina-

TABLE 5. General Formula for a Two-Dimensional Electron-Density Distribution

$$\sigma(xy) = \frac{4}{S_0}\sum_{\substack{hk\\0}}^{\infty}[A_{CC}CC - A_{SS}SS] + \frac{4}{S_0}\sum_{\substack{hk\\0}}^{\infty}[B_{CS}CS + B_{SC}SC]$$

I_A

$A_{CC}(hk) = {}^1/_2[F_A(hk) + F_A(\bar{h}k)]$
$A_{CC}(h0) = {}^1/_2F_A(h0)$
$A_{CC}(0k) = {}^1/_2F_A(0k)$
$A_{CC}(00) = {}^1/_4F_A(00)$

II_A

$A_{SS}(hk) = {}^1/_2[F_A(hk) - F_A(\bar{h}k)]$
$A_{SS}(h0) = 0$
$A_{SS}(0k) = 0$
$A_{SS}(00) = 0$

I_B

$B_{CS}(hk) = {}^1/_2[F_B(hk) + F_B(\bar{h}k)]$
$B_{CS}(h0) = 0$
$B_{CS}(0k) = {}^1/_2F_B(0k)$
$B_{CS}(00) = 0$

II_B

$B_{SC}(hk) = {}^1/_2[F_B(hk) - F_B(\bar{h}k)]$
$B_{SC}(h0) = {}^1/_2F_B(h0)$
$B_{SC}(0k) = 0$
$B_{SC}(00) = 0$

TABLE 6. Formulas for the Two-Dimensional Distribution for Various Dispositions of Symmetry Elements

I. Line of Symmetry Perpendicular to the X Axis

	Functions present in formula	Relation between F(hk)	A(hk) and B(hk)	Conditions on the indices: m lines, $x=0$	m lines, $x={}^1/_4$	g line, $x=0$	g line, $x={}^1/_4$
I	$[CC]_A$,	$F(hk) = F(\bar{h}k)$	$A_{CC}(hk) = F_A(hk)$	h, k	$h = 2n$	$k = 2n$	$h + k = 2n$
	$[CS]_B$	*	$B_{CS}(hk) = F_B(hk)$	All			
II	$[-SS]_A$,	$F(hk) = -F(\bar{h}k)$	$A_{SS}(hk) = F_A(hk)$	None	$h = 2n-1$	$k = 2n-1$	$h + k = 2n-1$
	$[SC]_B$	*	$B_{SC}(hk) = F_B(hk)$				

II. Inversion Center

	Functions present in formula	Relation between F(hk)	A(hk) and B(hk)	Conditions on the indices: $x=0$, $y=0$	$x={}^1/_4$, $y=0$	$x={}^1/_4$, $y={}^1/_4$
I	$[CC, -SS]_A$	$F(hk)=F(\bar{h}\bar{k})$	$A_{CC}(hk) = {}^1/_2[F_A(hk) + F_A(\bar{h}k)]$ $A_{SS}(hk) = {}^1/_2[F_A(hk) - F_A(\bar{h}k)]$	h, k All	$h = 2n$	$h + k = 2n$
II	$[CS, SC]_B$	$F(hk) = -F(\bar{h}\bar{k})$	$B_{CS}(hk) = {}^1/_2[F_B(hk) + F_B(\bar{h}k)]$ $B_{SC}(hk) = {}^1/_2[F_B(hk) - F_B(\bar{h}k)]$	None	$h = 2n-1$	$h + k = 2n-1$

*In addition, $F(hk) = F^*(\bar{h}\bar{k})$, i.e., $F_A(hk) = F_A(\bar{h}\bar{k})$ and $F_B(hk) = -F_B(\bar{h}\bar{k})$.

tions of functions that persist in the presence of symmetry elements in various positions in the cell (Table 6).

LITERATURE CITED

1. Internationale Tabellen zur Bestimmung von Kristallstrukturen. I. Gebrüder Bortraeger (Berlin, 1935).
2. K. Lonsdale, Simplified Structure Factor and Electron Density Formulas for the 230 Space Groups (G. Bell and Sons Ltd., London, 1936).
3. International Tables for X-Ray Crystallography. I. (The Kynock Press, Birmingham, 1952).
4. N. V. Belov, "Simplified formulas for the structure factor," Tr. Inst. kristallografii AN SSSR, 7, 3 (1952).
5. Handbook on X-Ray Structure Analysis (edited by A. I. Kitaigorodskii) [in Russian](Moscow, 1940).
6. C. A. Beevers and H. Lipson, "The use of Fourier strips for calculating structure factors," Acta cryst., 5, 673 (1952).
7. L. Alexander, "A simple but versatile strip technique for calculating structure factors," Acta cryst., 6, 727 (1953).
8. C. A. Beevers and H. Lipson, "A rapid method for summation of a two-dimensional Fourier series," Phil. Mag., 17, 855 (1934).
9. J. M. Robertson, "Numerical and mechanical methods in double Fourier synthesis," Phil. Mag., 21, 176 (1936).
10. W. Nowacki, Fourier Synthese von Kristallen und ihre Anwendung in der Chemie. Birkhäuser (Basel, 1952).

STRUCTURE OF THE DIHALIDE-DIAMINES OF COBALT

G. B. Bokii, T. I. Malinovskii, and A. V. Ablov

Moldavian Branch, Academy of Sciences of the USSR; and
N. S. Kurnakov Institute of General and Inorganic Chemistry
Translated from Kristallografiya, Vol. 1, No. 1,
pp. 49-52, January-February, 1956
Original article submitted November 1, 1955

The structure of the addition compounds formed by two amines with the halides of divalent cobalt is considered. The crystal structure of $CoCl_2 \cdot 2C_7H_9N$, which proves molecular, is determined. The coordination number for the cobalt is 4, the coordination polyhedron a tetrahedron. The authors confirm that the α- and β-modifications of compounds of divalent cobalt (blue and violet) are not cis and trans isomers. The first has molecular tetrahedral structure, while a chain structure with coordination number 6 for the cobalt must be ascribed to the second.

The structure of the addition compounds of general formula $CoX_2 \cdot 2A$, formed by two ammonia molecules, or two molecules of an organic amine, with halides of divalent cobalt has attracted the attention of many authors. Biltz and Fetkenheuer [1] found that the diamine of cobalt chloride, $CoCl_2 \cdot 2NH_3$, existed in two forms. A similar observation was made for the dipyridinate $CoCl_2 \cdot 2Py$ [2]. Various views have been published regarding the structure of these compounds. Biltz [1] and Hantzch [2] thought they dealt with cases of cis-trans isomers, as in the compounds of divalent platinum. Cox [3] used chemical and crystallographic methods to study the two forms of the dipyridinate of cobalt chloride: the stable, violet, α form and the unstable, blue, β form. Considering the dimensions of the unit cell in the violet form, he came to the conclusion that the lattice contained plane $CoCl_2 \cdot 2Py$ molecules with the pyridine groups in the trans position. From the magnetic properties of the two forms of $CoCl_2 \cdot 2Py$, Mellor concluded [4] that the violet form had a chain octahedral structure and the blue a tetrahedral structure. X-ray studies of Cs_3CoCl_5 [5, 6] and x-ray [7] and electron-diffraction [6] studies of Cs_2CoCl_4 showed that these compounds contained isolated $CoCl_4$ tetrahedra. Electron-diffraction examination of the dihydrate $CoCl_2 \cdot 2H_2O$ indicated that this compound had a chain octahedral structure [8].

Since the structure of the diamine dihalides of cobalt thus seems to be in doubt, we undertook an x-ray investigation of the addition compound of two molecules of p-toluidene with cobalt chloride, $CoCl_2 \cdot 2H_2NC_6H_4CH_3$.

Quite large single crystals of this compound are obtained on evaporating a mixture of solutions of anhydrous cobalt chloride and p-toluidene in ethyl alcohol. Rose crystals of the dialcoholate $CoCl \cdot 2C_7H_9N \cdot 2C_2H_5OH$ were found at the bottom of the beaker, while at the sides there was a gradual growth of blue plates of $CoCl_2 \cdot 2C_7H_9N$.

Found %: Co 17.21; Cl 20.67.

Calculated %: Co 17.12; Cl 20.60.

The crystals form concretions parallel to the extension. From optical data, the crystals are biaxial, the angle between the optic axes being $2v \approx 90°$. The refractive indices are Ng = 1.701, Nm = 1.652, and Np = 1.610.

The dimensions of the unit cell were determined from oscillation x-ray diffraction photographs and then improved by photographs obtained on a KFOR x-ray goniometer. The dimensions were: $a = 12.3 \pm 0.05$ Å, $b = 4.59 \pm 0.01$ Å, $c = 26.1 \pm 0.1$ Å, $\beta = 93°45' \pm 5'$. The density, determined pycnometrically, was 1.483, which gives for the number of formula units in the unit cell $n = 3.83 \approx 4$. The density determined by x rays was 1.55.

The Fedorov symmetry group was determined by indexing the x-ray goniometer photographs. The indices of the reflections satisfied the following conditions:

hkl only with $h + k + l = 2n$;

$h0l$ only with $h = 2n$ and $l = 2n$;

$0k0$ only with $k = 2n$,

which characterizes the Fedorov groups C_{2h}^6 and C_S^4.

The structural investigation was carried out from goniometric photographs taken on the KFOR with Mo $K\alpha$ radiation. The intensities were estimated by comparison with a blackening scale. Only the polarization and kinematic factors were taken into account. Some 556 independent reflections were obtained, taken from five layer lines ($h0l$, $h1l$, $h2l$, $h3l$, $h4l$).

From these data we constructed a series of interatomic vectors and the projection of the electron density on the XOZ plane. The Fedorov group and atomic position were established by analyzing the three-dimensional F^2 series and the electron-density projection.

Maxima lying in the XOZ and $X\frac{1}{2}Z$ planes indicate the presence of two-fold rotation and screw axes and thus unequivocally give the Fedorov group $C_{2h}^6 = I2/a$.

The cobalt atom occupies a fourfold particular position with one degree of freedom, lying on the two-fold rotation axes. The chlorine, nitrogen, and carbon atoms occupy an eightfold general position.

The coordinates of the atoms are

$$\text{Co: } \frac{1}{4},\ y,\ 0;\ \frac{3}{4},\ \bar{y},\ 0;$$

$$\frac{3}{4},\ \frac{1}{2}+y,\ \frac{1}{2};\ \frac{1}{4},\ \frac{1}{2}-y,\ \frac{1}{2};\ y = 0.386.$$

The general eightfold position for the Fedorov group C_{2h}^6 in the $I2/a$ arrangement is

$$xyz;\ \bar{x}\bar{y}\bar{z};\ \bar{x},\ \frac{1}{2}+y,\ \frac{1}{2}-z;$$

$$x,\ \frac{1}{2}-y,\ \frac{1}{2}+z;\ \frac{1}{2}+x,\ \bar{y},\ z;$$

$$\frac{1}{2}-x,\ \frac{1}{2}-y,\ \frac{1}{2}-z;$$

$$\frac{1}{2}+x,\ \frac{1}{2}+y,\ \frac{1}{2}+z;\ \frac{1}{2}-x,\ y,\ \bar{z}.$$

$$\text{Cl: } x = 0.384;\ y = 0.120;\ z = 0.034.$$

$$\text{N: } x = 0.182;\ y = 0.618;\ z = 0.052.$$

$$C_1\text{: } x = 0.166;\ y = 0.472;\ z = 0.096.$$

The structure of $CoCl_2 \cdot 2p\text{-}H_2NC_6H_4CH_3$ is molecular. The cobalt atom lies in the center of an almost-regular tetrahedron, two vertices of which are occupied by Cl atoms and two by N atoms (Fig. 1). As seen from Table 1, the Co–Cl and Co–N bonds are predominantly covalent. It is ex-

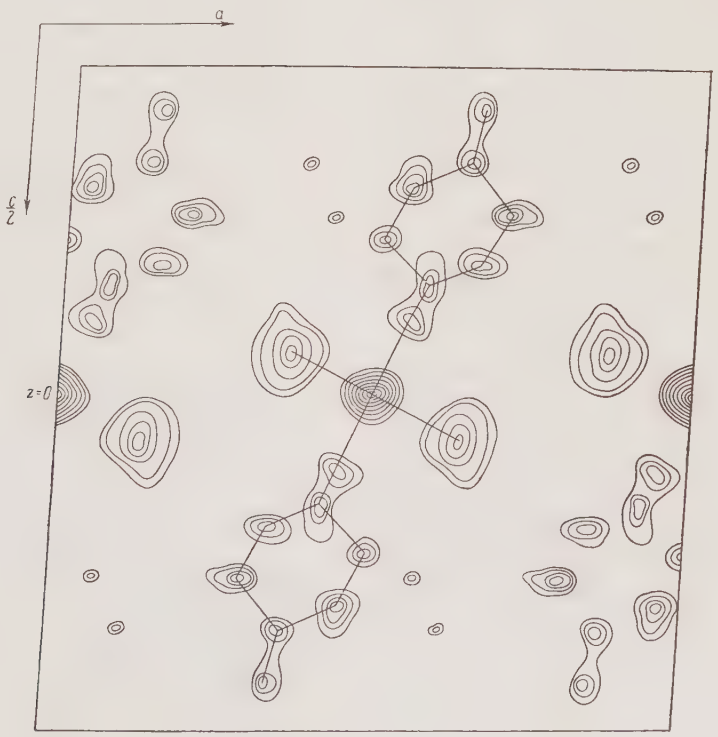

Fig. 1. Projection of the electron density of the $CoCl_2 \cdot 2H_2NC_6H_4CH_3$ unit cell on the XOZ plane.

TABLE 1. Interatomic Distances in A

Inside the molecules	Between neighboring molecules	Valence angles
Co — Cl 2.24	Cl — N 3.40	Cl—Co—N 109°
Co — N 1.92	Cl — Cl 3.50	Cl—Co—Cl 111°
N — C_1 1.38		N—Co—N 111°
Cl — Cl 3.70		Co—N—C_1 102°
Cl — N 3.40		
N — N 3.15		

tremely probable that tetrahedral structure must also be ascribed to other addition compounds of cobalt halides of composition $CoX_2 \cdot A_2$ and blue color, including the pyridinate.

As regards the violet modifications, we should probably assign these a chain structure with coordination number 6, analogous to the structure of $CoCl_2 \cdot 2H_2O$ [8].

It follows that the α- and β-forms of the compounds $CoX_2 \cdot A_2$ are not cis and trans isomers.

This view regarding the structure of the two forms of cobalt dipyridinate was discussed earlier on the basis of magnetic measurements by Mellor [4]. In support of the fact that the blue color of compounds $CoX_2 \cdot A_2$ is connected with the tetrahedral configuration, we may cite the fact that, with 1,10-phenanthroline, which occupies two neighboring coordination sites, cobalt chloride gives a blue crystalline substance of composition $CoCl_2-C_{12}H_8N_2$.

The tetrahedral disposition of the Cl and N atoms around the Co in the ditoluidinate of cobalt chloride enables us to solve the problem regarding the nature of the bond in the so-called "normal" complexes [9, 10, 11], such as the ammoniates and aminates of the salts of divalent metals. It is usually considered that in these compounds the metal-addend bond is ionic–dipolar. In this case, the dipole should occupy a position of minimum potential energy relative to the metal ion, i.e., the metal ion should lie on the line of the vector of the dipole molecule. For the symmetrical molecules NH_3 and C_5H_5N the direction of the vector of the dipole molecule coincides with that of the metal–nitrogen bond. In unsymmetrical molecules, such as aniline or p-toluidene, this is not so. Our value for the Co–N–C_1 angle differs from 109° only within the limits of experimental error; hence, the four atoms coordinated around the nitrogen are disposed at the vertices of a tetrahedron, as in the salts of ammonia. The directional aspects of the nitrogen valences in the additional product $CoCl_2 \cdot 2C_7H_9N$ further confirm the covalent nature of the metal–nitrogen bond.

Thus, from the crystallochemical point of view, there is no difference between normal complexes and interstitial complexes, which latter include the compounds of tervalent cobalt, platinum, chromium, etc., that are stable in aqueous solution.

The authors consider it their pleasant duty to thank M. A. Porai-Koshits for consultation in the work.

LITERATURE CITED

1. W. Biltz and B. Fetkenheuer, Über Ammoniakverbindungen der Halogenide des zweiwertigen Kobalts, Z. anorg. allgem. Chem., 89, 97, 133 (1914).
2. A. Hantzch, Solvatation und Komplexbildung als Ursache des Farbenwechsels der Kobalthaloide, Z. anorg. allgem. Chem., 159, 273-303 (1926).
3. E. G. Cox, A. J. Shorter, W. Wardlaw, and W. J. Way, "The stereochemistry of quadricovalent atoms: cobalt and manganese," J. Chem. Soc., 1556-1559 (1937).
4. D. P. Mellor and C. D. Corrvel, "The magnetic properties and structures of manganous and cobaltous dipyridine chlorides," J. Am. Chem. Soc., 60, 1786-1787 (1938).
5. H. M. Powell and A. F. Wells, "The structure of cesium cobalt chloride," J. Chem. Soc., 359-362 (1935).
6. G. N. Tishchenko and Z. G. Pinsker, "Electron-diffraction determination of the structure of $CsCoCl_4$," DAN SSSR, 100, 913-916 (1955).
7. M. A. Porai-Koshits, "X-ray study of complex compounds of divalent cobalt and nickel," Tr. Inst. kristallografii, No. 10, 269-287 (1954).
8. B. K. Vainshtein, "Electron-diffraction determination of the structure of $CoCl_2 \cdot 2H_2O$," DAN SSSR, 68, 301-4 (1949).
9. E. Lippmann and G. Vortmann, Über die Verbindungen des Kobalt- und Nickelchlorürs mit Theerbasen, B12, 79-82 (1879).
10. P. Pfeiffer and B. Werdelmann, Phenanthrolinhaltige Komplexsalze mit ein- und zweiwertigen Zentralatomen, Z. anorg. allgem. Chem., 261, 197-209 (1950).
11. F. Hein, Chemische Koordinationslehre (Leipzig, 1954).

AN X-RAY STRUCTURAL STUDY OF INDIGO AND THIOINDIGO

E. A. Gribova, G. S. Zhdanov, and G. A. Gol'der

L. Ya. Karpov Physicochemical Institute; and K. E. Voroshilov Scientific Research Institute for Intermediates and Dyestuffs

Translated from Kristallografiya, Vol. 1, No. 1, pp. 53-60, January-February, 1956
Original article submitted October 10, 1955

An x-ray study has been carried out on crystals of indigo and thioindigo by two-dimensional electron density projections and by linear and planar sections of the three-dimensional Fourier series. It has been shown that simple σ bonds and classical double bonds are not present in the indigo molecule. In the indigo molecule there is a single system of π-electron interactions. It has been established that there are intermolecular hydrogen bonds between the carbonyl and imino groups in indigo molecules.

There is considerable interest in the current literature in the structure of one of the longest-known organic dyes, indigo, and of related substances. The structural formula of indigo which correctly expresses the positions of the atoms in the molecule (1) was first established by Baeyer [1]. However, the indigo molecule has a number of properties which indicate that this formula does not express the actual character of the bonds and the distribution of the valences within the molecule.

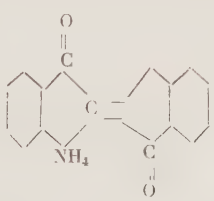

(1)

These properties are: the absence of geometrical isomers, the intensity of color, the great stability of the molecule, etc. Since these properties are not explained by formula (1), many other formulas have been proposed for indigo in which the basic skeleton is maintained but the nature of the bonds is changed. Some authors connect the special properties of indigo with an o-quinonoid zwitterionic structure [2, 3], while others connect them with the existence of intramolecular hydrogen bonding between the carbonyl and imino groups [4-8]. A number of authors draw particular attention to intermolecular interactions [9-11].

It seemed interesting to use the x-ray structural method to elucidate some of the peculiarities of the indigo structure, since this method permits the determination of the spatial distribution of atoms and molecules in the crystal, and the interatomic distances and bond angles in the molecule.

Recently, Eller [8, 12] published a number of short reports which cited x-ray structural data on indigo, thioindigo, and selenoindigo. We deciphered the crystal structures of indigo and thioindigo at the same time as Eller [13].

Crystals of indigo and thioindigo suitable for structural analysis were obtained by sublimation at atmospheric pressure. Crystallization from solutions did not give good results because of the extremely limited solubility of indigo and thioindigo in normal solvents.

The lattice constants, space groups, and numbers of molecules in the unit cell are given in Table 1. They are in agreement with those published by Eller. It follows from these data that the indigo and thioindigo molecules in the sublimed crystals exist in the trans forms. But the sublimation was carried out under vigorous conditions, so that it would be expected that one isomer could be converted to the other.

Our x-ray phase analysis showed that the dyes obtained by oxidation of the leucocompounds had the same structures as those obtained by sublimation. Consequently, it is concluded that the molecules of

TABLE 1. Lattice Parameters of Indigo and Thioindigo Crystals

Substance	a	b	c	β	Space group	z
Indigo . . .	9.23	5.74	12.25	116°30′	$P4/c$	2
Thioindigo . .	7.82	3.92	20.34	92°40′	$P4/c$	2

indigo and thioindigo exist in the trans form in normal crystals.

The orientation of the thioindigo molecules in the unit cell was determined by geometric analysis and analysis of intensities. The experimental values of the structure amplitudes were obtained from intensities of reflections of the zero-layer lines on a photograph taken with rotation of the crystal around the b axis. The photographs were taken with copper radiation in an RGNS camera. In all, 141 reflections of type h0l were obtained with maximum values of h = 10 and l = 26. From the coordinates for the chosen structural model, the signs of the structure amplitudes were chosen, and further structure decipherment was carried out from an electron-density projection on the (010) plane of the unit cell of the crystal.

The method of successive approximations was used to refine the x and z coordinates. Four approximations were carried out. The inclination of the molecules to the (010) plane was determined from the deformation of the benzene ring in the projection, assuming that all the atoms were coplanar. In Table 2 the values of the x and z coordinates of the atoms of the thioindigo molecule are given in fractions of the lattice parameters.

An electron-density projection along the b axis is shown in Fig. 1, and the values of the interatomic distances and bond angles are shown in Fig. 3. In Fig. 3 the experimental and calculated structure amplitudes are compared for certain regions of $\sin\theta$.

It was established by geometrical analysis that the plane of the indigo molecule in the crystal is at a considerable inclination to all three coordination planes of the unit cell. Hence, three-dimensional electron-density series were used for solution of the crystal structure.

Photographs were taken in copper radiation with an RGNS camera with rotation of the crystal around the b axis, and the layer lines h0l, h1l, h2l, h3l, and h4l were developed, 707 reflections in all. The signs of the h0l structure amplitudes were first determined from the structural model found from intensity analysis, and were then refined from the atomic coordinates in the electron-density projection on the (010) plane. The method

TABLE 2. Atomic Coordinates (x, z) in the Thioindigo Molecule

No. of atom	x/a	z/c	No. of atom	x/a	z/c
C_1	0.454	0.023	C_6	0.068	0.177
C_2	0.513	0.091	C_7	0.071	0.113
C_3	0.370	0.125	C_8	0.217	0.091
C_4	0.370	0.188	S	0.230	0.009
C_5	0.226	0.214	O	0.656	0.108

Fig. 1. Electron density projection of the thioindigo crystal along the b axis.

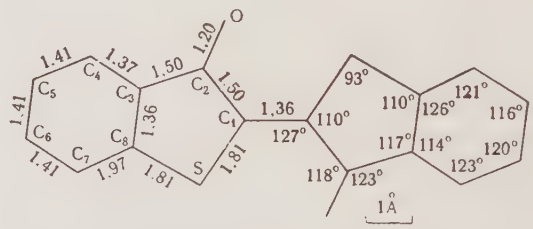

Fig. 2. The thioindigo molecule: values of the interatomic distances and the bond angles.

of successive approximations was used to determine exact values of the x and z coordinates. It was established from the size of the benzene ring that the plane of the molecule coincided, or almost coincided, with the (210) plane. The signs of all the structure amplitudes were determined from the x and z coordinates [from electron-density projection on the (010) plane] and the coordinates y = 1 − 2x, which correspond to the position of the molecule in the (210) plane. A section of the three-dimensional electron-density series on the plane (210) (Fig. 4), and ten linear sections parallel to the y axis, passing through centers of atoms, were then constructed. The atomic coordinates, determined from the projection and sections of the electron density, are given in Table 3.

Figure 5 depicts the molecule of indigo and includes bond length and bond angle data. In Fig. 6 is given a comparison of the experimental and calculated structure amplitudes of the h0l type for

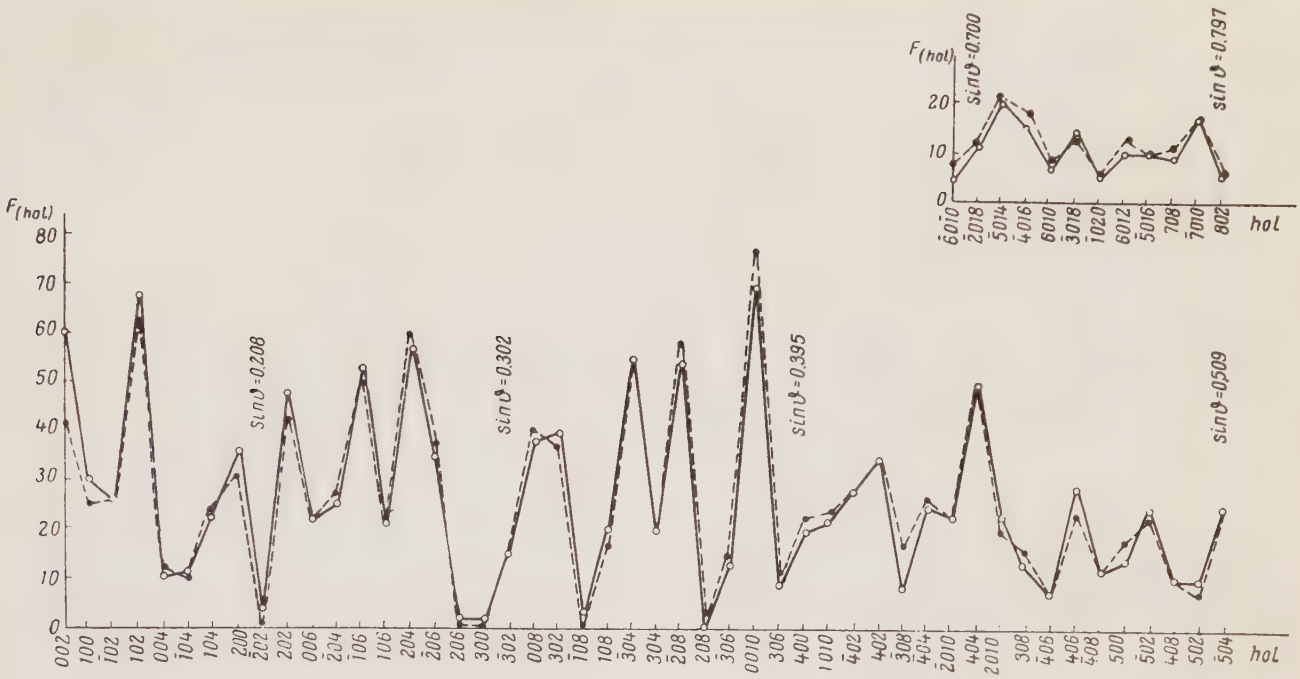

Fig. 3. Comparison of the experimental and calculated structure amplitudes for some regions of $\sin\theta$ in thioindigo. Solid line – calculated; dashed line – experimental.

Fig. 4. Section on the plane (210) of the three-dimensional electron density series for the indigo crystal.

TABLE 3. Atomic Coordinates (x, y, z) in the Indigo Molecule

No. of atom	x/a	y/b	z/c	No. of atom	x/a	y/b	z/c
C_1	0.049	0.907	0.020	C_6	0.373	0.261	0.087
C_2	0.103	0.793	0.142	C_7	0.293	0.432	0.004
C_3	0.197	0.593	0.138	C_8	0.208	0.602	0.029
C_4	0.277	0.421	0.222	N	0.124	0.793	0.038
C_5	0.364	0.256	0.196	O	0.059	0.847	0.219

certain regions of $\sin\theta$. It has been established that all the atoms of each half of the molecule (except nitrogen and C_2 and C_8 and the center of symmetry) lie in a single plane (with a precision of a few thousandths of an Angstrom unit), and this plane is defined by the formulas

$$x_1 = x\cdot\cos 26.5^\circ, \quad z_1 = z - x\cdot\sin 26.5^\circ.$$

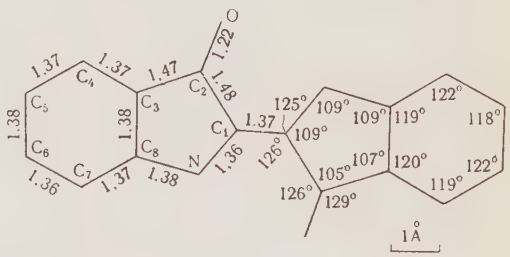

Fig. 5. Indigo molecule, showing interatomic distances and bond angles.

The divergence of the atoms N, C_2, C_8, and the center of symmetry from this plane are, respectively, +0.07 Å, +0.05 Å, +0.03 Å, and –0.03 Å.

An analysis of the interatomic distances in the indigo molecule shows that there are no simple σ bonds (except the bond to hydrogen) nor classical double bonds. The bond lengths are intermediate between single and double in both the benzene ring and in the heterocyclic ring. The fact that the $C_{(1)}-N$ and $N-C_{(8)}$ distances are shorter than those characteristic of an aliphatic single bond (1.47 Å) may be explained by formation of π-bonds between the unshared pair on nitrogen and its neighboring atoms. The very weak basicity of the imino group in indigo confirms this view. There is but a single system of π-electronic interactions in indigo. The results obtained show that there is no reality in the proposed o-quinonoid zwitterionic structure.

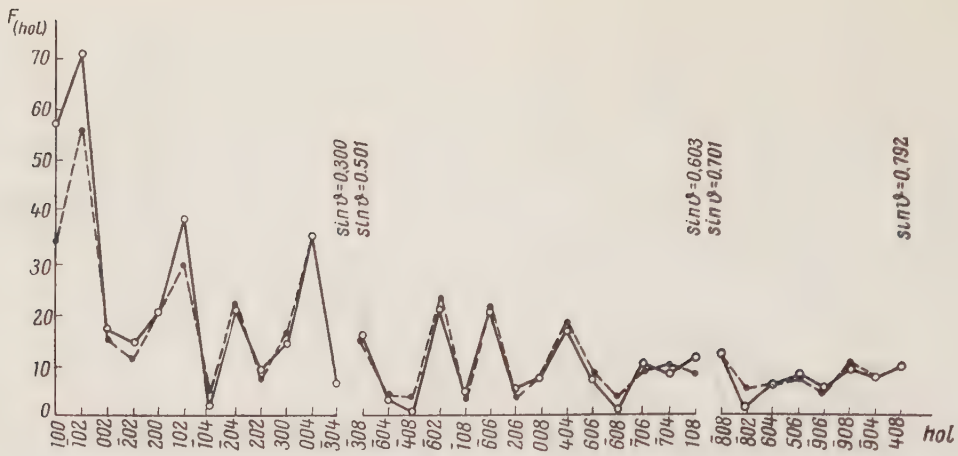

Fig. 6. Comparison of the experimental and calculated structural amplitudes of the h0l type for some regions of $\sin\theta$ in indigo. Solid line – calculated; dashed line – experimental.

Less conjugation in the heterocyclic ring was observed in the thioindigo molecule. The interatomic distances between carbon and sulfur (1.81 Å) show that the C_1-S and $S-C_8$ bonds cannot be considered to be intermediate between single and double. The sulfur atom either plays no part or plays a negligible part in the π-bond interaction.

The N...O distance within the indigo molecule is 2.94 Å, i.e., approximately equal to the sum of the intermolecular radii of nitrogen and oxygen. The position of the hydrogen atom in the iminio group, like those of the other hydrogen atoms, was not determined. But, to judge from the distance between the oxygen and nitrogen atoms, and from the relative position of imino and carbonyl groups, there are no internal hydrogen bonds in the indigo molecule, or in any case they are very weak. This conclusion is confirmed by a study of the vibrational absorption spectra of indigo, its tetrahalogenoderivatives, and thioindigo [14].

In the indigo crystal, each nitrogen atom is at a distance of 2.88 Å from an oxygen atom in the neighboring molecule, related by a glide plane. This indicates the existence of intermolecular hydrogen bonds between the imino and carbonyl groups of indigo molecules. Each molecule is linked by hydrogen bonds to four neighboring molecules. Therefore, bonds appear between all molecules whose centers of symmetry lie on the same plane perpendicular to the *a* axis of the crystal. It is natural that all these hydrogen bonds in the indigo crystal should increase its thermal stability. It may also explain the higher melting point of indigo (390-392°) relative to thioindigo (288°).

Some authors have observed in x-ray structural studies of molecular crystals that the heights of the electron-density maximum for the same atom depends on its position in the molecule [15, 16]. A similar phenomenon was observed in this study of indigo and thioindigo. The electron density at maxima decreased steadily as the atom was moved away from the center to the periphery of the molecule. The maximum difference in heights of maxima was 17% in indigo and 28% in thioindigo. The difference in heights of maxima of atoms at equal distances from the center of the molecule did not exceed 3% of the average for thioindigo and 5% for indigo. It may be suggested that the decrease in electron density from the center to the periphery of the molecules observed in the x-ray study of indigo and thioindigo crystals is connected with thermal vibrations of the whole molecule about the center of gravity.

The further the atoms from the center of the molecule, the greater their limits of vibration and the greater the blurring of the electron density. In the indigo crystal in which the molecules are linked by hydrogen bonds, thermal vibration may not be as strong as in thioindigo and, therefore, the decrease in the height of electron-density maxima is not so great for indigo.

On the basis of the x-ray structural study, it can be concluded that if cis isomers of indigo and thioindigo exist, the distance between oxygen atoms in their molecules would be about 2.0-2.1 Å. Such short distances between nonbonded atoms with the same excess charge cannot exist in molecules. For there to be larger distances between the oxygen atoms in the cis isomers, there would have to be strong distortion of the bonding angles or destruction of the coplanarity of the molecule, and this is energetically unsuitable. This may be the cause

of the lack of geometrical isomers in indigo and thioindigo. Recently, Brode, Pearson, and Wiman [7] reported the preparation of the cis isomer of thioindigo and some of its derivatives, but the results of their study are not completely unambiguous.

LITERATURE CITED

1. A. Baeyer, Ber., 33, Sonderheft, 51 (1950).
2. R. Kuhn, Naturwiss., 20, 618 (1932).
3. H. Hodgson, J. Soc. Dyers Colourists, 62, 176 (1946).
4. N. S. Dokunikhin and É. S. Levin, DAN SSSR, 35, 120 (1942).
5. N. S. Dokunikhin, Collection: Proceedings, Seventh Conference on the Chemistry and Technology of Aniline Dyes [in Russian] (Izd. AN SSSR, 1950), p. 121.
6. R. Gill and H. Stonchill, J. Soc. Dyers Colourists, 60, 183 (1944).
7. W. Brode, E. Pearson, and G. Wiman, J. Am. Chem. Soc., 76, 1034 (1954).
8. H. Eller, Compt. rend. Acad. Sci., 238, 1894 (1954); 239, 975 (1954).
9. S. Sheppard, P. Newsome, and H. Brigham, J. Am. Chem. Soc., 64, 2937 (1942).
10. V. A. Izmail'skii, Proceedings, Fourth Conference on the Chemistry and Technology of Aniline Dyes [in Russian](Izd. AN SSSR, 1941), p. 41.
11. V. A. Izmail'skii, Proceedings, Eighth Conference on the Chemistry and Technology of Aniline Dyes [in Russian] (Izd. AN SSSR, 1950), p. 108.
12. H. Eller, Compt. rend., Acad. Sci., 5, 142 (1952).
13. E. A. Gribova, DAN SSSR, 102, 279 (1955).
14. D. N. Shigorin, N. S. Dokunikhin, and E. A. Gribova, Zhur. Fiz. Khim., 21, 874 (1955).
15. G. Jeffrey, Ann. Reports, 40, 92 (1943).
16. G. Goldschmidt and F. Glewellyn, Acta Cryst. 3, 294 (1950).

X-RAY STRUCTURAL STUDY OF A METHYLENE BLUE DYE

G. S. Zhdanov, Z. V. Zvonkova, and L. G. Vorontsova

L. Ya. Karpov Physicochemical Institute

Translated from Kristallografiya, Vol. 1, No. 1,
pp. 61-65, January-February, 1956
Original article submitted October 10, 1955

The lattice parameters of methylene blue $[C_{16}H_{18}N_3S]^+Cl^- \cdot nH_2O$ have been refined to $a = 9.68_6$, $b = 31.86_9$, $c = 7.07_4$ Å, and $\beta = 97°11'$. An electron-density projection on the plane (001) has been constructed from F^2-series data and by isomorphous replacement of the chlorine atom by bromine. From this the ionic structure of methylene blue has been confirmed and it has been established that the atom of the cation closest to halogen is a sulfur atom.

The structures of dyes have seldom been studied. A systematic x-ray structural study would be of considerable interest for the elucidation of the relation between structure and properties of dyes.

In the present work, we have studied by x-ray methods the structure of the thiazine dye, methylene blue, which is much used in practice.

In x-ray and physicochemical papers, two forms of the formula have been suggested:

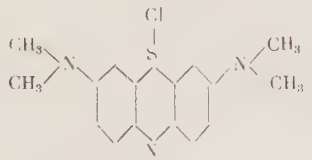

and

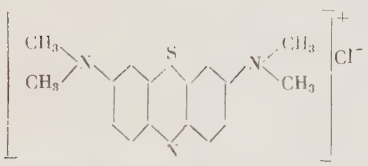

Absorption spectroscopic studies favor the ionic structure [1]. In this paper it was suggested that on hydrolysis the OH^- group became attached to the central nitrogen atom of the molecule and the H^+ to a nitrogen atom of an amino group. The charge localization in the complex ion was not established. In many chemical papers it has been suggested that the positive charge is averaged over the three nitrogen atoms.

Taylor [2] has carried out x-ray and optical studies of the methylene blue chloride, bromide, and iodide, and for the selenium-substituted bromide. He established that all the crystals except the iodide were twins. The twinning plane was parallel to the direction of elongation of the crystal. Taylor's data are cited in Table 1. They establish that the chloride, bromide, and selenium-substituted bromide are isomorphous.

Structure determination was carried out only for the iodide I, and this was by trial and error. The projection of the structure of iodide I on the (001) plane is shown in Fig. 1. The figures represent atomic coordinates along the Z axis.

All the atoms of the complex ion $[C_{16}H_{18}SN_3]^+$ lie in a single plane and the ions are associated in chains. The chains are distributed in layers parallel to the plane $(0\bar{1}2)$ and at a distance 3.45 Å apart. Taylor suggested that all the compounds in Table 1 were isostructural, i.e., they had a layer structure and consisted of the ions $[C_{16}H_{18}N_3S]^+$ with the methyl groups as points of contact. The nearest neighbors of the halogen atoms are the methyl groups and the water molecules.

To elucidate the structure of the methylene blue dye $[C_{16}H_{18}N_3S]^+Cl^- \cdot nH_2O$, we determined the structure by the electron-density series method. The dye crystals were obtained from the colorimetry laboratory of the Scientific Research Institute

TABLE 1.

Substance	a	b in A	c	α°	β°	γ°	z, No. of mol. H_2O	Class	Space group	σ_n
Chloride	9.5	31.3	6.9	90	97	90	4	Monoclinic	$C_{2h}^5-P2_1/c$	1.29
Bromide	9.7	31.5	6.9	90	97	90	5	Monoclinic	$C_{2h}^5-P2_1/c$	1.41
Iodide I	16.9	15.8	6.9	98	95	89	3	Triclinic	$C_1^1-P\bar{1}$	1.68
Iodide II	14.8	15.7	7.6	98	98	90	1	Triclinic/ monoclinic	Not deter.	1.64
Seleno-bromide	9.65	31.5	7.0	90	97	90	5	Monoclinic	$C_{2h}^5-P2_1/c$	1.57

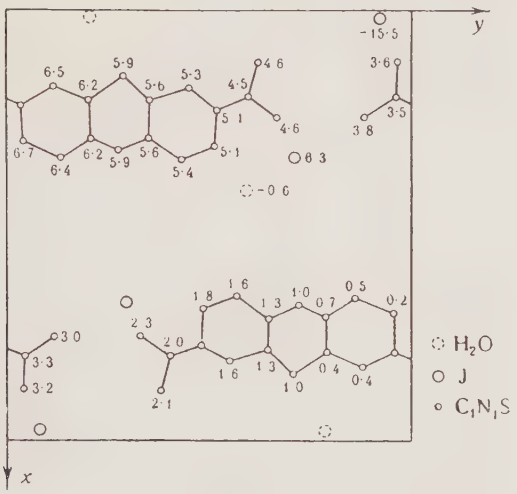

Fig. 1.

for Organic Semifinished Materials and Dyes. Several recrystallizations were carried out by V. P. Glushkova to obtain the best x-ray quality. X-ray photographs were taken of the industrial and recrystallized products.

The crystals were deep blue needles with a bronze metallic luster, 1-2 mm long, and 0.2-0.3 mm in thickness. The crystals were very brittle, and most appeared as fragments of needles.

Refinement of the lattice constants was carried out from an x-ray oscillation photograph taken on an RKU camera constructed by M. M. Umanskii. The following values were obtained: $a = 9.68_6$, $b = 31.86_9$, $c = 7.07_4$ Å, $\beta = 97°11'$. The photograph was indexed in terms of the space group $C_{2h}^5 = P2_1/c$. Ninety-eight reflections were revealed by development of the zero-layer lines relative to the c axis in Cu radiation. Three x-ray photographs with exposures of 18, 36, and 70 h were taken for more precise estimation of the intensities. The intensities were estimated quantitatively by comparison with a standard blackening scale.

Projections of the interatomic vector functions on the planes (001) (Fig. 2) and (100) (Fig. 3) were constructed for methylene blue chloride.

Since the number of atoms in the unit cell is 84 (excluding the hydrogen atoms), there is considerable superposition of maxima in the projection on (001), as was to be expected. The peaks belonging to the heavy Cl and S atoms were revealed, but it was not possible to distinguish between them because of their very similar diffracting power.

The isomorphous replacement of chlorine by bromine was used to find the coordinates of the Cl atoms from the F^2 series. The approximate coordinates of the Cl (Br) and S atoms were determined by a comparison of the peak heights of the interatomic vectors for the chloride and bromide:

$$x_{Cl} = 0.93, \quad y_{Cl} = 0.21,$$

$$x_S = 0.21, \quad y_S = 0.19.$$

The projection of the interatomic vector function on the plane (100) showed that the structure was layered.

These coordinates of the halogen and sulfur atoms permit the determination of the signs of 78

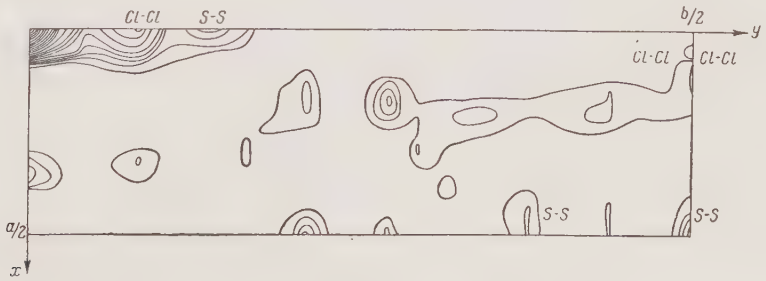

Fig. 2.

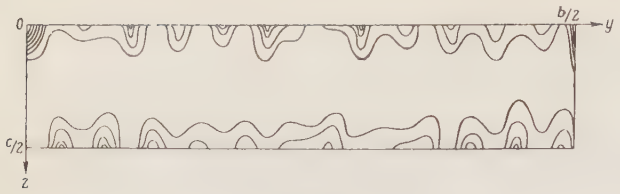

Fig. 3.

structure amplitudes from a comparison with the moduli of the structure amplitudes for the chloride and bromide with uniform (hk0). The electron-density projections were found by using these signs. The electron-density distribution diagram for the $[C_{16}H_{18}N_3S]^+Cl^- \cdot nH_2O$ crystal in the projection of the (001) plane (Fig. 4a) confirmed the Cl and S coordinates found previously from the F^2 series:

Cl (0.94; 0.21),

S (0.23; 0.19),

and allowed some conclusions to be drawn about the molecular structure of methylene blue: the complex ion is extended along the y axis. The distribution of the electron-density maxima corresponding to the projection of this structure model is shown in Fig. 4b. The distribution of regions of negative electron density correspond to the projections of the central "holes" in the benzene and heterocyclic rings. It must be taken into account that severe superposition of maxima occurs, especially in the part of the projection, as a result of projections of molecules from different layers. The false maximum at (x = 0.21, y = 0.25) probably occurs from a break in the series and the probable errors in determining the signs of some of the structural amplitudes.

A geometric analysis was carried out to confirm the structural model. A model of the complex ion $[C_{16}H_{18}N_3S]^+$ (Fig. 5) was constructed from literature values for interatomic and intermolecular radii, taking account of errors arising from the directionality of covalent bonds. The observed electron density distributions (Figs. 4a and 4b) agreed with the data from the geometrical analysis (Fig. 6).

Thus, by the successive use of the following methods: construction of the interatomic vector function, isomorphous replacement, construction of electron-density projections, and geometrical analysis – the principles of the structure of methylene blue were established for the (001) projection.

Analysis of the S–Cl distance even in the approximate model of the structure in the (001) projection, makes possible the conclusion that the S–Cl bond is not covalent, since the closest S–Cl distance, 2.8 Å in projection, is considerably longer than that of a covalent bond (2.03 Å). Consequently, the chemical formula of methylene blue should be given in the form $[C_{16}H_{18}N_3S]^+Cl^- \cdot nH_2O$.

It is also seen from Fig. 5 that the sulfur atom of the cation is closest to the chloride ion, and not the methyl groups as Taylor suggested. This is possibly explained by placement of the positive charge on sulfur. An earlier study of complex metal thiocyanates [3] established that the electron density was redistributed between the sulfur and nitrogen atoms in the covalent SCN group and in the SCN^- ion as a result of which the nitrogen atom had an excess of electron density in comparison with sulfur – $(N^{-\delta_1})$ and $(S^{-\delta_2})$, respectively. A similar

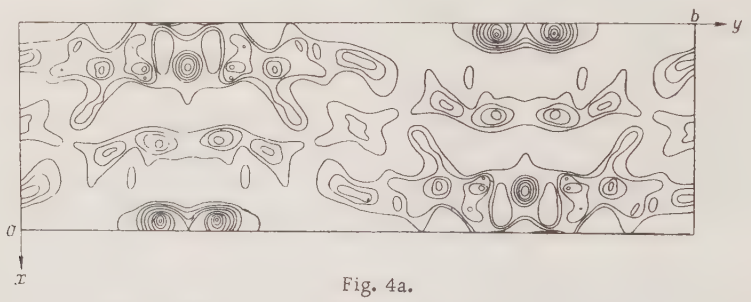

Fig. 4a.

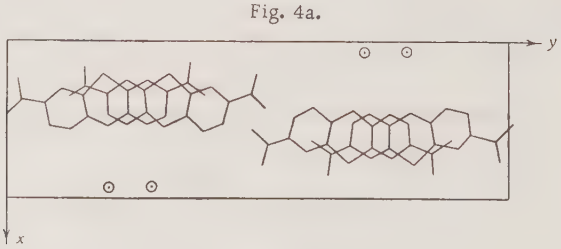

Fig. 4b.

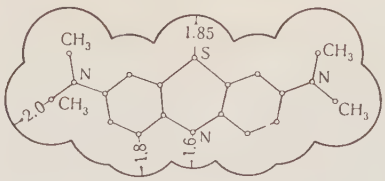

Fig. 5.

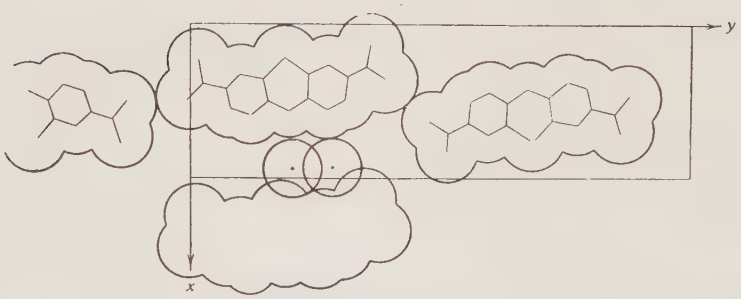

Fig. 6.

redistribution of electron density has also been established in the molecules N_4S_4 and As_4S_4 [4]. Thus our work has not confirmed Taylor's suggestion that methylene blue chloride and iodide are isostructural.

It is possible that the trial-and-error method used by Taylor can lead to an incorrect structural model when applied to a complex model with 75 atomic parameters.

A further study of the structure of $[C_{16}H_{18}N_3S]^+ \cdot Cl^- \cdot nH_2O$ by the construction of a three-dimensional electron-density section will allow for refinement of the interatomic distances and bonding angles, and will reveal more precise details of the structure.

LITERATURE CITED

1. C. F. Davidson, "The determination of methylene blue," J. Textile Inst., 38, 11, 408 (1947).
2. W. H. Taylor, "X-ray determination of methylene blue," Z. Krist., A91, 450-460 (1935).
3. G. S. Zhdanov and Z. V. Zvonkova, "Electron density distributions in crystalline complexes," Zh. Éksperim. i Teor. Fiz., 22, 3 (1952).
4. K. I. Tobelko, Z. V. Zvonkova, and G. S. Zhdanov, "The structure of realgar and the atomic radius of arsenic," DAN SSSR, 96, 4 (1954).

ELECTRON-DIFFRACTION DETERMINATION OF THE STRUCTURE OF IRON CARBIDE Fe_4C

Z. G. Pinsker and S. V. Kaverin

Faculty of Crystallography and X-Ray Diffraction, Gor'kii State University; Gor'kii Physicotechnical-Research Institute; Institute of Crystallography, Academy of Sciences of the USSR

Translated from Kristallografiya, Vol. 1, No. 1, pp. 66-72, January-February, 1956
Original article submitted October 15, 1955

During electron-diffraction study of α-Fe films subjected to cementation at 400 to 480°C in a current of CO or at approximately 650 to 700°C in a current of acetylene, a new cubic carbide of iron with lattice spacing a = 3.878 ± 0.002 Å was observed. Following structural analysis by means of Φ^2 and Φ series, and also minimization of the confidence factor for the new carbide (of probable composition Fe_4C), a structure based on the slightly distorted lattice of α-Fe was established. There was a single "molecule" of Fe_4C in the unit cell. The Fedorov group was T_d^1; 1C in (a): 000; 4Fe in (e): xxz with x = 0.265. The carbon had tetragonal coordination with Fe–C distance 1.78 Å.

Despite the large number of investigations devoted to the structure of the crystal lattices of various interstitial phases, the results obtained are by no means complete. This is especially true of the carbides of iron. It is evidently generally accepted that at temperatures above 721°C austenite is a stable carbide. Below this temperature we know martensite and cementite as metastable phases. The only stable phase in this temperature range is the cubic α solid solution with a negligible carbon content.

However, other carbides of iron undoubtedly exist. Investigations concerning these seem to proceed in two different directions: the study of processes and structure during the tempering of quenched steels, and the structure of iron catalysts used in the synthesis of hydrocarbons. We may take the existence of iron carbides richer in carbon than cementite (Fe_3C) as established. The well-known carbide of Hägg, and also the hexagonal carbide are assigned the composition Fe_2C [1,2,3]. There is also evidence of the existence of a carbide with formula $Fe_{20}C_9$. For the hexagonal carbide we have lattice spacings a = 2.74 and c = 4.32 Å. For the analogous iron nitride Fe_2N, the spacings are a = 2.77 and c = 4.42 Å, which disagrees with the usually given atomic radii: carbon 0.77 and nitrogen 0.71 Å. The incomplete nature of structural data on the carbides of iron is demonstrated by the absence of any indication of lattice spacings for Hägg's carbide, although the list of interplane spacings for reflections ascribed to this phase was first published more than twenty years ago and reproduced in other work. All data on the carbides of iron are usually based on Debye photographs from samples constituting multiphase systems. There are no reliable determinations of the chemical composition of the separate phases. All this is in sharp contrast to the remarkable achievements of structural x-ray diffraction in other fields.

In addition to purely structural results, there are a considerable number of chemical and physicochemical investigations into the interaction of iron and its oxides with CO and H_2 (synthesis of hydrocarbons) which have been reported.[1] Various authors have suggested the possible formation of the following compounds: Fe_4C, Fe_2C, FeC, FeC_2,

[1] Literature indicated in review [4].

Fe_3C, and Fe_4C_3. These results, however, require structural verification.

We note that the structures of long-established carbide phases are also insufficiently well known. In particular, the position of the carbon in the austenite, cementite, and martensite lattices has never been reliably established by direct experimental determination. The data for austenite and martensite are not well founded, since the proportion of x-ray scattering introduced by the carbon atoms is of the same order as the error in measuring (and calculating) the intensities of the diffraction photographs. For cementite, the position of the carbon atoms in the lattice has been established only from geometrical considerations.

The inadequacy of structural data for the carbides of iron, together with the extreme importance of an all-around knowledge of these phases and the difficulties found in x-ray examination, led us to develop a new method of studying them by electron diffraction. After we had obtained experimental data on the new carbide, some other papers were published on the electron-diffraction study of iron–carbide structures, using a completely analogous method. In these papers, however, only the formation of cementite and the hexagonal carbide was mentioned, and no new structural data were presented [5].

In order to obtain iron carbides, we subjected iron films with some degree of orientation to treatment in the gas phase. Treatment in a current of CO or $CO + H_2$ was used, as well as cementation in a current of acetylene.

In developing the method of study, we tried to create conditions favorable toward as detailed as possible a structural examination of the carbide phases formed. Results obtained for the structure of nitrides illustrate the possibilities created by electron-diffraction analysis of films prepared by treating iron in a gaseous medium [6]. The original layers of single-crystal or polycrystalline iron were obtained by condensation from the vapor onto the surface of heated rocksalt crystals. After control photographs were taken of films stripped from the salt crystals, samples of crystals bearing iron films were placed in a furnace for cementation. The carbon monoxide was produced by decomposing formic acid, and was purified and dried. Before passing the carbon monoxide, the system was flushed with pure, dry hydrogen. Interaction with the CO was effected at temperatures from 400 to ~520° for various periods from 5 min to 5 h. Treatment with dry acetylene was effected at 400 to 500° and 650 to 700° for 15 min. Then the carbide films were stripped from the salt crystals in the usual way and placed in the electron-diffraction camera for study. Structural study showed that, apart from oxides of iron formed by oxygen accidentally drawn in from the air, this treatment gave three carbide phases, including cementite and the hexagonal carbide. As regards the third phase, we were able to obtain electron-diffraction photographs containing only the lines of this phase on treatment in a current of CO at 400 and 480°, and also on 15-min treatment in a current of acetylene at 700° (Figs. 1-5). In some samples obtained by treatment with CO, we noted partial orientation. Apart from this, with this treatment we obtained some films containing completely nonoriented crystals of the new phase. We must assume that the degree of orientation of the

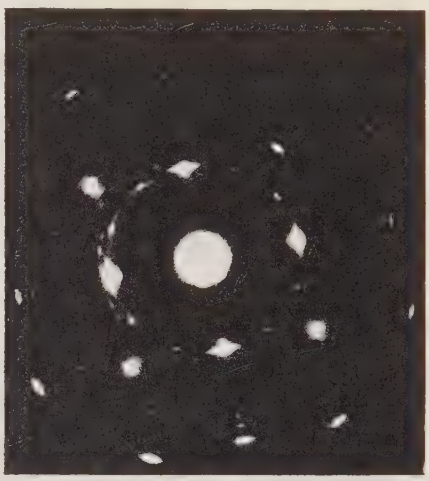

Fig. 1. Electron-diffraction photograph of a two-phase film containing Fe_4C (mosaic single crystal) and oriented cementite.

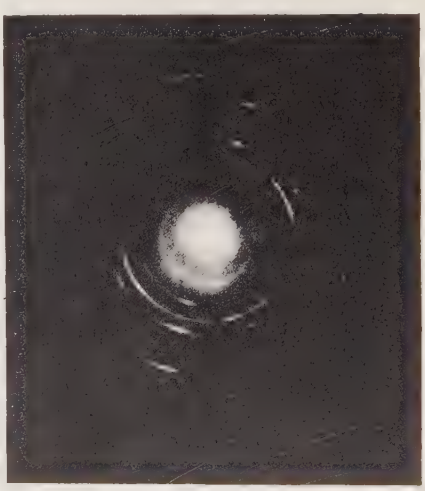

Fig. 2. Electron-diffraction photograph of a partly oriented film of the carbide Fe_4C.

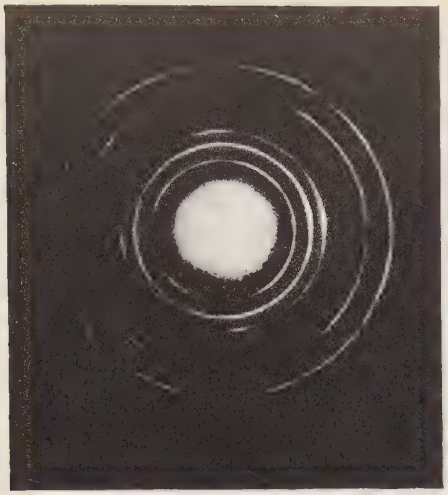

Fig. 3. Electron-diffraction photograph of a partly oriented film of the carbide Fe_4C.

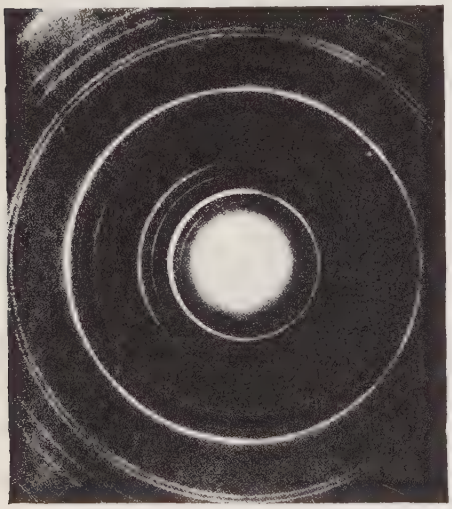

Fig. 4. Electron-diffraction photograph of a polycrystalline film of Fe_4C containing NaCl lines.

samples does not depend on the composition of the cementing gas, but is determined by the structure of the original iron film and various other factors.

Electron-diffraction photographs of the new phase clearly demonstrate its cubic symmetry. The network of reflections observable in the diffraction picture, where the main pattern appertains to Fe_3O_4, is immediately indexed by means of indices hk0. The electron-diffraction photographs of Figs. 2 and 3, with partial orientation of the scattering crystallites, show texture typical of cubic phases: the directions [111], [110], and – to a smaller extent – [100] lie perpendicular to the plane of the film.

In determining the lattice spacing of the new phase, we used electron-diffraction photographs

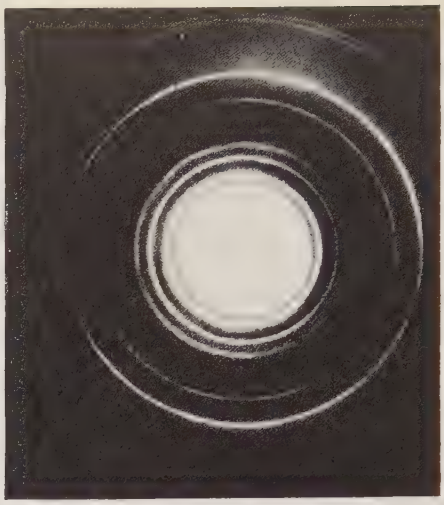

Fig. 5. Electron-diffraction photograph of a polycrystalline film of Fe_4C; reflections from NaCl are noticeable in the form of spotty lines.

containing NaCl lines as well as those of the new phase itself. The lattice spacing proved to be $a = 3.878 \pm 0.002$ Å. An extremely important result is the constancy of this quantity on determining the lattice spacing of the new phase in a series of experiments carried out under different conditions over a number of years.

The experimental intensities of the electron-diffraction photographs were estimated on the well-known ten-point scale.

Electron-diffraction photographs obtained in the series of experiments using carbon monoxide (Figs. 2 and 3) correspond to partly oriented samples. The diffraction pattern is formed by the superposition of more intense arcs on the continuous Debye ring. Fairly perfect orientation of the crystallites produced short arcs, and on all the rings (though less so for planes with a large recurrence factor), the sections between the intense arcs could be used for estimating intensities. Error in intensity measurement is nevertheless increased by these features of the diffraction pictures.

The electron-diffraction photographs of the nonoriented polycrystalline specimens (Figs. 4 and 5) obtained in experiments with acetylene also proved unsuitable for exact intensity measurements. In some photographs the superposition of NaCl lines caused confusion; in others, there was serious fogging. It should be noted that, in order to determine the position of the light carbon atoms in the presence of iron (especially for composition Fe_4C), microphotometer intensity measurements are required if precise results and good agreement between theory and experiment are to be achieved.

Our Fourier synthesis based on experimental Φ^2 and Φ values has the advantage of being less sensitive to the accuracy of intensity measurements. Table 1 shows the corresponding averaged data obtained by using a large number of electron-diffraction photographs.

Considering the data of Table 1, we may conclude that our carbide has a lattice based on γ iron. In favor of this supposition is the value of the lattice spacing a = 3.878 Å, which is in reasonable agreement with those of austenite (3.62 Å) and the γ phase of Fe_4N (3.79 Å). We also note that reflections with nonmixed indices in general have greater intensities than the rest. We calculated one-dimensional sections of the Φ^2 series along the [110] and [111] directions. The first section gave a quite definite result: a strong maximum in the center of the face. As regards the second, in the [111] direction there was a slight maximum near the center of the octant ($\frac{1}{4}$ $\frac{1}{4}$ $\frac{1}{4}$).

The sensitivity of the Φ^2 function was insufficient to fix the coordinates of the end of the Fe–C vector reliably.

It should be noted that the data presented do not contradict a lattice of three iron atoms in the unit cell, disposed in the centers of the faces, which corresponds, for example, to the group $O^1(c)$. Considering the possible composition and structure of the carbide on the basis of such a lattice with a carbon atom at the vertex of the cube, we arrive at the extremely unlikely Fe–C distance of 2.74 Å. Hence, without further investigation, considering this lattice as extremely loose, we reject this variant.

Just as improbable is the structure on the α-Fe basis.

Turning to the possible distribution of the carbon atoms in the fcc lattice of iron, and to the composition of the present carbide, we must also reject the simplest solution: a carbon atom in the octahedral position (center of the cell). Such a structure should give extremely weak reflections with mixed indices, rapidly diminishing with increasing hk$l$; here, the scattering power $4f_{Fe} \pm f_C$ compares with f_C. The fairly large intensity of reflections with mixed indices compels us to relinquish this model. We note furthermore that the considerable intensity of the 110 and 210 reflections may be determined by the considerable scattering power of carbon at low angles.

It is clear that, on placing one carbon atom in a tetrahedral vacancy, we should expect a similar scattering picture.

TABLE 1. Experimental Electron-Diffraction Data for the Carbide Fe_4C

hkl	d_{hkl} in Å	$\Phi_{exp} = \sqrt{I_{exp}/pd^2}$	hkl	d_{hkl} in Å	$\Phi_{exp} = \sqrt{I_{exp}/pd^2}$
100	3.875	4.8	422	0.79	17.1
110	2.74	11.1	430	0.775	2.4
111	2.237	34.5	500	0.775	3.7
200	1.935	24.6	431	0.76	2.3
210	1.732	4.7	333	0.746	12.8
211	1.58	7.3	511	0.746	12.1
220	1.37	25.6	520	0.72	2.6
300	1.29	5.8	521	0.708	1.8
221	1.29	2.3	440	0.685	9.2
310	1.224	3.7	522	0.675	1.9
311	1.169	20.3	441	0.675	1.9
222	1.118	10.1	530	0.665	1.9
230	1.074	3.4	433	0.665	1.9
231	1.035	3.7	531	0.655	6.8
400	0.968	9.4	600	0.646	8.9
410	0.94	0	442	0.646	9.1
322	0.94	4.7	611	0.627	4.6
411	0.913	3.9	620	0.612	7.6
330	0.913	3.2	533	0.85	6.0
331	0.888	17.3	622	0.583	5.0
420	0.866	13.9			
421	0.845	3.0			
332	0.8255	4.8			

Is it possible to have a number of carbon atoms greater than unity in the unit cell? The symmetry of the cubic groups T_h^1, T_d^1, O^1, and O_h^1 admits placing three carbon atoms in octahedral vacancies (centers of edges). In this case, however, the reflections with unmixed indices are strengthened, while the others will again be determined by the scattering of only one carbon atom. Clearly, by placing four carbon atoms in octahedral vacancies, we obtain an NaCl-type lattice with corresponding extinctions.

The only solution which we can suggest is based on the fact that the iron atoms also take part in the formation of reflections with mixed indices, which is possible with a slight rearrangement of the ideal fcc lattice. This rearrangement may be called the "implantation" of a carbon atom into a tetrahedral vacancy, since, for a period $a \approx 3.88$ Å the distance from the center of an iron atom to the center of the nearest tetrahedron is 1.675 Å. Thus we find a carbide of composition Fe_4C with carbon in a tetrahedron and four iron atoms displaced from the ideal positions along the space diagonals. This structure is described by group T_d^1. The carbon is in (a): 000 and the iron in (e): xxx. In order to check this model and determine the value of x, we examined the Φ series from the experimental structure amplitudes. The model proposed has no center of symmetry; hence, calculation of the three-dimensional series requires knowing the phases of the structure amplitudes. So as not to introduce a substantial arbitrary element into the calculation in

view of the sensitivity of the phase values to the parameter taken for iron, we decided to limit the investigation to the centrosymmetrical projection of the structure on the cube face.

In calculating the theoretical structure amplitudes, we met some indeterminacy of the data for the scattering power of the carbon atoms. In fact, the literature contains no less than four tables for f_p^C, calculated by different authors. Table 2 gives the corresponding values of the atomic amplitudes for electrons. The most serious discrepancies occur for small angles of reflection. We note that this fact introduces difficulty into accounting for the cation or anion state of the carbon atom in calculating the theoretical Φ. In calculating Φ, we used the values II in Table 2. As calculation of the structure amplitudes showed, the signs of Φ_{hkl}, except for two weak reflections, did not vary over a wide range of values of the parameter x. Figure 6, representing the projection of the lattice potential of our carbide on the cube face, gives an unequivocal solution for its structure; the four maxima near the centers of the quadrants correspond to iron atoms, and the maxima in the vertices of the cell to carbon (Fig. 7). The parameter x for the iron atoms, as determined from this projection, is 0.26. By using the method of minimizing the confidence factor $R = \sum \| \Phi_E | - | \Phi_T \| / \sum | \Phi_E |$ we established that the most probable value was 0.265. For this, the R is quite large (0.28), which of course is chiefly due to insufficient accuracy in estimating the experimental reflection intensities. The overall picture of the relation between theoretical and experimental structure amplitudes is shown in Fig. 8.

For the parameter value in question, the minimum Fe–C distance in the lattice is 1.78 Å, for the "average" distance in austenite 1.81 Å, and for cementite, 1.86 Å. The small Fe–C distance and the tetrahedral coordination of the carbon atom in

Fig. 6. Projection of the potential of the Fe_4C lattice on the cube face, calculated from experimental Φ values.

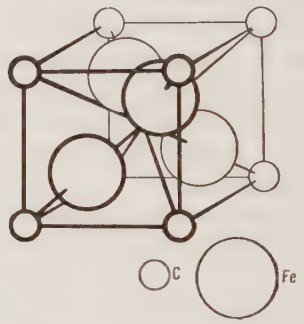

Fig. 7. Structure of the carbide Fe_4C.

TABLE 2. Atomic Scattering Amplitudes of Electrons by Carbon $f = (Z - f_p)d^2$ from Various Data

$\sin\vartheta/\lambda \cdot 10^8$	0.0	0.05	0.7	0.15	0.20	0.25	0.30	0.40	0.50	0.60	0.70	0.80	0.90	1.00
		10	5	3.33	2.5	2	1.67	1.25	1.00	0.833	0.714	0.625	0.555	0.500
I *	52		35		18.75		10.55	6.40	4.30	3.06	2.34	1.84	1.49	1.25
II **	23.8	21.9	19.9	16.8	14.9	12.2	9.7	6.54	4.5	3.10	2.35	1.84	1.49	1.25
III ***		80	60	41	25.5	17.2	12.2	7.22	4.83					
IV ****		23.6	21.5	18.05	14.9	12.0	9.65	6.26	4.29	3.10				

*X-ray amplitudes by Hartree. Internationale Tabellen z. Bestimmung v. Kristallstrukturen. No. II, 571 (1935).

**Taken from tables of V. K. Vainshtein. "Atomic scattering factors of electrons," ZhÉTF, 25, 2, 157-168 (1953).

***X-ray amplitudes by MacWeeny. "X-ray scattering of aggregates of bound atoms," Acta Cryst., 7, 2, 180-186 (1954).

****X-ray amplitudes by I. Berghuis, I. Iberta, et al., "New calculations of atomic scattering factors," Acta Cryst., 8, 8, 478-483 (1955).

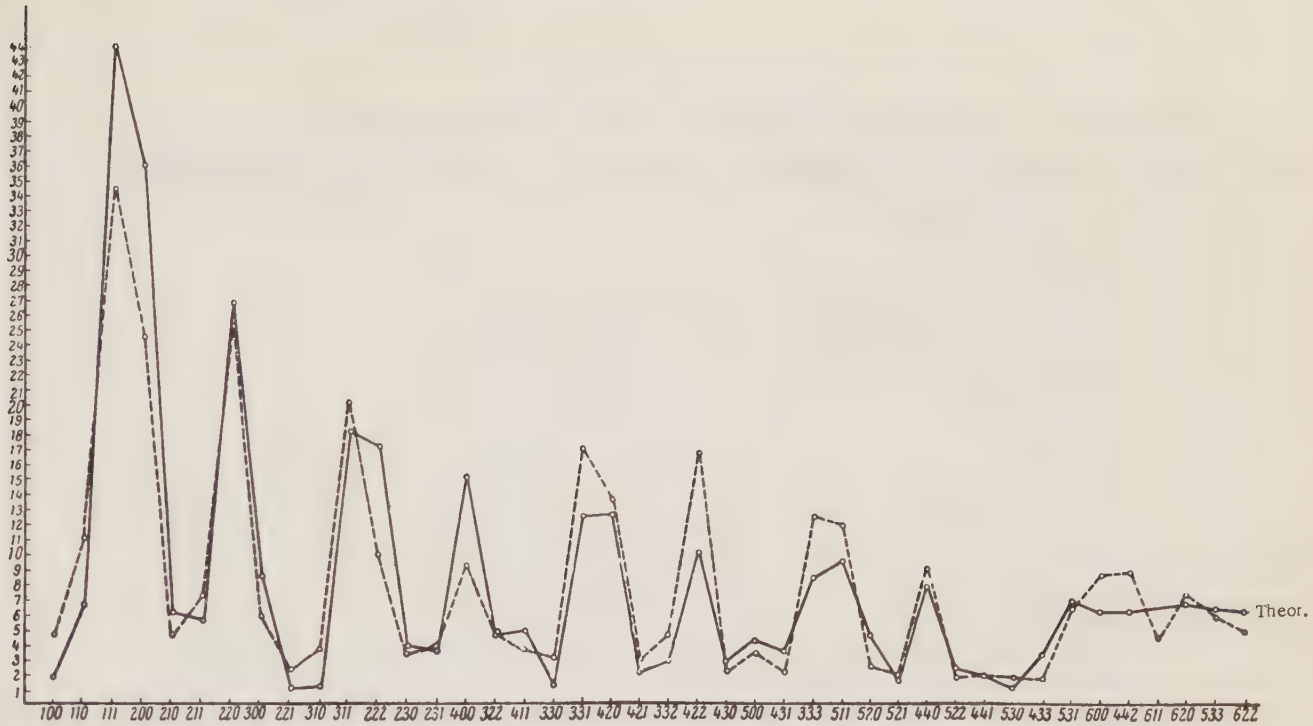

Fig. 8. Relation between theoretical and experimental structure amplitudes.

the lattice possibly indicate that this carbide is a chemical compound and distinguish it from solid solutions such as austenite. This hypothesis is also supported by the constancy of the lattice spacing of the carbide Fe_4C, which indicates a constant composition.

In conclusion, we express thanks to former graduate students of Gor'kii State University, E. Krasotskaya, M. Grinberg, and G. Pinsker, and also to ourco-workerat the Gor'kii Physicotechnical-Research Institute at the University, N. V. Gudkova, who took part in obtaining the experimental material. We also express thanks to E. L. Lapidus, who carried out a large part of the computing work.

LITERATURE CITED

1. M. P. Arbuzov, "On the crystal structure and particle size of the carbide phase of tempered steel," DAN SSSR, 73, 1, 83-86; Ibid., bibliog. of papers by G. V. Kurdyumov and colleagues.
2. I. T. McCartney, L. I. E. Hofer, B. Seligman, J. A. Lecky, W. S. Peebles, and R. B. Anderson, "Electron-diffraction and x-ray study of iron catalysts," J. Phys. Chem., 57, 7, 730-736 (1953); Ibid., bibliog. of papers on questions of the production, treatment, and structure of catalysts.
3. K. H. Jack, "Results of further x-ray studies of the Fe–C and Fe–N systems and corresponding interstitial alloys," Acta Cryst., 3, 392-393 (1950).
4. O. A. Esin and P. V. Gel'd, "Forms of existence of metalloids dissolved in metal," Usp. khimii, 22, 1, 62 (1953).
5. J. J. Trillat and S. Oketani, "Orientation relationships between cementite and α-iron," Acta cryst., 5, 469-471 (1952); J. J. Trillat and N. Takahashi, "Recent achievements in the diffraction of electrons and their use," J. phys. et radium, 14, 5, 17S-18S (1953).
6. Z. G. Pinsker and S. V. Kaverin, "Electron-diffraction study of the structure of the cubic nitride of iron," DAN SSSR, 95, 4, 797-799 (1954); "Electron-diffraction study of the structure of the hexagonal nitrides of iron," DAN SSSR, 96, 3, 519-522 (1954).

A CRYSTALLOCHEMICAL STUDY OF THE NATURE OF THE DONOR–ACCEPTOR BONDS IN BORON COMPLEXES

Z. V. Zvonkova

L. Ya. Karpov Physicochemical Institute

Translated from Kristallografiya, Vol. 1, No. 1,
pp. 73-80, January-February, 1956
Original article submitted October 10, 1955

The crystal structure of the boron trifluoride pyridine complex has been determined. The parameters of the monoclinic lattice are: $a = 17.71$, $b = 5.89$, $c = 14.34$ Å; $\beta = 118°42'$. The number of molecules per unit cell was $z = 8$. The space group was $C_{2h}^5 - P2_1/c$. The method of statistical equalities was used to determine the signs of the structure amplitudes and also the method of three-dimensional electron-density sections. The interatomic distances found for the compound $F_3B \rightarrow NC_5H_5$ were: B–F, 1.41; B–N, 1.53; F–F, 2.30; N–C, 1.36; C–C, 1.39 Å, and the bond angles were $\sphericalangle FBF = 109.5°$, $\sphericalangle NBF = 108.5°$, $\sphericalangle C_1NC_2 = 117.5°$, $\sphericalangle NC_1C_3 = 123°$, $\sphericalangle C_1C_3C_5 = 119°$, $\sphericalangle C_3C_5C_4 = 118.5°$. The crystallochemical theory of donor–acceptor bonds is discussed.

There are many important theoretical and practical problems in the field of physical chemistry for crystallochemical study. One of the central problems of chemical bonding theory is the elucidation of the nature of donor–acceptor bonds in complex compounds. The theoretical side of this problem provides for an explanation of the part played by the unshared pairs of atoms in molecule formation and the discovery of the nature of the chemical bond formed between the donor and acceptor molecules. The practical side is connected with broad problems of synthesizing materials with a variety of technological properties.

The object of x-ray structural study in the present work was the crystalline complex formed from boron trifluoride and pyridine, $F_3B \leftarrow NC_5H_5$. Boron trifluoride and its derivatives are very important catalysts which have been studied vigorously of late. It is sufficient to mention that there are more than a thousand papers and monographs on the study of these compounds [1,2]. Of the x-ray structural studies, those of Hoard and his coworkers must be noted first. They studied $F_3B \leftarrow NH_3$, $F_3B \leftarrow NH_2CH_3$, $F_3B \leftarrow N(CH_3)_3$, and $F_3B \leftarrow NCCH_3$. They cited the results of their studies in a review [3] as interatomic distances and bond angles (Table 1).

TABLE 1

Interatomic distances and bond angles	$F_3B \leftarrow NH_3$	$F_3B \leftarrow NH_2CH_3$	$F_3B \leftarrow N(CH_3)_3$	$F_3B \leftarrow NCCH_3$
N — B	1.60	1.57	1.585	1.635
B — F	1.38	1.39	1.39	1.33
F — F	2.27	2.27	2.24	2.23
N — F	2.40	2.40	2.46	2.34
N — CH_3	—	1.50	1.50	—
∠ FBF	111°	110.5°	107°	114°
∠ FBN	107°	108.5°	112°	103°
∠ BNC	—	114°	105°	—
∠ CNC	—	—	114°	—
∠ CNB	—	114°	105°	—

It is known that the nitrogen atom is found in molecules in three basic valence states: (1) three σ bonds $\diagup\!\!\diagdown\!\!-$, e.g., ammonia, NH_3; (2) two σ and one π bond $\diagup\!\!\diagdown\!\!=$, e.g., pyridine, NC_5H_5; and, (3) one σ and 2 π bonds, $N\equiv$, e.g., methyl cyanide, CH_3CN. The crystalline compounds studied by Hoard contain nitrogen atoms in the first and third valence states. The current data on the dissociation energy of the compounds $F_3B-NC_5H_5$, 50.6 kcal [4], $F_3B \leftarrow N(CH_3)_3$, 28 kcal; and $F_3B \leftarrow NH_3$, 17 ± 10 kcal, and the energy of formation of the crystalline compounds $F_3B \leftarrow NCCH_3$, 26.5 kcal, $F_3B \leftarrow NH_2CH_3$, 42.7 kcal, and $F_3B \leftarrow NH_3$, 42 kcal, indicate that the greatest effect of the donor–ac-

TABLE 2

Formula	System	a in Å	b in Å	c in Å	$\beta°$	σ_x	σ_n	z	Space group
$F_3B \leftarrow NC_5H_5$	monoclinic	17,71	5.89	14.34	118°42′	1.49	1.48	8	$C_{2h}^5 - P2_1/c$

ceptor bond is observed for the second valence state of nitrogen. It was therefore of interest for crystallochemical correlations to study the structure of $F_3B \leftarrow NC_5H_5$.

The crystals were protected against moisture while the x-ray photographs were taken by covering with a thin layer of paraffin. The results of determining the crystal class, the lattice parameters, the number of particles per unit cell, the x-ray and pycnometric densities, and the space group of crystals of $F_3B \leftarrow NC_5H_5$ are cited in Table 2.

This structure is complex to decipher because the general position 4(e) of the space group $C_{2h}^5 - P2_1/c$ is doubly occupied by atoms of the molecule. It is therefore necessary to determine the parameters of 60 atoms (excluding hydrogen atoms). However, the determination of this structure is also essential for the extension to the pyridine ring of the previously established shortening of the intermolecular radius of the hydrogen in the benzene ring to 0.74 Å in the structure of $[ClTlC_6H_5]Cl$. It can be postulated that this effect facilitates the close similarity of the b axis of the monoclinic unit cells of $[ClTlC_6H_5]Cl$ (b = 5.77 Å) and $F_3B \leftarrow NC_5H_5$ (b = = 5.89 Å].

The direct method of statistical equalities, which we have used before [6], was used to determine the signs of the structure amplitudes. The methodology for the decipherment of the $F_3B \leftarrow NC_5H_5$ structure was described at the Fifth All-Union Conference on X-Ray Crystallography. Two electron-density projections were constructed on the planes (010) and (100). Further refinement of the structure was carried out from sections of the three-dimensional electron density constructed for k = 0, 1, 2, and 3. To construct the three-dimensional series, 890 experimental structure amplitudes were used. These were taken from films of crystals obtained on the RGNS x-ray goniometer constructed by M. M. Umanskii.

The coordinates of the atoms of two molecules are given in Table 3. Two projections of the interatomic bonds in the compound $F_3B \leftarrow NC_5H_5$ are shown in Figs. 1 and 2. The positions of the molecules in the unit cell are shown in Fig. 3 in a projection on the (010) plane. The average interatomic distances in the structure are:

B–F, 1.41; B–N, 1.53; F–F, 2.30 Å;
N–C, 1.36; C–C, 1.39 Å.

TABLE 3

Atom	x'	z'	x''	z''	y''''
N	0.125	0,320	0.379	0.254	0.079
C_1	0.122	0.274	0.377	0.208	0.878
C_2	0.122	0.266	0.377	0.200	0.269
C_3	0,116	0.177	0.371	0.111	0.873
C_4	0.116	0.169	0.371	0.103	0.279
C_5	0.113	0.122	0.368	0.056	0.054
	0.130	0.427	0,385	0.361	0.093
F_1	0.175	0.487	0.430	0.421	0.902
F_2	0.175	0.479	0.430	0.413	0.292
F_3	0.045	0.409	0.300	0.343	0.097

The precision of determination of the interatomic distances is 0.01-0.02 Å, which can be seen from the coincidence of the results of the independent determination of interatomic distances in two molecules. The bond angles are: ∢ FBF = 109.5°, ∢ NBF = 108.5°; ∢ C_1NC_2 = 117.5°; ∢ NC_1C_3 = 123°; ∢ $C_1C_3C_5$ = 119°; ∢ $C_3C_5C_4$ = 118.5°.

In a much earlier electron-diffraction study of the pyridine molecule by Schomaker and Pauling, the bond angles were assumed to be approximately 120°. The deformation of the bond angles in the pyridine molecule which has now been established for $F_3B \leftarrow NC_5H_5$ is in accord with radiospectroscopic data on the structure of pyridine [7].

The large value of the structure amplitude with the index (400) is caused by superposition of the pyridine rings at approximately x = 1/8 and 3/8. Refinement of the atomic coordinates shows that the planes of the pyridine rings of both molecules make an angle of 4° with the (100) plane. This circumstance leads to the same values of the coordinates for the two molecules, because both intermolecular $F_2 - H_5$ distances correspond to the sum of the F and H radii. The construction of sections of the electron density at different heights shows that the lines along which the atoms $B_1N_1C_5$ and H_5 are distributed make an angle of 3° with the (010) plane. The closest intermolecular distances are: $F_3' - C_3'$ = 2.95 Å; $F_3'' - C_2'$ = 2.96 Å, and $F_2' - C_3''$ = 3.04 Å (primes and double primes are used to differentiate between the two systems of molecules). The variation in these distances is determined by the B–F–C bond angles, so that the values of the interatomic radii depend on mutual orientation of the covalent bonds in the molecules [5]. The plane of the pyridine ring is perpendicular to the plane (010). They are precluded from being angled because of the short distances $F_3' - C_3'$, $F_3'' - C_2'$, and $F_2 - H_5$.

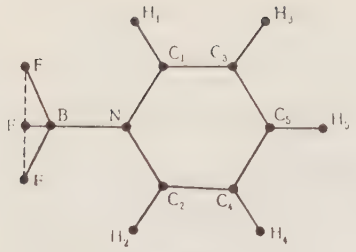

Fig. 1.

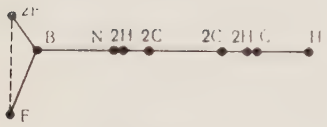

Fig. 2.

An experimental value of the intermolecular fluorine radius (r_F = 1.34 Å) was calculated from the intermolecular distance $F_I'' - F_I'$. Belov and Bokii [8] give an ionic radius of fluorine r_F = 1.33 Å, while Pauling gives an intermolecular radius r_F = 1.35 Å [9].

A considerable shortening of the intermolecular hydrogen atomic radius r_H = 0.80 Å occurs in the structure of $F_3B \leftarrow NC_5H_5$ from the H–H distance of molecules from neighboring unit cells. This effect confirms calculations of the intermolecular radius r_H = 0.74 Å in the phenyl ring of [ClTl–C_6H_5]Cl. The occurrence of this effect in different structures indicates that the basic reason for the shortening of the intermolecular hydrogen radius is the covalent nature of the C–H bond [5] and not thermal vibrations of the atoms in the crystals, as was proposed by Cochrane. It is interesting that the hydrogen radius in the water molecule, as determined by nuclear resonance [10], is 0.78 Å.

The accumulation of a large quantity of data on crystallochemical intermolecular atomic radii shows the necessity for constructing new data tables of intermolecular distances containing maximum and minimum values of the radii, i.e., values of the radii along the direction of the covalent bond and at right angles to this.

It is possible that the presence of H–H and F–F contacts in the structure cause the low melting point (t = 45°).

To judge from the interatomic distances and the energies of formation, the strength of the donor-acceptor bonds increases in the series $F_3B \leftarrow NCCH_3$, $F_3B \leftarrow NH_3$, $F_3B \leftarrow NC_5H_5$. This indicates that the asymmetry and elongation of the unshared pair of electrons on the nitrogen atom is much greater in pyridine than in methyl cyanide.

The widely accepted explanation of the nature of the donor–acceptor bond is that the nitrogen atom donates electrons to the boron atom (i.e., $\overset{+}{N} \rightarrow \overline{B}$) to form a positively charged quadricovalent nitrogen atom and a negatively charged quadricovalent boron atom. This is incorrect. It does not correspond to the crystallochemical electronegativity scale, according to which the nitrogen atom is more electronegative than the boron atom. Consequently, the reverse redistribution of charges on the boron and nitrogen atoms, $B^{+\delta_1}$ and $N^{-\delta_2}$, should occur on compound formation.

A crystallochemical study of the influence of the unfilled bonding orbitals of the metal atom on the formation of complexes of mercury and thallium has led to the conclusion that the orbitals of these elements are unable to accept more electrons than are necessary to form normal covalent bonds in molecules [11, 12].

The donor–acceptor bond is different in nature from the covalent bond. To form a donor–acceptor

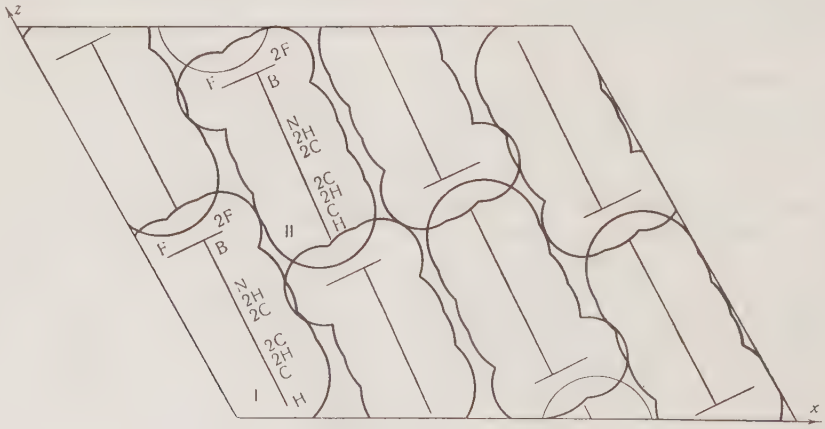

Fig. 3.

bond, an unshared pair of electrons from an atom of the donor molecule is used.

The important role of unshared pairs of electrons in the formation of molecules arises because these pairs take part in the hybridization of orbitals and hence take up a definite direction in space. For example, the nitrogen atom has the following electron distribution: $\boxed{s^2 \mid p \mid p \mid p}$. The unshared pair of s^2 electrons has spherical symmetry. In forming the pyridine molecule sp^2 hybridization occurs to give three σ bonds with a plane trigonal configuration and one π bond in the direction of the remaining p orbital. Two of the three σ bonds are attached to carbon atoms, while the third is filled by the fifth nitrogen electron, in the pyridine molecule. Thus asymmetry and elongation of the unshared pair of electrons on nitrogen arises in the pyridine molecule. This asymmetry and directionality of the unshared pair of electrons is a necessary condition for taking part in the formation of donor–acceptor bonds. The directionality of the nitrogen valences in the pyridine molecule is shown in Fig. 4, where the arrow indicates the direction of the unshared pair of electrons, the thin lines represent the directions of the π bonds, and the thick lines indicate σ bonds.

The overlap of the directional unshared pair of the nitrogen atom with the vacant orbital of the boron atom leads to the formation of a donor–acceptor bond between the BF_3 molecule and the NC_5H_5 molecule. In fact, in the formation of the coordination compound, the electronegativity is little changed because the unshared pair of electrons remains to a considerable degree with the nitrogen atom. This is seen from the x-ray structural data. The greatest changes occur in the BF_3 molecule: the B–F bond length increases from 1.30 Å in the free molecule [13] to 1.41 Å in the complex, and the stereochemistry around boron changes from planar to tetrahedral. The hybridization changes from sp^2 to sp^3 on forming the fourth bond to boron. The interatomic distances in the pyridine molecule in the $BF_3 \leftarrow NC_5H_5$ molecule change within the limits of 0.01-0.02 Å, but there is a small change in the electron density in the pyridine molecule.

The results of the x-ray structural study effectively supplement data on the energy of formation of a compound, since thermodynamic measurements only give the overall effect without an analysis of the separate chemical bonds in the molecule. At the present time, the role of the unshared pair of electrons is being studied by a variety of physicochemical methods. A calculation of the dipole

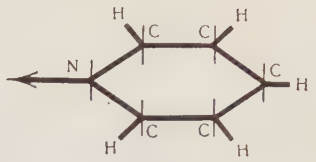

Fig. 4.

moment of water by Coulson [14] showed that the asymmetry of the unshared pairs of electrons on oxygen played the main part in creating the dipole moment. The measurements of the dipole moments of boron complexes with nitrogen showed that the polarization of the bond $\overline{B}-\overset{+}{N}$ was absent – they can be explained in terms of the asymmetry of the unshared pair of electrons in nitrogen [15].

Crystallochemical studies have great value in elucidating the nature of donor–acceptor bonds. In a recent review on the nature of donor–acceptor bonds in complex compounds, Nyholm [16] noted that the understanding of the nature of the donor–acceptor bond in complex compounds, and the elucidation of factors which affect its stability, are of great importance in the stereochemistry, thermodynamics, and kinetics of complex compounds, but the theory has weak points and, in particular, it does not explain that many compounds which contain atoms with unshared pairs of electrons, e.g., halides, do not form coordination compounds with metal salts.

However, crystallochemical theory can be used to explain these facts. As an example, we shall discuss the reason why boron trifluoride does not form coordination compounds with organic molecules which contain halogen atoms. In the light of the discussion, this indicates that the fluorine atom does not have the asymmetry and elongation of the unshared pairs necessary to form donor–acceptor bonds between the molecules.

A great deal of experimental crystallochemical material on directed covalency in molecules and in complex compounds is now available. The directions of the covalencies in elements of the Vth, VIth, and VIIth groups of the periodic system can be illustrated by the structures of the molecules PCl_5, $TeCl_4$, and ClF_3 (Fig. 5). The halogen atoms can form three covalent bonds in a T structure. To form the additional bonds, a p^2 pair of electrons is promoted from the ground state of chlorine: $\boxed{s^2 \mid p^2 \mid p^2 \mid p}$ The direction of the T bonds is such that the formation of the donor–acceptor bonds avoids steric hindrance. The effect of steric hindrance appears to be stronger in donor–acceptor

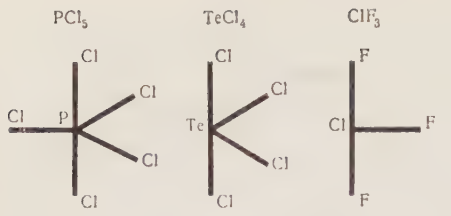

Fig. 5.

bonds than in covalent bonds [17]. The B ← N donor–acceptor bond is weaker than the B–N covalent bond. This is seen from the dissociation energy of the compound, $B(NMe_2)_3$, which is 89.7 kcal [18], a compound in which the B–N covalent bond distance is 1.50 Å, the sum of the covalent radii.

Finally, it must be remembered that the chemical bonds in molecules are usually intermediate in type and in their structures molecules display predominantly characteristic features of different types of chemical bonds.

Attention is now turned to the fact that three equal bonds are formed in the BF_3 molecule with sp^2 hybridization, while in the ClF_3 molecule the bonds have different strengths, the equatorial bond being stronger than the two axial bonds. This is evident from radiospectroscopic data on the molecular structure of ClF_3 [19], for the Cl–F bond lengths are 1.598 and 1.698 Å, respectively, and the bond angle FClF = 87°29'. This is explained by the differences in energy of the 2s, 2p, and 3s electronic states.

The following rule exists: As the filling of the outer electron orbitals occurs with a change from s^2 to p^2, the directional character of the additional valence bonds changes. These are formed by unshared electron pairs taking part in hybridization of the electrons in the molecule. Hence, the stability of the donor–acceptor bonds in complex compounds decreases in order of donor atoms: nitrogen, oxygen, fluorine, and their electronic analogs.

Since nitrogen and chlorine atoms have the same directions for separate valence bonds perpendicular to the equatorial plane, they should have some properties in common when the atoms are in combination. This is not observed in the formation of donor–acceptor bonds between molecules, but it is observed in intramolecular covalent bonds. In derivatives of benzene in which hydrogen is replaced by a chlorine atom or an amino group, shortening of the interatomic distances is observed, Cl–C to 1.706 A [20] and N–C to 1.37 Å [21] in comparison with Cl–C = 1.78 Å and N–C = 1.47 Å in aliphatic compounds. Thus, the C–Cl and C–N bonds are strengthened because the unshared pairs take part in hybridization. The sp^2 electrons take part to some extent in the three σ bonds at the nitrogen atom in the group $\begin{matrix} H \\ H \end{matrix}\!\!>\!N-C<$ because, x-ray data show, that the group is planar. The effect of the unshared pairs of electrons on the nitrogen and chlorine atoms is in the formation of sp hybrid orbitals directed at right angles to the equatorial plane and parallel to the p orbitals of the carbon atoms of the benzene ring, so that they take part in π-interaction with the benzene ring.

In crystallochemistry, the difference in the contributions of the s and p electrons to hybridization is estimated from the bond angles in molecules; for example, the larger size of the bond angles at nitrogen in comparison with those at bismuth is connected with the greater participation of the nitrogen s^2 electrons in the general hybridization. It can be confirmed from an analysis of the internuclear distances that the effect of the unshared pair of electrons on nitrogen is much greater in the pyridine molecule than in the nitrile group.

Crystallochemical studies of interatomic distances are an important additional criterion in deciding the question of the role of the unshared pair of electrons in the formation of chemical bonds in molecules and chemical compounds.

The author expresses her deep thanks to G. S. Zhdanov for discussing this work. Thanks are also expressed to Z. P. Lipina, A. N. Khvatkina, and A. N. Abramov for help in taking the x-ray photographs, preparing the crystals, and determining the pycnometric density.

LITERATURE CITED

1. A. V. Topchiev and Ya. M. Paushkin, Boron Trifluoride as a Catalyst in Alkylation, Polymerization, and Condensation [in Russian] (Moscow, 1949).
2. G. Buz and D. Martin, The Chemistry of Boron Trifluoride and Its Derivatives [Russian translation] (IL, Moscow, 1955).
3. I. L. Hoard, S. Geller, and T. B. Owen, "Structures of molecular addition compounds," Acta cryst., 4, 405 (1951).
4. P. A. van der Meulen and H. A. Heller, "Pyridine boron trifluoride," J. Am. Chem. Soc., 54, 4404 (1932).
5. G. S. Zhdanov and Z. V. Zvonkova, "Development of crystallochemical ideas on the nature

of intermolecular interaction and intermolecular radii on the basis of x-ray structural data," Tr. Inst. Kristallogr. AN SSSR, 10, 30 (1954).
6. K. I. Tobelko, Z. V. Zvonkova, and G. S. Zhdanov, "The structure of realgar and the atomic radius of arsenic," DAN SSSR, 749 (1954).
7. Billy B. DeMore, W. S. Wilcox, J. H. Goldstein, B. Bak, K. E. McCulloh, Gilbert F. Pollnow, and B. Bax, J. Chem. Phys., 21, 1305 (1953); 92, 565, 681, 876, 2013 (1954).
8. First Conference on Crystallochemistry: N. V. Belov and G. B. Bokii, "The current state of crystallochemistry and its problems," [in Russian] (Izd. AN SSSR, Moscow, 1954), p. 7.
9. L. Pauling, Nature of the Chemical Bond [Russian translation] (Goskhimizdat, 1947).
10. M. Soutif and Y. Ayant, "Etude de la molecule d'eau dans le cristal $Zi_2SO_4 \cdot H_2O$ par la methode de la resonance nucleaire," J. Chim. Phys., 50, 107 (1953).
11. Z. V. Zvonkova, V. V. Samodurova, and L. G. Vorontsov, "New results on the crystallochemistry of complex halides of mercury," DAN SSSR, 102, 1115 (1955).
12. Z. V. Zvonkova, "Crystal structures of molecular and complex compounds of thallium," ZhFKh.
13. H. Levy and L. O. Brockway, "The molecular structures of boron trimethyl, trifluoride, trichloride, and tribromide," J. Am. Chem. Soc., 59, 2085 (1937).
14. C. A. Coulson, "Critical survey of the method of ionic-homopolar resonance, Proc. Roy. Soc. 207, 63 (1951).
15. H. I. Becher, Über den Bindugszustand in Bor-Stickstoff Verbindungen, Z. anorg. allgem. Chem., 270, 273 (1952).
16. R. S. Nyholm, "The nature of the metal–ligand bond in complex compounds," Rev. Pure Appl. Chem., 4, 15 (1954).
17. H. C. Brown, H. I. Schelsinger, and S. Z. Gardon, "Studies in stereochemistry," J. Am. Chem. Soc., 64, 325 (1942).
18. H. A. Skinner and N. B. Smith, "The thermochemistry of organoboron compounds," J. Chem. Soc., 6, 4025 (1953).
19. D. F. Smith, "The microwave spectrum and structure of chlorine trifluoride," J. Chem. Phys., 21, 609 (1953).
20. Gunnar Erlandsson, "Microwave spectrum of chlorobenzene," Arkiv. Fysik., 8, 341 (1954).
21. S. C. Abrahams and J. Monteath Robertson, "The crystal structure of p-nitroaniline," Acta cryst., 1, 252 (1948).

NEW IONIC REFRACTION VALUES

G. B. Bokii and S. S. Batsanov

M. V. Lomonosov Moscow State University
Translated from Kristallografiya, Vol. 1, No. 1,
pp. 81-89, January-February, 1956
Original article submitted October 1, 1955

Ionic refraction determinations were made on ions which did not have noble-gas structures, using experimental data on crystalline materials containing the ions. The determinations were carried out by comparing the molar refractions of salts containing complex anions, since the additive law is most closely followed under these conditions. The ionic refraction values obtained were $Zn^{2+} = 0.6$; $Ni^{2+} = 0.6$; $Co^{2+} = 0.7$; $Fe^{2+} = 1.15$; $Cu^{2+} = 1.2$; $Mn^{2+} = 1.4$; $Pb^{2+} = 9.0$; $Ga^{3+} = 0.5$; $Cr^{3+} = 2.1$; $Fe^{3+} = 3.4$ cm^3; these agreed with values calculated by independent methods in all cases.

Refraction data are used widely in chemistry to solve the most diverse problems, included among which are structural questions. In the organic field, the refractometer method has been applied to structural chemistry studies for a considerable time [1], but its application to inorganic chemistry is comparatively recent. Refractometer results were successfully used to determine ionic radii by Wasastjerna [2] and, in particular, by Kordes [3,4], and have been applied by us [5-11] to the determination of geometric configurations of complex compounds, and to the study of hydrogen bonding in inorganic crystals.

The refractometric method has some decided advantages over other structural chemistry methods; it provides a rapid result, and does not need a high-quality specimen. It therefore appeared of interest to extend the use of the refractometer method to the most widespread and practically important class of inorganic substances, the silicates. One of the biggest obstacles to this was the lack of data on refraction in the crystalline state for many of the nonnoble-gas type cations met with in silicates. The present investigation included a determination of the refractions of a series of di- and trivalent cations, first among which were iron and manganese.

At the present time there are many different systems of ionic refraction determination but, of these, only the ones described by Fajans [12], Pauling [13], and Kordes [3] are complete and consistent. Fajans derived his ionic refraction values from experimental data on aqueous solutions of electrolytes, Pauling used the relationship between refraction and the secondary Stark effect, and Kordes worked from the relationship between ionic refraction and ionic radii. In principle, none of these three methods can give characteristic refraction values for ions not of the noble-gas type. In fact, since there is no rigorous quantitative theory relating the refractions of these ions and their spectral properties and dimensions, the Pauling and Kordes methods cannot, in general, be used to find the refractions of nonnoble-gas ions accurately. The Fajans method, based on the principle of additive superposition of refractions of infinitely diluted aqueous electrolyte solutions, also cannot lead to the desired result, since the method gives only the apparent ionic refractions. In aqueous solutions, the ions exert a distorting influence on the water molecules surrounding them, decreasing their refraction. The magnitude of this decrease can be estimated for noble-gas type ions, since it is known for the sodium ion. For ions not of the noble-gas type, this starting point does not exist, and so data on solutions cannot be used to determine refractions of ions in the gaseous and crystalline states (these states being equivalent where the cations are con-

cerned [7]). In Fajan's opinion, data on characteristic refractions of ions of this type can be obtained only from measurements on crystals.

1. Not long ago, some American workers [14] attempted to determine the polarizability of the iron ion using data on crystalline iron halides. However, when these authors subtracted the polarizability of a halogen ion, derived from results from alkaline salts, from the molar polarizability of the iron halide, they arrived at a physically meaningless result – the ionic polarizability turned out to be negative. It appeared that this result could only be due to an incorrect method of calculation, the error arising in not taking into account the considerable reduction of the halogen ion refractions in the field of the iron ions. To avoid this error, it is obviously necessary, first, to use anionic refractions calculated from results on salts with cations of identical charge and, second, to use complex rather than simple anions, since the former are more difficult to distort and, therefore, obey the additive law better. These conditions are approached most closely in the case of isomorphic salts containing chemically identical anions.

A comparison of the molar refractions of isomorphic salts gives the difference in cationic refractions, just as a comparison of refractions of neighboring members of a homologous series gives the value of the homologous difference refraction, this being the basic method of determining atomic refractions in organic chemistry. Table 1 lists the refractions of a series of calcium and lead salts, worked out from results given in Winchell's handbook [15].

From the table it can be seen that the difference between the refraction of the lead and calcium salts varies around 7.94 cm^3. On adding the refraction of the calcium ion (1.40 cm^3 according to Fajans [12]), we obtain an ionic refraction value for Pb^{2+} of 9.34 cm^3. According to independent measurements made by Kordes [16] on lead glass, the ionic refraction of lead is 9.13 cm^3. Thus, a comparison of the refractions of analogous complex salts can give quite accurate results for the refractions of ions not possessing noble-gas electron shells.

TABLE 1

Compound	R_D, cm^3	ΔR, cm^3
$PbCO_3$	20.05	7.44
$CaCO_3$	12.61	
$PbSO_4$	22.14	6.31
$CaSO_4$	15.83	
$PbWO_4$	31.51	9.18
$CaWO_4$	22.33	
$PbMoO_4$	32.05	9.51
$CaMoO_4$	22.54	
Pb_2SiO_4	37.08	8.08
Ca_2SiO_4	20.92	
$Pb_3(PO_4)_2$	56.44	7.12
$Ca_3(PO_4)_2$	35.08	

Table 2 shows a comparison between the molar refractions of iron and magnesium salts, calculated from the most reliable experimental data. For all the substances only one refractive index is given, averaged by the formula $\bar{n} = (n_g \cdot n_m \cdot n_p)^{1/3}$, this being necessary for calculation of refractions by the Lorentz – Lorenz formula.

From Table 2 it can be seen that the difference between the molar refractions of analogous iron and magnesium salts averages 2.27 cm^3. The additive rule is obeyed in this case quite closely, since the spread of results lies within the range of experimental error (± 0.10-0.15 cm^3). Since, for increasing molecular weights, errors in measurement of density have an increasing effect on calculations of molar volumes, and hence also on refractions, we cut short the Tutton salt series at the rubidium salts for the sulfates, and at the calcium salts for the selenates. We acted similarly in the comparisons shown in the other tables.

If the complex anions had undergone no change in refraction at all on exchanging the cations, then to calculate the refraction it would be sufficient to add the refraction of the magnesium ion (0.28) onto the difference in refractions found (2.27). However, the polarizabilities of the complex ions do in fact change, although this change may be quite insigni-

TABLE 2

Compound	$\frac{M}{d}$	$\bar{n}_D$	R_D, cm^3	ΔR, cm^3
$FeCO_3$	29.33[17]	1.791 [17]	12.43	2.44
$MgCO_3$	28.30[17]	1.624 [17]	9.99	
$FeSO_4 \cdot 7H_2O$	146.50[18]	1.4784[19]	41.52	2.13
$MgSO_4 \cdot 7H_2O$	146.80[20]	1.4492[15]	39.39	
Fe_2SiO_4	47.16[21]	1.854 [15]	20.76	2.38
Mg_2SiO_4	43.75[21]	1.652 [15]	16.00	
$K_2Fe(SO_4)_2 \cdot 6H_2O$	198.05[12]	1.4850[22]	56.76	2.15
$K_2Mg(SO_4)_2 \cdot 6H_2O$	196.58[22]	1.4664[22]	54.61	
$(NH_4)_2Fe(SO_4)_2 \cdot 6H_2O$	208.86[22]	1.4925[22]	60.66	2.20
$(NH_4)_2Mg(SO_4)_2 \cdot 6H_2O$	207.78[22]	1.4744[22]	58.46	
$Rb_2Fe(SO_4)_2 \cdot 6H_2O$	207.81[22]	1.4889[22]	59.98	2.30
$Rb_2Mg(SO_4)_2 \cdot 6H_2O$	206.18[22]	1.4713[22]	57.68	
$K_2Fe(SeO_4)_2 \cdot 6H_2O$	210.39[23]	1.5207[23]	64.03	2.33
$K_2Mg(SeO_4)_2 \cdot 6H_2O$	208.63[23]	1.5033[23]	61.70	
$(NH_4)_2Fe(SeO_4)_2 \cdot 6H_2O$	220.39[23]	1.5292[23]	68.00	2.25
$(NH_4)_2Mg(SeO_4)_2 \cdot 6H_2O$	219.42[23]	1.5111[23]	65.75	

ficant. Because of its small volume, the magnesium ion exerts a strong polarizing effect on its partners, and it therefore is possible that part of the difference ΔR is due to a reduction in anionic refraction. To check this possibility, we must compare the molar refractions of iron salts with the refractions of analogous calcium and strontium compounds, since, in the latter, we are dealing with underformed anions [24]. Table 3 shows the corresponding molar refractions, wholly calculated from data given in Winchell [15].

From the information shown in Table 3, it follows that the difference in refraction between the Ca^{2+} and Fe^{2+} ions is 0.17 cm^3, and that between Sr^{2+} and Fe^{2+} is 1.44 cm^3. Using the ionic refraction values quoted by Fajans (Ca^{2+} = 1.40 cm^3 and Sr^{2+} = 2.58 cm^3), we obtain the following refraction values for divalent iron: from the Ca salts, 1.23 cm^3; and from the Sr salts, 1.14 cm^3, giving a weighted mean value of $R_{Fe^{2+}}$ = 1.20 cm^3. This last value differs considerably from that obtained from the comparison of iron and magnesium salt refractions. The disagreement is due to the lowered refraction of the anions in the magnesium salts because of the strong polarizing influence of the Mg^{2+} ion. This effect can be allowed for by comparing the molar refractions of the magnesium salts with those of the analogous Ca and Sr compounds.

The difference between the ionic refractions of Ca^{2+} and Mg^{2+} is equal to 1.40 − 0.28 = 1.12, while the difference between the molar refractions of identical anions is equal to 2.54 cm^3, as shown by Table 4. Since the cations do not alter their refractions, the difference of 1.42 cm^3 (2.54 − 1.12) is the drop in anionic refraction due to the field of the magnesium ion. A similar value is obtained from a comparison of magnesium and strontium salts: $R_{SrX} - R_{MgX}$ = 2.30 cm^3, which means that the refraction drop is equal to 3.88 − 2.30 = 1.58 cm^3. From this, it can be concluded that a reduction in anionic refraction takes place in magnesium salts, averaging 1.47 cm^3. When this correction is taken into account, the results in Table 2 give a value for the refraction of the Fe^{2+} ion which agrees well with that obtained from Table 3 (1.20 cm^3). In fact, if we subtract from the difference ΔR_{Fe-Mg} = 2.27 cm^3 the quantity 1.47 cm^3 (the "magnesium drop"), then, on adding the Mg^{2+} ion refraction of 0.28 cm^3, we obtain a refraction value for the Fe^{2+} ion of 1.08 cm^3. This leads to a final result of $R_{Fe^{2+}}$ = 1.15 cm^3.

Thus, the ionic refraction of iron, worked out from a comparison of iron and magnesium salts (allowing for the refraction-drop correction) agrees, within the limits of experimental error, with the value obtained from a comparison of iron salts with calcium or strontium salts. This circumstance allows us to make future comparisons using only Mg salts, which is very convenient, since they are isomorphic with Zn, Mn, Co, Ni, and Cu salts, and have been studied much more extensively than any other salts containing divalent cations.

The validity of this method of calculating ionic refractions can be checked through a study of zinc salts, since the ionic refraction of Zn^{2+} has been determined by a number of authors in various ways. Table 5 shows a comparison of the molar refractions of analogous zinc and magnesium salts.

The average difference between these refractions of zinc and magnesium salts is 1.82. From this, the refraction of the Zn^{2+} ion is equal to 0.63 cm^3. According to Kruis [27], the refraction of the Zn^{2+} ion is equal to 0.60 cm^3. Kordes, working from a relationship between ionic refractions and radii [3] gives a value of 0.71 cm^3. So our value of the zinc ion refraction agrees with values obtained by completely different methods, and the method of calculation we have described can be applied to the determination of the refraction of other ions.

Table 6 lists experimental data from which the molar refractions of copper, nickel, cobalt, and manganese salts have been calculated.

From these results (Table 6) we can determine the ionic refractions of Cu^{2+}, Ni^{2+}, Co^{2+}, and Mn^{2+}. To do this, we need only to subtract, from the molar refractions of the metal salts listed, the molar refraction of their magnesium analog, and then from this difference subtract a further 1.19 cm^3 (i.e., subtract 1.47 cm^3, the "magnesium

TABLE 3.

Compound	R_D, cm^3	ΔR, cm^3
$CaCO_3$	12.61	0.18
$FeCO_3$	12.43	
Ca_2SiO_4	20.92	0.16
Fe_2SiO_4	20.76	
$SrCO_3$	13.87	1.44
$FeCO_3$	12.43	

TABLE 4.

Compound	R_D, cm^3	ΔR, cm^3
$CaCO_3$	12.61	2.62
$MgCO_3$	9.99	
Ca_2SiO_4	20.92	2.46
Mg_2SiO_4 . . .	16.00	
$SrCO_3$	13.87	3.88
$MgCO_3$	9.99	

TABLE 5

Compound	$\frac{M}{d}$	$\overline{n}D$	R_D, cm^3	ΔR, cm^3
$ZnCO_3$	28.31[15]	1.772[15]	11.79	1.80
$MgCO_3$	28.30	1.624	9.99	
$ZnSO_4 \cdot 7H_2O$	143.78[21]	1.4738[25]	41.37	1.98
$MgSO_4 \cdot 7H_2O$	146.80	1.4492	39.39	
$K_2Zn(SO_4)_2 \cdot 6H_2O$	196.16[26]	1.4859[26]	56.32	1.71
$K_2Mg(SO_4)_2 \cdot 6H_2O$	196.58	1.4664	54.61	
$(NH_4)_2Zn(SO_4)_2 \cdot 6H_2O$	206.38[26]	1.4937[26]	60.06	1.60
$(NH_4)_2Mg(SO_4)_2 \cdot 6H_2O$	207.78	1.4744	58.46	
$Rb_2Zn(SO_4)_2 \cdot 6H_2O$	205.58[26]	1.4897[26]	59.41	1.73
$Rb_2Mg(SO_4)_2 \cdot 6H_2O$	206.18	1.4713	57.68	
$K_2Zn(SeO_4)_2 \cdot 6H_2O$	208.80[26]	1.5212[26]	63.62	1.92
$K_2Mg(SeO_4)_2 \cdot 6H_2O$	208.63	1.5033	61.70	
$(NH_4)_2Zn(SeO_4)_2 \cdot 6H_2O$	217.73[26]	1.5308[26]	67.36	1.61
$(NH_4)_2Mg(SeO_4)_2 \cdot 6H_2O$	219.42	1.5111	65.75	

TABLE 6

Compound	$\frac{M}{d}$	$\overline{n}_D$	R_D, cm^3
$MnCO_3$	31.23[15]	1.739[15]	12.58
Mn_2SiO_4	49.98[21]	1.7967[21]	21.29
$(NH_4)_2Mn(SO_4)_2 \cdot 6H_2O$	212.13[22]	1.4851[22]	60.80
$Rb_2Mn(SO_4)_2 \cdot 6H_2O$	212.26[22]	1.4827[22]	60.59
$(NH_4)_2Mn(SeO_4)_2 \cdot 6H_2O$	223.35[23]	1.5217[23]	68.09
$CoCO_3$	29.01[15]	1.766[15]	12.00
$CoSO_4 \cdot 7H_2O$	14.34[21]	1.483[21]	40.96
$K_2Co(SO_4)_2 \cdot 6H_2O$	195.68[22]	1.4892[28]	56.49
$(NH_4)_2Co(SO_4)_2 \cdot 6H_2O$	206.40[22]	1.4962[28]	60.31
$Rb_2Co(SO_4)_2 \cdot 6H_2O$	205.03[22]	1.4930[28]	59.57
$K_2Co(SeO_4)_2 \cdot 6H_2O$	208.60[23]	1.5252[23]	63.95
$(NH_4)_2Co(SeO_4)_2 \cdot 6H_2O$	218.10[23]	1.5335[23]	67.74
$NiSO_4 \cdot 7H_2O$	14.40[21]	1.4836[21]	41.18
$K_2Ni(SO_4)_2 \cdot 6H_2O$	193.99[22]	1.4934[28]	56.41
$(NH_4)_2Ni(SO_4)_2 \cdot 6H_2O$	203.91[22]	1.5012[28]	60.09
$Rb_2Ni(SO_4)_2 \cdot 6H_2O$	203.43[22]	1.4969[28]	59.52
$K_2Ni(SeO_4)_2 \cdot 6H_2O$	206.14[23]	1.5293[23]	63.61
$(NH_4)_2Ni(SeO_4)_2 \cdot 6H_2O$	216.53[23]	1.5372[28]	67.64
$CuSO_4 \cdot 7H_2O$	14.83[21]	1.48[21]	42.14
$K_2Cu(SO_4)_2 \cdot 6H_2O$	196.49[22]	1.4907[22]	56.88
$(NH_4)_2Cu(SO_4)_2 \cdot 6H_2O$	206.08[22]	1.4990[22]	60.52
$Rb_2Cu(SO_4)_2 \cdot 6H_2O$	206.24[22]	1.4943[22]	60.08
$K_2Cu(SeO_4)_2 \cdot 6H_2O$	209.66[23]	1.5226[23]	64.01
$(NH_4)_2Cu(SeO_4)_2 \cdot 6H_2O$	220.64[23]	1.5311[23]	68.27

drop," and add 0.28 cm^3, the magnesium ion refraction). Table 7 lists the refraction differences $R_{EX} - R_{MgX}$ and the refractions calculated for the cations mentioned above.

2. This method of determining ionic refractions from a comparison of the molar refractions of complex compounds can be extended to cover trivalent cations. Of course, the concept of ionic refraction cannot strictly be applied to highly charged atoms, since they form bonds of partially covalent character. Since, however, the compounds met with in nature often include, say, trivalent iron, it would be useful to know how to calculate the proportion of the molar polarizability of the whole compound which was due to the iron. As well as the refraction of trivalent iron, we also worked out the ionic refractions of trivalent chromium and gallium, to see how far we would be justified in applying the method to the calculation of the refraction of positively charged trivalent ions.

In Table 8 are compared the molar refractions of aluminum and iron (ferri) compounds, only the most suitable for comparison being chosen, i.e., the alums include only the potash and ammonium members. Rubidium, cesium, and thallium alums have such high molecular weights that, for an error in specific gravity of ± 0.02, the error in calculating the refractions would be more than a cubic centimeter.

On the average, the molar refractions of analogous iron and aluminum compounds differ by 4.98 cm^3.

To determine the refraction of trivalent iron, we need only to calculate what part of this difference ΔR is due to the drop in anionic refraction because of the strong distorting influence of the aluminum. This problem can be solved by comparing the refractions of identical anions in aluminum and calcium salts. Table 9 shows such a comparison, with values of aluminum and calcium ion refractions taken from Fajans (0.17 and 1.40 cm^3, respectively).

It can be seen here that the aluminum ion reduces the refraction of its partners by 1.7 cm^3.

TABLE 7

Compound	E = element			
	Cu	Co	Ni	Mn
ECO_3	—	2.01	—	2.59
E_2SiO_4	—	—	—	2.64
$ESO_4 \cdot 7H_2O$	2.75	1.57	1.79	—
$K_2E(SO_4)_2 \cdot 6H_2O$	2.27	1.88	1.80	—
$(NH_4)_2E(SO_4)_2 \cdot 6H_2O$	2.06	1.85	1.63	2.34
$Rb_2E(SO_4)_2 \cdot 6H_2O$	2.40	1.89	1.84	2.91
$K_2E(SeO_4)_2 \cdot 6H_2O$	2.31	2.25	1.91	—
$(NH_4)_2E(SeO_4)_2 \cdot 6H_2O$	2.52	1.99	1.89	2.34
ΔR average	2.39	1.92	1.81	2.56
$R_{E^{+2}}$	1.2	0.7	0.6	1.4

TABLE 8

Compound	R_D, cm^3	ΔR, cm^3
$KFe(SO_4)_2 \cdot 12H_2O$	78.35[22]	5.00
$KAl(SO_4)_2 \cdot 12H_2O$	73.35[22]	
$NH_4Fe(SO_4)_2 \cdot 12H_2O$	80.35[22]	4.72
$NH_4Al(SO_4)_2 \cdot 12H_2O$	75.63[22]	
$FePO_4 \cdot 2H_2O$	25.65[29]	5.22
$AlPO_4 \cdot 2H_2O$	20.23[29]	

TABLE 9

Compound	$\frac{M}{d}$	$\bar{n}_D$	R_D, cm^3	R anion	ΔR, cm^3
$CaSO_4$	46.45[15]	1.586[15]	15.59	14.19	1.72
$Al_2(SO_4)_3$	126.3[30]	1.510*	37.75	12.47	
$Ca_3(PO_4)_2$	107.2[15]	1.628[15]	35.50	15.65	1.67
$AlPO_4$	46.19[15]	1.525[15]	14.15	13.98	

*From our measurements.

Thus, the difference in refraction between the Fe^{3+} and Al^{3+} ions works out at $4.98 - 1.70 = 3.28$ cm^3. Adding the refraction of the aluminum ion, we find that $R_{Fe^{3+}} = 3.45$ cm^3.

In a similar manner, the refractions of trivalent chromium and gallium can be calculated. These calculations are shown in Table 10.

According to Kordes [3] and Pauling [13], the refraction of the Ga^{3+} ion is equal to 0.49 or 0.50 cm^3, respectively, which is almost exactly the same as our value. So the refractions of trivalent cations can be determined quite accurately from a comparison of the molar refractions of their crystalline salts.

3. In conclusion, we will compare (Table 11) the characteristic refraction values obtained by us for nonnoble-gas ions, with their values in aqueous solutions, determined by Fajans and Joos [31].

This comparison of the refractions of "crystalline" and "dissolved" ions shows that the pairs of

TABLE 10

Compound	R_D, cm^3	ΔR, cm^3	$\overline{\Delta R}$	$R_{E^{+3}}$
$KCr(SO_4)_2 \cdot 12H_2O$	77.02[22]	3.67	3.68	2.15
$KAl(SO_4)_2 \cdot 12H_2O$	73.35			
$NH_4Cr(SO_4)_2 \cdot 12H_2O$	79.32[22]	3.69		
$NH_4Al(SO_4)_2 \cdot 12H_2O$	75.63			
$KGa(SO_4)_2 \cdot 12H_2O$	75.44[22]	2.09	2.06	0.52
$KAl(SO_4)_2 \cdot 12H_2O$	73.35			
$NH_4Ga(SO_4)_2 \cdot 12H_2O$	77.67[22]	2.04		
$NH_4Al(SO_4)_2 \cdot 12H_2O$	75.63			

values are, in general, similar; the refractions of the divalent ions, nickel, iron, manganese, and lead are the same, within the limits of experimental accuracy, the refractions of the Zn^{2+}, Cu^{2+}, and Fe^{3+} ions are less in solution, and only with Co^{2+} is the refraction of the "dissolved" ion significantly greater than that of the "crystalline" ion.

Since our ionic refractions coincide in two known cases (see above) with the "gaseous" ionic refractions, we can deduce that some of the differences in comparison to "dissolved" ions are due to the influence of the water. We know that the molecules of water around cations have reduced refractions. On subtracting the refraction of the water from the general refraction of a solution, this fixed refraction drop is transferred to the cations. This effect operates in the case of divalent zinc and copper, and for trivalent iron. The discrepancy in the case of the cobalt refraction is apparently due to an inaccurate determination of its ionic refraction in solution, since divalent nickel and cobalt ions are very similar in all their properties, and it is impossible to understand why the polarizability of cobalt in solution should be twice that of nickel.

It is an interesting point that the refractions of nonnoble-gas ions increase with increase in their positive valences. Thus, the refraction of $Cu^{1+} = 1.08$, according to Kodes' data [3], while that of $Cu^{2+} = 1.2$ cm^3; the refraction of $Fe^{2+} = 1.1$, and that of $Fe^{3+} = 3.4$ cm^3. The increase in refraction of the cations is due to a shift in the nature of the chemical bonding, from ionic to covalent, because of the increase in polarizing action of the nonnoble-gas ions as their charge increases. Since the ionization of atoms to form cations is accompanied by a loss of electrons, and ionization to form anions involves a gain in electrons, it is clear that on going from an ionic bond to a covalent one the electronic polarizabilities (refractions) of cations will increase, while those of anions will fall.

TABLE 11

R_D	Ion									
	Zn^{+2}	Ni^{+2}	Co^{+2}	Fe^{+2}	Cu^{+2}	Mn^{+2}	Pb^{+2}	Ga^{+3}	Cr^{+3}	Fe^{+3}
Crystal	0.6	0.6	0.7	1.15	1.2	1.4	9.0	0.5	2.1	3.4
Solution	0.29	0.67	1.28	1.22	0.39	1.37	9.38[32]	—	—	2.86

This change in the type of chemical bonding imposes a natural limitation on the application of the very concept of ionic refraction and, consequently, on methods of determining it. The method described in the present article can therefore only be applied to di- and trivalent ions.

The method of determining refraction values of nonnoble-gas cations derived in the present work supplements the available systems of finding ionic refractions in the crystalline state, and at the same time extends the area of application of refractometric methods in inorganic chemistry.

LITERATURE CITED

1. I. I. Kanonnikov, The Light-Refracting Abilities of Chemical Compounds [in Russian] (Kazan', 1884).
2. J. Wasastjerna, "On the radii of ions," Soc. Sci. Fenn., Comm. Phys. Math., 38, 22-28 (1923).
3. E. Kordes, "Ermittlung von Atomabständen aus der Lichtbrechung," Z. phys. Chem., 44, 249, 327 (1939).
4. E. Kordes, "Jonenradien und Polarisierbarkeiten in Steinsalzgittern mit Jonen gleicher Edelgasschale," Naturwiss., 69, 488-489 (1952).
5. G. B. Bokii and S. S. Batsanov, "A new method of determining the structures of complex compounds. 1," Vestn. Mosk. Univ., 2, 147-163 (1952).
6. G. B. Bokii and S. S. Batsanov, "A new method of determining the structures of complex compounds. 2," Vestn. Mosk. univ., 9, 89-94 (1952).
7. G. B. Bokii and S. S. Batsanov, "A new method of determining the structures of complex compounds. 3," Vestn. Mosk. univ., 10, 87-96 (1954).
8. G. B. Bokii, M. N. Lyashenko, and S. S. Batsanov, "A new method of determining the structures of complex compounds. 4," Vestn. Mosk. Univ., 12, 75-78 (1954).
9. G. B. Bokii and S. S. Batsanov, "The refraction of hydrogen bonds," DAN SSSR, 92, 6, 1179-1180 (1953).
10. S. S. Batsanov, "Refraction of hydrogen bonds in inorganic compounds. 1," Vestn. Mosk. univ., 9, 95-110 (1954).
11. S. S. Batsanov, "Development and application of refractometry in chemistry," Usp. khim., 24, 688-729 (1955).
12. K. Fajans, "Über Refraktion und Dispersion von Gasen und Dampfen," Z. Phys. Chem., 24, 103-155 (1934).
13. L. Pauling, "The theoretical prediction of the physical properties of many-electron atoms and ions," Proc. Roy. Soc., A114, 181-200 (1927).
14. J. Tessmann, A. Kahn, and W. Shockley, "Electronic polarizabilities of ions in crystals," Phys. Rev., 92, 890-895 (1953).
15. N. H. Winchell and A. N. Winchell, Elements of Optical Mineralogy [Russian translation](IL, 1953).
16. E. Kordes, "Physikalisch-chemische Untersuchungen über den Feinbau von Gläsern," Z. anorg. Chem., 241, 1-38 (1939).
17. A. Winchell and W. Meck, "Birefringence–dispersion ration as a diagnostic," Am. Miner., 32, 336-343 (1947).
18. E. Moles and M. Grespi, "Zur Kenntnis des Volumens des Wassers in Metallsalzhydraten," Z. Phys. Chem., 130, 337-344 (1927).
19. M. Erofejeff, "Lichtbrechung des Minerals," Ber. Wien Akad., 56, 63-70 (1867).
20. M. Porter, "The refractive indices of mixed crystals of magnesium sulfate and zinc sulfate," Z. Krist., 75, 288-300 (1930).
21. A. N. Winchell, The Optic and Microscopic Characters of Artificial Minerals [Russian translation](ONTI, 1933).
22. A. Tutton, "The hexahydrated double sulphates containing thallium," Proc. Roy. Soc., A118, 367-392 (1928).
23. A. Tutton, "The hexahydrated double selenates containing thallium," Proc. Roy. Soc., A118, 393-415 (1928).

24. E. Kordes, "Jonendeformation in binären Verbindungen der Alkalien und Erdalkalien," Z. Krist., 105, 337-363 (1944).
25. M. Dufet, "Sur les proprietes optiques des melanges de sels isomorphes," Bull. Soc. Fr. Min., 3, 180-188 (1880).
26. A. Tutton, "The relation of ammonium to the alkali metals," J. Chem. Soc., 87, 1123-1183 (1905).
27. A. Kruis, "Refraktometrische Untersuchungen," Z. Phys. Chem., B34, 51-66 (1936).
28. A. Tutton, "The monoclinic double sulphates containing thallium," Proc. Roy. Soc., A108, 240 (1925).
29. D. McConnell, "The refractive indices of phosphates," Am. Miner., 25, 719-723 (1940).
30. L. Nilson and O. Petterson, "Über Molekularwärme und Molekularvolumina der seltenen Erden und deren Sulfate," Ber., 13, 1462-1465 (1880).
31. K. Fajans and G. Joos, "Molrefraktion von Jonen und Molekülen im Lichte der Atomstruktur," Z. Phys., 23, 1-44 (1924).
32. P. Wulf and A. King, "Molrefraktion, Dispersion und Adsorption isomorpher Sr-, Ba- und Pb-Salze, sowie einiger Tl-Salze," Z. Krist., 87, 72-99 (1934).

CONSTANCY AND MULTIPLE PROPORTIONS AS FUNDAMENTAL PRINCIPLES IN CRYSTALLOGRAPHY AND CHEMISTRY

A. F. Kapustinskii

N. S. Kurnakov Institute of General and Inorganic Chemistry

Translated from Kristallografiya, Vol. 1, No. 1,
pp. 90-94, January-February, 1956
Original article submitted November 5, 1955

It is established empirically that the fundamental principles of crystallography with regard to constancy of the angles between the faces and the integral nature of the ratios of the parameters of the faces are equivalent to the principles of chemistry with regard to constancy of composition and multiple proportions by weight, these being also a consequence of the atomic structure of matter. It is shown that constancy and multiple proportions also appear in the actual building units of the crystal, i.e., the atoms and ions.

The fundamental principles of crystallography, which were discovered empirically, are the law of constancy of the angles between the crystal faces of a given substance (Steno, Rome de Lisle), and the law of rational proportions, expressing the integral nature of the ratios of the parameters of the faces in axial units (Haüy) [1]. These two principles appear to be completely equivalent to the two fundamental laws of chemistry, namely, constancy of the chemical individual (Proust), and the principle of multiple proportions by weight (Dalton). All these generalizations are essentially the logical consequence of the real existence of atoms and molecules. Outside the atomic theory, all these laws would be obscure, incomprehensible, and would be deprived not only of inner unity, but also of physical meaning. In different ways, they express the same thing: the discrete nature of matter; chemistry in terms of mass, crystallography in terms of spatial forms. This unity of crystallography and chemistry can be shown in various ways and hardly calls for further examination; in view, however, of its particularly convincing nature, one of these ways deserves special mention; this is the Shubnikov law [2], establishing a connection between the chemical formula expressing composition and the crystallographic characteristics of a compound.

Although the foregoing general principles of crystallography and chemistry are quite important and reveal the specific chemistry of the atoms most distinctly, they can by no means claim to be rules which have no exceptions. On the contrary, as shown by Kurnakov [3], compounds of constant and variable composition are possible, i.e., daltonides and berthollides, the latter, while they do not possess a singular point in the limits of the representation of the homogeneous individual phase in composition–property diagrams, are nonetheless equally chemical individuals with the daltonides. Crystal chemistry indeed provides an interesting approach to the understanding of this problem as a whole. The point is that, for an isolated molecule (gas), the principles of constant composition and multiple proportions know of no exceptions. There are also almost no exceptions for typical ionic lattices, in which the interchangeability of differently charged ions is impossible on the basis of electrostatic considerations alone. On the other hand, it is a priori probable, in the case of covalent and intermetallic compounds, in which it is relatively an easy matter to effect variation of the components, and, therefore, precisely for such crystals, the propagation of individuals of variable composition is quite natural.

As in chemistry, departures from the observance of the laws of constancy and multiple proportions are well known and have been explained, so in crystallography it is not difficult to predict such departures from its fundamental laws, and since these

very laws are the consequence of the atomic nature of matter, the deviations from these laws, which constitute an over-abstraction of the reality, are also due to the atomic structure of crystals.

In fact, crystal faces are far from being plane structures, but possess "irregularities," which are by no means negligibly small. Tolanski [4] has demonstrated experimentally the existence of a relief exceeding 1000 Å on some crystals, which, figuratively speaking, constitutes almost the same "irregularity" as does a mountain 1000 m high compared with the height of a man. The resulting relative constancy of the angles of a crystal, and also the repetition of the parameters of the faces, are obvious. These generalizations have thus rather a limited character; they are statistically true on the average. This, of course, is not to depreciate their functions as generalizations which, in themselves, reveal the essential features of the solid state.

The question naturally arises that, if the principles of constancy and multiple proportions occur in chemistry as a consequence of the discrete nature of matter, are they not also applicable in some degree to the very building units of crystal chemistry, the atoms and ions. The special examination of this question is of considerable interest since, as applied to the masses of atoms, it was raised more than a century ago by Proust (formation of complex atoms by the "polymerization" of hydrogen atoms); at that time, it was answered in the negative, in view of the clearly nonintegral nature of atomic masses, but now, following the discovery of isotopes, it has been answered in the affirmative, since the atomic weight of any isotope is an integral repetition of the weight of the nucleus.

By following this simple analogy, it might be expected that the principle of multiple proportions, as applied to individual atoms and ions, ought to result in the multiple relationship of the dimensions of all atoms (or ions) to the dimension of the particle appearing as the smallest. It is well known, however, that such expectation is by no means justified.

There is, however, another possible approach to the solution of this problem, which is based on a consideration of the comparative "thickness" of the various electron levels (K, M, N, L, O, P, etc.), and which is particularly simple for particles having spherical symmetry, since, in such cases, the question is always one of the distance corresponding to two successive minima of radial electron density. In principle, such minima can be calculated, a definite solution of the problem being obtained, both from the geometrical point of view, and that of theoretical physics. In fact, Odiot [5], making use of the Hartree function, obtained quite good results for a number of chemical elements, close to the results obtained by calculation of the radial density minima.

These methods, however, are somewhat complicated, and the results are comparatively limited. It will be shown below that there is another possible approach to the same problem, the theoretical basis of which will be considered later. Following this method, it is possible to show convincingly that the principle of multiple proportions actually applies also to atomic and ionic dimensions.

We commence with an examination of those particles which have been studied most reliably, and which are closest to the spherical form in their electronic "architecture." This requirement is satisfied by ionic radii of the rare-gas type. More particularly, we choose to consider the cations.

The electrons of any ion (and atom) form two groups, sharply distinguished in character, the electrons of the K-layer, closest to the nucleus, (two-electron group), and all the others (eight-electron environment in the case of ions of rare-gas type).

The electrons of the K-layer, which are closer than the others to the nucleus, form a sphere, the dimensions of which depend on the number of charges of the ion. This may be shown as follows.

An examination of the more reliable system of ionic radii, the well-known Goldschmidt system [6], already shows that $Me^{\cdots}$ ions are quite rare, $Me^{5\cdot}$ ions actually do not exist in lattices, and the estimate of their dimensions is only tentative. Ions of period II of the periodic table are examples of rare-gas type ions having a single K-shell. The largest is the lithium ion and the smallest the nitrogen ion (0.1 Å). Confining ourselves in all subsequent calculations to an accuracy of 0.1 Å, we may practically assume the radius of the last-mentioned ion to be zero.

The dimension of the K-shell decreases linearly from the lithium ion with increase in size of the ion charge η. Taking the foregoing into account, we have

$$K = 0.2(5 - \eta). \qquad (1)$$

This dimension of the K-shell also represents the radius of the ion as a whole, since the dimensions of the nucleus are negligibly small. With the exception of $Be^{\cdot\cdot}$, equation (1) is confirmed satisfactorily (see Table 1 and Fig. 1).

For all the electron shells occurring after the K-level, the dependence on the magnitude of the

TABLE 1. Verification of Multiple Proportions in Ionic Dimensions [Eq. (4)]. Radii of Rare-Gas Type Ions in A

Element	r	
	calculated acc. to (4)	acc. to Goldschmidt
Lithium	0.8	0.8
Sodium	1.0	1.0
Potassium	1.2	1.3
Rubidium	1.4	1.5
Cesium	1.6	1.6
Francium	1.8	1.9
Beryllium	0.6	0.3
Magnesium	0.8	0.8
Calcium	1.0	1.1
Strontium	1.2	1.3
Barium	1.4	1.4
Radium	1.6	1.5
Boron	0.4	0.3
Aluminum	0.6	0.6
Scandium	0.8	0.8
Yttrium	1.0	1.1
Lanthanum	1.2	1.2
Actinium	1.4	1.4
Carbon	0.2	0.2
Silicon	0.4	0.4
Titanium	0.6	0.6
Zirconium	0.8	0.9
Cerium	1.0	1.0
Thorium	1.2	1.1

charge is negligibly small, since these shells are comparatively remote from the nucleus. They exhibit a surprising regularity: The "thickness" of each of the shells is the same, namely 0.23 Å, to an accuracy of 0.03 Å. Roughly speaking (see diagram, Fig. 2), an atom or ion "puts on" more electron shells of the same thickness as its structure becomes more complex. The radius of an ion may therefore be expressed by the simple formula

$$r = K + L,\ M,\ N,\ O,\ P, \qquad (2)$$

where the K-level is specially selected, or taking (1) into account

$$r = 0.2\,(5 - \eta) + 0.2n, \qquad (3)$$

where n is the number of quantum levels in the ion, following the K-shell closest to the nucleus.

Substituting in this principal quantum number m = n + 1, we have

$$r = 0.2\,(5 - \eta) + 0.2\,(m - 1) \qquad (4)$$

and

$$r = 0.8 + 0.2\,(m - \eta_i). \qquad (4a)$$

Table 1 gives the results calculated according to (4) compared with Goldschmidt's data. The radii of the ions not given in Goldschmidt's book have been taken from Yatsimirskii [7] for francium, and from Ormont [8] for radium and thorium. The radius of $B^{\cdot\cdot}$ has been interpolated from $B^{\cdot\cdot}$ and $C^{\cdot\cdot\cdot\cdot}$. The data obtained by Zackhariasen [9] for actinium have been converted for the Goldschmidt system.

The only element to show any pronounced discrepancy is beryllium. All the others, within the limits of the established accuracy, obey the rule which has been found, and this rule is obeyed much better than, for instance, the rules of Dulong and Petit, Trouton, and Hume-Rothery.

Similar calculations have been performed, although with lesser accuracy, for the radii of atoms, since the latter, in the case of rare-gas type structures, differ from ionic radii approximately by the same constant quantity. Here, again, there is the repetition of the same quantity 0.20, evidently representing some "universal thickness of the electron layer"; as was to be expected, however, the number of discrepancies is here greater. Out of 26 atoms of different elements, there are six discrepancies exceeding 0.1 Å, instead of the single similar discrepancy in the case of the cations.

Charge η	1	2	3	4	5
Radius equal to 0.2 (5—η)	0.8	0.6	0.4	0.2	Less than 0.1

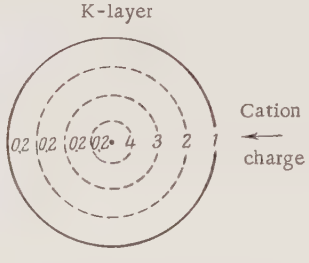

Fig. 1. Diagram showing the occurrence of constancy and multiple proportions in the K-shell closest to the nucleus. The size of the K-shell varies as a function of the cation charge (dotted lines). All the dimensions are expressed in an integral repetition of 0.2 A.

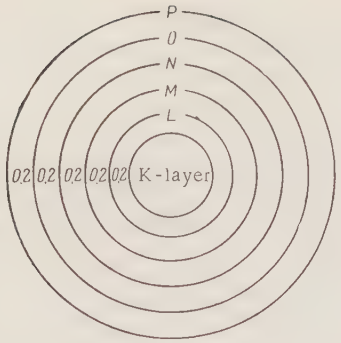

Fig. 2. Diagram of the occurrence of constancy and multiple proportions in the dimensions of ions. The thickness of each "electron layer" (quantum level) is 0.2 A. The integral repetition of this level gives the radius of any cation of rare-gas type. The K-layer closest to the nucleus is specially marked. The principal P, O, N, M, L layers are marked along a vertical.

Even for rare-gas type cations, however, the structure of which is ideally simple and symmetrical, and for which the ionic radii are most reliable, it would be illusory to expect high accuracy, measured, for example, in hundredths of an angstrom. First, in hundredths, there is nonadditivity, i.e., inconstancy of the radii themselves and, second, it would be quite unlikely for the volume of the atom or ion to increase by an exactly observed increase in the number of electron shells of equal thickness.

The rule which has been found points to a steady decrease in electron density with increase in distance of the levels from the nucleus, in qualitative agreement with wave-mechanics calculations. This, however, is unessential for us in the plan in which the consideration of the question is developed in this communication. It is important to note that for all the ideally spherical rare-gas type of ions (with one exception), there occurs a quite definite factor of multiple dimensions, both for the K-shell closest to the nucleus, constructed by repetition of the standard unit of 0.20 Å, and for all the other shells (L, M, N, O, P, Q, etc.), built up by an (m – 1)-fold repetition of the same unit 0.20 Å.

The establishment of this simple rule permits us to return once more to the general statement of the problem, with which the article began. Summing up the foregoing, we may draw the following conclusions.

1. Constancy and multiple proportions in crystallography and chemistry represent a natural consequence of the corpuscular (atomic) structure of matter.

2. Constancy and multiple proportions also appear in atomic (ionic) dimensions, here again, evidently, precisely as a consequence of the corpuscular (electronic) structure of the particles (atoms and ions) forming the crystal lattices. With the exception of the K-layer closest to the nucleus, all the other electron levels of cations of rare-gas type have a "thickness" of the order of 0.20 Å, so that the dimensions of an ion are determined by the (m – 1)-fold repetition of this standard multiple plus the radius of the K-layer.

LITERATURE CITED

1. See, for example, A. V. Shubnikov, E. E. Flint, and G. V. Bokii, Principles of Crystallography [in Russian] (Izd. AN SSSR, Moscow – Leningrad, 1940).
2. A. V. Shubnikov, "The fundamental law of crystal chemistry," Izv. AN SSSR, 515 (1922).
3. N. S. Kurnakov, Introduction to Physicochemical Analysis [in Russian] (Leningrad, 1928).
4. S. Tolanski, "The topography of crystal faces," Proc. Roy. Soc., London, A184, 41-51 (1945).
5. S. Odiot, "Determination geometrique des couches K, L, M des atomes et ions Be, F^-, Al^{3+}, Ca^{2+}, Rb^+, and Hg," Compt. rend. Acad. Sci., 237, 22, 1399-1401 (1953).
6. V. M. Goldschmidt, Kristallchemie [Russian translation edited by V. G. Khlopin] (ONTI, Leningrad, 1937).
7. K. B. Yatsimirskii, "Ionic radii and ionization potential," Zh. obshch. khim., 13, 180 (1953).
8. B. F. Ormont, Structures of Inorganic Substances [in Russian] (GTTI, Moscow – Leningrad, 1950).
9. W. Zachariasen, "Crystal radii of the heavy elements," Phys. Rev., 73, 1104-1105 (1948).

SOME PECULIARITIES IN THE THERMAL DEFORMATION OF CRYSTALS

A. V. Shubnikov

Institute of Crystallography, Academy of Sciences of the USSR
Translated from Kristallografiya, Vol. 1, No. 1,
pp. 95-104, January-February, 1956
Original article submitted September 20, 1955

The article shows that the thermal expansion of crystals cannot be reduced merely to a simple elongation of the crystal in all directions passing through any point in its interior. A correct pattern of the thermal expansion of crystals is given by the transformation of the unit radii of a sphere to the radius-vectors of an ellipsoid OB by means of translation vectors AB (Fig. 2). The coefficients of thermal expansion of crystals are assumed to be the intercepts AC and not the intercepts AD. The dependence of the coefficients of expansion of a crystal on direction is given by formula (8), by means of which it is possible to construct all imaginary surfaces of coefficients of expansion of crystals (Figs. 9-15). A more complete picture of the thermal deformation of crystals calls for an investigation of the surfaces of the coefficients of thermal displacement BC (Fig. 2) of crystals.

It is well known that crystals undergo homogeneous deformation on thermal expansion. One of its peculiarities is that a sphere, imagined to be separated somewhere inside a crystal, is transformed by the deformation into an ellipsoid, and a cube into a parallelepiped. In the homogeneous deformation of plane figures, a circle is transformed into an ellipse and a square into a parallelogram.

Such a definition of the thermal deformation of crystals allows the thermal deformation to be understood in different ways. We shall consider two treatments of this phenomenon: one definitely incorrect and the other correct; or, better, more correct, since it is amenable to further improvement. We shall commence with the first.

Incorrect Concept of the Thermal Deformation of Crystals

We assume that the thermal expansion of crystals occurs in such a manner that every radius of a sphere, imagined to be separated inside the crystal, is transformed into an identically directed radius-vector of an ellipsoid by simple elongation or compression. This means that in a plane diagram the radius of a circle OA is transformed into a radius-vector of the ellipse OB, OC into OD, OE into OF, etc. (Fig. 1).

We assume as principal coefficients of expansion, the magnitudes

$$\alpha_1 = \frac{AB}{OA \cdot t} = \frac{a_1 - r}{rt}, \quad \alpha_2 = \frac{DC}{OC} = \frac{a_2 - r}{rt},$$

where a_1 is the length of the principal horizontal semiaxis of the ellipse; a_2 is the length of the principal vertical semiaxis of the ellipse; r is the length of the radius of the circle; and t is the increase in temperature.

If the thermal deformation of crystals actually occurred by simple elongation of all the radii of the circle, we should have to assume as coefficient of expansion of the crystal along any oblique direction the magnitude

$$\alpha' = \frac{EF}{OE \cdot t} = \frac{R - r}{rt},$$

where R denotes the length of the variable radius-vector of the ellipse. It is not difficult to see, however, that the described mechanism of thermal de-

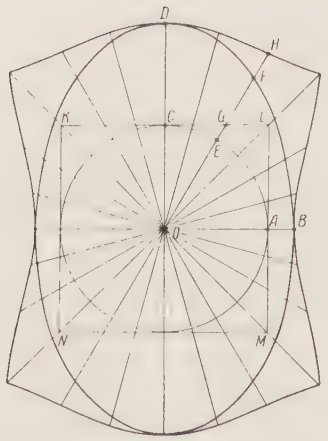

Fig. 1. If the deformation of a circle to form an ellipse occurs in such a manner that any point E on the circumference passes to the point F, the point G on the side of the square ought to pass to the point H. Accordingly, the square ought to be transformed into the curvilinear shown in the diagram.

formation of crystals, with all its simplicity and apparent clarity, is greatly in error, if not from the practical standpoint, at least from the theoretical standpoint. This becomes perfectly obvious if we apply this mechanism not to the deformation of a circle, but to that of a square KLMN. In this case, it appears that the square is not transformed into a parallelogram, but into some curvilinear figure, shown in the diagram. To construct any point H of this figure, the length of the intercept GH must be determined. If we assume that the coefficient α' has the value given above, the length of the intercept GH may easily be found from the relationship

$$\frac{GH}{OG} = \frac{R-r}{r},$$

since the length of the radius-vector OG of the square is known for each of its points G. If the crystal were deformed by thermal expansion in the manner indicated, its lattice would be distorted. This means that it could have a strictly lattice structure at only one definite temperature with which, of course, it is impossible to agree.

We have examined this incorrect treatment of homogeneous deformation in such detail because, following the footsteps of earlier authors [1], certain contemporary crystal physicists [2], including in the past the author of the present article [3], have unfortunately resorted to it.

By way of example, we shall cite one of the usual discussions based on the incorrect mechanism of homogeneous deformation which we have considered. We shall consider essentially the derivation of one of the most important formulas of crystal physics, although specifically the same thermal expansion of crystals will be borne in mind.

If we assume that the radius of a deformed circle is equal to unity, the equation of the ellipse obtained from it may be written in Cartesian coordinates, referred to the principal axes of the ellipse, as follows:

$$\frac{x_1^2}{(1+\alpha_1)^2} + \frac{x_2^2}{(1+\alpha_2)^2} = 1.$$

Making use of the substitutions

$$x_1 = R\cos(RX_1) = (1+\alpha')c_1,$$
$$x_2 = R\cos(RX_2) = (1+\alpha')c_2$$

and ignoring squares and derivatives of the small quantities $\alpha', \alpha_1, \alpha_2$, we reduce the equation of the ellipse to the form

$$\alpha' = \alpha_1 c_1^2 + \alpha_2 c_2^2.$$

We have obtained this formula bearing in mind the deformation of plane figures. If we repeated our argument as applied to three-dimensional figures, we should arrive at the formula

$$\alpha' = \alpha_1 c_1^2 + \alpha_2 c_2^2 + \alpha_3 c_3^2, \qquad (1)$$

enabling us to calculate the coefficient of expansion α' from the three known principle coefficients α_1, α_2, α_3 for any direction in the crystal defined by the direction cosines c_1, c_2, c_3.

More Correct Concept of the Thermal Expansion of Crystals

This concept is based on the assumption that the thermal deformation of a crystal may be described by the system of equations

$$\left.\begin{aligned} x_1' &= a_1 x_1 \\ x_2' &= a_2 x_2 \\ x_3' &= a_3 x_3 \end{aligned}\right\}, \qquad (2)$$

where x_1, x_2, x_3 are the Cartesian coordinates of any point of the crystal before deformation, x_1', x_2', x_3' are the coordinates of the same point after deformation, and a_1, a_2, a_3 are some constants (positive or negative real numbers). It is assumed that the coordinates are referred to the system of the principal axes of the crystal which theoretically may always be found (for monoclinic and triclinic crystals, the position of the principal axes is fixed only for a given temperature). If it is a ques-

tion of the deformation of a sphere which we imagine to be separated inside the crystal, or actually ground out of it, we take the center of the sphere as the origin of the coordinates.

We assume that all the points of interest to us are arranged after deformation on the surface of this sphere and that the radius of the latter is equal to unity. This means that the coordinates x_1, x_2, x_3 are connected together by the equation

$$x_1^2 + x_2^2 + x_3^2 = 1. \qquad (3)$$

Having determined from equation (2) the coordinates x_1, x_2, x_3 and substituting the values found for them in the equation (3) for the sphere, we obtain the expression

$$\frac{x_1'^2}{a_1^2} + \frac{x_2'^2}{a_2^2} + \frac{x_3'^2}{a_3^2} = 1, \qquad (4)$$

which represents the equation of an ellipsoid. We have shown that the sphere is transformed by equations (2) into an ellipsoid. Similarly, it may be shown that a cube is converted by them into a parallelepiped. For this purpose, it is necessary to take as starting equation not that of a sphere, but the equation for two parallel sides of a cube, and to show that by means of equations (2) it is transformed into the equations of two planes equidistant from the origin of the coordinates and parallel to each other.

As is known, the equation of a plane may be represented in the form

$$\frac{x_1}{A_1} + \frac{x_2}{A_2} + \frac{x_3}{A_3} = 1,$$

where A_1, A_2, A_3 are the lengths of the intercepts of the plane with the coordinate axes. If this equation is taken as the equation for one face of a cube, the cube face parallel to it will have the equation

$$\frac{x_1}{-A_1} + \frac{x_2}{-A_2} + \frac{x_3}{-A_3} = 1.$$

Substituting in both these equations the values of x_1, x_2, x_3 found from equations (2), we get

$$\frac{x_1'}{a_1 A_1} + \frac{x_2'}{a_2 A_2} + \frac{x_3'}{a_3 A_3} = 1,$$

$$\frac{x_1'}{-a_1 A_1} + \frac{x_2'}{-a_2 A_2} + \frac{x_3'}{-a_3 A_3} = 1.$$

These are the equations for two parallel planes equidistant from the origin of the coordinates, which was to be demonstrated.

We shall examine the process of thermal deformation, described by equations (2) in greater detail with reference to the plane scheme (Fig. 2). We shall take a circle having a radius equal to unity. We divide it into 4n equal parts (24 parts in the diagram). We connect the points of division to the center of the circle; we have a system of radii of the circle before its transformation into an ellipse. We now apply to each point of division of the circle, and correspondingly to each radius of the latter, the transformation (2), assuming $x_3 = 0$. We take first the point K with the coordinates $x_1 = 1$, $x_2 = 0$. Multiplying them respectively by a_1 and a_2, we get $x_1' = a_1$, $x_2' = 0$. This result shows that the point K, after deformation while remaining on the X_1 axis, ought to be displaced to the right if $a_1 > 1$, or to the left, if $a_1 < 1$. In constructing the diagram we assumed $a_1 = 1.25$, $a_2 = 2.00$. In accordance with this, our point was displaced to the position E on the right of K. It follows from the foregoing that $a_1 = OE$. Similarly, it may be shown that $a_2 = OF$. As will be seen, the constants a_1, a_2, from the geometrical point of view, are the semiaxes of the ellipse into which the circle is transformed as the result of deformation. If we apply our transformation to the point A, we find that, after deformation, it will have moved to the point B along the displacement vector AB. In accordance with

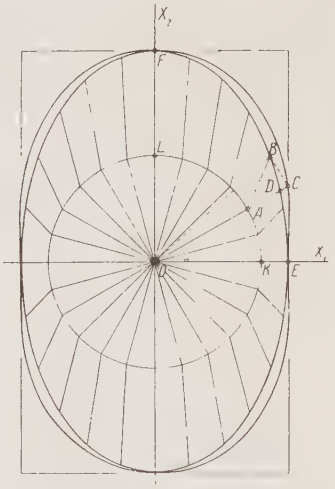

Fig. 2. Transformation of a circle into an ellipse as described by equations (2) and corresponding exactly to the observed thermal deformation of crystals. In this case, the vector OA is transformed into the vector OB by means of the displacement vector AB, which transfers the point A to B. In this case, a magnitude proportional to the length of the intercept AC is taken as coefficient of expansion in the OA direction.

this, the radius of the circle OA is transformed into the radius vector OB of the ellipse. If we complete this construction for all the points of division of the circle, without representing for the sake of simplicity the radius vectors of the ellipse, we obtain the complete deformation pattern shown in Fig. 2. It will be seen that this pattern differs substantially from that previously considered (Fig. 1).

By using formulas (2), it is easy to calculate and construct the diagram for the transformation of a square into a parallelogram (Fig. 3).

Returning to Fig. 2, there is to be seen in it the point D, coinciding with the point of intersection of the ellipse and the prolonged straight line OA, and the point C, which is located at the intersection of the same straight line with the normal BC dropped from the point B onto this straight line. We transfer these and other points of the diagram considered to a special diagram (Fig. 4). We denote the angles formed by the straight line OC with the axes of the coordinates by φ_1, φ_2, and their cosines, which are the direction cosines of this straight line, by c_1, c_2. It is evident that the coordinates of the point A for OA = 1 are c_1, c_2 and the coordinates of point B, in agreement with formulas (2) are equal to a_1c_1; a_2c_2. We furthermore denote the length of the intercept of the straight line OC by a'.

The diagram shows that the normal equation of the straight line GH for this notation may be written in the form

$$a' = x_1c_1 + x_2c_2.$$

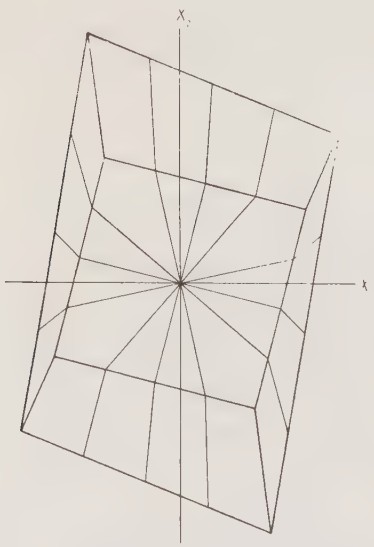

Fig. 3. Diagram to show that a square is transformed into an oblique parallelogram by equations (2).

Since this straight line passes through the point B, the equation cited will not be violated if, instead of x_1, x_2 we substitute the coordinates of these points a_1c_1; a_2c_2. After this substitution, the equation cited becomes the equation

$$a' = a_1c_1^2 + a_2c_2^2. \tag{5}$$

We must here digress slightly from the main theme of our article and point out that if, in the equation (5) we have obtained, the quantities a_1, a_2 are regarded as constants and the quantities a', c_1, c_2 as variables, taking into account, of course, the fact that the sum of the squares of the direction cosines is always equal to unity,

$$1 = c_1^2 + c_2^2, \tag{6}$$

this equation (5) will define in Cartesian coordinates some curve which, after due examination, is found to be an oval-like curve, with four points in common with the ellipse under consideration (Fig. 2), and situated outside the latter with all its other points.

We return to our subject. We subtract equation (6) from (5)

$$a' - 1 = (a_1 - 1)c_1^2 + (a_2 - 1)c_2^2.$$

As we already know, the quantities $a_1 - 1$ and $a_2 - 1$ represent the principal coefficients of expansion α_1 and α_2. If, in agreement with this, we denote the quantity $a' - 1$ by α', the last-mentioned equation becomes

$$\alpha' = \alpha_1c_1^2 + \alpha_2c_2^2. \tag{7}$$

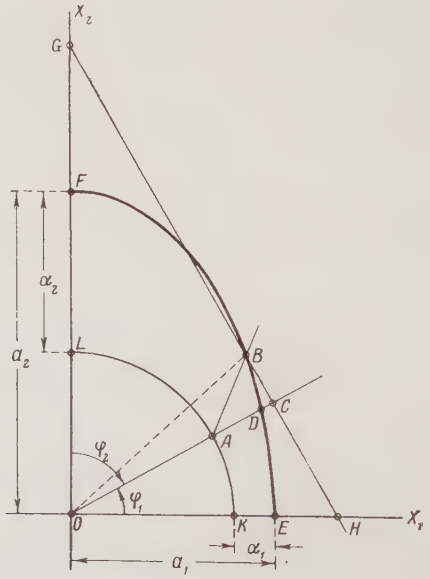

Fig. 4. Diagram for deduction of Eq. (8).

Formula (7) describes the thermal expansion of plane figures. If we repeated our considerations, having in mind three-dimensional figures, we should obtain the equation

$$\alpha' = \alpha_1 c_1^2 + \alpha_2 c_2^2 + \alpha_3 c_3^2. \quad (8)$$

We now direct our attention to the fact that formulas (1) and (8) do not differ from each other in outline, despite the fact that the first of them is approximate (since, in deriving it we ignored squares and derivatives of the quantities α', α_1, α_2, α_3) and the second is perfectly accurate. This is due to the fact that in formula (1), by the quantity α' we understood the intercept AD (see Fig. 4), which is actually defined approximately by this formula, whereas, in formula (8) by the quantity α' we understood the intercept AC, which is defined perfectly accurately by this formula.

Taking this into account, and bearing in mind the fact that formula (8) has been derived on the basis of more exact concepts of thermal deformation, we shall henceforth understand by the coefficient of expansion α' a quantity proportional to the intercept AC and not the intercept AD.

At first sight, such a definition of the coefficient of expansion – in fact not novel – may appear to be too artificial, since the point C is situated outside the ellipse (i.e., outside the crystal, if before deformation it is given the shape of a sphere). It is necessary, however, to take into consideration the fact that the real transformation of the vector OA (Figs. 2 and 4) into the vector OB by means of the displacement vector AB occurs not only by extension of the vector OA to the magnitude of the intercept AC, but also on account of the shift CB, as the result of which the point C coincides with the point B, where it ought to be.

It is very important to note that the formula (8) we have derived, being an equation of second degree with regard to the variables c_1, c_2, c_3, is an equation of fourth degree with regard to the variables x_1, x_2, x_3. This may easily be verified by replacing the variables c_1, c_2, c_3, α' by their equivalent quantities

$$\frac{x_1}{\alpha'}, \frac{x_2}{\alpha'}, \frac{x_3}{\alpha'}, \sqrt{x_1^2 + x_2^2 + x_3^2}.$$

It follows from this that equation (8), despite often-encountered statements, cannot express in Cartesian coordinates any surface of a second order, in particular the surface of an ellipsoid.

The fact that in individual cases equation (8) cannot express an ellipsoid even approximately is clear from the following. We know that the coefficient of calcite along the principal axis has a positive sign, and along directions perpendicular thereto a negative sign. This means that in certain oblique directions the coefficient of expansion ought to be exactly equal to zero, i.e., certain radius vectors of the ellipsoid ought also to be equal to zero. Such ellipsoids do not exist.

We should here like to point out that, despite the previously often-repeated view [4,5], in the thermal expansion of calcite there is not only no contradiction of the ellipsoid law, but, on the contrary, a most elegant confirmation of this law, since, in this case also, the sphere is transformed by equations (2) into an ellipsoid and a circle into an ellipse (Fig. 5).

Form, Symmetry, and Antisymmetry of Surfaces of the Coefficients of Expansion of Crystals

By means of equation (8), it is possible to find from the three known principal coefficients of expansion $\alpha_1, \alpha_2, \alpha_3$, the coefficient of expansion α' for any direction in the crystal, determined by the cosines c_1, c_2, c_3, which affords the possibility, by plotting from one point in different directions radius vectors proportional to α', to construct theoretically all conceivable forms of surfaces of coefficients of expansion of crystals for α_1, α_2, α_3 differing from each other in magnitude and sign.

For crystals of the cubic system, all three principal coefficients of expansion are equal to each other and all three are positive ($\alpha_1 = \alpha_2 = \alpha_3 > 0$). In this case, equation (8) assumes the form

$$\alpha' = \alpha_1 (c_1^2 + c_2^2 + c_3^2) = \alpha_1. \quad (9)$$

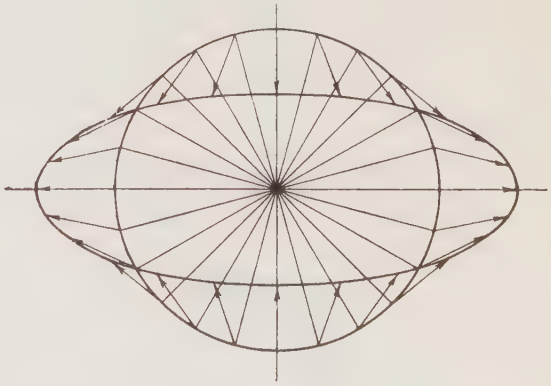

Fig. 5. Diagram showing that the ellipsoid law for thermal deformation remains valid even if one of the principal coefficients has a negative sign.

The corresponding surface evidently is a sphere with positive radii, a white sphere having the symmetry $\infty/\infty \cdot m$.

For $\alpha_3 \neq \alpha_2 = \alpha_1$; α_1, $\alpha_3 > 0$, the surface of the coefficients of expansion, expressed by the equation

$$\alpha' = \alpha_1 (c_1^2 + c_2^2) + \alpha_3 c_3^2, \tag{10}$$

becomes an oval-like, positive (white) surface of revolution, prolate (for $\alpha_3 > \alpha_1$), or oblate (for $\alpha_3 < \alpha_1$) along the X_3 axis (Figs. 6 and 7), and, in both cases having the symmetry $m \cdot \infty : m$. Such surfaces describe the simplest and most frequently encountered case of the thermal expansion of optically uniaxial crystals.

It was pointed out in the foregoing that, in calcite, α_3 has a positive sign and α_1 a negative sign. In accordance with this, equation (8) for this and similar uniaxial crystals will have the form

$$\alpha' = -\alpha_1(c_1^2 + c_2^2) + \alpha_3 c_3^2. \tag{11}$$

Figure 8 shows the corresponding surface of revolution having the symmetry $m \cdot \infty : m$. As will be seen, it consists of two ovoid positive (white) regions and one toroidal negative (black) region.

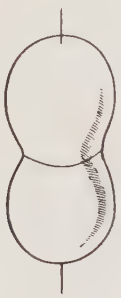

Fig. 6. Surface of coefficients of expansion of crystals satisfying the equation $\alpha' = \alpha_1(c_1^2 + c_2^2) + \alpha_3 c_3^2$ for $\alpha_3 > \alpha_1$.

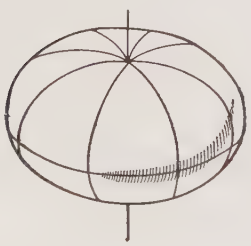

Fig. 7. Surface satisfying the equation $\alpha' = \alpha_1(c_1^2 + c_2^2) + \alpha_3 c_3^2$ for $\alpha_3 < \alpha_1$.

If all the principal coefficients of expansion are positive and all differ from each other ($\alpha_1 \neq \alpha_2 \neq \alpha_3$; $\alpha_1, \alpha_2, \alpha_3 > 0$), equation (8) assumes the form

$$\alpha' = \alpha_1 c_1^2 + \alpha_2 c_2^2 + \alpha_3 c_3^2. \tag{12}$$

The corresponding surface having the $m \cdot 2 : m$ symmetry is shown in Fig. 9. It describes the most frequently encountered cases of the thermal expansion of the majority of optically biaxial crystals.

If one of the principal coefficients, say α_3, has a negative sign, equation (8) becomes

$$\alpha' = \alpha_1 c_1^2 + \alpha_2 c_2^2 - \alpha_3 c_3^2. \tag{13}$$

The corresponding surface (Fig. 10) consists of two negative (black) ovoid regions, and one elongated

Fig. 8. Surface satisfying the equation $\alpha' = -\alpha_1(c_1^2 + c_2^2)\alpha_3 c_3^2$.

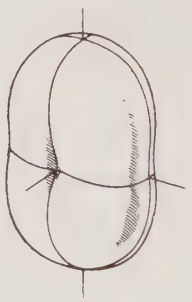

Fig. 9. Surface satisfying the equation $\alpha' = \alpha_1 c_1^2 + \alpha_2 c_2^2 + \alpha_3 c_3^2$.

Fig. 10. Surface satisfying the equation $\alpha' = \alpha_1 c_1^2 + \alpha_2 c_2^2 - \alpha_3 c_3^2$.

positive (white) region, having the form of an elongated annulus (bread roll). Theoretically, it may be predicted that such surfaces, having the symmetry m · 2 : m, may describe the thermal expansion of some biaxial crystals.

The surfaces described change their form substantially when one or two of the principal coefficients of expansion become equal to zero.

For $\alpha_1 = 0$, equation (10) becomes

$$\alpha' = \alpha_3 c_3^2. \tag{14}$$

The corresponding surface of revolution, shown in Fig. 11, has the symmetry m · ∞ : m and represents a pair of ovoid (white) regions, osculating at one point.

The same equation (10) for $\alpha_3 = 0$ assumes the form

$$\alpha' = \alpha_1 (c_1^2 + c_2^2). \tag{15}$$

The corresponding surface of revolution, shown in Fig. 12, has the form of a round bread roll (white) with two funnel-shaped depressions osculating at their apices. The surface has the symmetry m · ∞ : m.

If one of the principal coefficients in equation (12) is equated to zero, then (for $\alpha_3 = 0$), it assumes the form

$$\alpha' = \alpha_1 c_1^2 + \alpha_2 c_2^2. \tag{16}$$

Fig. 11. Surface satisfying the equation $\alpha' = \alpha_3 c_3^2$.

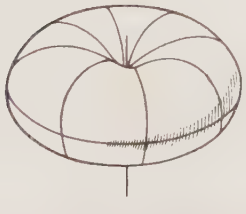

Fig. 12. Surface satisfying the equation $\alpha' = \alpha_1(c_1^2 + c_2^2)$.

The corresponding surface, shown in Fig. 13, has the form of an elongated bread roll with two funnel-shaped depressions, osculating at their apices. The surface has the symmetry m · 2 : m.

It remains to consider surfaces in which, for equality to zero of one coefficient, the other two have different signs. If, in equation (13), we put $\alpha_3 = 0$ and change the sign of c_1, it becomes

$$\alpha' = -\alpha_1 c_1^2 + \alpha_2 c_2^2. \tag{17}$$

The corresponding surface, shown in Fig. 14, represents a pair of identical negative (black), and a pair of identical, but of another size, positive (white) ovoid regions, connected by their apices at one point. The surface has the symmetry m · 2 : m.

If, in the last-mentioned equation, the principal coefficients of expansion are antiequal to each other, it assumes the form

$$\alpha' = \alpha_1 (c_2^2 - c_1^2). \tag{18}$$

The corresponding surface, shown in Fig. 15, a pair of identical white ovoid regions and a pair of black ovoid regions, antiequal to the former, connected together by their apices at one point. The surface has the symmetry m · 2 : m, and it also has the property of antisymmetry (m · 4 : m).

Fig. 13. Surface satisfying the equation $\alpha' = \alpha_1 c_1^2 + \alpha_2 c_2^2$.

Fig. 14. Surface satisfying the equation $\alpha' = -\alpha_1 c_1^2 + \alpha_2 c_2^2$.

Fig. 15. Surface satisfying the equation $\alpha' = \alpha_1(c_2^2 - c_1^2)$.

We consider the last five surfaces (Figs. 11-15) constructed theoretically on the assumption that one or two principal coefficients of expansion are equal to zero, to be unreal for crystals, but assume that it will be possible artificially to produce uniform anisotropic materials, the thermal deformation of which will correspond to these surfaces.

In conclusion, we would point out that the pattern of thermal deformation of crystals we have outlined is not final, since we have restricted ourselves merely to the investigation of the surfaces of the coefficients of thermal expansion and have left entirely out of consideration the surfaces of the coefficients of thermal shear of crystals. We propose to deal with this second problem in a future article.

LITERATURE CITED

1. T. Liebisch, Grundriss der physikalischen Krystallographie (1896), pp. 184-187.
2. W. Wooster, A Textbook on Crystal Physics, (1949) p. 21.
3. A. V. Shubnikov, E. E. Flint, and G. B. Bokii, Principles of Crystallography [in Russian], (1940) pp. 282-283.
4. E. S. Fedorov, Course on Crystallography [in Russian] (1901), p. 317.
5. E. S. Fedorov, Short Course on Crystallography [in Russian], (1910) p. 158.

DIELECTRIC ELLIPSOIDS AND DIELECTRIC-CONSTANT SURFACES

I. S. Zheludev

Institute of Crystallography, Academy of Sciences of the USSR

Translated from Kristallografiya, Vol. 1, No. 1,
pp. 105-111, January-February, 1956
Original article submitted November 1, 1955

A geometrical interpretation is given for the dielectric-constant tensor, which gives the Fresnel ellipsoid, and also a geometric interpretation of the reciprocal tensor, which gives the refractive-index ellipsoid. An anisotropic dielectric may be characterized in terms of these two ellipsoids, in which case a simple graphical method gives any two of the vectors **D**, **E**, and **P** from the other one. The analogy with optics is employed with the refractive indices n_S along the ray and n_N along the normal to give the ray dielectric constant ε_S (in the direction of the given vector **E**) and normal one ε_N (in the direction of the given vector **D**). Double dielectric-constant surfaces are constructed.

The following simple relations apply to a homogeneous isotropic dielectric:

$$\mathbf{P} = \alpha \mathbf{E}, \tag{1}$$

$$\mathbf{D} = (1 + 4\pi\alpha)\,\mathbf{E} = \varepsilon \mathbf{E} = \mathrm{E} + 4\pi \mathbf{P}, \tag{2}$$

where **D** is electrical induction, **P** is electrical polarization, **E** is electric field strength, ε is dielectric constant, and α is polarizability; ε and α are scalars here, so **D**, **P**, and **E** coincide in direction.

Equations (1) and (2) allow of a very simple geometrical interpretation. If, for example, we mark out vectors **D** in all directions (keeping the absolute magnitude constant) from some point, the ends of these vectors will lie on a sphere. The ends of the corresponding **E** vectors will also lie on a sphere, so (1) and (2) represent the geometrical operation of transformation of a sphere into a sphere. In the present case, the radius of sphere **D** will be ε times the radius of sphere **E**.

An anisotropic dielectric (crystal or homogeneous anisotropic medium) has a tensor relation between these quantities:

$$\mathbf{P} = \Pi_\alpha \mathbf{E},$$

$$\mathbf{D} = \Pi_\varepsilon \mathbf{E},$$

where Π_α and Π_ε are symmetric tensors of the second rank. The expressions can be put as

$$P_1 = \alpha_{11}E_1 + \alpha_{12}E_2 + \alpha_{13}E_3$$
. . . . . .
. . . . . .
$$D_1 = \varepsilon_{11}E_1 + \varepsilon_{12}E_2 + \varepsilon_{13}E_3$$
. . . . . .
. . . . . .

in which $P_1 \ldots$ and $D_1 \ldots$ are the components of vectors **P** and **D** along the coordinate axes.

Π_ε and Π_α are symmetric ($\varepsilon_{ik} = \varepsilon_{ki}$, $\alpha_{ik} = \alpha_{ki}$); the coefficients of the form ε_{ii} and α_{ii} are usually termed longitudinal, while ε_{ik} and α_{ik} ($i \neq k$) are called transverse.

An orthogonal coordinate system may also be used to describe phenomena in crystals; the axes are chosen to coincide with the symmetry axes of the crystal as far as possible. If the crystal has less than three mutually perpendicular axes, one of the axes is taken as coinciding with one of the symmetry axes, the other two passing through edges or perpendicular to faces to give an orthogonal system. Two axes lie in the symmetry plane for monoclinic crystals of class m, the third being perpendicular to this plane. The coordinate system is chosen arbitrarily for a triclinic crystal, in general.

These tensor relations also allow of a geometrical interpretation.

Dielectric Ellipsoids

Tensor calculus [1] shows that a symmetric second-rank tensor may be put in diagonal form by transformation of the coordinate system; it also shows that such a tensor has a fairly simple geometrical interpretation. Here we consider only the geometrical interpretation of Π_ε already in diagonal form; there is no difference of principle in the consideration of Π_α and Π_ε.

Consider the equation of the surface

$$\mathbf{E}\cdot(\Pi_\varepsilon\cdot\mathbf{E}) = 1, \tag{3}$$

formed by the ends of the variable vector $\mathbf{E}$ in various directions. In coordinate form this is

$$\varepsilon_1 E_1^2 + \varepsilon_2 E_2^2 + \varepsilon_3 E_3^2 = 1, \tag{4}$$

and is the equation of an ellipsoid ($\varepsilon_i > 0$); equation (4) in canonical form is

$$\frac{E_1^2}{\left(\frac{1}{\sqrt{\varepsilon_1}}\right)^2} + \frac{E_2^2}{\left(\frac{1}{\sqrt{\varepsilon_2}}\right)^2} + \frac{E_3^2}{\left(\frac{1}{\sqrt{\varepsilon_3}}\right)^2} = 1. \tag{5}$$

The scalar product $\Pi_\varepsilon \cdot \mathbf{E} \equiv \mathbf{D}$ of (3) has a simple geometrical meaning; if vector $\mathbf{E}$ ends at point M on the surface of (3), then vector $\Pi_\varepsilon \cdot \mathbf{E} = \mathbf{D}$ has the direction of the normal to the plane tangential to the surface at M (Fig. 1). The absolute value of this scalar product is given by

$$|\Pi_\varepsilon\cdot\mathbf{E}| = |\mathbf{D}| = \frac{1}{ON},$$

where ON is the distance along the normal $\bar{\mathbf{n}}$ from the center of the ellipsoid to the plane tangential to the surface at M. We leave aside the proofs that the surface of (3) has these properties, because these are given in general form in textbooks on tensor calculus.

Consider also the equation of the surface

$$\mathbf{D}\cdot(\Pi_\varepsilon^{-1}\cdot\mathbf{D}) = 1, \tag{6}$$

formed by the ends of vectors $\mathbf{D}$ in various directions.

Here, Π_ε^{-1} is a tensor reciprocal to Π_ε; if Π_ε takes the form

$$\Pi_\varepsilon = \begin{pmatrix} \varepsilon_1 & 0 & 0 \\ 0 & \varepsilon_2 & 0 \\ 0 & 0 & \varepsilon_3 \end{pmatrix},$$

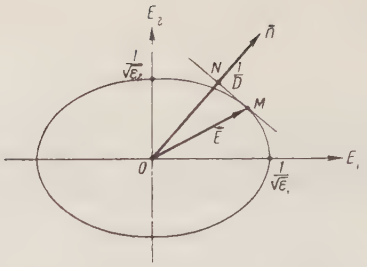

Fig. 1. Determination of the direction and magnitude of vector $\mathbf{D}$ from the Fresnel ellipsoid (section of an ellipsoid of rotation by a plane passing through the axis of rotation).

then Π_ε^{-1} takes the form

$$\Pi_\varepsilon^{-1} = \begin{pmatrix} \frac{1}{\varepsilon_1} & 0 & 0 \\ 0 & \frac{1}{\varepsilon_2} & 0 \\ 0 & 0 & \frac{1}{\varepsilon_3} \end{pmatrix}.$$

Equation (6) in coordinate form is

$$\frac{D_1^2}{\varepsilon_1} + \frac{D_2^2}{\varepsilon_2} + \frac{D_3^2}{\varepsilon_3} = 1,$$

and in canonical form,

$$\frac{D_1^2}{(\sqrt{\varepsilon_1})^2} + \frac{D_2^2}{(\sqrt{\varepsilon_2})^2} + \frac{D_3^2}{(\sqrt{\varepsilon_3})^2} = 1. \tag{7}$$

Surface (6) has properties analogous to those of (3); the scalar product $\Pi_\varepsilon^{-1} \cdot \mathbf{D} \equiv \mathbf{E}$ has the direction of the normal to the plane tangential to the surface of (6) at M', while the absolute value of the product (of the vector $\mathbf{E}$) is given by

$$|\Pi_\varepsilon^{-1}\cdot\mathbf{D}| = |\mathbf{E}| = \frac{1}{ON'},$$

where ON is the distance along the normal $\mathbf{n}'$ from the center of the ellipsoid to the plane tangential to the ellipsoid at M' (Fig. 2).

Turning now to (5) and (7), we see that here the variables are the components of $\mathbf{E}$ and $\mathbf{D}$, the constants being ε_1, ε_2, and ε_3. The semiaxes of the ellipsoids are $1/\sqrt{\varepsilon_1}$, $1/\sqrt{\varepsilon_2}$, $1/\sqrt{\varepsilon_3}$, and $\sqrt{\varepsilon_1}$, $\sqrt{\varepsilon_2}$, and $\sqrt{\varepsilon_3}$, respectively. Comparing (5) with the equation of the Fresnel ellipsoid

$$\frac{x_1^2}{v_1^2} + \frac{x_2^2}{v_2^2} + \frac{x_3^2}{v_3^2} = 1,$$

where the v are the principal velocities of light in the crystal, and comparing (7) with that for the optical indicatrix

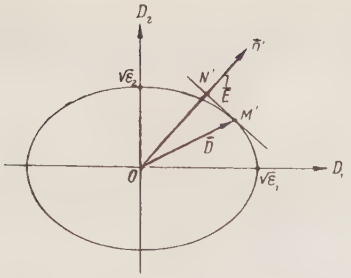

Fig. 2. Derivation of the direction and absolute magnitude of vector **E** for the ellipsoid of refractive indices (section of an ellipsoid of rotation by a plane passing through the axis of rotation).

$$\frac{x_1^2}{n_1^2}+\frac{x_2^2}{n_2^2}+\frac{x_3^2}{n_3^2}=1,$$

where the n_i are the principal refractive indices of the crystal, we have, because optics gives

$$n=\sqrt{\varepsilon},\quad v=\frac{c}{n}=\frac{c}{\sqrt{\varepsilon}},$$

(where c is the speed of light in vacuo), that (5) defines the Fresnel ellipsoid and (7) the optical indicatrix. The ellipsoids defined by (5) and (7), or by (3) and (6), are called reciprocal, because they are defined by tensors Π_ε and Π_ε^{-1}.

A very important property of these ellipsoids is that the ends of vectors **D** describe the ellipsoid of (6) if those of **E** describe that of (3), the direction of **D** being defined by that of the normal to a plane tangential to the ellipsoid of (3) at the end of vector **E** (point M), and conversely: the ends of **E** describe the ellipsoid of (3) if those of **D** describe that of (6), the direction of **E** being defined by that of the normal to a plane tangential to the ellipsoid of (6) at the end of vector **D** (point M'). Figure 3 shows this construction for a section of an ellipsoid of rotation by a plane passing through the axis of rotation.

Let

$$\Pi_\varepsilon \cdot \mathbf{E}^* = \mathbf{D}^*, \tag{8}$$

where the * denotes that $\mathbf{E}^*$ corresponds to $\mathbf{D}^*$ in accordance with ellipsoid (3). Now let a **D**, equal to $\mathbf{D}^{**}$ in (6), be equal to $\mathbf{D}^*$; if we can show that the $\mathbf{E}^{**}$, derived from (6), is equal to $\mathbf{E}^*$, we have the proof of the above assertion. In fact, from

$$\mathbf{E}^{**} = \Pi_\varepsilon^{-1} \cdot \mathbf{D}^{**} = \Pi_\varepsilon^{-1} \cdot \mathbf{D}^*,$$

and from (8) we have

$$\mathbf{E}^{**} = \Pi_\varepsilon^{-1} \cdot \Pi_\varepsilon \cdot \mathbf{E}^* = \mathbf{E}^*,$$

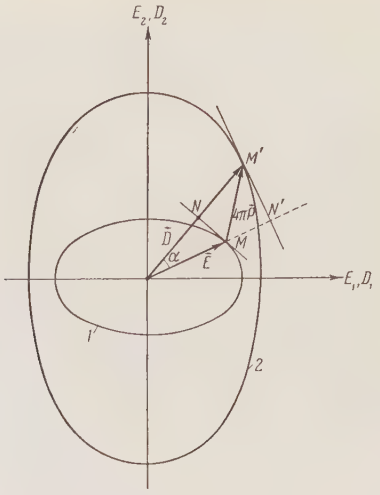

Fig. 3. Vectors **D**, **E**, and $4\pi\mathbf{P}$ in an anisotropic dielectric for the particular case of ellipsoids of rotation in section by a plane passing through the axis of rotation: 1) Fresnel ellipsoid; 2) optical indicatrix.

which was to be proved. We can also use (6) and specify $\mathbf{D}^*$ to show that this vector and the $\mathbf{D}^{**}$ derived from (3) will be equal, provided that the corresponding vectors $\mathbf{E}^*$ and $\mathbf{E}^{**}$ are also equal. This demonstrates the one-to-one relation between the vectors **D** and **E** defined by (3) and (6).

These features make it very simple to find one vector given the other.

In addition,

$$\mathbf{D} = \mathbf{E} + 4\pi\mathbf{P},$$

which gives a simple means of finding the vector $4\pi\mathbf{P}$ (Fig. 3). Any homogeneous isotropic dielectric may thus be characterized by (5) and (7) as regards its electrical parameters. Sections of the ellipsoids are used by laying off one of the quantities (**D**, **P**, or **E**) in a suitable scale in a given direction and then by construction determining the two others as to direction and absolute magnitude in the same scale.

The following are some points on the shape of the Fresnel and refractive-index ellipsoids. The ε_i are not distinct for all crystal systems, on account of the symmetry; the number of distinct ε_i gives us either a general ellipsoid ($\varepsilon_1 \neq \varepsilon_2 \neq \varepsilon_3$), an ellipsoid of rotation ($\varepsilon_1 = \varepsilon_2 \neq \varepsilon_3$), or a sphere ($\varepsilon_1 = \varepsilon_2 = \varepsilon_3$). A prolate Fresnel ellipsoid corresponds to an oblate optical indicatrix, etc.

This is not the only method of considering the polarization of anisotropic media or of interpreting the dielectric-constant tensor. For instance, Shubnikov [2] has treated the tensor relation be-

tween two polar vectors in a plane as the transformation of a circle (whose points are the ends of one of the vectors) into an ellipse (whose points are the ends of the other vector). This treatment is especially valuable in the thermal deformation of a crystal, hydrostatic compression, etc. Polarization of a dielectric can be considered in this way, and the final results must be the same. The two methods are thus complementary, and either may prove the more convenient for a particular problem.

The above method of interpretation is suitable for a linear dielectric (one with a linear relation between field and polarization). A special study is needed to determine whether the method can be applied to dielectrics of other types.

Dielectric-Constant Surfaces

By these surfaces are meant ones formed by the ends of the radius vector **r** from a point O in the crystal, the length being equal to the dielectric constant. An electrically isotropic body has spheres as its surfaces, and these are simple to construct.

The dielectric constant is a tensor for any anisotropic medium; **D** and **E** coincide in direction only along the principal axes, so the concept of a dielectric constant as the coefficient of proportionality between **D** and **E** becomes meaningless.

We now examine the meaning to be given to the dielectric constant of an anisotropic body.

The refractive index n_N is defined in optics as

$$n_N = \frac{c}{v_N},$$

where c is the velocity of light in vacuo and v_N is the velocity along the normal to the wave front. This is the refractive index measured in optics. The refractive index n_S along a ray is defined by

$$n_S = \frac{c}{v_S},$$

where v_S is the ray speed or the speed of energy transport.

It is shown in optics [3] that the velocity along the normal is equal to the projection of v_S on the wave normal:

$$v_N = v_S \cdot \cos\alpha,$$

where α is the angle between the directions of the normal and the ray. Then the ray refractive index n_S is related to n_N by

$$n_S = n_N \cdot \cos\alpha.$$

The two indices are clearly the same along the principal axes of the Fresnel ellipsoid and optical indicatrix:

$$n_S = n_N = n.$$

Also, the refractive index n of an isotropic medium is shown in electromagnetic theory to be related to the dielectric constant ε:

$$n = \sqrt{\varepsilon}.$$

Then we have two ε for an anisotropic medium, namely ε_N in the direction of **D**, and ε_S in the direction of **E**, with

$$\varepsilon_N = n_N^2, \quad n_N = \sqrt{\varepsilon_N},$$
$$\varepsilon_S = n_S^2, \quad n_S = \sqrt{\varepsilon_S}.$$

But

$$n_S = n_N \cdot \cos\alpha,$$

so ε_N should be related to ε_S by

$$\varepsilon_S = \varepsilon_N \cdot \cos^2\alpha. \tag{9}$$

Condition (9) essentially defines ε_S and ε_N. It is simple to show that (9) is obeyed if, by ε_N, we understand the quantity that indicates by what factor **D** (as defined by its direction cosines c_1, c_2, c_3) is larger than the projection (in the direction of **D**) of the corresponding vector **E**; by ε_S we understand the quantity that indicates by what factor **E** is less than the projection (on the direction of **E**) of **D** (Fig. 3). We then set

$$\varepsilon_N = \frac{D}{\overline{ON}} = \frac{D}{E \cdot \cos\alpha}, \tag{10}$$

$$\varepsilon_S = \frac{D \cdot \cos\alpha}{E}. \tag{11}$$

From (10) and (11),

$$\varepsilon_N = \frac{\varepsilon_S}{\cos^2\alpha}$$

or

$$\varepsilon_S = \varepsilon_N \cos^2\alpha,$$

which coincides with (9).

The equations for the surfaces of ε_N and ε_S are as follows. From (10) and (11) we have

$$\varepsilon_N = \frac{D}{E \cdot \cos\alpha} = \frac{D}{E \cdot \frac{\mathbf{D} \cdot \mathbf{E}}{D \cdot E}} = \frac{D^2}{\mathbf{D} \cdot \mathbf{E}},$$

$$\varepsilon_S = \frac{D \cdot \cos\alpha}{E} = \frac{D \cdot \mathbf{D} \cdot \mathbf{E}}{E \cdot D \cdot E} = \frac{\mathbf{D} \cdot \mathbf{E}}{E^2}.$$

From the construction of the Fresnel ellipsoid and optical indicatrix

$$\mathbf{D}\cdot\mathbf{E}=1,$$

and, so,

$$\varepsilon_N = D^2, \tag{12}$$

$$\varepsilon_S = \frac{1}{E^2}. \tag{13}$$

Expressing in (5) and (7) the components of **E** and **D** via the direction cosines of these vectors, we put these equations in the form

$$\frac{1}{D^2}=\frac{c_1^2}{\varepsilon_1}+\frac{c_2^2}{\varepsilon_2}+\frac{c_3^2}{\varepsilon_3}, \tag{14}$$

$$\frac{1}{E^2}=\varepsilon_1 c_1^2+\varepsilon_2 c_2^2+\varepsilon_3 c_3^2. \tag{15}$$

Comparison of (12) with (14), and of (13) with (15), gives

$$\frac{1}{\varepsilon_N}=\frac{c_1^2}{\varepsilon_1}+\frac{c_2^2}{\varepsilon_2}+\frac{c_3^2}{\varepsilon_3}, \tag{16}$$

$$\varepsilon_S=\varepsilon_1 c_1^2+\varepsilon_2 c_2^2+\varepsilon_3 c_3^2, \tag{17}$$

where c_1, c_2, and c_3 are the direction cosines of **D** and **E**, respectively. Figure 4 shows the method of constructing the surfaces for ε_N and ε_S. The dielectric-constant surface is thus double for an anisotropic body; ε_N and ε_S are equal only along the principal axes of the Fresnel ellipsoid and optical indicatrix.

This method of interpreting the electrical polarization can be extended to other phenomena described by symmetric second-rank tensors.

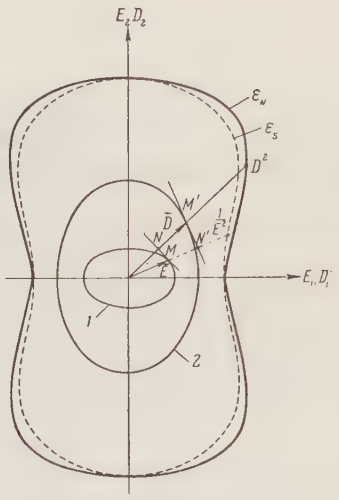

Fig. 4. Double surfaces for ε_S and ε_N for the particular case of a section of surfaces of rotation by a plane through the axis of rotation: 1) Fresnel ellipsoid; 2) optical indicatrix.

We are indebted to Academician A. V. Shubnikov for a valuable discussion of the present results.

LITERATURE CITED

1. N. E. Kochin, Vector Calculus and the Principles of Tensor Calculus [in Russian] (Moscow, 1951).
2. A. V. Shubnikov, "Symmetry and geometrical interpretation of two-dimensional polar tensors," Izv. AN SSSR, ser. fiz., 13, 3, 376-391 (1949).
3. A. V. Shubnikov, Optical Crystallography [in Russian] (Moscow, 1950).

TANGENTIAL GROWTH RATES OF ELEMENTARY LAYERS ON PARATOLUIDINE CRYSTALS

G. G. Lemmlein and E. D. Dukova

Institute of Crystallography, Academy of Sciences of the USSR
Translated from Kristallografiya, Vol. 1, No. 1,
pp. 112-118, January-February, 1956
Original article submitted November 1, 1955

Growth from the vapor state is reported for p-toluidine, with emphasis on the relation of tangential growth rate on (001) faces to thickness for elementary layers at 1.2% supersaturation. The thickness is measured from the birefringence, by Senarmont's method, and in reflection. The results are considered to show that there is an adsorbed layer on a growing surface; the differences in growth rates are due to surface diffusion, which is especially important for elementary layers, which grow more rapidly than thicker ones. Dislocations also occur at the junctions between parts of a skeletal structure.

Surface morphology and direct examination show that crystals grow via very thin layers. Theory shows that more energy is released when an ion is attached to an incomplete layer on a NaCl crystal than when it starts a new layer, so the growth probability for an existing layer is higher than the nucleation probability for a new one [1]. The current theory of crystal growth from the vapor state deals only with the motion of a layer of elementary height [2], although observation shows that actual layers are tens or hundreds of units high.

Quantitative empirical relations for layer growth are needed as a basis for further advances in crystal growth theory. We especially need evidence on the effects of layer weight on propagation rate (tangential growth rate).

Marcelin (1914) [3] was the first to observe the formation of very thin layers on faces for p-toluidine growing from alcoholic solution. The crystals were thin enough to give low-order interference colors in reflection, so the thickness of any layer was easily measured. The minimum thickness appeared to be that of two molecules (about 18 Å).

In 1922, Volmer [4] reported layered growth on PbI_2 crystals formed at an interface between $PbNO_3$ and KI solutions; he found that thick layers grow more slowly than thin ones, and he supposed that the lower limit of thickness would be of molecular order, but he did not measure the thickness. Some general observations on growth from solution for layers 1600-4000 Å thick have been reported by Bunn and Emmett [5].

We have examined layer growth in p-toluidine in the vapor at low supersaturation, which was produced in a chamber with a horizontal temperature gradient. This consisted of a glass cylinder having a heating wire in the base and also a small internal heater surrounding a crucible containing the material. This chamber was set up on the stage of a microscope, the crystals growing on the flat glass top (Fig. 1). The bottom heater controlled the gen-

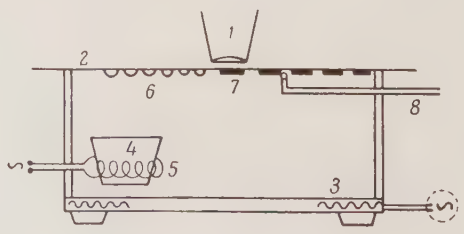

Fig. 1. Chamber for observing crystals growing from the vapor. 1) Microscope; 2) glass cover; 3) glass base with heater wire; 4) crucible; 5) heater; 6) drops of liquid; 7) crystals; 8) thermocouple.

Fig. 2. Stepped layers on crystals of p-toluidine between crossed polarizers; first-order colors occur in the thin parts (× 400).

eral temperature, while the crucible heater controlled the supply of vapor. The appropriate horizontal temperature gradient was thereby set up on the cover. The temperature near the surface was measured with a copper–constantan couple. Growth could be observed around the melting point (44°). The layers on (001) faces had rounded outlines at 1-5° away from that point (tangential growth rate not dependent on the azimuth). Layered growth involving liquid droplets was observed at the same temperature [6], but these could appear on the surface only at a certain temperature and vapor pressure. A constant vapor pressure was provided by keeping the evaporator at a fixed temperature; the temperature at the crystal was controlled with the bottom heater. The drops and protuberances indicate certain definite conditions. The supersaturation was calculated from the temperature; in the above case it was 1.2%, or about 10^{-2}.

Paratoluidine is orthorhombic and has a layered structure; the unit cell contains 8 molecules (two layers of four) and has the large value of c = 23.5 Å. The birefringence is very high (0.22).

The layered growth on (001) faces is very prominent. The tangential growth rates were measured without reference to the crystallographic direction, as the layers were rounded. Layers of elementary thickness could be observed at ×400 on account of the large c parameter, as in Marcelin's [3] and Kowarski's [7] work. The above conditions allowed us to examine layers from elementary thickness up to 150c, on account of the high birefringence.

The growth rate was measured with a seconds clock and an ocular micrometer.

Heights from 20c to 150c were measured between crossed nicols, the thickness being given by

$$\Delta = (n_g - n_p)\, e_1,$$

where Δ is path difference, $(n_g - n_p)$ is birefringence, and e_1 is thickness. These measurements could be made only on stepped crystals 3-10 μ thick, giving first- or second-order colors in the thin part. An increase of 150c in the second order gave a sharp change of color. The thicknesses on the two sides of a step gave the height of the step. Similarly, the mean thickness of several layers can be deduced in the same way, as in Fig. 2.

Smaller thicknesses were measured in reflection by Perrin's method [8]: $\Delta = 2ne_2$, where Δ is path difference, n is refractive index for the given direction, and e_2 is thickness.

Combination of these two formulas gives $e_1/e_2 = 2n/(n_g - n_p)$; the ratio is 15 for p-toluidine, so a given path difference is produced by a thickness 15 times smaller. A crystal only 1 μ thick gives no color between crossed polarizers, while the height of a step that produces a sharp change of color in the second order is only 10c. There is an appreciable color change from the passage of very thin identical layers. Measurements were made in this way on layers of thickness up to 10 units.

The results were verified and extended by using Senarmont's method with a $\lambda/4$ plate. (The Senarmont compensator is suitable for very small path differences.) The path difference Δ is

$$\Delta = \frac{2\theta}{360}\lambda,$$

where θ is the angular displacement of the analyzer from the crossed position, and λ is wavelength. The mercury green line (λ = 546 mμ) is equivalent to 30 Å per 1°, which corresponds to 136 Å thickness (about 6c) for p-toluidine.

Growth occurs via spiral layers under the conditions we used [6], but we took measurements only at points where the radius of curvature of the growth front was not less than 100 μ, in order to eliminate any effects from the curvature. The usual formula [2] indicates that the tangential rate for a front of radius 100 μ differs by only 0.2% from that for a straight front if the height is 15c and the distance between steps is 10 μ. The mean rates were measured to 4-5%, so the correction for curvature is quite negligible.

The thickness was reduced to the number of elementary layers n = h/c, in which h is height; the actual heights were always close to integers on this basis, and the rate always showed a distribution related to the height, with few intermediate values.

There was good agreement between growth rates measured in different ways for layers of the same thickness (Table 1). The third line is the volume deposited on unit length of a step in 1 sec.

The amount is least for the layer of unit height; it is rather larger for 2c but then remains roughly constant up to 25c, after which it rises again. This difference arises from variation in the spacing between successive steps in spiral-layer growth; the steps on thin layers are close together, whereas those on thick ones are far apart. The influx of material per unit area of face is presumably fixed under specific conditions, so the distance between steps should be determined by the thickness and tangential growth rate. This feature requires more detailed examination.

It is clear that the crystal grows only via propagation of layers under these conditions. The

TABLE 1

Height, in units of c	1	2	3	4	5	6	7	8	9	10	15	25	40*	50	100	150	200*
Growth rate, μ /sec	8.0	6.5	5.0	3.8	3.0	2.5	2.1	1.9	1.6	1.5	1.0	0.6	0.49*	0.4	0.3	0.25	0.27
Volume deposited per unit length, $\mu^2 \cdot 10^4$	188	305	353	358	353	353	346	357	339	353	353	353	460	470	705	981	1269

Note. The asterisks denote Kowarski's values for crystals in vapor under conditions similar to ours. The thicknesses have been converted to c units.

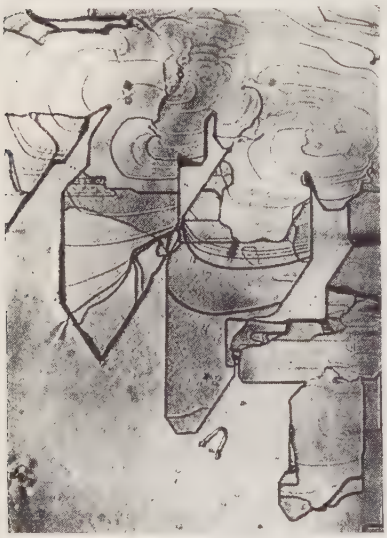

Fig. 3. Propagation of successive layers from growth centers.

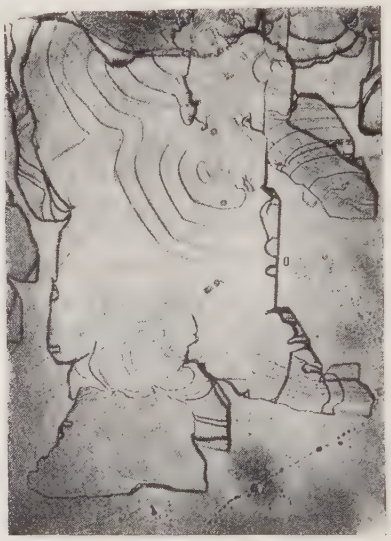

Fig. 4. Dislocations arising at the junction of parts of a skeletal structure.

sources of the layers are indicated by the current theory as lying at the points where dislocations emerge, these giving rise to steps that are the growth centers for the layers [2].

These dislocations (Fig. 3) do act as layer courses; we have previously considered the origin of the dislocations [6], which arise where parts of a skeletal crystal meet. Paratoluidine usually starts to grow from the corners, and the points where layers meet may be ones where the two lattices do not fit exactly, so a dislocation arises. This provides a highly active center for further growth and a source of spirals, as in Fig. 4. Turns far from the center are of large radius and produce nearly straight growth fronts (Figs. 2 and 3).

Figure 5 shows the growth rate as a function of thickness for straight fronts.

It is clear that the rate for an elementary layer is very different from that for a thick one at the same temperature and supersaturation. The difference may be due to growth via a mobile adsorbed layer instead of direct from the vapor [9]. Frenkel [10] discussed surface fluctuations in relation to the observed roughness of crystal faces; he showed that there should be such an adsorbed layer, in which the atoms or molecules can migrate freely over the surface. Barton et al. [2] also assigned an important part to surface diffusion in the growth of elementary steps.

The growth rates for straight fronts show that surface diffusion does play a very large part in the growth of the elementary layers. The diffusion flux reaches a limit for a height of 3c, and the curve of Fig. 5 is a hyperbola, as Table 1 indicates. The proportion entering by surface diffusion becomes relatively small for large thicknesses, for then much material is received directly from the vapor.

These processes cause the growth rate to become independent of the thickness; the curve of Fig. 5 becomes nearly horizontal above 25c, where it tends asymptotically to a constant value. The growth rate for an infinitely thick layer (by extrapolation) is

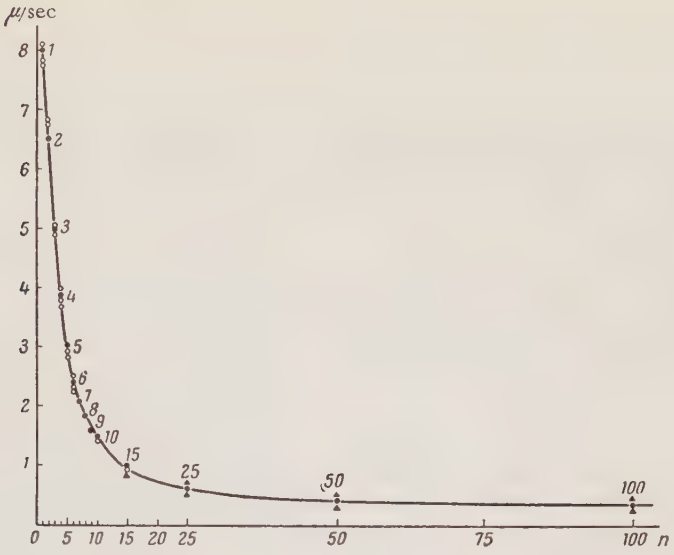

Fig. 5. Tangential growth rate as a function of thickness: filled circles, Senarmont compensator; open circles, Perrin's method; triangles, measurements between crossed polarizers.

0.1 μ/sec, which thus gives us the rate for a macroscopic platelet under these conditions, as the tangential rate on (001) may be taken as equal to the normal rate for a side face, which is 8.6 mm/day under the above conditions. This agrees roughly with results for platy substances similar to p-toluidine when grown from the vapor.

LITERATURE CITED

1. I. N. Stranski, "Zur Theorie des Kristallwachstums," Z. Phys. Chem., 136, 259-278 (1928).
2. W. K. Burton, N. Cabrera, and F. Frank, "The growth of crystals and the equilibrium structure of their surfaces," Phil. Trans. Royal Soc., London, A243, 299-358 (1951).
3. R. Marcelin, "Etude experimentale sur le developement des cristaux (Note posthume)," Ann. de Phys., ser. 9, 10, 189-191 (1918).
4. M. Volmer, "Zum Problem des Krystallwachstums," Z. Phys. Chem., 102, 267-281 (1922).
5. C. W. Bunn and U. Emmett, "Crystal growth from solution," Dis. Faraday Soc., 5, 119-128 (1949).
6. G. G. Lemmlein and E. D. Dukova, "Observations on spiral growth on growth on crystals of p-toluidine," DAN SSSR, 102, 77-79 (1955).
7. L. Kowarski, "Sur la croissance des cristaux tres mincés," J. Chem. Phys., 32, 303-331 (1935).
8. J. Perrin, "La stratification des lames liquides," Ann. de Phys., ser. 9, 10, 160-188 (1918).
9. M. Volmer, Kinetik der Phasenbildung (Dresden, 1939).
10. Ya. I. Frenkel', "Surface motion of particles on crystals and the natural roughness of crystal faces," ZhÉTF, 16, 39-52 (1946).

TANGENTIAL GROWTH RATES OF ELEMENTARY LAYERS ON THE SURFACE OF A CRYSTAL

A. A. Chernov

Institute of Crystallography, Academy of Sciences of the USSR
Translated from Kristallografiya, Vol. 1, No. 1,
pp. 119-122, January-February, 1956
Original article submitted November 10, 1955

A study is made of the kinetics of the tangential growth of elementary layers of various thicknesses on the surface of a growing crystal. On the basis of the concept of "creeping" molecules adsorbed by the surface, and on the assumption of slight supersaturation, a formula is derived connecting the rate of movement of the front of the elementary layer with the thickness of the latter. A comparison is made with experimental data.

According to modern concepts, first developed by Frenkel' [1], the crystal face of any substance, in equilibrium with another phase of the same substance, comprises a multitude of microscopic steps of different heights. The "staircase" formed by these steps has rises and falls, so that the macroscopic face is plane, and is characterized by simple indices. The front of each step is also not a straight line, but has "Frenkel' discontinuities" of molecular order of magnitude. The molecules adsorbed on the face of the crystal form an adsorbed layer in equilibrium with the "Frenkel' discontinuities" and the medium surrounding the crystal. If the equilibrium is disturbed, a transfer of molecules to the solid phase occurs at the positions of these discontinuities, leading to the formation of plane (superficial) diffusion streams. The consumption of substance in the adsorbed layer is made good by the deposition of fresh molecules from the medium surrounding the crystal. It is thus significant that direct condensation of the substance to the solid phase occurs only on the lateral surfaces of the steps, which we shall call the absorbent or active surfaces.

Applying these concepts to steps of the height of one molecule, Burton, Cabrera, and Frank [2] developed a theory of the growth of crystals from the gas phase. Direct microscopic observation of the face of a growing crystal, however, shows that steps of a thickness of up to 1000 molecules or more play a very important part in the growth process. Furthermore, experiments by Lemmlein and Dukova [3] have revealed that the thinnest of the propagating layers have a thickness of one unit cell of the structure, and this, in the case, for example, of the organic substance paratoluidine, forms four molecules. From this follows the necessity to study the kinetics of the movement of the fronts of layers of polymolecular thickness. The present work examines the possibility of such a movement.

We shall examine the mechanism macroscopically and characterize the absorbent surface of a step, the mean profile ab of which is shown in the figure, by the coefficient of absorption β, the coefficient of diffusion $D_1 = a^2\nu e^{-U/kT}$ (where U is the activation energy of plane movement, $a \sim 5$ Å, the size of a molecule, $\nu \sim 10^{12}$ sec^{-1}, the frequency of vibration of a molecule as a whole), and some effective length $l = \theta h$. We shall characterize the points of the profile by the distance s to the center of the profile O. We denote the mean path of the adsorbed molecules on this surface by $\bar{s}_1$, and their chemical potential by μ_1. The same quantities, but referring to the nonabsorbent surface, will be provided with the subscript 2. The chemical potentials of the gas and solid will be μ_g and μ_s

As will be seen from Fig. 1, we are dealing with diffusion along the bent surface of an anisotropic body. Therefore, the equilibrium concentrations of the adsorbed molecules depend, generally

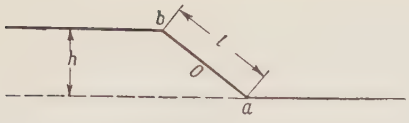

Fig. 1.

speaking, already on the coordinate of s. Due to this, it is more convenient to operate with the chemical potential of these molecules, which in equilibrium is contant along the entire surface.

The experiments of Lemmlein and Dukova [3] indicate that the front of a step moves at a velocity of not more than about 10 μ/sec, which is much less than the mean velocity of the molecules diffusing over the surface (of the order of hundreds of meters per second). When considering the diffusion of such molecules to the front of the step, their velocity may therefore be ignored.

With regard to the dependence of the velocity of movement of the front of the layer on the thickness of the latter, which is of interest to us, it may be noted that asymptotically for large values of h we should have

$$v(h) = v_\infty + a^3 j/h, \tag{1}$$

where v_∞ is determined by the quantity of substance arriving on the absorbent surface directly from the gas phase, while j is the density of flow of plane diffusion. Subsequently, however, we shall be mainly concerned with the range of small values of h.

We consider the case where $D_1 = \infty$, i.e., $\mu_1 = \text{const} = \mu_{1\infty}$. We shall consider the diffusion process to be stationary. The density of diffusion flow of adsorbed molecules to the nonabsorbent surface is $\gamma_2(d\mu_2/ds)$. The number of molecules deposited from the vapor per unit of this surface of the crystal, for small deviations from thermodynamic equilibrium, is evidently $\alpha(\mu_g - \mu_2)$; here, γ and α are coefficients of proportionality, connected, in the case of low densities n of molecules adsorbed on the surface, with the usual coefficient of plane diffusion D and the mean lifetime of a molecule in the adsorbed state τ by the relationships

$$\gamma_i = \frac{n}{kT} D_i,\ i = 1.2,\quad \alpha = \frac{n_1}{kT\tau_1} \approx \frac{n_2}{kT\tau_2}.$$

Generally speaking, they depend on μ, but for small values of μ, this dependence may be ignored. From the foregoing, it is clear that the law of conservation of matter leads to the following equation for the chemical potential on the nonabsorbent surface ($s > l/2$):

$$\gamma_2 \frac{d^2\mu_2}{ds^2} - \alpha(\mu_2 - \mu_g) = 0. \tag{2}$$

We now formulate the boundary condition for $s = l/2$. In unit time on the part aO, $\beta l/2(\mu_{1\infty} - \mu_s)$ molecules are absorbed, $(\alpha l/2)(\mu_g - \mu_{1\infty})$ molecules are deposited from the gas, and $a\gamma_2(d\mu_2/ds)$ molecules diffuse through the point a. Therefore,

$$\gamma_2 \frac{d\mu_2}{ds} + \frac{\alpha l}{2}(\mu_g - \mu_{1\infty}) = \frac{\beta l}{2}(\mu_{1\infty} - \mu_g). \tag{3}$$

By virtue of the continuity of the chemical potential, $\mu_2 = \mu_{1\infty}$. Hence,

$$\gamma_2 \frac{d\mu_2}{ds} + \frac{\alpha l}{2}(\mu_g - \mu_2) = \frac{\beta l}{2}(\mu_2 - \mu_s). \tag{4}$$

By solving (2) together with (4), it is easy to see that

$$\begin{aligned} v &= \beta l a^3 (\mu_{1\infty} - \mu_s)/h \\ &= v_\infty + a^3\beta\vartheta(\mu_g - \mu_s)/1 + \beta l/2\sqrt{\gamma_2\alpha}. \end{aligned} \tag{5}$$

We shall now take into account the finite nature of the quantity D_1. For this purpose, $\mu_{1\infty}$ in (4) must be replaced by some mean value $\bar{\mu}_1$; the difference between these values $\mu_{1\infty} - \bar{\mu}_1$ may be represented by a series of powers of the ratio of the length of the step to the value of the mean path of a molecule in the adsorbed state $l/\bar{s}_1$, commencing with a term of first order (for $D_1 = \infty$, $\bar{s}_1 = \infty$ and $\mu_{1\infty} - \mu_1$ ought to disappear). The finite nature of D_1 may therefore be allowed for by adding to the right-hand part of (4) terms with successive powers of $l/\bar{s}_1$. It is clear, however, that in the first place, for calculating the coefficients of such an expansion, some additional considerations of a physical nature are required and, in the second place, it will not be true for large values of h. It is therefore more expedient to start from a natural model of the uniformly absorbing surface of a step, and solve the following boundary problem exactly:

$$\begin{gathered} \gamma_1 \frac{d^2\mu_1}{ds^2} + \alpha(\mu_g - \mu_1) + \beta(\mu_s - \mu_1) = 0,\ 0 < s < \frac{l}{2}, \\ \gamma_2 \frac{d^2\mu_2}{ds^2} + \alpha(\mu_g - \mu_2) = 0,\ s > \frac{l}{2} \\ \text{for } s = 0 \quad \frac{d\mu_1}{ds} = 0, \text{ for } s = \frac{l}{2}, \quad \gamma_1 \frac{d\mu_1}{ds} = \gamma_2 \frac{d\mu_2}{ds}. \end{gathered} \tag{6}$$

Here, the term $\beta(\mu_s - \mu_1)$ takes into account the transfer of substance to the solid phase.

From this, considering that $\beta \gg \alpha$, we have

$$\begin{aligned} v(h) &= \frac{a^3}{h}\int_0^l \beta(\mu_1 - \mu_s)\,ds \\ &= a^3\delta\mu\left[\theta\alpha + \frac{1}{h}\frac{2\sqrt{\gamma_2\alpha}}{1 + \sqrt{\frac{\gamma_2\alpha}{\gamma_1\beta}}\coth\sqrt{\frac{\beta}{\gamma_1}}\frac{\theta h}{2}}\right] \end{aligned} \tag{7}$$

where $\delta\mu = \mu_g - \mu_s$.

TABLE 1

$h/4a$	1	2	3	4	5	6	7	10	15	50	100
v_{exp}, μ/sec	8	6.5	5	3.8	3	2.5	2.1	1.5	1.0	0.4	0.3
v_{calc}, μ/sec	9	6.1	4.5	3.5	2.9	2.5	2.2	1.6	1.1	0.4	0.25

For $D_1 \to \infty$, $\gamma_1 \to \infty$, and (7) becomes (5). Here, the quantity $\theta = l/h$, determining the mean deviation of the absorbent surface from the vertical obviously varies from values of the order of several units for small values of h (in the comparison with experiment, we considered $\theta = 4$), and approaches unity as h increases. At the same time, for low values of h, the first term of the sum in (7) plays altogether a relatively minor part, and in it we may therefore put $\theta = 1$. In the second term, θ forms part of an expression which rapidly tends to a constant limit as h increases, so that the variation of h may here be ignored and this quantity may be regarded as constant. The problem of the strict determination of the dependence of θ on h is one of surface structure and currently has not been solved.

Proceeding to a brief discussion of the expression obtained, we note first of all that it is proportional to $\delta\mu$. Just as in expression (1), the first term represents the contribution of the flow of substance from the gas phase directly onto the absorbing surface, while the second term represents the plane diffusion flow. The coefficients in formula (7) vary according to the properties of the substance. With increase in the energy of sublimation and the bond energy per molecule proportional to it, the mean length of the plane path of the adsorbed molecule increases and the coefficient $\alpha \sim \nu e^{-W/2kT}$ falls (W is the bond energy per molecule). In view of the fact that the first term of (7) is proportional to α, while the second is proportional to $\sqrt{\alpha}$, plane diffusion flow plays a relatively larger part in the growth of difficultly volatile substances than in the growth of volatile substances. A decrease in the frequency of vibration ν of the adsorbed molecules as a whole acts in the same way as an increase in the energy of sublimation.

The second term of (7) shows that those values of h, commencing with which the dependence of interest to us assumes the character (1), are determined by the quantity β or, more exactly, by the ratio between the mean paths $\bar{s}_1$ and $\bar{s}_2$ of the molecules in the adsorbed state on the absorbent and nonabsorbent surfaces, respectively.

The presence of an impurity, i.e., the presence of foreign molecules in the adsorbed layer, must alter the value of the diffusion coefficients D_1 and D_2, and hence the rate of growth itself.

Since the same kinetic mechanism evidently operates in the growth of crystals from solution, the results obtained are also applicable to that case.

A number of circumstances make comparison with experiment difficult: first, the value of the constants α and $\gamma_1 \sim \gamma_2$ are expressed merely in order of magnitude through sublimation energy and frequency ν; second, the only measurements of this kind (of G. G. Lemmlein and E. D. Dukova) have been made on one substance only, i.e., paratoluidine. We considered $\theta = 4$, $W/kT \sim 20$, corresponding to a sublimation energy of ~15 kcal/mole, and $\bar{s}_2 = 200\ a$, and hence found α and γ_2. It was then possible to select in (7) a value of $\beta \gg \alpha$ ($\beta \sim 40\ \alpha$), such that there was sufficiently close approximation of the experimental data in the limits of the approximate examination. The selected value[1] of $\delta\mu$ determines the additive component in (7), while β determines the form of the curve. Table 1 shows the calculated and experimental values of the velocities of movement of the fronts of layers of different thicknesses as calculated and found experimentally.

It is not difficult to see from Table 1 that there is an appreciable departure from law (1) at $h < \sim 12\ a$, i.e., three heights of the unit cell of the structure. Diffusion flow plays an important part up to $h \sim 300 \cdot 4a$.

We are happy to take this opportunity of thanking I. M. Lifshits and G. G. Lemmlein for their interest in the work, and valuable discussions.

LITERATURE CITED

1. Ya. I. Frenkel', "Surface creep of particles in crystals and the natural roughness of crystal faces," ZhÉTF, 16, 1, 39-52 (1946).
2. W. K. Burton, N. Cabrera, and F. C. Frank, "The growth of crystals and the equilibrium structure of their surfaces," Phil. Trans., Ser. A: No. 866, 243, 299-358 (1951).
3. G. G. Lemmlein and E. D. Dukova, "Investigation of the rates of tangential growth of elementary layers on paratoluidine crystals," Kirstallografiya, 1, 112-118 (1956).

[1] In the experiments described above, supersaturation was not measured; it is merely known that it was constant.

THE MOLECULAR SCATTERING OF LIGHT AND THE $\alpha \rightleftharpoons \beta$ TRANSFORMATION IN QUARTZ

I. A. Yakovlev, L. F. Mikheeva, and T. S. Velichkina

M. V. Lomonosov Moscow State University

Translated from Kristallografiya, Vol. 1, No. 1,
pp. 123-131, January-February, 1956
Original article submitted November 1, 1955

In investigation of molecular statistical phenomena in solid bodies close to phase transition points, measurements were made of the intensity of the molecular scattering of light in quartz, over the temperature range 15-600 °C. The phenomenon of opalescence was detected in the crystal at 573°C, indicating intense and reversible formation of small optical nonuniformities in the quartz in the vicinity of the phase transition temperature.

Introduction and Experimental Method

In the detailed investigation of the molecular mechanism of phase transformations in solids, the topics to be studied may conveniently include phenomena bearing on the statistical side of molecular processes. The phenomena in this category include the molecular scattering of light, the existence of which, in crystals, was first established by Landsberg [1].

Molecular scattering of light occurs at small nonuniformities in the optically pure medium, these being continuously created and reabsorbed as a result of thermal movements of the molecules.

The intensity of the light scattered in the medium is $I \sim I_0 \overline{\Delta\varepsilon^2}/\lambda^4$, where I_0 is the intensity of the primary beam and λ is the wavelength of the light [2]. The quantity $\overline{\Delta\varepsilon^2} = \overline{(\varepsilon - \varepsilon_0)^2}$, which supplies a quantitative expression for the factor of most importance in considering the phenomenon, is the mean-square fluctuation of the optical dielectric permeability from its average value ε_0. If we use the variables ρ and T, in the case of an isotropic liquid the quantity $\overline{\Delta\varepsilon^2}$ can be written in the form

$$\overline{\Delta\varepsilon^2} = \left(\frac{\partial\varepsilon}{\partial\rho}\right)_T^2 \overline{\Delta\rho^2} + \left(\frac{\partial\varepsilon}{\partial T}\right)_\rho^2 \overline{\Delta T^2}, \qquad (1)$$

where ρ and T are the density and temperature of the medium, and $\overline{\Delta\rho^2}$ and $\overline{\Delta T^2}$ are the corresponding mean-square fluctuations of these quantities in the microvolume under consideration. Experience has shown that in all known cases of scattering of light, $(\partial\varepsilon/\partial\rho)_T^2 \overline{\Delta\rho^2} >> (\partial\varepsilon/\partial T)_\rho^2 \overline{\Delta T^2}$. Then, $\overline{\Delta\varepsilon^2} = \rho^2 (\partial\varepsilon/\partial\rho)_T^2 kT\beta_T$, since $\overline{\Delta\rho^2} = \rho^2 kT\beta/v$, where k is Boltzmann's constant and β is the compressibility of the medium [2]. The value of $\overline{\Delta\varepsilon^2}$ in an anisotropic medium will not be considered for the moment. It is important to note that the quantity $\overline{\Delta\varepsilon^2}$ is proportional to the compressibility of the medium, which shows that a relationship exists between the intensity of the light scattered and the elastic properties of the medium. The quantity $\Delta T^2 = kT^2/C_V$, where C_V is the specific heat of the bulk material within the fluctuation range. It will be shown below that under solid-body phase-transition conditions, the dependence of the scattered-light intensity on the temperature term cannot be neglected, which lends a special character to the present light-scattering study in comparison with earlier investigations. The characteristic relationship between I and λ^4, holding only in the case of optical nonuniformities of size $l < \lambda$, provides an important experimental criterion in considering the average size of the light-scattering nonuniformities in the medium.

From the foregoing it will be apparent that the intensity of the scattered light will be intricately bound up with statistical phenomena occurring in the medium, and can be used in investigating these phenomena. It is only necessary to select effective conditions in applying the scattering of light to the

study of the fluctuation processes taking place during solid-body phase transitions.

As the first case for investigation, we selected the $\alpha \rightleftharpoons \beta$ transformation in quartz (T = 573°). Our choice was determined by the high quality of quartz single crystals, which have been thoroughly studied under the most diverse conditions [3,4]. The quartz phase transformation must be considered, in the thermodynamic sense, as a transition of the second kind, since it is virtually unaccompanied by stepwise changes in specific volume and entropy [5,6,7]. Supporting the view that the quartz phase transition is a λ-point, is the increase in symmetry of the crystal on attaining the high-temperature form: $A_3 3A_2 \rightarrow A_6 6A_2$ [8]. According to results given by Perrier and Mandrot [9], the elastic constants of quartz pass through a minimum close to the transition point, and the refractive index of quartz alters extremely rapidly under the same conditions [10]. From these facts we may expect, according to formula (1), that the intensity of the scattered light will increase markedly during the phase transformation, and may serve to indicate statistical phenomena taking place within the quartz. An important consideration in favor of the choice of quartz as the experimental material was the availability of data on scattering of light in it. This information appears in the series of articles [1], while an exhaustive experimental and theoretical study of the molecular scattering of light in quartz was carried out by Motulevich [11], who investigated the phenomenon up to a temperature of 250°C. Thus, the normal course of a projected experiment could be reliably checked by comparing it with the results of work carried out previously.

Description of Experiments

To pursue the objectives stated above, the apparatus shown diagrammatically in Figs. 1 and 2 was assembled. A light beam from a mercury lamp passes through a quartz crystal held in a furnace. The light scattered by the quartz at right angles to the primary light beam is registered by a photoelectronic multiplier.

Oriented 20 × 20 × 40-mm parallelepipeds of polished quartz were prepared from best-quality specimens of optical quartz, not containing twins.[1] However, the ultimate criterion for the suitability of a specimen for further work was the temperature–intensity behavior [1] shown by scattered light up to 250°, and according to experimental and theoretical data the relationship should be linear; during our experiments we were able to compare the behavior with the painstaking measurements made by Motulevich [11].

In order that the results of the projected experiments would be of interest with regard to the practical study of phase transitions in crystals, the experimental temperature conditions needed particular attention. It was necessary to keep to a minimum the temperature gradients in the crystals, because of the extreme variations with temperature of the properties of the crystal close to the transition point. Analysis of the appropriate data showed that it would be inadvisable to work with a furnace temperature gradient over 1 deg/cm. This was a very harsh requirement for a furnace working at a temperature of about 600°C, and having three windows on the level of the working zone to boot.[2] On the other hand, it was necessary to bring about a temperature distribution in the crystal which would satisfy the optical demands of the experimental layout (see below). The furnace had a square 120 mm^2 horizontal cross section, was 250 mm high, and was welded from 8-mm thick iron (see Fig. 2). Windows of diameter about 20 mm were arranged at a height of 160 mm above the base of the furnace. To reduce heat losses through radiation, at 600°, the windows were occupied by heatproof glass light filters. Inside the furnace, the windows were provided with thin lightproof metal sleeves. The outer surface, under the Nichrome heating coil and above this, was smeared with a mixture of alumina and fireclay.

The removable lid to the furnace was thermally insulated by a ceramic fitting containing a heating coil. The quartz crystal Q was placed on a metal platform P attached to a thin porcelain tube PT. The furnace stood on a massive ceramic slab CS. A ceramic fitting containing a heating coil was placed inside the furnace on this ceramic slab. After the crystal had been placed in position, the removable furnace lid and the lower perimeter of the furnace were hermetically sealed with fireclay; the furnace thus contained a closed thermal zone. A metal jacket MJ was placed over the furnace, forming an air pocket 50 mm thick between each of the outer walls of the furnace and the metal jacket. The three heating coils mentioned above were inde-

[1] Through the kind cooperation of Academician A. V. Shubnikov, some of the quartz specimens used were prepared by A. B. Gil'varg at the Institute of Crystallography of the Academy of Sciences; to these persons the authors are deeply grateful.

[2] The authors are deeply grateful to V. A. Sokolov for valuable consultations on the problems involved in achieving the necessary experimental temperature conditions.

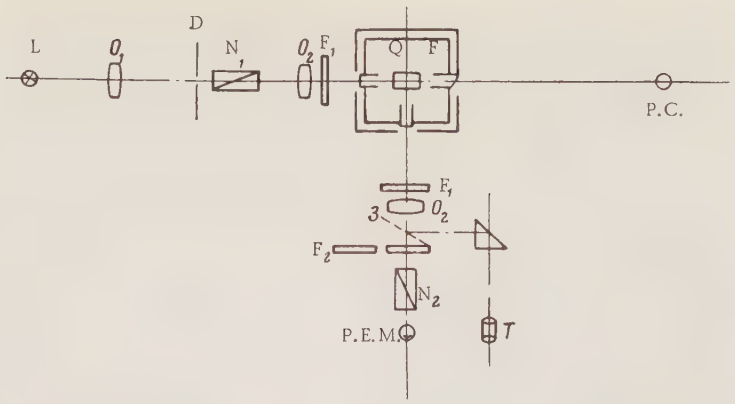

Fig. 1. General layout of the apparatus (horizontal projection). L) Ultra high-pressure mercury lamp; O_1, O_2, O_3) object lenses; F_1) heatproof light filter; F_2) colored light filter; N_1, N_2) Nicol prisms; PC) photocell; PEM) photoelectronic multiplier; M) mirror gate; T) telephoto lens; F) furnace.

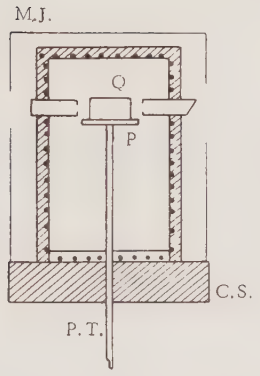

Fig. 2. Vertical section through the furnace. MJ) Metal jacket; Q) quartz crystal; CS) ceramic slab.

pendently fed from a battery supply. The currents through the coils were maintained to an accuracy of 0.05 A, using an ELA-type ammeter. Temperatures were measured with a Pt/PtRh thermocouple and a potentiometer; one of the thermocouple junctions was placed in melting ice. The thermocouple and the crystal could be adjusted by microscopic amounts in vertical, horizontal, and rotational senses, while in the sealed furnace. Temperature gradients were measured by altering the thermocouple position under rigidly constant furnace conditions. Gradients detected in the working zone were compensated for by altering the currents in the base and lid heating coils. At temperatures near 573°, it was found possible to keep the vertical temperature gradient in the crystal zone down to 0.01 deg/mm. The horizontal gradient in the direction of propagation of the light beam was kept down to 0.03 deg/mm. The highest temperature in the crystal was that near the entry window, brought about by the use of unequal-sized entry and exit windows in the furnace. From the above, it will be seen that the isothermal layers in the crystal lay practically perpendicular to the light beam passing through the crystal. This meant that as the furnace was heated, the phase transformation region, passing along the light beam because of the temperature gradient, automatically had to pass by the observation window in the furnace and the photoelectronic multiplier or telephoto lens and camera placed at this window. Finally, some special experiments were carried out to determine the temperature–time curves for which the thermocouple temperature corresponded to the temperature of the crystal alongside it. The furnace was heated extremely slowly; a complete experimental cycle (15° → 600° → 15°) occupied more than 72 hours. The rate of temperature change near the phase transition point was about 0.3 deg/h.

Experimental Results: The Opalescence Phenomenon

The final measurements on the relationship between the intensity of light scattered by quartz and the temperature of the quartz, were made on three specimens. Two of the quartz specimens came from the same deposit, while the third was obtained from another source. Several experiments were carried out on each specimen. Investigations were made of various combinations of directions of primary and scattered beams in the quartz, using different polarization conditions; these are indicated in the table.

TABLE 1

Case No.	Primary beam		Scattered beam	
	Direction of propagation	Intensity and polarization state	Direction of propagation	Intensity and polarization state
1	y	I_Z	x } specimens	I_X, I_y
2	x	I_Z	z } 2 and 3	$I_X + I_y$
3	x	I_Z	y specimen 1	I_Z, I_X

Separate measurements of the individual intensity components were necessary to determine the depolarization of the scattered light, this being an essential parameter in considering the anisotropy of the scattering medium. The sum of the quantities I_X and I_y (in the second case) is given because, when the scattered light is propagated along the z axis, the optical activity of the quartz leads to a difference appearing between the values of I_X and I_y. Measurements were made of each of the values I_X, I_y, I_Z for the total light of the mercury lamp, for the 4360, 4078, and 4047 Å group of mercury lines, and for the 5460 Å line. From the relationship between the intensity of the scattered light and its wavelength, the dimensions of the optical nonuniformities could be estimated, this being one of the salient points of our experiment. It was important to use light filters, so that the percentage of parasitic light in the complete beam of light being registered would be lower for the shortwave part of the spectrum than for white light. The results obtained from measurements using a violet light filter were therefore the most reliable. These are the ones shown in the figures which follow. However, in our apparatus, because of the constancy of the weak parasitic light, the relationships found between the scattered light intensity and the temperature were exactly the same for blue, white, or green light.

In Figs. 3, 4, and 5 are shown the results of our measurements, in the order in which they are listed in Table 1.

The x axis of each graph shows the temperature, and the y axis the ratio $I_T/I_{20°}$, i.e., the intensity of the light scattered by the quartz at temperature T over the intensity at room temperature. A correction for the temperature-independent parasitic light, in our experiments not accounting for more than $0.3I_{20°}$, was introduced by the usual method of extrapolation of the linear part of the curve to absolute zero.[3] In Fig. 5, the maximum of $I_T/I_{20°}$, corresponding to the phase transition point, was inserted separately, since the main experiment had been accidentally stopped at the peak of the maximum, and we did not feel it was expedient to linkup results of subsequent tests on a single point of the curves with the results of the other experiments.

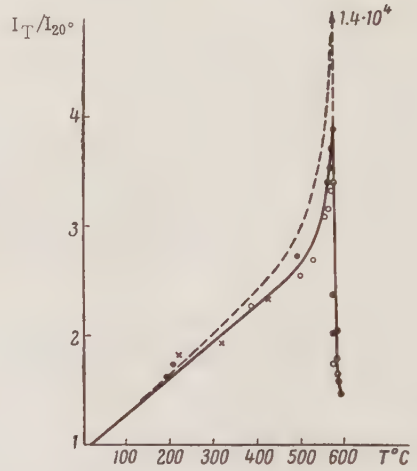

Fig. 3. Plot of intensity of scattered light against temperature (case 1 in Table 1). ● — Heating; ○ — cooling; × — repeat run; dashed line — theoretical curve (for the 573-600° range, this lay exactly on the experimental curve).

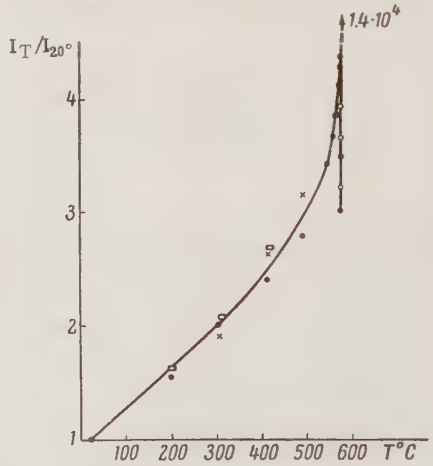

Fig. 4. Plot of intensity of scattered light against temperature (case 2 in Table 1). ● — Heating; ○ — cooling; × — repeat run.

[3]No correction was introduced into our results for the Raman effect because of its uncertain value under these conditions. The thermal radiation of the furnace was, of course, allowed for by making a direct measurement of the photoelectronic multiplier current when the mercury lamp was switched off. Thanks to the use of heatproof filters, even at 600° the thermal radiation of the furnace had only ≈5% of the intensity of the light scattered by the quartz at this temperature.

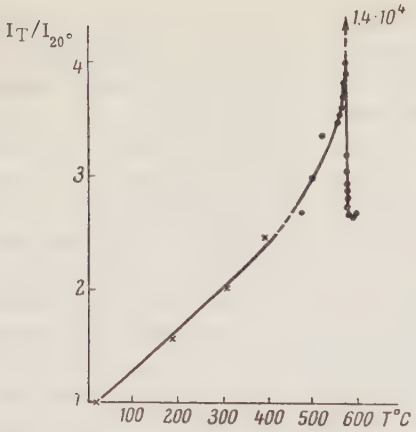

Fig. 5. Plot of intensity of scattered light against temperature (case 3 in Table 1). ×, ● – Heating.

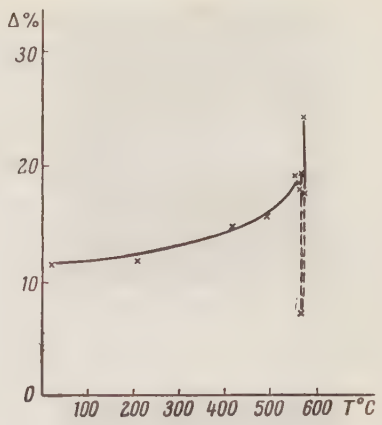

Fig. 6. Plot of depolarization of scattered light against temperature.

The slopes of the linear parts of our curves were all within 4% of Motulevich's results [11], obtained by the photographic photometry method in the temperature range 20-250°.

Figure 6 shows typical results for the depolarization – temperature relationship of the scattered light, with the temperature plotted along the x axis of the graph and the depolarization $\Delta = I_X/I_Z$ along the y axis. The results refer to case 1 in Table 1, but similar results were obtained in the other cases.

In Figs. 3, 4, and 5, the maxima on the curves are marked with an arrow and the figure $1.4 \cdot 10^4$. This indicates that over a 0.1-deg temperature range, close to 573°, there is a particularly rapid increase in the intensity of the scattered light, this reaching 10,000 times its room-temperature value $I_{20°}$. This intensity jump is due to a specific phenomenon, quartz opalescence, occurring near the phase transition temperature. Visual and photographic observations of the crystal, carried out in parallel with the scattered-light intensity measurements, showed that the "boundary" of the α and β phases is an area of marked optical nonuniformity in the crystal. At a temperature of 573°, it appeared as if a strongly light-scattering band of mist ($I \simeq 1.4 \cdot 10^4 I_{20°}$) began to move slowly from the hotter end of the quartz[4] to the colder end. On one side of the mist band lay α-phase quartz, and on the other side lay β-phase. As the temperature of the furnace was raised further, the mist band traveled to the opposite end of the crystal, and the whole crystal became transparent and weakly light scattering again.

On cooling the furnace, the mist band again appeared, at the cooler end of the crystal, and then moved away from this point toward the hotter end of the crystal. The band extended across the whole width of the crystal, and was 0.5 to 3 mm thick. We were able to vary its thickness by altering the horizontal temperature gradient in the quartz. The temperature range in the band was ≃0.1°. By stabilizing the furnace temperature, we were able to hold the mist band in the center of the crystal for 3 h. In Figs. 7, 8, and 9 are shown a series of photographs, showing the primary beam of light in the quartz before the appearance of the mist band at the phase boundary (exposure 1 h), the intersection of the mist band and the primary light beam for a horizontal temperature gradient of 0.3 deg per cm (exposure 1 sec), and another photograph of the latter for a gradient of 1 deg/mm. The photographically very unfavorable relationship between the intensity of scattered light in the mist band and that in the transparent parts of the crystal, on both sides of the band, meant that it was not possible to photograph the primary light beam satisfactorily in both the mist band and the adjacent transparent crystal phases simultaneously. In the last two photographs, therefore, the outlines of the primary light beams have been picked out with dashed lines.

The phenomenon in question occurred in all the quartz specimens investigated, and could be reproduced several times with any specimen. X-ray tests on specimens before and after heating did not show up any changes in their structures as a result of the treatment. There are thus no irreversible changes occurring in the crystal which are associated with the phenomenon we observed. The depolarization of the light scattered by the mist band was ≃6%, while that of light scattered by quartz under normal conditions is ≃12%, which indicates

[4]It will be recalled that the crystal virtually contained only a horizontal temperature gradient, directed along the primary light beam.

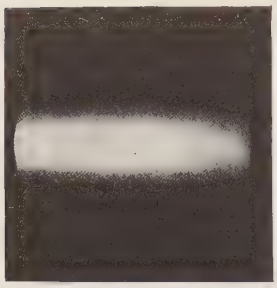

Fig. 7. Photograph of the primary light beam in quartz (exposure 1 h).

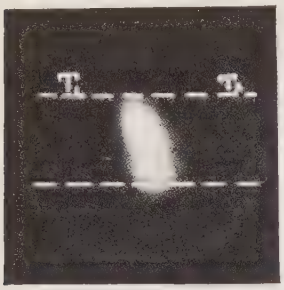

Fig. 8. Photograph of the intersection of the primary light beam and the mist band in quartz (exposure 1 sec; horizontal temperature gradient ≃0.03 deg/mm).

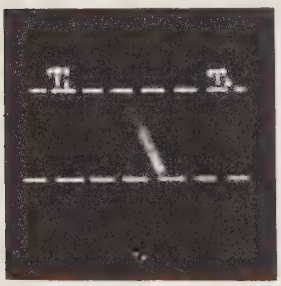

Fig. 9. Photograph of the intersection of the primary light beam and the mist band in quartz (exposure 1 sec; horizontal temperature gradient ≃1 deg/mm).

that the structure of the mist band is more weakly anisotropic than that of a normal quartz crystal (see Fig. 6).

Visual observations of the mist band in white light showed that when the band was viewed from the beam entry side, scattered blue light predominated, but when viewed from the exit side, more yellow light was scattered. Such behavior is typical for the passage of light through a strongly scattering medium. In order to estimate the size of the optical nonuniformities in the mist band, it was necessary to verify that the λ^{-4} law, for the intensity of scattering of light of different wavelengths, was obeyed. Over the whole experimental temperature range, beginning at room temperature, we monitored the scattering intensity ratio for blue to green light. The value of this ratio was ≃5. Under our conditions, the value of this ratio for the direct light of the mercury lamp was 1.6. For the light scattered by the mist band, this quantity was increased to a value of 10. So that the deductions to be drawn from this value should be unambiguous, we measured in our apparatus the ratio of intensities of scattered blue and green light for pure benzene, which has an undisputed molecular light-scattering character. Benzene, which is a liquid which scatters light extremely strongly, was chosen because its scattering was of roughly equal intensity to that observed in the mist band under consideration. The value for benzene of the ratio we were interested in was 4.2, in our apparatus. This provided grounds for the assumption that in the mist band we were dealing with optical nonuniformities smaller in size than the wavelength of the light. The increase in the ratio of intensities of blue to green light scattered by the mist band, above the corresponding value for scattering by benzene, was due to the fact that the relative proportion of parasitic direct light from the lamp was less in the experiments with the strongly light-scattering mist band than in the experiments with benzene.

Discussion of Experimental Results General Conclusions

The experimental results described above can be most simply discussed by following the natural division of the whole temperature range investigated into a series of intervals, characteristic of the phenomena described.

Over the temperature interval 20-400°, a linear relationship was established between the intensity of scattered light I, and the temperature T. In Motulevich's paper [11], this linear relationship was followed up to temperatures of 250°. In view of the fact that theoretical calculations also lead to a linear function for the explicit relationship between I and T, our results indicate that up to 400° the elastic and elasto-optical parameters of quartz which, with the temperature, determine the intensity of scattered light, are weakly temperature-dependent.

The temperature intervals 400-573° and 573-600° are two regions in which the relationship between I and T is not linear. Both the sharp increase

and the rapid fall in intensity of scattered light within these two intervals are in accord with other experimental data, indicating that quartz takes on quite different properties in the vicinity of its phase transition point. Thus, the sharp drop in the elastic modulus E of quartz, observed in [9] (to 1.7 of the original for $E_{\parallel z}$ and to 2.5 times the original for $E_{\perp z}$), points to an increase in the compressibility of quartz at about 573°, leading to greater fluctuations of density in the medium. In Fig. 3, the dashed curve shows the theoretical relationship between I and T for quartz, allowing only for the change in compressibility which is due to the variation with temperature of Young's modulus. The path of the dashed curve is in good agreement with the experimental results. In constructing the theoretical curve, it would be necessary to take into account not only the dependence of the compressibility on temperature, but also the relationship between refractive index and temperature, i.e., the temperature term in formula (1). The measurements made by Rinne and Kolb [10] established a relationship between n and T, but under the natural conditions of their experiments they measured this value at constant pressure, while formula (1) has the expression $(\partial\varepsilon/\partial T)_\rho$. The transformation from $(\partial\varepsilon/\partial T)_p$ to $(\partial\varepsilon/\partial T)_\rho$ does not present any mathematical difficulties, since $(\partial\varepsilon/\partial T)_\rho = (\partial\varepsilon/\partial T)_p + (\partial\varepsilon/\partial p)_T(\alpha/\beta_T)$, where α is the coefficient of volumetric expansion for the substance.[5] However, the value of $(\partial\varepsilon/\partial p)_T$ was not measured for the temperature range of interest to us, which forms an obstacle to the conversion.[6] Qualitatively, however, the relationship between ε and T will undoubtedly also have an effect in the light-scattering behavior under study here, where, because of the large values of $(\partial\varepsilon/\partial T)_\rho$, fluctuations in temperature $\overline{\Delta T^2}$ will develop [see (1)].

Let us return now to discussion of the opalescence phenomenon arising in quartz in the immediate vicinity of the phase transformation point. Our experiments were the first to detect the phenomenon of reversible opalescence in a solid body. It turns out here, when we compare our measurements with opalescence intensity measurements made at the critical points of various materials [12, 13], that opalescence is stronger in quartz than in certain liquids in their critical state. The very fact that opalescence appears is an indication of the abrupt formation of small optical nonuniformities in the quartz. The explanation of the origin of these nonuniformities is directly derived from the quite unambiguous interpretation given above of the nonlinear portions of the I–T curves. In a case such as this, we must recognize that opalescence occurs as a result of a special intensification of fluctuations in dielectric permeability at the phase transition point. But, since we have no grounds for assuming that, in the solid state the compressibility may attain values similar to those at the critical point of the substance, we must look for the cause of formation of large optical nonuniformities, above all, in large values of $(\partial\varepsilon/\partial T)_\rho$, which provide for the possibility of temperature fluctuations appearing over small volumes. Calculation shows that the value of $(\overline{\Delta T^2})^{1/2}$ is of the same order of magnitude as the mist-band temperature range in our experiments, and further calculations lead to a value for the intensity of the scattered light which is acceptable in explanation of the effect observed. This point of view corresponds, in our opinion, to treating the phase transition in quartz as a λ point.

In this phenomenon, it is undoubtedly significant that the $\alpha \rightleftharpoons \beta$ transition in quartz is close to the critical Curie point on the line of phase transitions of the second kind [8].

We will observe that the behavior shown in our experiments, and the visual picture of a single intermediate zone between the two phases, can be assumed to solidly confirm the existence of a single phase transformation in quartz near 573°. We consider it necessary to make this observation, since Steinwehr [14] has asserted that other intermediate phases exist between the α and β phases of quartz. Steinwehr's statement was based on interferometer measurements of the difference in path of two light beams, one of which passed through a quartz plate. The step-type relationship between the temperature and this path difference was interpreted by the author as reflecting a series of phase transformations. It is perfectly obvious that measurements of optical path differences in quartz close to the phase transformation point, without preliminary detection and careful localization of the mist band, will, in general, be meaningless and cannot lead to any well-founded conclusions.

In conclusion, we will list the following basic results of the work reported.

1. An experimental method has been devised which permits quantitative study of the intensity of molecular Rayleigh scattering of light in quartz in the 15-600° temperature range, and also allows lo-

[5] For greater physical clarity, we will again use the relationships for an isotropic medium.

[6] There is a further difficulty in that the variables p and T are not statistically independent like ρ and T.

cation and observation of the boundary region between the two crystal structures of quartz.

2. For the first time, a λ-type intensity maximum has been shown to exist in the scattering of light near the phase transition point of a solid body. From the existence of this maximum, it was deduced that fluctuations in the dielectric permeability of quartz were intensified as its temperature approached the phase transition point.

3. For the first time in a solid body, the phenomenon of molecular opalescence was detected and quantitatively investigated, in a crystal lying near its polymorphic transformation temperature. On the basis of the experimental results, an examination was made of a possible molecular mechanism for the abrupt formation of optical nonuniformities in a crystal at its phase transition temperature.[7]

LITERATURE CITED

1. G. S. Landsberg, "Molekulare Lichtzerstreung in festen Körpern I," Zs. Phys., 43, 773-778 (1927); "Molekulare Lichtzerstreung in festen Körpern II. Abhängigkeit der Intensität des zerstreuten Lichtes von der Temperatur," Zs. Phys., 45, 442-448 (1927).
2. M. A. Leontovich, Statistical Physics [in Russian] (Moscow – Leningrad, 1944).
3. R. B. Sosman, The Properties of Silica (New York, 1927).
4. A. V. Shubnikov, Quartz and Its Uses [in Russian] (Izd. AN SSSR, 1940).
5. P. G. Strelkov and G. I. Kosourov, "A dilatometer for small-sized specimens," Izv. AN SSSR, ser. fiz., 17, 3, 383-388 (1953).
6. N. N. Sinel'nikov, "The vacuum adiabatic calorimeter and some new data on the $\alpha \rightleftharpoons \beta$ transformation in quartz," DAN SSSR, 92, 369-372 (1953).
7. H. Moser, "Messung der wahren spezifischen Wärme von Silber, Nickel, β-Messing, Quarzkristall und Quartzglass zwischen + 50 u. 700°C nach einer verfeinerten Methode," Zs. Phys. 37, 737-752 (1946).
8. L. D. Landau and E. M. Lifshits, Statistical Physics [in Russian] (Moscow – Leningrad, 1951).
9. A. Perrier and R. Mandoro, "Elasticité et symetrié du quartz au temperatures elevées," Compt. rend. Acad. Sci., 175, 622-625 (1922).
10. P. Rinne and R. Kolb, "Optisches zur Modifikationsänderung von α in β Quarz sowie von α in β Leuzit," Neues Jahrbuch der Mineralogie 2, 138-158 (1910).
11. G. P. Motulevich, "Molecular scattering of light in crystals," Tr. fiz. inst. AN SSSR, 5, 12-61 (1950).
12. W. H. Keesom, "Spektrophotometrische Untersuchung der Opaleszenz eines einkomponentigen Stoffes in der Nähe des kritischen Zustandes," Ann. Phys., 35(340), 591-598 (1911).
13. O. Mass and S. G. Mason, "The critical opalescence of ethylene," Canad. J. Res., B26, 592-595 (1948).
14. H. Steinwehr, "Umwandlung $\alpha \rightleftharpoons \beta$ in Quarz," Z. Kristallographie, B99, 4, 293-313 (1938).

[7] While our article was in the press, an article by V.L. Ginzburg was published which predicted, quite independently, the phenomenon we had looked for, i.e., anomalous scattering of light in a solid body at a phase transformation of the second kind (V. L. Ginzburg, "The scattering of light near a phase transformation of the second kind," DAN SSSR, 105, 240-243, 1955).

BRIEF COMMUNICATIONS

THE STRIPS METHOD OF COMPUTING FOURIER ANALYSES IN CRYSTAL STRUCTURE ANALYSIS

N. V. Belov and T. N. Tarkhova

Institute of Crystallography, Academy of Sciences of the USSR
Translated from Kristallografiya, Vol. 1, No. 1,
pp. 132-136, January-February, 1956
Original article submitted November 20, 1955

The effective speed of a computing machine is presently only 2-3 times that of the manual method in two-dimensional Fourier syntheses, as experience here and elsewhere has shown.[1] One reason for this is that at least four workers are needed in the machine method, in the later stages at least, whereas one person can do all the work in the manual method. Computing machines are also exceptionally costly, and we have very little access to foreign machines, so it would seem that the strips method is likely to remain with us as the basic method for a long time yet. This makes it extremely desirable to rationalize the work; the number of operations is not reduced, but the strain on the worker is reduced.

One of the tiring operations in summing the numbers in the columns arises from the need to add the black figures but subtract the red. The negative values on the strips may be replaced by the difference from 100, whereupon all the numbers are simply added; it merely remains to subtract from each column the appropriate number of 100s (the number used in the column).

Red ink (or a bar over the number) is used also for these differences, but the color is ignored in the summation, the red entries merely being counted at the end to give the number of 100s to be subtracted.

This treatment is of considerable value if the numbers are added by means of a manual or electrical adding machine such as the SASL-Pz by Rheinmetall (and then it is convenient to add up three columns at once); but it does not work so well with those who prefer oral counting, because the sums increase continuously in this method and give a large final number, whereas the sequence of plus and minus values usually gives a relatively small final sum.

The following is a new cosine strip for h = 1 and amplitude 100 (sixtyfold division of the edge of the elementary parallelepiped):

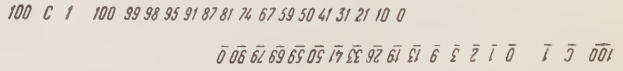

The first 16 numbers ($x_0, x_1, x_2, \ldots, x_{15}$) correspond to the positive side of the strip, and the last 16 ($x_{15}, x_{16}, \ldots, x_{30}$) to the negative side; it is assumed that the long strip will be folded along the dotted line, the second half being glued to the first in that position (the numbers in the second set of 16 are best written upside down if this is actually done).

100	99	98	95	91	87	81	74	67	59	50	41	31	21	10	0
99															$\overline{90}$
98															$\overline{79}$
95															$\overline{69}$
91															$\overline{59}$
87															$\overline{50}$
81															$\overline{41}$
74															$\overline{33}$
67															$\overline{26}$
59															$\overline{19}$
50															$\overline{13}$
41															$\overline{9}$
31															$\overline{5}$
21															$\overline{2}$
10															$\overline{1}$
0	$\overline{90}$	$\overline{79}$	$\overline{69}$	$\overline{59}$	$\overline{50}$	$\overline{41}$	$\overline{33}$	$\overline{26}$	$\overline{19}$	$\overline{13}$	$\overline{9}$	$\overline{5}$	$\overline{2}$	$\overline{1}$	$\overline{0}$

Scheme No. 1

[1] Machines give a very great saving in time in more routine processes, e.g., refinement of coordinates.

TABLE 1. Cosines

100	C	0	100	100	100	100	100	100	100	100	100	100	100	100	100	100	100	100
100	C	1	100	99	98	95	91	87	81	74	67	59	50	41	31	21	10	0
100	C	2	100	98	91	81	67	50	31	10	90	69	50	33	19	9	2	0
100	C	3	100	95	81	59	31	0	69	41	19	5	0	5	19	41	69	0
100	C	4	100	91	67	31	90	50	19	2	2	19	50	90	31	67	91	100
100	C	5	100	87	50	0	50	13	0	13	50	0	50	87	100	87	50	0
100	C	6	100	81	31	69	19	0	19	69	31	81	100	81	31	69	19	0
100	C	7	100	74	10	41	2	13	69	41	91	95	50	79	19	1	33	0
100	C	8	100	67	90	19	2	50	31	91	91	31	50	2	19	90	67	100
100	C	9	100	59	69	5	19	0	81	95	31	41	0	41	31	95	81	0
100	C	10	100	50	50	0	50	50	100	50	50	0	50	50	100	50	50	0
100	C	11	100	41	33	5	90	87	81	79	2	41	50	99	31	26	9	0
100	C	12	100	31	19	19	31	100	31	19	19	31	100	31	19	19	31	100
100	C	13	100	21	9	41	67	87	69	1	90	95	50	26	19	41	98	0
100	C	14	100	10	2	69	91	50	19	33	67	81	50	9	31	98	90	0
100	C	15	100	0	0	0	100	0	0	0	100	0	0	0	100	0	0	0
100	C	16	100	90	2	31	91	50	19	67	67	19	50	91	31	2	90	100
100	C	17	100	79	9	59	67	13	69	99	90	5	50	74	19	59	98	0
100	C	18	100	69	19	81	31	0	31	81	19	69	100	69	19	81	31	0
100	C	19	100	59	33	95	90	13	81	21	2	59	50	1	31	74	9	0
100	C	20	100	50	50	100	50	50	100	50	50	100	50	50	100	50	50	100
100	C	21	100	41	69	95	19	0	81	5	31	59	0	59	31	5	81	0
100	C	22	100	33	90	81	2	50	31	9	91	69	50	98	19	10	67	0
100	C	23	100	26	10	59	2	87	69	59	91	5	50	21	19	99	33	0
100	C	24	100	19	31	31	19	100	19	31	31	19	100	19	31	31	19	100
100	C	25	100	13	50	0	50	87	0	87	50	0	50	13	100	13	50	0
100	C	26	100	9	67	69	90	50	19	98	2	81	50	10	31	33	91	0
100	C	27	100	5	81	41	31	0	69	59	19	95	0	95	19	59	69	0
100	C	28	100	2	91	19	67	50	31	90	90	31	50	67	19	91	2	100
100	C	29	100	1	98	5	91	13	81	26	67	41	50	59	31	79	10	0
100	C	30	100	0	100	0	100	0	100	0	100	0	100	0	100	0	100	0

The strip for h = 2 (positive side) will contain the zero, second, fourth, etc., entries up to the 30th on the previous long strip provided that the final zero on the first half and the first zero on the second half will read identically as number 15, and both be black. The strip for h = 3 similarly consists of the zero, third, sixth, and so on; position 10 will contain No. 30 of the basic strip. No. 11, and so on, may be obtained by adding to this a similar strip of 31 entries $(x_{30}, x_{31}, \ldots, x_{60})$ with a mirror-image array, namely red figures first and black ones last; here, again, identical red figures at position 30 on the first strip and the zero on the reversed one will be given the same number, namely 30.

Position 11 on the strip for h = 3 has entry 33; position 15 has entry 45, which finishes h = 3.

The double strip with 60 entries is the cosine part of the fundamental, whose length equals a_j, the side of the unit cell. The h = 2 and h = 3 strips give harmonics corresponding to $\lambda = a_j/2$ and $\lambda = a_j/3$. All the strips for the harmonics are derived from the double strip if this is folded to bring entry 60 into coincidence with No. 1 (scheme No. 1), the strip for h = 4 being obtained by taking the entries zero, fourth, and so on up to the 60th, which occupies position 15. No. 64 reproduces (in sequence) No. 4, and so on.

The formula for the strip for a given h may be written as follows on the basis of this very elementary method. Let $x_0^h, x_1^h, \ldots, x_n^h$ be the numbers appearing at the positions on such a strip; then $x_0^h = x_0^1$, $x_1^h = x_h^1$, $x_2^h = x_{2h}^1, \ldots, x_n^h = x_{nh}^1$. If nh exceeds 60, we take the remainder from division by 60, which may be written as $x_n^h = x_{nh}^1 = x_m^1$, where $m \equiv nh \pmod{60}$.

The cosine is symmetrical about argument π [$\cos(\pi + \alpha) = \cos(\pi - \alpha)$], so we may take as m

TABLE 2. Sines

100	S	1	0	10	21	31	41	50	59	67	74	81	87	91	95	98	99	100
100	S	2	0	21	41	59	74	87	95	99	99	95	87	74	59	41	21	0
100	S	3	0	31	59	81	95	100	95	81	59	31	0	$\overline{69}$	$\overline{41}$	$\overline{19}$	$\overline{5}$	$\overline{0}$
100	S	4	0	41	74	95	99	87	59	21	$\overline{79}$	$\overline{41}$	$\overline{13}$	$\overline{1}$	$\overline{5}$	$\overline{26}$	$\overline{59}$	0
100	S	5	0	50	87	100	87	50	0	$\overline{50}$	$\overline{13}$	$\overline{0}$	$\overline{13}$	$\overline{50}$	0	50	87	100
100	S	6	0	59	95	95	59	0	$\overline{41}$	$\overline{5}$	$\overline{5}$	$\overline{41}$	0	59	95	95	59	0
100	S	7	0	67	99	81	21	$\overline{50}$	$\overline{5}$	$\overline{9}$	$\overline{59}$	31	87	98	59	$\overline{90}$	$\overline{26}$	$\overline{0}$
100	S	8	0	74	99	59	$\overline{79}$	$\overline{13}$	$\overline{5}$	$\overline{59}$	41	95	87	21	$\overline{41}$	$\overline{1}$	$\overline{26}$	0
100	S	9	0	81	95	31	$\overline{41}$	$\overline{0}$	$\overline{41}$	31	95	81	0	$\overline{19}$	$\overline{5}$	$\overline{69}$	59	100
100	S	10	0	87	87	0	$\overline{13}$	$\overline{13}$	0	87	87	0	$\overline{13}$	$\overline{13}$	0	87	87	0
100	S	11	0	91	74	$\overline{69}$	$\overline{1}$	$\overline{50}$	59	98	21	$\overline{19}$	$\overline{13}$	10	95	67	$\overline{59}$	$\overline{0}$
100	S	12	0	95	59	$\overline{41}$	$\overline{5}$	0	95	59	$\overline{41}$	$\overline{5}$	0	95	59	$\overline{41}$	$\overline{5}$	0
100	S	13	0	98	41	$\overline{19}$	$\overline{26}$	50	95	$\overline{90}$	$\overline{1}$	$\overline{69}$	87	67	$\overline{41}$	$\overline{9}$	21	100
100	S	14	0	99	21	$\overline{5}$	$\overline{59}$	87	59	$\overline{26}$	$\overline{26}$	59	87	$\overline{59}$	$\overline{5}$	21	99	0
100	S	15	0	100	0	$\overline{0}$	0	100	0	$\overline{0}$	0	100	0	$\overline{0}$	0	100	0	$\overline{0}$
100	S	16	0	99	$\overline{79}$	$\overline{5}$	41	87	$\overline{41}$	$\overline{26}$	74	59	$\overline{13}$	$\overline{59}$	95	21	$\overline{1}$	0
100	S	17	0	98	$\overline{59}$	$\overline{19}$	74	50	$\overline{5}$	$\overline{90}$	99	$\overline{69}$	$\overline{13}$	67	59	$\overline{9}$	$\overline{79}$	100
100	S	18	0	95	$\overline{41}$	$\overline{41}$	95	0	$\overline{5}$	59	59	$\overline{5}$	0	95	$\overline{41}$	$\overline{41}$	95	0
100	S	19	0	91	$\overline{26}$	$\overline{69}$	99	$\overline{50}$	$\overline{41}$	98	$\overline{79}$	$\overline{19}$	87	10	$\overline{5}$	67	41	$\overline{0}$
100	S	20	0	87	$\overline{13}$	0	87	$\overline{13}$	0	87	$\overline{13}$	0	87	$\overline{13}$	0	87	$\overline{13}$	0
100	S	21	0	81	$\overline{5}$	31	59	$\overline{0}$	59	31	$\overline{5}$	81	0	$\overline{19}$	95	$\overline{69}$	$\overline{41}$	100
100	S	22	0	74	$\overline{1}$	59	21	$\overline{13}$	95	$\overline{59}$	$\overline{59}$	95	$\overline{13}$	21	59	$\overline{1}$	74	0
100	S	23	0	67	$\overline{1}$	81	$\overline{79}$	$\overline{50}$	95	$\overline{9}$	41	31	$\overline{13}$	98	$\overline{41}$	$\overline{90}$	74	$\overline{0}$
100	S	24	0	59	$\overline{5}$	95	$\overline{41}$	0	59	$\overline{5}$	95	$\overline{41}$	$\overline{0}$	59	$\overline{5}$	95	$\overline{41}$	$\overline{0}$
100	S	25	0	50	$\overline{13}$	100	$\overline{13}$	50	0	$\overline{50}$	87	$\overline{0}$	87	$\overline{50}$	0	50	$\overline{13}$	100
100	S	26	0	41	$\overline{26}$	95	$\overline{1}$	87	$\overline{41}$	21	21	$\overline{41}$	87	$\overline{1}$	95	$\overline{26}$	41	0
100	S	27	0	31	$\overline{41}$	81	$\overline{5}$	100	$\overline{5}$	81	$\overline{41}$	31	0	$\overline{69}$	59	$\overline{19}$	95	$\overline{0}$
100	S	28	0	21	$\overline{59}$	59	$\overline{26}$	87	$\overline{5}$	99	$\overline{1}$	95	$\overline{13}$	74	$\overline{41}$	41	$\overline{79}$	0
100	S	29	0	10	$\overline{79}$	31	$\overline{59}$	50	$\overline{41}$	67	$\overline{26}$	81	$\overline{13}$	91	$\overline{5}$	98	$\overline{1}$	100

TABLE 3. Cosines

100	C	1	100	99	98	95	91	87	81	74	67	59	50	41	31	21	10	0
90	C	1	90	90	88	86	82	78	73	67	60	53	45	37	28	19	9	0
80	C	1	80	80	78	76	73	69	65	59	54	47	40	33	25	17	8	0
70	C	1	70	70	68	67	64	61	57	52	47	41	35	28	22	15	7	0
60	C	1	60	60	59	57	55	52	49	45	40	35	30	24	19	12	6	0
50	C	1	50	50	49	48	46	43	40	37	33	29	25	20	15	10	5	0
40	C	1	40	40	39	38	37	35	32	30	27	24	20	16	12	8	4	0
30	C	1	30	30	29	29	27	26	24	22	20	18	15	12	9	6	3	0
20	C	1	20	20	20	19	18	17	16	15	13	12	10	8	6	4	2	0
10	C	1	10	10	10	10	9	9	8	7	7	6	5	4	3	2	1	0
5	C	1	5	5	5	5	5	4	4	4	3	3	3	2	2	1	1	0
4	C	1	4	4	4	4	4	3	3	3	3	2	2	2	1	1	0	0
3	C	1	3	3	3	3	3	3	2	2	2	2	2	1	1	1	0	0
2	C	1	2	2	2	2	2	2	2	1	1	1	1	1	1	0	0	0
1	C	1	1	1	1	1	1	1	1	1	1	1	1	0	0	0	0	0

TABLE 3. Sines

100	S	1	0	10	21	31	41	50	59	67	74	81	87	91	95	98	99	100
90	S	1	0	9	19	28	37	45	53	60	67	73	78	82	86	88	90	90
80	S	1	0	8	17	25	33	40	47	54	59	65	69	73	76	78	80	80
70	S	1	0	7	15	22	28	35	41	47	52	57	61	64	67	68	70	70
60	S	1	0	6	12	19	24	30	35	40	45	49	52	55	57	59	60	60
50	S	1	0	5	10	15	20	25	29	33	37	40	43	46	48	49	50	50
40	S	1	0	4	8	12	16	20	24	27	30	32	35	37	38	39	40	40
30	S	1	0	3	6	9	12	15	18	20	22	24	26	27	29	29	30	30
20	S	1	0	2	4	6	8	10	12	13	15	16	17	18	19	20	20	20
10	S	1	0	1	2	3	4	5	6	7	7	8	9	9	10	10	10	10
5	S	1	0	1	1	2	2	3	3	3	4	4	4	5	5	5	5	5
4	S	1	0	0	1	1	2	2	2	3	3	3	3	4	4	4	4	4
3	S	1	0	0	1	1	1	2	2	2	2	2	3	3	3	3	3	3
2	S	1	0	0	0	1	1	1	1	1	1	2	2	2	2	2	2	2
1	S	1	0	0	0	0	0	1	1	1	1	1	1	1	1	1	1	1

the least in absolute value of the remainders from division by 60, no matter whether this is positive or negative, i.e., we always have one of the first 30 entries on the strip for h = 1.

Table 1 gives the cosine strips for amplitude 100 and h = 0,1,2,...30; the values will be altered proportionately for other amplitudes. The positive sides are shown, the negative sides bearing (in red) the differences from 100 of the black numbers on the positive side. Experience over more than 15 years has shown that it is unnecessary to use more than two significant figures in the entries.

The sine strips are derived from the cosine ones by 90° shift; Table 2 gives these for h from 1 to 30.

The strips are drawn up as follows. We compile two tables for h = 1 with 100 lines having amplitudes F from 1 to 100. On one side we insert x^1_m = F cos mb for the positive amplitudes, and on the other (rear side), the same for the negative ones. All those on the rear side are negative, so the differences are written; but the red 100 is most simply replaced by a black zero. One completed sheet is cut up horizontally and gives 100 strips for h = 1; the other is cut up into 16 narrow bands along vertical lines. The positive sides of the latter are numbered 0 to 15; the negative ones, 15 to 30. These are laid out in accordance with these numbers and $x^h_n = x^1_{nh}$ to form tables for h = 2,3,4, and so on, which are then cut up along horizontal lines.

Further economy is attained by restricting the strips to steps of unity for amplitudes 1-10, etc., for multiples of ten; any amplitude with an intermediate value will correspond to two strips. Fifteen strips for each h suffice if two significant figures are used for differences as well as sums.

Table 3 gives the complete set of 15 strips for h = 1 (divisible once horizontally and twice vertically).

LITERATURE CITED

1. N.V. Belov, Vestn. AN SSSR, 11, 75-80 (1954).

DERIVATION OF THE FORMULA FOR THE TEMPERATURE FACTOR FROM A CONVOLUTION THEOREM

B. K. Vainshtein

Institute of Crystallography, Academy of Sciences of the USSR
Translated from Kristallografiya, Vol. 1, No. 1,
pp. 137-138, January-February, 1956
Original article submitted November 1, 1955

Convolution is becoming increasingly used in structure analysis and scattering theory (see [1] for review); this is capable of giving new results, and also of giving known results more simply. This note deals with the latter aspect.

The f curves are defined by the Fourier integral over the distribution $\rho(\mathbf{r})$ of the scattering matter in the atom at rest:

$$f(\mathbf{s}) = \int \rho(\mathbf{r})\, e^{i(\mathbf{sr})}\, dv_r = F\{\rho(\mathbf{r})\} \qquad (1)$$

(F is the Fourier operator). Consider the distribution $\rho_T(\mathbf{r})$ in an atom subject to thermal motion whose effect on the average distribution of the center of gravity about the equilibrium is a known probability function $w(\mathbf{r})$; here we envisage the random part of the thermal motion, which is not dependent on the bonds between the atoms. We normalize $w(\mathbf{r})$ via

$$\int w(\mathbf{r})\, dv_r = 1. \qquad (2)$$

An atom displaced from its equilibrium position to point $\mathbf{r}'$ has a distribution $\rho(\mathbf{r} - \mathbf{r}')$. The probability of finding it in that position is $w(\mathbf{r}')$. So $\rho_T(\mathbf{r})$ is to be found by integrating $\rho(\mathbf{r} - \mathbf{r}')w(\mathbf{r}')$, over all $\mathbf{r}'$:

$$\rho_T(\mathbf{r}) = \int \rho(\mathbf{r} - \mathbf{r}')\, w(\mathbf{r}')\, dv_{r'}. \qquad (3a)$$

But this is the convolution of $\rho(\mathbf{r})$ and $w(\mathbf{r})$:

$$\rho_T(\mathbf{r}) = \widehat{\rho w}(\mathbf{r}) \qquad (3b)$$

in complete accordance with the physical meaning of the convolution operation. The convolution theorem states that the Fourier integral of a convolution of two functions is the product of the Fourier integrals of each of the functions:

$$F\{\widehat{\rho w}(\mathbf{r})\} = F\{\rho(\mathbf{r})\} \cdot F\{w(\mathbf{r})\}. \qquad (4)$$

Then we have the result that the atomic temperature factor (the scattering power of an atom in thermal motion) is $f(\mathbf{s}) \cdot f_T(\mathbf{s})$, namely the product of the $f(\mathbf{s})$ of (1) by the temperature factor $f_T(\mathbf{s})$ as defined by the Fourier integral of $w(\mathbf{r})$:

$$f_T(\mathbf{s}) = F\{w(\mathbf{r})\} = \int w(\mathbf{r})\, e^{i(\mathbf{sr})}\, dv_r. \qquad (5)$$

Here the $f(\mathbf{s})$ of (1) and the $f_T(\mathbf{s})$ of (5) have been put in the most general form, which imposes no restrictions on $\rho(\mathbf{r})$ and $w(\mathbf{r})$. It is usually assumed that both of these functions have spherical symmetry, in which case (1) and (5) are expressed in spherical coordinates; an ellipsoidal form has been used for $w(\mathbf{r})$ in some structure studies. A spherical Gaussian form for $w(\mathbf{r})$, namely $w(\mathbf{r}) = (2\pi\overline{u^2}) \cdot \exp\{-\mathbf{r}^2/2\overline{u^2}\}$, gives us, from (5), the Debye temperature factor $f_T(s) = e^{-M}$, $M = \frac{1}{2}\overline{u^2}s^2$, where $\overline{u^2}$ is the mean-square displacement from the equilibrium position.

LITERATURE CITED

1. R. Hosemann, F. Motzkus, and G. Schoknecht, "Verwendung von Faltungsoperationen zur eindeutigen Röntgenstrukturanalyse," Fortschr. Phys., 2, 1-41 (1954).

SPECIAL CASE OF THE PROPAGATION OF ELASTIC WAVES IN CRYSTALS

K. S. Aleksandrov

Institute of Crystallography, Academy of Sciences of the USSR
Translated from Kristallografiya, Vol. 1, No. 1,
pp. 138-139, January-February, 1956
Original article submitted October 20, 1955

This communication deals with one of the special questions of the propagation of elastic waves in anisotropic media – the case of the propagation of ultrasonic waves in the direction of the two-fold (Y) axis in a crystal of the tetragonal system.

It is known from theory [1,2] that three ultrasonic plane waves may be propagated in this direction – a longitudinal wave and two transverse waves. The velocities of these waves are determined, respectively, by the elastic constants c_{11}, c_{44}, and c_{66}. We shall here confine ourselves only to the transverse waves. The directions of the displacements in transverse waves are perpendicular to each other and parallel to the crystallographic axes Z and X, where Z is the four-fold axis and X the two-fold axis. In the case of ammonium dihydrogen phosphate, $c_{44} = 8.30 \cdot 10^{10}$ and $c_{66} = 6.04 \cdot 10^{10}$ dyn/cm^2, i.e., a wave with a direction of displacement along Z is propagated at a lower speed than a wave with a direction of displacement along X.

By means of a Y-cut quartz plate, a short ultrasonic pulse of transverse vibrations of a frequency of 1.67 Mc is sent into a single crystal specimen of ammonium dihydrogen phosphate, 60 mm long. The ultrasonic pulses passing through the specimen are received by a second Y-cut plate, are amplified, and are fed to the plates of a cathode-ray tube. The Y-cut quartz plate irradiates and receives the transverse waves with a fixed direction of displacement, and, in this sense, it is analogous to a polarizer in optics. In what follows we shall use the terminology adopted in optics, both for brevity of the discussion and to emphasize the very close analogy between the phenomena studied and similar phenomena in optics.

This analogy has already been noted in the literature [3].

Figure 1 shows oscillograms of pulses, which have passed through the specimen with change in the direction of displacement of the excited oscillations relative to the Y and Z axes. It will be seen that if the wave excited in the crystal is polarized parallel to the X or Z axis (1a and 1c), one pulse is received, the time of propagation of which depends on the length of the specimen and the value of the elastic constant. The direction of displacement in each of the pulses may be determined by rotation of the receiving plate. In the crossed position of "polarizer" and "analyzer," the pulses disappear. If the excited wave is polarized in the direction of the bisector between the axes, the screen shows two pulses, propagating at different speeds (Fig. 1b). This is direct confirmation of the existence of two "permitted" directions of displacement of transverse waves for a given direction of propagation.

As in the case of the propagation of light perpendicularly to the optical axis of a uniaxial crystal, two plane transverse waves are propagated in one direction at different speeds.

Figure 2 shows the variation in the oscillograms received when the receiver (analyzer) is rotated for constant diagonal position of the radiator (polarizer). Figure 2a repeats Fig. 1b, but with lower amplification. If the direction of the oscillations of the receiver coincide with one of the permitted directions of displacement, sometimes one, sometimes the other wave, is received. It will be seen from Figs. 2a and 2c that the patterns are practically the same for parallel and crossed Nicols. Similar to this, in optics for diagonal position of the crystal, the patterns with crossed and parallel Nicols in monochromatic light are similar, while in white light the color changes to the complementary color.

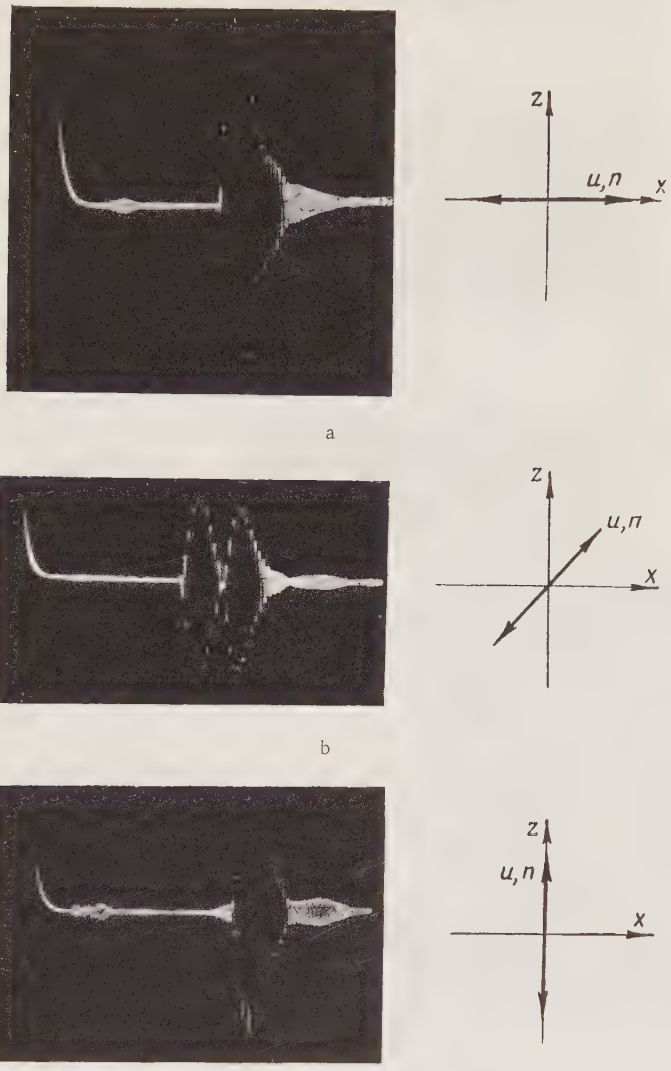

Fig. 1. Oscillograms of ultrasonic pulses, which have passed through a specimen of ammonium dihydrogen phosphate, as a function of the direction of displacement in the excited wave relative to the permitted directions X and Z. "Polarizer" and analyzer" parallel.

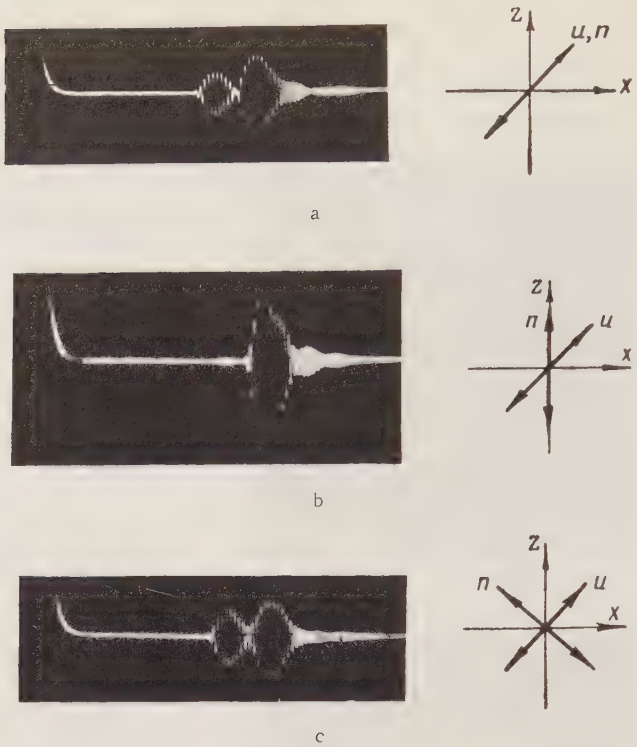

Fig. 2. Variation in oscillograms on rotation of the receiver n around the direction of propagation Y. The radiator u excites an ultrasonic wave with a direction of displacement along the bisector of the angle between the X and Z axes.

These phenomena may be observed not only in crystals of the tetragonal system, but in any crystals with directions in which two purely transverse waves are propagated at different speeds. This requirement is met by any of the three orthogonal axes in crystals of the rhombic system, any direction perpendicular to the six-fold axis in crystals of the hexagonal system, and the [110] and similar directions in crystals of the cubic system, etc. For cubic crystals, in the [110] direction, the difference in the speeds of transverse waves increases with increase in anisotropy of the crystal ($c_{11} - c_{12} - 2c_{44}$).

We thank I. M. Sil'vestrov for discussing the questions examined.

LITERATURE CITED

1. R. Meier and K. Schuster, Ann. Phys., 11, 8, 397-406 (1953).
2. F. E. Borgnis, Phys. Rev., 98, 4, 1000-1005 (1955).
3. J. Klerk and M. Musgrave, Proc. Phys. Soc., 63, 12, 81-88 (1954).

PRODUCTION OF ETCH FIGURES BY MEANS OF ULTRASONIC VIBRATIONS

Kh. S. Bagdasarov and A. P. Kapustin

Institute of Crystallography, Academy of Sciences of the USSR
Translated from Kristallografiya, Vol. 1, No. 1,
pp. 139-140, January-February, 1956
Original article submitted October 10, 1955

It is well known that when crystals dissolve, multifaceted depressions, called etch figures, are formed on their faces. The formation of etch figures is due to the different solubility of crystals in different directions and is connected with the initial stage of solution of the crystals. In many cases, a knowledge of the etch figures enables a correct conclusion to be made regarding the symmetry of a crystal.

For the production of etch figures, unsaturated mother liquor is used. However, it is not always possible to obtain etch figures in an unsaturated solution. It is often necessary to select special solvents, which alter considerably the form of the etch figures.

In the new method of producing etch figures in an ultrasonic field, the crystal is placed in saturated mother liquor, and is exposed to short-time irradiation (of the order of 2-3 min) in a weak ultrasonic field. In this way, etch figures have been produced on the octahedral face of a crystal of potash alum (Fig. 1), on the cleavage plane parallel to the pinacoid of a crystal of benzophenone, and on a piece of a potassium bichromate crystal of random form.

For producing the ultrasonic field, a magnetostriction generator with a power of 1 kW and a frequency of 40 kc was used.

The idea of producing etch figures by means of ultrasonic vibrations was suggested by A. V. Shubnikov.

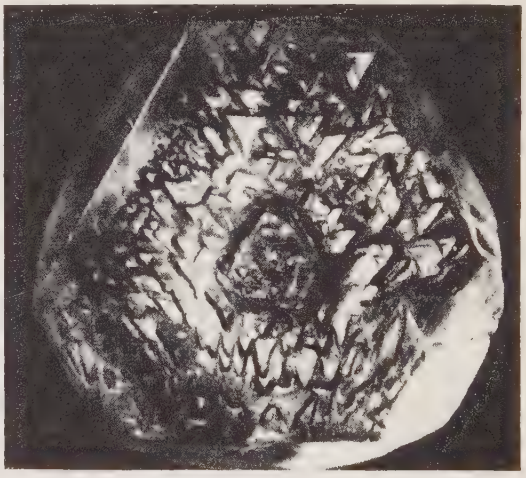

Fig. 1. Etch figures on the octahedral face of a potash alum crystal.

RELATION BETWEEN THE MELTING POINTS AND REFRACTIVE INDICES OF IONIC CRYSTALS

S. S. Batsanov

M. V. Lomonosov State University, Moscow
Translated from Kristallografiya, Vol. 1, No. 1,
pp. 140-142, January-February, 1956
Original article submitted October 1, 1955

It is known that the optical spectra of crystals depend on the electron polarizability of the ions of which they are composed. The polarizabilities (refractions) of the ions depend on their radii [1]. The melting points of crystals are functions of their lattice energies, and are hence also connected with the ionic radii [2]. Since the refractive indices and melting points of ionic crystals depend on a single common source, these two characteristics ought to be interlinked with each other. The present article is devoted to establishing this link.

The table gives the refractive indices (upper line) and melting points (lower line) of alkali halides. The refractive indices in all cases were extrapolated to $\lambda = \infty$ by the Wulff method [3] in order to avoid the effects of dispersion.

These data are shown graphically in Fig. 1 (points enclosed by circles indicating the limits of experimental error).

We see from the graph that the dependence of the n_∞ of the alkali halides on their melting point is linear and inverse.

This type of relationship is quite understandable. On passing from the fluorides to the iodides, and maintaining the type of structure, there is an increase in the interatomic distances and consequent fall in the crystal-lattice energy and melting point. In the same direction the polarizability of the anion increases:

$$R_{F^-} = 2.98 \text{ cm}^3, \quad R_{Cl^-} = 8.31,$$
$$R_{I^-} = 11.32, \text{ and } R_{I^-} = 16.63 \text{ [7]}$$

and hence so does the refractive index.

The rectilinear nature of the relationship is due to the approximately additive character of the optical and energy properties of ionic crystals. In the already-cited paper by G. B. Bokii and S. S. Batsanov, it was shown that the refraction (and hence the refractive indices) of alkali halides is connected with their composition in an additive fashion. On the other hand, the crystal-lattice energy may also be represented as a sum of terms corresponding to the individual ions [9]. Hence, it is clear that the melting point of ionic crystals may also be connected with their composition by an additive function.

Thus, both the refractive indices and melting points of ionic crystals are determined by functions having an additive character and depending finally

TABLE 1

Cations	Anions			
	F	Cl	Br	I
Na	1.320 [4] 980 [5]	1.526 [6] 801 [5]	1.613 [4] 760 [5]	1.725 [4] 663 [5]
K	1.355 [7] 856 [5]	1.474 [7] 771 [5]	1.536 [7] 730 [8]	1.628 [7] 681 [5]
Rb	1.390 [7] 760 [5]	1.477 [7] 726 [5]	1.529 [7] 683 [5]	1.610 [7] 642 [5]
Cs	1.468 [1] 680 [5]	1.517 [4] 646 [5]	1.538 [4] 636 [5]	1.622 [4] 621 [5]

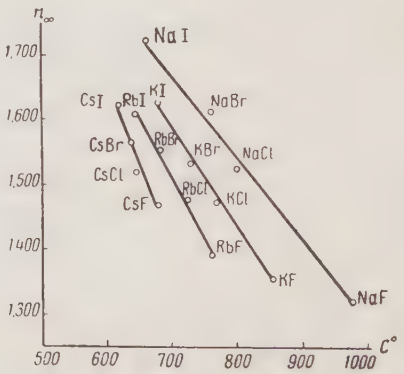

Fig. 1.

on the same thin, the interatomic distances. This also produces the simple proportional relation between n and the mp of the crystals.

In analytical form the relationship may be described as follows: the refractive indices of alkali salts are

$$n_{Na} = 2.420 - 0.001039 \cdot t^0_m,$$
$$n_K = 2.500 - 0.001250 \cdot t^0_m,$$
$$n_{Rb} = 2.650 - 0.001553 \cdot t^0_m,$$
$$n_{Cs} = 3.017 - 0.002208 \cdot t^0_m.$$

It is interesting to note that an equation of exactly the same type connects the boiling point of organic compounds with their refractive indices [10]. Hence, we may conclude that the refractive index of chemical substances depends linearly on their melting point or boiling point.

LITERATURE CITED

1. E. Kordes, "Die Ermittlung von Atomabständen aus der Lichtbrechung," Z. Phys. Chem., B44, 249-260 (1939).
2. G.B. Bokii, Introduction to Crystallochemistry [in Russian] (Izd. MGU, 1954), p. 197.
3. P. Wulff, "Ein neues Verfahren zur Dartstellung des Diespersionsverlaufes im Sichtbaren und Ultravioletten," Z. Phys. Chem., B21, 368-382 (1933).
4. K. Spangenberg, "Dichte und Lichtbrechung der Alkalihalogenide," Z. Krist., 57, 494-534 (1922).
5. F. Jäger, "Über die Temperaturabhängigkeit der molekularen freien Oberflächenenergie von Flüssigkeiten," Z. anorg. Chem., 101, 1-214 (1917).
6. F. Martens, "Über die Dispersion von Flusspat, Sylvin, Steinsaltz, Quarz und Kalkspat, sowie über die Dispersion von Diamant," Ann. Phys., 8, 459-465 (1902).
7. G.B. Bokii and S.S. Batsanov, "New method of determining the structure of complex compounds. III," Vestn. MGU, 10, 87-96 (1954).
8. G. Kellner, "Die binären Systeme aus den Bromiden der Alkali-und Erdalkalimetalle," Z. anorg. Chem., 99, 137-183 (1917).
9. A.F. Kapustinskii, "Electronegativity and crystal-lattice energy," DAN SSSR, 67, 467-470 (1949).
10. M.M. Samygin, "Relation between boiling points and refractive indices," ZhFKh, 11, 325-330 (1938).

ON THE POSSIBILITY OF FORMING THE STRUCTURE OF THE DEUTERIDES (HYDRIDES) OF METALS, RETAINING HYDROGEN MOLECULES OR PAIRS OF ATOMS IN THE LATTICE

B. F. Ormont

L. Ya. Karpov Physicochemical Institute

Translated from Kristallografiya, Vol. 1, No. 1,
pp. 142-144, January-February, 1956
Original article submitted December 1, 1955

The generally accepted mechanism for the development of solid solutions of nonmetals (nitrogen, oxygen, etc.) in metals, in particular those formed by ds elements (titanium, zirconium, etc.), provides for the splitting of the nonmetal molecule into atoms on interaction with the metal.

At the same time, in regard to the hydrides of the same ds elements, since the time of Hägg's work [1], opinion has strengthened (see, for example, [2]), that unsplit hydrogen molecules might penetrate directly into the lattice of a metal, with the formation of a structure analogous to that of ThC_2. We indicated in [3] that this model (proposed by Hägg, for example, for the "dihydride" of zirconium ZrH_2) was improbable, since the effect of the considerable expansion of the metal lattice as the hydrogen penetrated could scarcely be compensated from the energy side by forces arising between the H_2 molecules and the Zr crystal. We indicated that, from general theoretical considerations, we should expect the formation of structures with the pairs of atoms (H_2) split up, i.e., with isolated hydrogen atoms. Otherwise, if Hägg's model for the structure of ZrH_2 were confirmed, quantum chemistry would have the difficult theoretical problem of handling the mechanism and nature of this linkage. This question is of fundamental interest.

In the light of what has been said, we cannot fail to turn attention to the fact that in contemporary literature the description of the structure of zirconium hydride on Hägg's model is still continuing (see [4], 1955).

It therefore seems appropriate, for elucidating the true state of affairs, to consider the important study of the dihydrides (dideuterides) of thorium and zirconium by x-ray, neutron-diffraction, and magnetic methods made by Rundle, Shull, and Wollan [5]. These authors found a tetragonalized cell belonging to the fluorspar type. Unfortunately, the authors, after obtaining extremely important experimental data regarding the Me–Me and Me–D interatomic distances, did not publish the D–D distances or consider the question of the relation between these data and the Hägg model. The absence of a sketch of the unit cell in this paper may be responsible for the fact that subsequent discussion of this structure is usually based on the "old" unit cell which, after [5,6], ought to be considered as unfounded.

We therefore think it appropriate to demonstrate the connection between the fcc unit cell of fluorspar (Fig. 1 shows two such cells) and the bc tetragonal unit cell of the dideuterides (dihydrides) of zirconium and thorium [6], and to derive the corresponding interatomic distances D–D.

The positions of the metal are 000 and $\frac{1}{2},\frac{1}{2},\frac{1}{2}$.

Analysis of intensities led the authors of [5] to the conclusion that of the five possible variants of hydrogen-atom distribution, the correct one was 000; $\frac{1}{2}$, $\frac{1}{2}$, $\frac{1}{2}+{}^{0.1}\frac{1}{2}$, $\frac{1}{4}$; $\frac{1}{2}$, ${}^{0.1}\frac{1}{4}$. This description

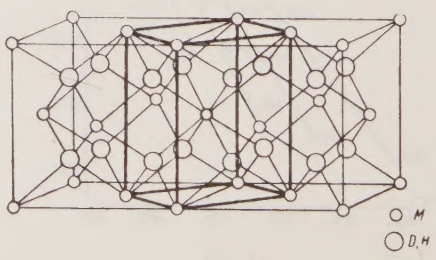

Fig. 1.

(unusual in our own literature) is equivalent to the following: $^{0.1}/_2$, $^1/_4$; $^1/_2$, $^{0.1}/_4$; $^1/_2$, $^{0.3}/_4$, $^{0.1}/_2$, $^3/_4$.

The unit cell of the dihydride is shown in final form in Fig. 2. Without deformation, the c/a ratio following from the fluorspar structure is $\sqrt{2}$ = 1.414. In zirconium dihydride it equals 4.443 : 3.520 = 1.26, in thorium dihydride 5.03 : 4.1 = 1.23. Thus, some contraction takes place along the c axis. As seen from Fig. 2 and from the coordinates of the D atoms, the D–D distance denoted by the broken line equals $c/2$ = 2.224 Å for zirconium dideuteride and 2.515 Å for thorium dideuteride. The Me–D distance in the first case equals 2.09 and in the second 2.41 Å, as in [5].

Thus, the D–D distance in the dideuterides is three times larger than in the D_2 molecule (where it equals 0.74 Å), i.e., there are no hydrogen molecules or groups of hydrogens in the lattice.

It should be noted that, as shown in [6], the structure of ThC_2 also differs from that given by all authors prior to [6], and, in particular, the C–C distance reaches 1.5 Å as against 1.2 Å in acetylene.

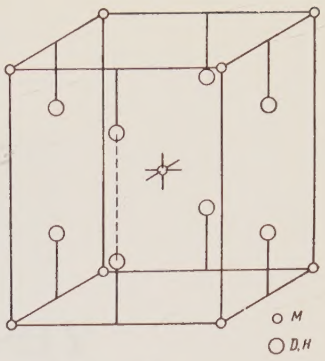

Fig. 2.

LITERATURE CITED

1. G. Hägg, "Röntgenuntersuchung über die Hydride von Ti, Zr, V, u. Ta," Z. Phys. Chem., B11, 433-454 (1930).
2. Ya. S. Umanskii, Carbides of Solid Alloys [in Russian] (Metallurgizdat, Moscow, 1947).
3. B. F. Ormont, Structures of Inorganic Materials [in Russian] (Tekhteorizdat, Moscow, 1950), p. 384.
4. Ya. S. Umanskii, B. N. Finkel'shtein, M. E. Blanter, S. T. Kishkin, N. S. Fastov, and S. S. Gorelik, Physical Metallurgy [in Russian] (Metallurgizdat, 1955), p. 213.
5. R. E. Rundle, C. G. Shull, and E. O. Wollan, "The crystal structure of Th and Zr Dihydrides by x-ray and neutron diffraction," Acta cryst., 5, 22 (1952).
6. E. B. Hunt and R. E. Rundle, "The structure of ThC_2 by x-ray and neutron diffraction," J. Am. Chem. Soc., 73, 4777 (1951).